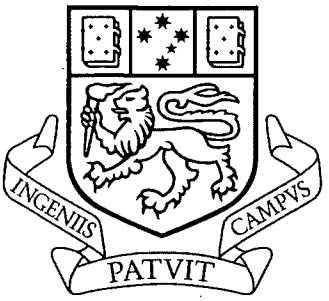

UNIVERSITY
OF TASMANIA

Structural and Reductive Chemistry of Low-valent Lanthanide Complexes Featuring Modified Porphyrinogens

By

Alistair Sydney Paul Frey, B. Sc. (Hons)

A thesis submitted in fulfillment
of the requirements for the degree of
Doctor of Philosophy

School of Chemistry, University of Tasmania, February 2009

This thesis contains no material which has been accepted for the award of any other degree or diploma in any University, and contains no copy or paraphrase of material previously presented by another person, except where due reference is made in the text.

This thesis is not to be made available for loan or copying for two years following the date this statement was signed. Following that time the thesis may be made available for loan and limited copying in accordance with the Copyright Act 1968.

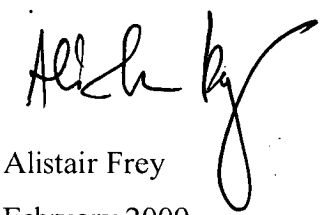

Alistair Frey

February 2009

ACKNOWLEDGEMENTS

Firstly I would like to sincerely thank my supervisor, Dr. Michael G. Gardiner, University of Tasmania, and my associate supervisor, Dr. Adrian V. George at the University of Sydney, for providing me with the project which this thesis is the final result of. I have thoroughly enjoyed being a member of their research groups and am grateful for their time and encouragement over the years. Thanks also go to Prof. Les D. Field, who provided valuable input and support while I was working at the University of Sydney. I would like to thank the University of Tasmania for the scholarship which made it possible for me to devote more than three years to this work.

I would like to acknowledge Dr. Thomas Rodemann (University of Tasmania) and Dr. Ian Luck (University of Sydney) for valuable assistance with NMR spectroscopy, and Dr. Noel Davies (Central Science Laboratory, University of Tasmania) for his Mass Spectroscopy expertise. Various crystallographers have contributed to the collection and refinement of the molecular structures presented here, in particular I would like to thank Prof. Peter Junk, Dr. Marcus Cole and Dr. Matthias Hilder at Monash University, and of course Michael!

Special thanks go to my parents, Elizabeth and Otto, and sister Erika for their loving support while I was studying in Tasmania. This thesis is dedicated to my late Godparents, Orman and Marjorie Mansfield, whose relentless enthusiasm encouraged me and facilitated my educational pursuits throughout the years.

ABSTRACT

This thesis describes studies into the synthesis, characterisation and reactivity of samarium(II) and samarium(III), europium(II) and ytterbium(II) complexes derived from the modified porphyrinogens *trans-N,N'*-dimethyl-*meso*-octaethylporphyrinogen, $Et_8N_4Me_2H_2$, and *trans*-calix[2]benzene[2]pyrrole, $Me_8N_2Ph_2H_2$.

Chapter 2 is concerned with the synthesis of a new modified porphyrinogen *N,N'*-dimethyl-*meso*-octamethylporphyrinogen, $Me_8N_4Me_2H_2$, via a convergent "3+1" procedure from the condensation of 1-methyl-2,5-bis(1,1'-dimethylhydroxymethyl)pyrrole with 1-methyl-2,5-bis{(2'-pyrrolyl)dimethylmethyl}pyrrole in acetonitrile in the presence of scandium trifluoromethanesulfonate. The stepwise nature of the synthesis potentially allows independent functionalisation of various parts of the molecule.

The unique electronic and steric properties of complexes derived from doubly deprotonated *N,N'*-dimethyl-*meso*-octaethylporphyrinogen were exploited to force unusual reactivity and/or structural features in a range of lanthanide(II) and lanthanide(III) complexes. Chapter 3 details the synthesis of samarium(II), europium(II) and ytterbium(II) complexes of this macrocycle. Subsequent reaction with a range of 1,4-diazabuta-1,3-dienes (R-N=C(H)-C(H)=N-R, R = *t*-Bu, *i*-Pr and *n*-Bu) gave complexes featuring 1,4-diazabuta-1,3-diene binding to the lanthanide centres as neutral Lewis base donors, chelating radical anions and bridging reduced dianions. Steric limitations were found to alter these structural outcomes, and the complexes were characterised by X-ray crystal structure determination and NMR spectroscopy. Steric factors were also implicated in the observation of an unusual solvent mediated Sm(II)/Sm(III) reversibility in which a Sm(III) centre reverted to Sm(II) upon addition of coordinating solvent (R = *t*-Bu).

Steric competition in the *N,N'*-dimethyl-*meso*-octaethylporphyrinogen system was further examined in Chapter 4 by synthesis of a highly strained cyclopentadienyl Sm(III) complex $[(Et_8N_4Me_2)Sm(C_5H_5)]$ featuring a major conformational deformation in the macrocycle. Also synthesised was a centrosymmetric bimetallic

cyclooctatetraenediyl bound Sm(III) complex [{($Et_8N_4Me_2$)Sm}$_2$(μ:η^2:η^2-COT)] in which the cyclooctatetraenediyl dianion is forced to adopt an η^2-binding mode to each Sm centre. Solid state molecular structures of these strained molecules were complemented by ^{1}H, ^{13}C, 2D and variable temperature NMR studies of the cyclopentadienyl complex to examine fluctional processes in solution.

Chapter 5 describes ligand substitution reactions in which Sm(III) complexes of 1,4-diazabuta-1,3-dienes were reacted with reducible substrates. Samarium(III) complexes of *t*-butyl-1,4-diaza-1,3-diene and *i*-propyl-1,4-diaza-1,3-diene were found to reduce benzil to give the binuclear complex [{($Et_8N_4Me_2$)Sm}$_2${μ-OC(Ph)C(Ph)O}] with the concomitant formation of the free 1,4-diazabuta-1,3-diene. Also investigated was the highly strained [($Et_8N_4Me_2$)Sm(C_5H_5)], which was found to react with 1,4-benzoquinone to give the binuclear complex [{($Et_8N_4Me_2$)Sm}$_2${μ-O(C_6H_4)O}].

Chapter 6 describes the reductive chemistry of the Sm(II) complex [($Et_8N_4Me_2$)Sm(THF)$_2$]. It was found to reduce CO_2 in a disproportionation reaction to give carbon monoxide and a bridging CO_3^{2-} moiety. The resulting binuclear samarium(III) complex was characterised by X-ray crystal structure determination and NMR spectroscopy. The Sm(II) complex was also used in redox transmetallation reactions with mercury, thallium and silver salts. The reaction with silver tetrafluoroborate gave a Sm(III) tetrafluoroborate intermediate which underwent subsequent salt metathesis reactions with sodium cyclopentadienide and lithium iodide to give the respective samarium(III) derivatives.

Chapter 7 details the synthesis of *trans*-calix[2]benzene[2]pyrrole by condensation of pyrrole with 1,3-bis(1',1'-dimethylhydroxymethyl)benzene in acetonitrile. The literature procedure for the synthesis of this macrocycle was improved by the use of a catalytic amount of scandium trifluoromethanesulfonate in place of stoichiometric boron trifluoride as Lewis acid. As a counterpoint to the conformationally restricted *N,N'*-dimethyl-*meso*-octaethylporphyrinogen, the less rigid doubly deprotonated *trans*-calix[2]benzene[2]pyrrole was investigated as a ligand for lanthanide metals. The potassium salt was synthesised by deprotonation of the neutral porphyrinogen with potassium metal. The lanthanide chemistry was investigated by reaction of the dipotassium salt with SmI_2. The reaction was sensitive to conditions and resulted in mixtures from which a number of Sm(II) complexes featuring varying degrees

of solvation and an unsolvated "*N*-confused" dimer were isolated. Molecular structures of the dipotassium salt, mono- and bis-THF Sm(II) adducts and Sm(II) *N*-confused binuclear dimer were obtained. As derivatives, a cationic Sm(III) cyclooctatetraenediyl complex and a potassium containing Sm(III) cyclooctatetraendiyl complex were obtained and characterised by X-ray crystal structure determination. Macrocyclic binding modes fell between the extremes of the samarium(II) mono-THF adduct (featuring a bis(η^3-arene) structural motif with only a slight metallocene bend angle, η^5-bound pyrrolide rings) and the cyclooctatetraenediyl Sm(III) complexes in which the macrocycle splays back to allow the large, planar COT full access to the Sm coordination sphere, resulting in an η^8 Sm-COT interaction and concomitant reduction in arene hapticity to a slipped η^1-arrangement with pyrrolide rings η^1-bound through the nitrogen. The Sm(II) complexes were also characterised by ^{1}H NMR and/or variable temperature ^{1}H NMR spectroscopy.

Table of Contents

5 Ligand Based Reduction Chemistry of Strained Sm(III) Complexes

6 Carbon Dioxide and Transmetallation Reduction Chemistry

7 *trans*-Calix[2]benzene[2]pyrrolide Samarium Chemistry

8 Conclusion

ABBREVIATIONS

Å	Ångström, 10^{-10} m
Anal.	microanalysis
b	broad
n-Bu	*normal*-butyl
t-Bu	*tert*-butyl
Bz	benzyl
Calcd.	Calculated
COT	Cyclooctatetraenediyl dianion
18-crown-6	1,4,7,10,13,16-hexaoxacyclooctadecane
Cy	cyclohexyl
d	doublet
DME	1,2-dimethoxyethane
EI	electron ionisation
EPR	electron paramagnetic resonance
Et	ethyl
$Et_8N_4H_4$	*meso*-octaethylporphyrinogen
$Et_8N_4MeH_3$	*N*-methyl-*meso*-octaethylporphyrinogen
$Et_8N_4Me_2H_2$	*trans-N,N´*-dimethyl-*meso*-octaethylporphyrinogen
$Et_8N_4Me_3H$	*N,N´,N´´*-trimethyl-*meso*-octaethylporphyrinogen
$Et_8N_4Me_4$	*N,N´,N´´,N´´´*-tetramethyl-*meso*-octaethylporphyrinogen
Et_2O	diethyl ether
$Et_8O_2N_2H_2$	*meso*-octaethyl-*trans*-dioxaporphyrinogen
GC/MS	gas chromatography/mass spectrometry
gCOSY	gradient correlation spectroscopy
gHMBC	gradient heteronuclear multiple bond correlation
gHMQC	gradient heteronuclear multiple quantum correlation
gNOESY	gradient nuclear overhauser effect spectroscopy
IR	infra-red
L	ligand
Ln	lanthanide

M	metal
M^+	parent molecular ion peak
m	multiplet (NMR), medium (IR)
Me	methyl
m/e	mass to charge ratio
m.p.	melting point
MS	mass spectrum
NMR	nuclear magnetic resonance
Ph	phenyl
ppm	parts per million
q	quartet
R	alkyl, aryl
$R_8N_4H_4$	*meso*-octaalkylporphyrinogen
s	singlet (NMR), strong (IR)
t	triplet
THF	tetrahydrofuran
TMEDA	*N,N,N',N'*-tetramethylethylenediamine
TMS	trimethylsilyl
w	weak
X	halide
υ	frequency
δ	chemical shift

Chapter 1
Introduction

1.1 General considerations

The *lanthanide* elements (also known as *lanthanoids*, and in the past as *rare earths* or *lanthanons*) are defined as those with the $[Xe]4f^{0-14}5d^{0-2}6s^2$ electronic configuration, spanning the first row of the f-block of the periodic table. The Group 3 elements scandium and yttrium are chemically similar to the lanthanides, and so are commonly included in discussions of lanthanide chemistry. The historical title *rare earth elements* has proved to be a misnomer since the elements are hardly scarce, with terrestrial abundances similar to many historically "common" elements, such as molybdenum and tin.[1] However, *lanthanide*, derived from the Greek *lanthanein* (to lie hid),[2] would seem an apt description for a series of elements which waited not only to be discovered, but to be explored chemically as well. The lanthanides occur together in relatively common ores such as bastnasite ($LnFCO_3$) and monazite ($(Ln, Th, U)PO_4$) which can be reduced to produce *mischmetal*, an alloy of the metals in their naturally occurring proportions. The development of lanthanide chemistry only became possible in the mid-20th century when industrial scale ion-exchange methods of separating the chemically similar elements from one another became available.[3]

The most common oxidation state of the lanthanides is +3, whilst the +4 oxidation state has been observed in complexes of cerium.[4] Whilst the +2 oxidation state has been well established for complexes of samarium, europium and ytterbium, recent work has expanded this range to include neodymium, dysprosium and thulium. The ionic radii across the lanthanide series steadily decreases as the effective nuclear charge increases across the row, a trend commonly referred to as the *lanthanide contraction*. These electronic and steric properties will be referred to in later discussions of structure and reactivity of lanthanide complexes of dianionic modified porphyrinogens.

The first organometallic lanthanide complexes were the tris(cyclopentadienyl)lanthanide(III) complexes reported in 1954 by Wilkinson and Birmingham.[5] Subsequently, lanthanide complexes containing larger, bulkier ligands were synthesised to promote desirable properties such as crystallinity and reactivity. Bulkier π-bound ligands were thus employed, including pentamethylcyclopentadienyl[6]

($(C_5Me_5)^-$, Cp*) and cyclooctatetraenediyl[7] ($(C_8H_8)^{2-}$, COT). Examples of sterically demanding substituted cyclopentadienyl and cyclooctatetraenediyl organolanthanide complexes will be given in the introduction to Chapter 4.

An ever growing proportion of work in the field of organolanthanide chemistry has involved alternate ligand systems, of which the modified porphyrinogens featured in this thesis are an emerging part. Modified porphyrinogens were developed as lanthanide ligands as a means of exploiting the often unpredictable, but potentially very useful porphyrinogen lanthanide chemistry developed during the 1990s (*vide infra*). Porphyrinogens can be considered a subset of a broader class of pyrrolide ligands, which have been investigated as an alternative to the ubiquitous cyclopentadienyl ligand during the same period.

As a context for the chemistry of modified porphyrinogen ligands, the following introduction will briefly describe the lanthanide coordination chemistry of heterocyclic pyrrolide ligands, with a focus on porphyrinogen and modified porphyrinogen chemistry.

1.2 Lanthanide pyrrolide chemistry

The pyrrolide ligand is similar to the cyclopentadienyl ligand in that it is five membered, cyclic, aromatic and singly anionic. Like the cyclopentadienyl system, pyrrolide ligands can engage in η^5-binding between a lanthanide metal and the aromatic π-electrons. In addition, pyrrolide ligands offer the possibility of σ-binding to the lone pair of electrons present at the sp^2 hybridised nitrogen centre. The binding mode(s) actually adopted in a given complex depend on the properties of bound metal(s) (*e.g.* competition between different metal centres in heteronuclear complexes), other ligands and the bulk of substitutents present on the pyrrolide ring.

Heteronuclear ytterbium(II) complexes containing the 2,5-dimethylpyrrolide ligand were prepared *via* reaction of (2,5-$Me_2C_4H_2N$)Li or (2,5-$Me_2C_4H_2N$)K with ytterbium(II) iodide, Figures 1 and 2.[8] The alkali metal retained from the metathesis reaction was found to determine the binding mode of the ytterbium centre in the resultant complexes. The lithium complex $[\{(\mu\text{-}\eta^1\text{:}\eta^5\text{-}2,5\text{-}Me_2C_4H_2N)_2Yb(I)_2[Li(THF)]_2\}_2(toluene)]_n$, **(I)**, featured σ-binding between the lithium

cations and pyrrolide nitrogens with the ytterbium centres η^5-bound to the face of the pyrrolide ring. Conversely, the larger potassium cations in $\{(\mu\text{-}\eta^1\text{:}\eta^5\text{-}2,5\text{-}Me_2C_4H_2N)_4[K(THF)]_2Yb\}_n$, **(II)**, preferrentially bind η^5 to the face of the pyrrolide ring, with the ytterbium centres left to σ-bind to the heterocycle nitrogens.

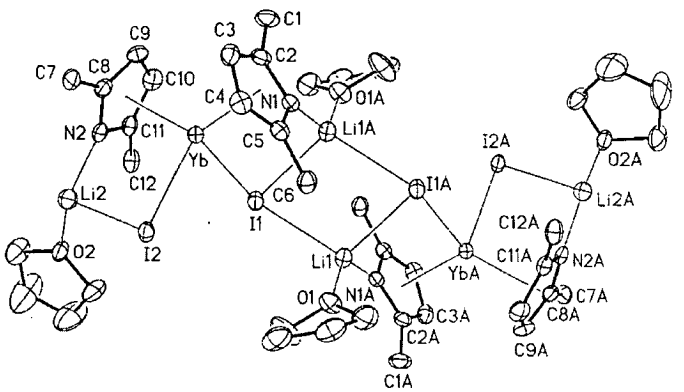

Figure 1: A portion of the linear chain of the π-bound ytterbium 2,5-dimethylpyrrolide complex, $[\{(\mu\text{-}\eta^1\text{:}\eta^5\text{-}2,5\text{-}Me_2C_4H_2N)_2Yb(I)_2[Li(THF)]_2\}_2(toluene)]_n$, **(I)**.[8]

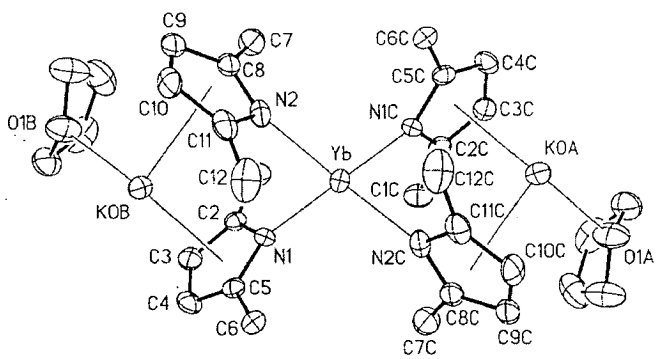

Figure 2: A portion of the linear chain of the σ-bound ytterbium 2,5-dimethylpyrrolide complex, $\{(\mu\text{-}\eta^1\text{:}\eta^5\text{-}2,5\text{-}Me_2C_4H_2N)_4[K(THF)]_2Yb\}_n$, **(II)**.[8]

The ytterbium(III) complex $[(2,5\text{-di-}t\text{-}BuC_4H_2N)YbCl_2(THF)_2]$, **(III)**, was prepared by the salt metathesis reaction between $YbCl_3(THF)_3$ and $(2,5\text{-di-}t\text{-}BuC_4H_2N)Na$, Figure 3.[9] The resultant mononuclear complex features a ytterbium centre η^5-bound to the pyrrolide ligand. The bulky *t*-butyl substituents present at the 2 and 5 positions of the pyrrolide ligand induce the η^5 interaction by hindering σ-N binding of the ligand to the Yb centre. There are examples of pyrrolides in other ligand

systems bearing tertiary carbons in the 2 and 5 positions which do not participate in η^5-binding with lanthanide metals, *e.g.*, porphyrinogens (see Section 1.5).

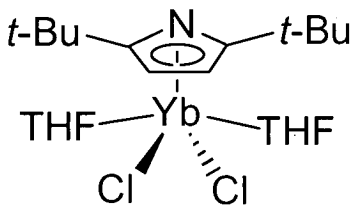

Figure 3: π-bound ytterbium 2,5-di-*t*-butylpyrrolide complex [(2,5-di-*t*-$BuC_4H_2N)YbCl_2(THF)_2$], **(III)**.

The heterocyclic samarium(III) cyclooctatetraenediyl sandwich complex [(2,5-di-*t*-$BuC_4H_2N)Sm(C_8H_8)(THF)$], **(IV)**, was prepared by reaction of [$\{(C_8H_8)Sm(\mu\text{-}Cl)(THF)\}_2$] with (2,5-di-*t*-$BuC_4H_2N)Na$ in THF, Figure 4.[10] The complex features the 2,5-di-*t*-butylpyrrolide ligand η^5-bound to the samarium centre with an η^8-bound cyclooctatetraenediyl dianion and THF molecule completing the coordination sphere. The analogous thulium(III) and lutetium(III) complexes contained no THF, presumably due to the smaller size of these cations.

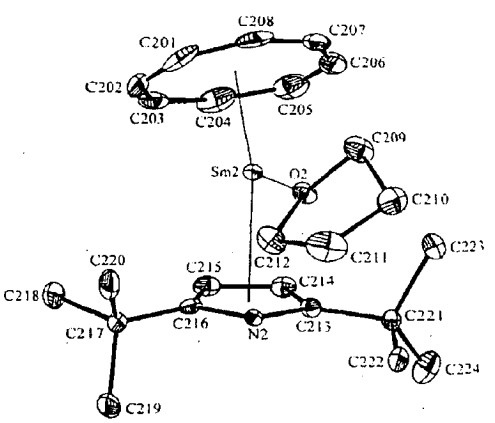

Figure 4: π-bound samarium 2,5-di-*t*-butylpyrrolide complex, **(IV)**.[10]

The η^5-binding mode displayed in the lanthanide(III) 2,5-di-*t*-butylpyrrolide complexes **(III)** and **(IV)** is not observed in the molecular structure of the lithium salt **(V)** of the same ligand.[11] Even though there is considerable steric bulk around the heterocyclic nitrogen the smaller lithium cation prefers to σ-bind to the nitrogen centre

rather than π-bind to the face of the heterocycle, Figure 5. However, there are reported cases of lithium cations π-bound to substituted pyrrolide ligands. The heteronuclear 2,3,4,5-tetramethylpyrrolide complex $[Li\{C_4Me_4NAlMe_2\}_2(\mu\text{-}Cl)]$, **(VI)**, contains two Lewis acidic alumunium centres σ-bound to each pyrrolide nitogen.[12] The electrons in the sp^2 orbital of the nitrogen centres thence become less available for further coordination and the lithium cation adopts an η^5-interaction between the faces of the two pyrrolide rings to form a sandwich type complex, Figure 5.

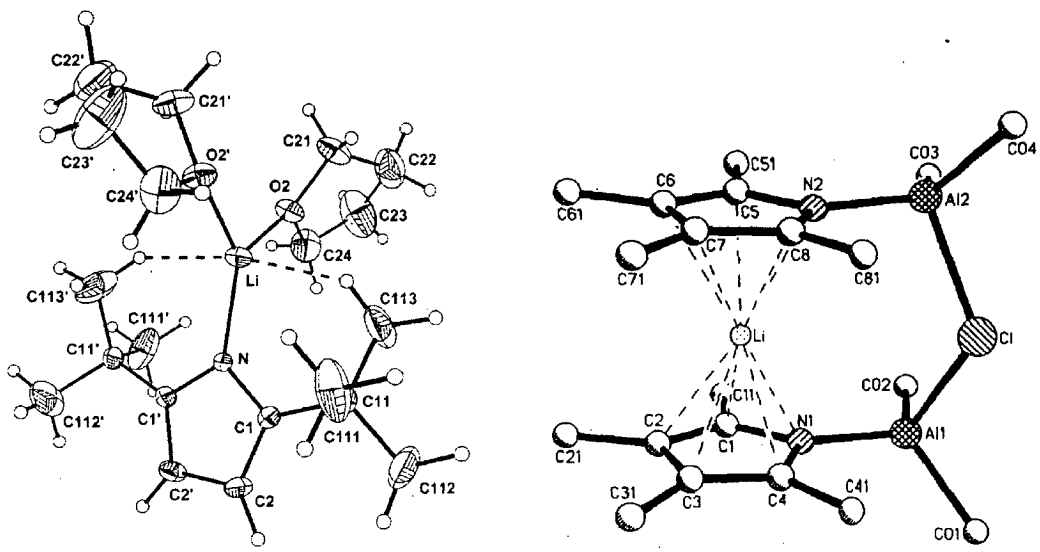

Figure 5: Substituted pyrrolide complexes: σ-bound Li **(V)** (left) and π-bound **(VI)** (right) Li centres.[11,12]

1.3 Lanthanide dipyrromethane chemistry

The dipyrromethane ligand contains two pyrrolide rings bridged at the 2-positions by a single carbon atom. The ligand can be considered the pyrrolyl analogue of an *ansa*-bis(cyclopentadienyl) system, with the presence of a nitrogen centre in each ring offering the possibility of σ- as well as π-binding modes. Dipyrromethane ligands typically bridge multiple metal centres with both σ- and π- interactions, leading to a wide variety of structural outcomes in lanthanide complexes. The lanthanide chemistry has been mainly developed with the diphenyl ($(Ph_2C(2\text{-}C_4H_3N)_2)^{2-}$, **(VII)**) and cyclohexyl ($((1,1\text{-}H_{10}C_6(2\text{-}C_4H_3N)_2)^{2-}$, **(VIII)**) substituted dipyrromethanes, Figure 6.

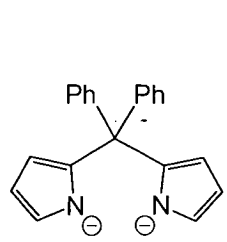

(VII)

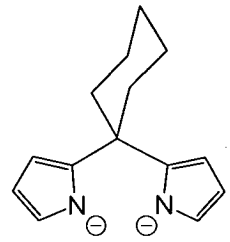

(VIII)

Figure 6: Common dipyrromethane ligands.

The samarium(II) complex $[\{(Ph_2C\{2\text{-}C_4H_3N\}_2)Sm\}_6(THF)_3]$, **(IX)**, was synthesised by the deprotonation of the neutral ligand with a samarium(II) bis{bis(trimethylsilyl)amide} complex under an argon atmosphere.[13] It features six samarium units arranged on the inside of a hexameric cluster, with each samarium centre bridging two dipyrromethane units *via* π- and σ-binding modes. The coordination spheres of the samarium centres are exposed on the inside of the cluster, resulting in high reactivity. Complex **(IX)** undergoes reaction with N_2 to give the dinitrogen complex $[\{(\mu\text{-}Ph_2C\{\eta^1\text{:}\eta^5\text{-}2\text{-}C_4H_3N\}_2)Sm\}_4(\mu\text{-}\eta^1\text{:}\eta^1\text{:}\eta^2\text{:}\eta^2\text{-}N_2)(THF)_2]$, **(X)**. Complex **(X)** is formed by reaction of four samarium(II) centres on an N_2 molecule, resulting in four-electron reduction of dinitrogen, Scheme 1.

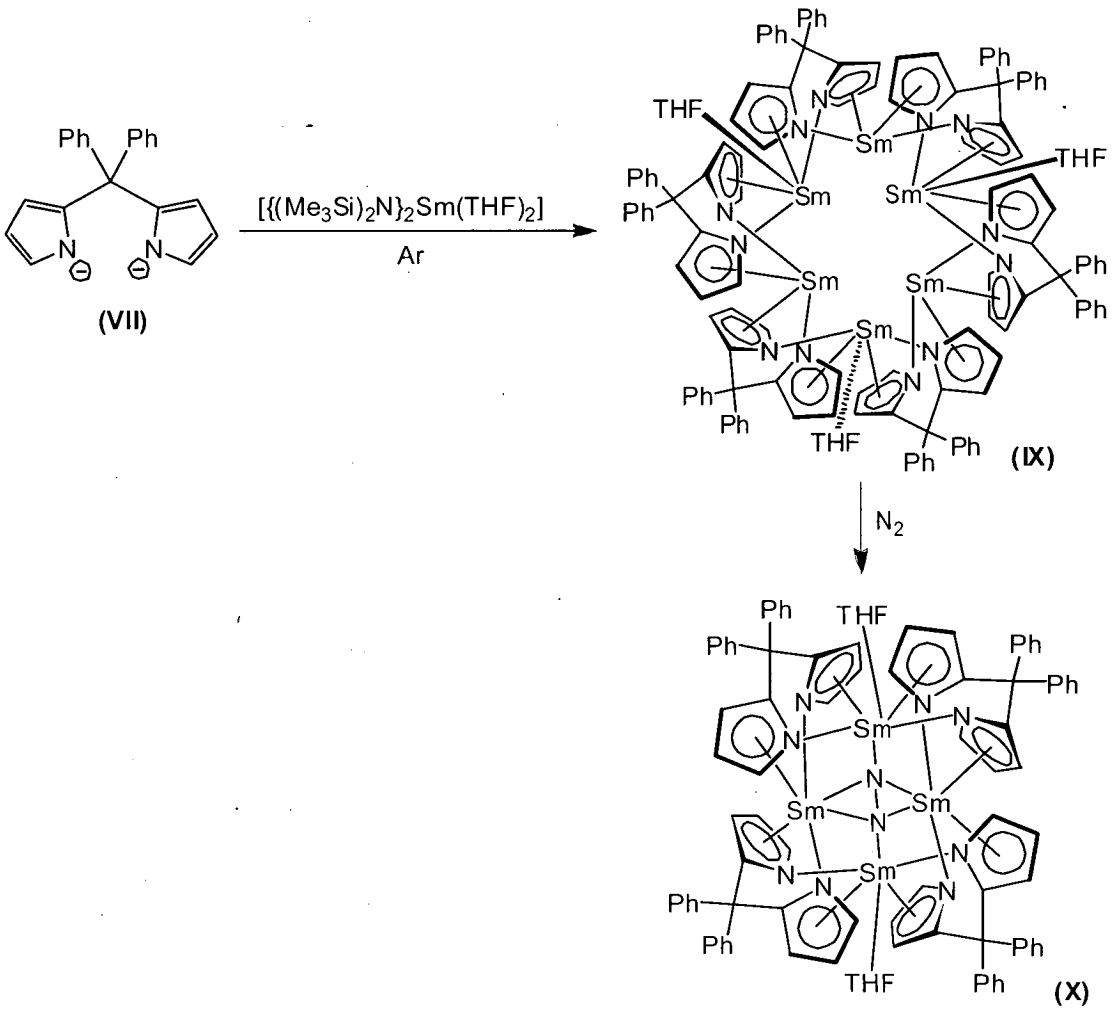

Scheme 1: Dinitrogen reduction by hexameric samarium(II) cluster.

The tetranuclear dinitrogen complex **(X)** was also formed by the reaction of $(Ph_2C(2\text{-}C_4H_3N)_2K_2$ with SmI_2 under a nitrogen atmosphere.[14] The same reaction under argon resulted in the formation of the ionic Sm(II) complex $[(\{\mu\text{-}Ph_2C(\eta^1{:}\eta^5\text{-}2\text{-}C_4H_3N)_2\}_2\{(Sm\{THF\}_3)_2Sm\})(\mu_3\text{-}I)]^+[\{(\mu\text{-}Ph_2C\{\eta^1{:}\eta^5\text{-}2\text{-}C_4H_3N\}_2)Sm\}_5(\mu_5\text{-}I)]^-$, **(XI)**. Reaction of **(XI)** with potassium hydride under nitrogen gave **(X)**, Scheme 2.

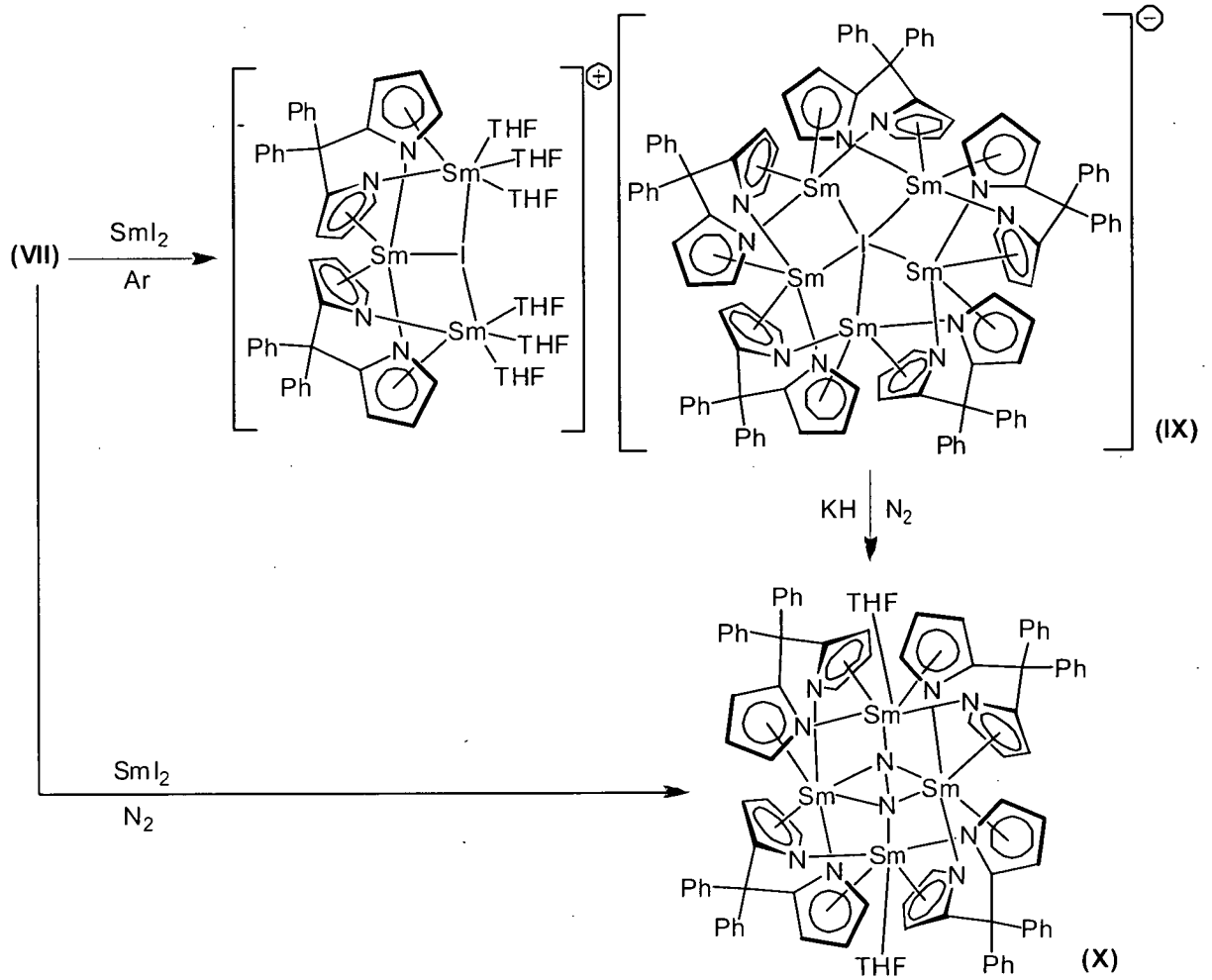

Scheme 2: Dinitrogen reduction.

Reaction of $(Ph_2C(2\text{-}C_4H_3N)_2)Na_2$ or $(Ph_2C(2\text{-}C_4H_3N)_2)K_2$ with $SmCl_3(THF)_3$ and subsequent reduction with metallic sodium or potassium in THF resulted in formation of a hydride complex[15] $[Na(THF)_6][\{Ph_2C(2\text{-}C_4H_3N)_2Sm\}_4(H)(THF)_2]$, **(XII)**, or a chloride complex[14] $[\{[\mu\text{-}Ph_2C(\eta^1\text{:}\eta^5\text{-}2\text{-}C_4H_3N)_2]Sm\}_4(THF)_2(\mu_4\text{-}Cl)\{K(THF)_2\}]$, **(XIII)**, respectively (Figure 7). The origin of the hydride moiety in **(XII)** was attributed by the authors to the degradation of THF by the alkali metal, although mechanistic proof was not offered. The chloride anion present in the molecular structure of **(XIII)** was retained from the metathesis precursor.

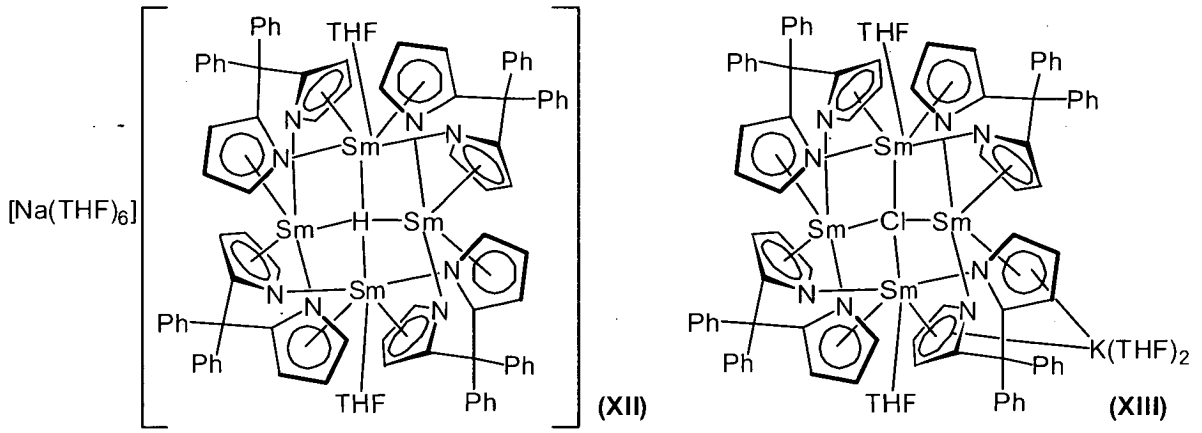

Figure 7: Hydride complex **(XII)** and chloride complex **(XIII)**.

The cyclohexyl substituted samarium(II) complex $[(\{1,1\text{-}(2\text{-}C_4H_3N)_2C_6H_{10}\}Sm)_8(THF)_4]\cdot$hexane, **(XIV)**, was synthesised by deprotonation of the neutral ligand with a samarium(II) bis{bis(trimethylsilyl)amide} complex.[13] It is an octameric cluster which reacts readily with N_2 to form the tetrameric dinitrogen complex $[(\{(CH_2)_5C(2\text{-}C_4H_3N)_2\}Sm)_4(THF)_2(N_2)]\cdot 0.5THF$, **(XV)**.[15] Complex **(XV)** reacted with metallic sodium to give $[(\{(CH_2)_5C(2\text{-}C_4H_3N)_2\}Sm)_4(THF)_2(\mu\text{-}N_2)(Na\{THF\})_2]\cdot 2THF$, **(XVI)**. Complex **(XVI)** contains a THF-solvated sodium atom η^1-bound to each nitrogen of the reduced dinitrogen moeity within the cavity and η^5-bound to two pyrrolide rings. Further reaction with sodium led to the linear polymeric $[(1,1\text{-}H_{10}C_6\{2\text{-}C_4H_3N\}_2)_2Sm(Na\{THF\})_2]_n$, **(XVII)**, the molecular structure of which features approximately pseudo-tetrahedral samarium(II) and sodium centres. The evolution of gaseous N_2 was not observed during reaction, and neither NH_3 nor N_2H_4 were detected upon acidification of the reaction mixture, leaving the fate of the dinitrogen moiety undetermined.[16] Complex **(XVI)** was also obtained from the reaction of $1,1\text{-}H_{10}C_6(2\text{-}C_4H_3N)_2Na_2$ with $SmCl_3(THF)_3$ followed by reduction with metallic sodium, Scheme 3.[15]

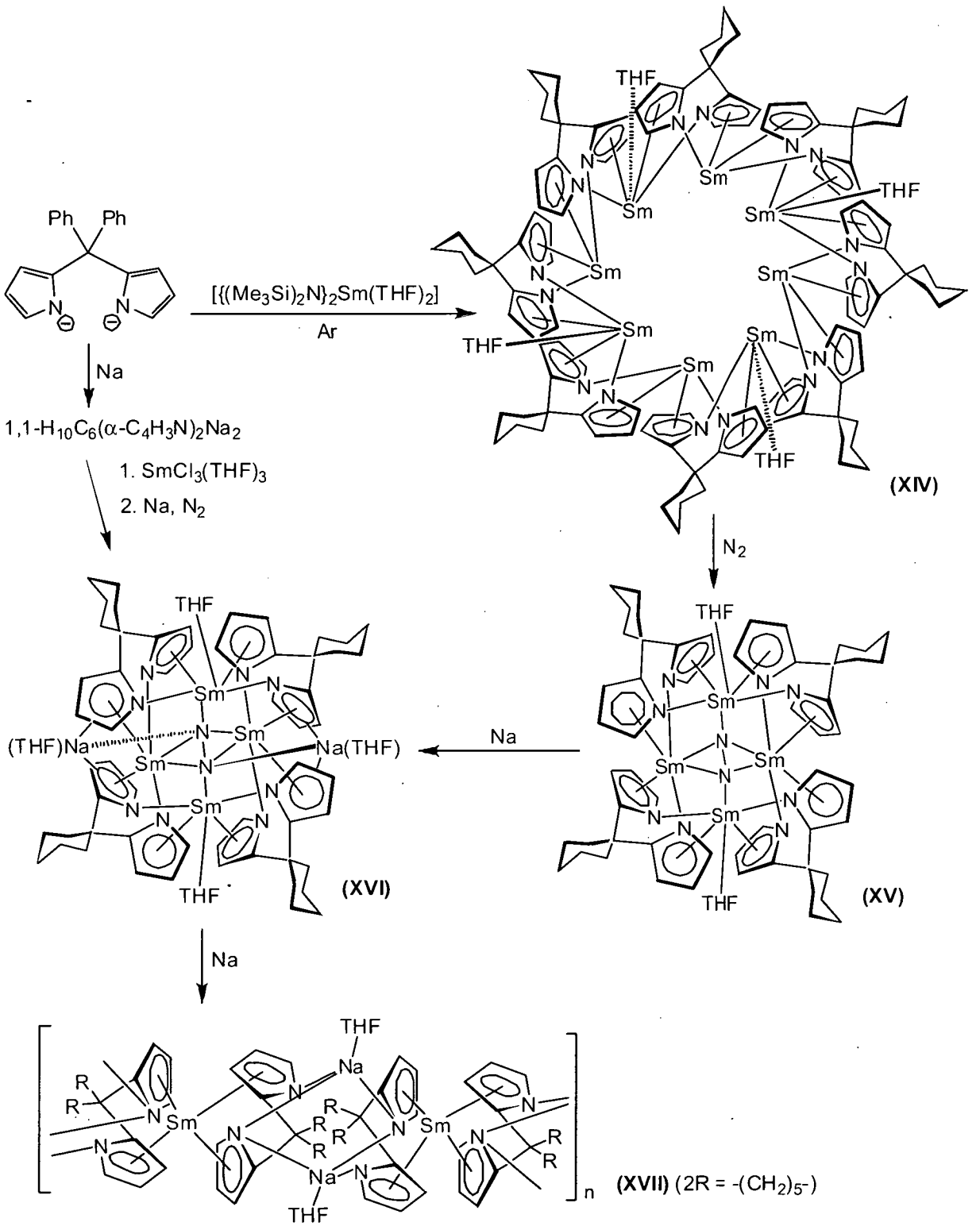

Scheme 3: Transformations involving the $(1,1\text{-}H_{10}C_6(2\text{-}C_4H_3N)_2)^{2-}$ ligand.

1.4 Lanthanide tetraanionic porphyrinogen chemistry

Porphyrinogens contain four pyrrole units linked by sp^3 hybridised carbon atoms at the *meso*-positions, forming a macrocyclic structure. The *meso*- positions are substituted with alkyl or aryl substitutents, thus preventing conversion to the corresponding porphyrin. Porphyrins are linked at the *meso*-positions by sp^2 hybridised carbons, leading to conjugated macrocyclic skeletons which adopt a planar conformation, Figure 8. The lack of conjugation between pyrrole units in porphyrinogens results in freedom to adopt non-planar macrocyclic conformations.

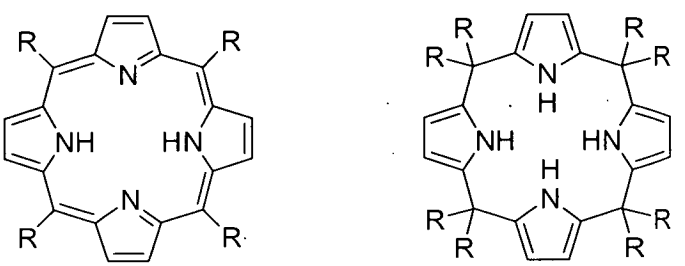

Figure 8: Porphyrin and porphyrinogen structures.

The possible conformations that can be adopted by porphyrinogens are often described using the same set of descriptors used for calixarene macrocycles, Figure 9. Some authors have suggested "calix[4]pyrrole" is a more correct term for describing the macrocycles than porphyringen owing to this feature; the term "porphyrinogen" is used in most discussions in this thesis except for those regarding the octamethyl-*trans*-di-*m*-phenylene substituted porphyrinogen (Chapter 7), for which the name *trans*-calix[2]benzene[2]pyrrole is used.

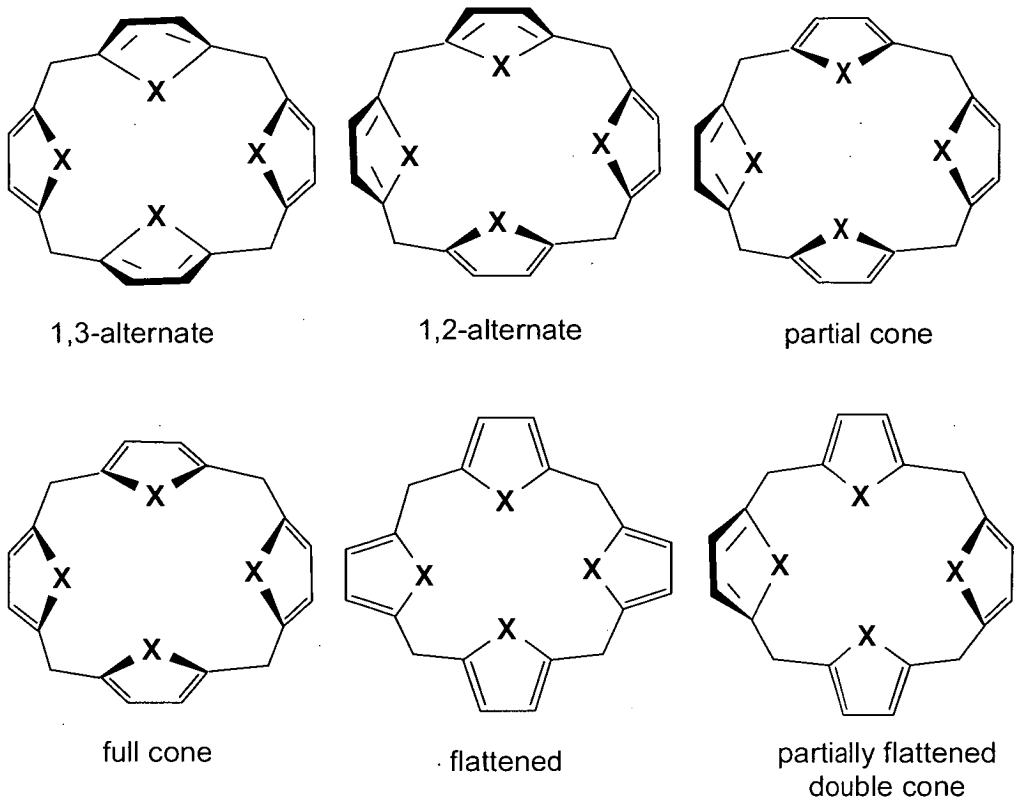

Figure 9: Porphyrinogen and calixarene conformations.

An abbreviated general formula '$R_nN_nH_n$' is used as an abbreviation throughout this thesis for *meso*-octaalkylporphyrinogens. 'R' refers to the *meso*-functionalities, 'N' refers to the pyrrole rings, 'H' refers to the acidic N-H pyrrollic protons. Thus, '$Et_8N_4H_4$' represents the *meso*-octaethylporphyrinogen containing four pyrrole rings, none of which is deprotonated, whilst the tetradeprotonated form of the same porphyrinogen would be '$(Et_8N_4)^{4-}$'. For clarity, *meso*-alkyl groups of porphyrinogens are commonly omitted from figures throughout this thesis. Modified porphyrinogens are referred to using the related abbreviation '$R_nN_nR'_nH_n$' where R_n is the type and number of *meso*-substituent, N_n is the number of pyrrole rings, R'_n refers to the type and number of functionalties used to modify the basic porphyrinogen, and H_n refers to the number of deprotonatable pyrrole N-H groups (≡ anionicity). The abbreviated names will be presented as each modified porphyrinogen is introduced.

The neutral porphyringen molecule can be deprotonated to give $(R_8N_4)^{4-}$ which typically retains the 1,3-alternate conformation observed for $R_8N_4H_4$, Figure 10. On each side of the macrocyclic plane a cavity is defined by two opposite anionic nitrogen centres and two opposite pyrrolide rings. An *endo*-bound metal can therefore σ-bind to two

pyrrolide nitrogens and π-bind to the other two pyrrolide rings, a binding mode commonly seen for lanthanides (*e.g.* samarium(II) complex $[(Et_8N_4)Sm_2(Et_2O)_2]$ **(XVIII)**.[17] In the case of the smaller Group 1 metals, multiple metal centres may share the cavity (*e.g.*, the lithium complex $[(Et_2O)Sm(Et_8N_4)(Li)(Li\{THF\})_2(\mu_3\text{-}OCH_2CH_2)(Et_2O)_{1.5}]$ **(XXIII)**, *vide infra*).[18]

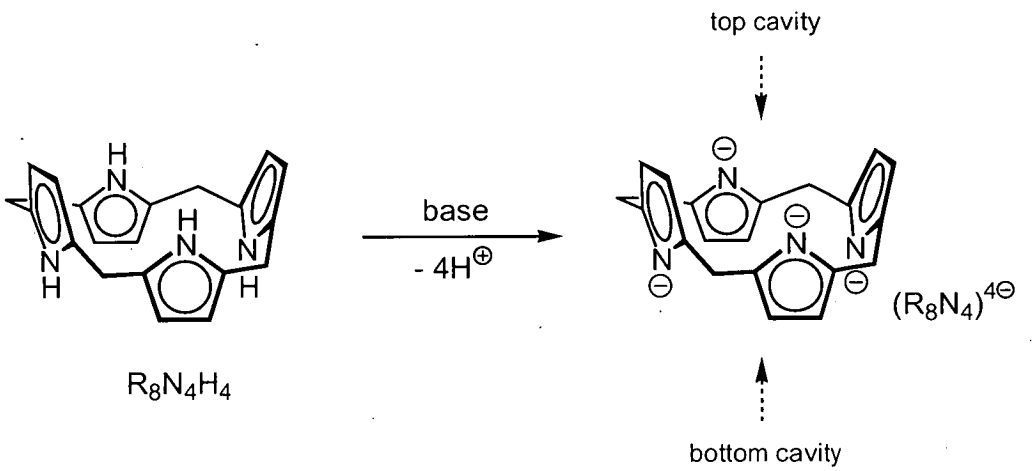

Figure 10: Tetradeprotonation of $R_8N_4H_4$.

The majority of lanthanide porphyrinogen complexes reported to date feature samarium bound to tetradeprotonated *meso*-octaethylporphyrinogen $(Et_8N_4)^{4-}$, or the *meso*-cyclohexyl substituted porphyrinogen $((C_6H_{10})_4N_4)^{4-}$. Both heterometallic and alkali-metal free complexes of these ligands have been prepared and structurally authenticated.

Deprotonation of the neutral $Et_8N_4H_4$ ligand with $[\{(SiMe_3)_2N\}_2Sm(THF)_2]$ gave the dinuclear samarium(II) complex $[(Et_8N_4)Sm_2(Et_2O)_2]$, **(XVIII)**,[17] Equation 1. The complex contains two samarium centres, and the macrocycle is in the same 1,3-alternate conformation as the neutral ligand. Each samarium centre is σ-bound to two opposite deprotonated pyrrolide donors, and η^5-bound *via* π-interactions to the two flanking pyrrolide rings. The overall coordination environment afforded to each samarium centre by the macrocycle is an alternate $\eta^1{:}\eta^5{:}\eta^1{:}\eta^5$ arrangement. The coordination sphere of each samarium atom is completed by a diethyl ether molecule coordinating *via* the oxygen atom which acts as a Lewis base donor. The O-Sm···Sm-O unit is approximately linear. The complex is of interest due to the short Sm···Sm distance of 3.3159(5) Å. Magnetic susceptibility data suggested a degree of interaction between the two samarium centres.

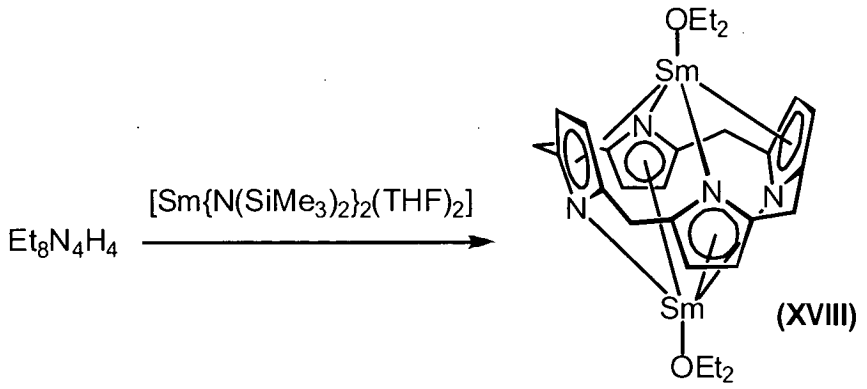

Equation 1

Metathetical exchange between an equivalent of $SmCl_3(THF)_3$ and half an equivalent of $(Et_8N_4)Li_4$ gave the heterometallic samarium(III) complex **(XIX)** (Scheme 4).[19] Complex **(XIX)** contains a solvated lithium centre tethered to each samarium *via* two bridging chlorides. The bridging chlorides can be replaced by reaction with methyllithium to give an analogous tetramethyl samarium/lithium complex **(XX)**. The bridging chloride and lithium centres in **(XIX)** were removed by reduction with metallic lithium or refluxing with $LiAlH_4$ to give $[(Et_8N_4)Sm_2(THF)_2]$, **(XXI)**, the THF-solvated analogue of **(XVIII)**. Throughout these transformations the two samarium centres remain bound within the macrocycle in the same $\eta^1:\eta^5:\eta^1:\eta^5$ arrangement observed in **(XVIII)**.

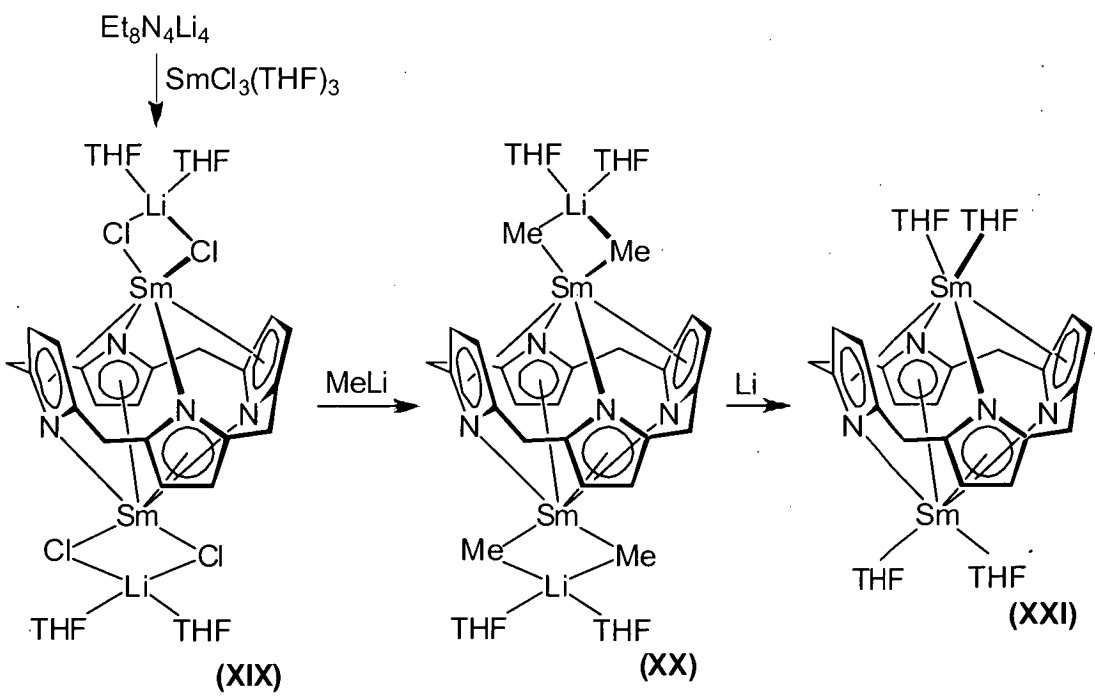

Scheme 4: Reaction of $SmCl_3(THF)_3$ with a half equivalent of $Et_8N_4Li_4$.

Reaction of $SmCl_3(THF)_3$ with a stoichiometric amount of $(Et_8N_4)Li_4$ gave the structurally uncharacterised samarium(III) chloride complex $[(Et_4N_4)(Cl)Sm\{Li_2(THF)_3\}]$, **(XXII)**, (Scheme 5).[20] Reduction of **(XXII)** with metallic lithium under argon gave the heterometallic samarium(II) enolate complex $[(Et_2O)Sm(Et_8N_4)(Li)\{Li(THF)\}_2(\mu_3\text{-}OCH_2\text{-}CH_2)(Et_2O)_{1.5}]$, **(XXIII)**.[18] Complex **(XXIII)** contains a samarium centre bound on one side of the macrocycle in the usual $\eta^1{:}\eta^5{:}\eta^1{:}\eta^5$ binding mode. The other face of the macrocycle accomodates three lithium centres, two σ-bound to pyrrolide nitrogens, the third π-bound to a pyrrolide ring. The three lithium centres are also bound to the oxygen of the enolate originating from ring-opened THF, with a weak interaction between the enolate double bond and one of the lithium atoms.

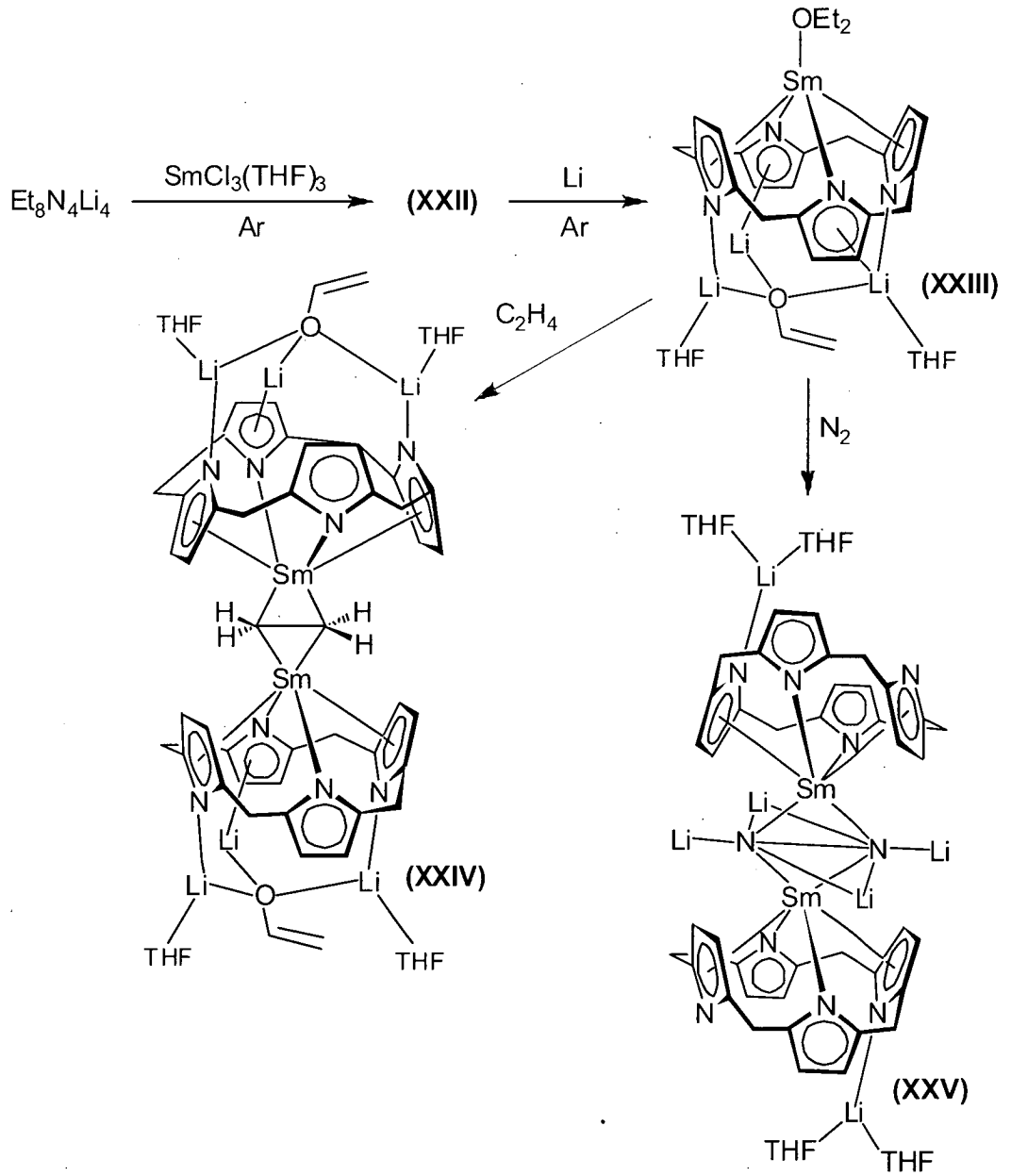

Scheme 5: Stoichiometric reaction of $SmCl_3(THF)_3$ with $(Et_8N_4)Li_4$ and some small molecule activation studies.

Complex **(XXIII)** was found to react with ethylene to give $[(\{(CH_2{=}CHO)Li\}\{Li(THF)\}_2\{Et_8N_4\}Sm)_2(\mu\text{-}CH_2CH_2)]$, **(XXIV)**, in a reversible reaction.[18] ^1H NMR analysis of solutions of **(XXIV)** in benzene-d_6 showed the presence of free C_2H_4 and starting **(XXIII)**, indicative of a reversible reaction, whilst the single bond character of the ethylene C-C bond in the molecular structure (length 1.487(10) Å) represented the reduced species in the solid state. Complex **(XXIII)** reacted with N_2 to give $[\{(THF)_2Li(Et_8N_4)Sm\}_2(N_2Li_4)]$, **(XXV)**, which features a central tetralithium hydrazide bound between two samarium(III) centres.[21] Since the reduction required four electrons it is necessary to implicate lithium centres in the reduction process. This assumption is congruent with the observation that the lithium-free complexes **(XVIII)** and **(XXI)** do not form reduced species with N_2.

Analogous reactions have been carried out using the cyclohexyl derivatised porphyrinogen, $(C_6H_{10})_4N_4H_4$. Reaction of $SmCl_3(THF)_3$ with $(\{C_6H_{10}\}_4N_4)Li_4$ followed by reduction with metallic lithium under argon gave $[((C_6H_{10})_4N_4)(THF)Sm(\mu_3\text{-}Cl)\{Li(THF)\}\{Li(THF)_2\}]$, **(XXVI)**, which contains a single samarium centre and three lithium atoms bridging a single chloride at the other face of the macrocycle, Scheme 6.[18] The chloride **(XXVI)** reacted with N_2 to give dimeric $[\{[Li(THF)]_3(\mu_3\text{-}Cl)((C_6H_{10})_4N_4)Sm\}_2(\mu\text{-}N_2)]\cdot 2THF$, **(XXVII)**, in which dinitrogen is bound side-on between the two samarium centres.[22] The short N-N distance (1.08(3) Å) indicated that reduction had not taken place, and dissolution in diethyl ether or THF resulted in liberation of N_2. However, reaction of **(XXVII)** with another molecule of **(XXVI)** caused reduction of the bound dinitrogen and the formation of trinuclear $[\{((C_6H_{10})_4N_4)_2Sm_3Li_2\}(\mu\text{-}N_2)\{Li(THF)_2\}]\cdot THF$, **(XXVIII)**, in which the third samarium centre is η^2-bound to the reduced dinitrogen moiety and η^5-bound to a pyrrolide ring of each macrocycle. The stability of **(XXVIII)** in refluxing toluene and the N-N distance of 1.502(5) Å indicated that dinitrogen reduction had indeed taken place.

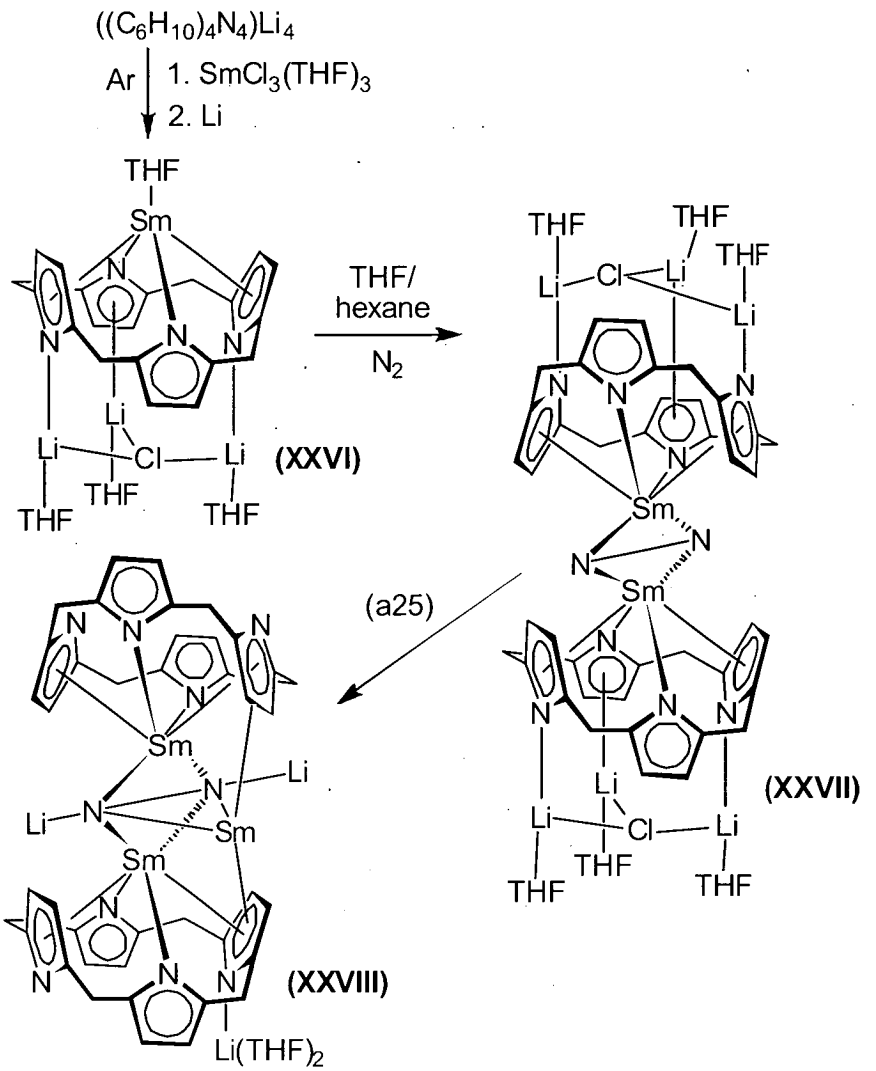

Scheme 6: Dinitrogen reductions.

The sodium salt of the *meso*-octaethylporphyrinogen has also been investigated as a precursor for lanthanide chemistry. Reaction of $LnCl_3(THF)_3$ with $(Et_8N_4)Na_4$ in THF under argon gave $[(THF)_2Na(Et_8N_4)Ln(THF)]$, **(XXIX)**,(Ln = Pr, Nd, Sm, Eu, Gd, Yb), Scheme 7.[23] Complex **(XXIX)** (Ln = Pr, Nd) underwent reduction with sodium napthalenide under N_2 to give the two-electron reduced dinitrogen complex **(XXX)**, structurally characterised as the 1,4-dioxane (Ln = Nd) and DME (Ln = Pr) derivatives **(XXXI)** and **(XXXII)**, respectively.[24] Complexes **(XXXI)** and **(XXXII)** contain reduced dinitrogen side-bound to both neodymium centres. Complex **(XXXI)** contains four solvated sodium counter cations bound to the macrocyclic pyrrolide rings, whilst the ionic complex **(XXXII)** contains two solvated sodium cations bound directly to the macrocycle and two charge separated solvated sodium cations.

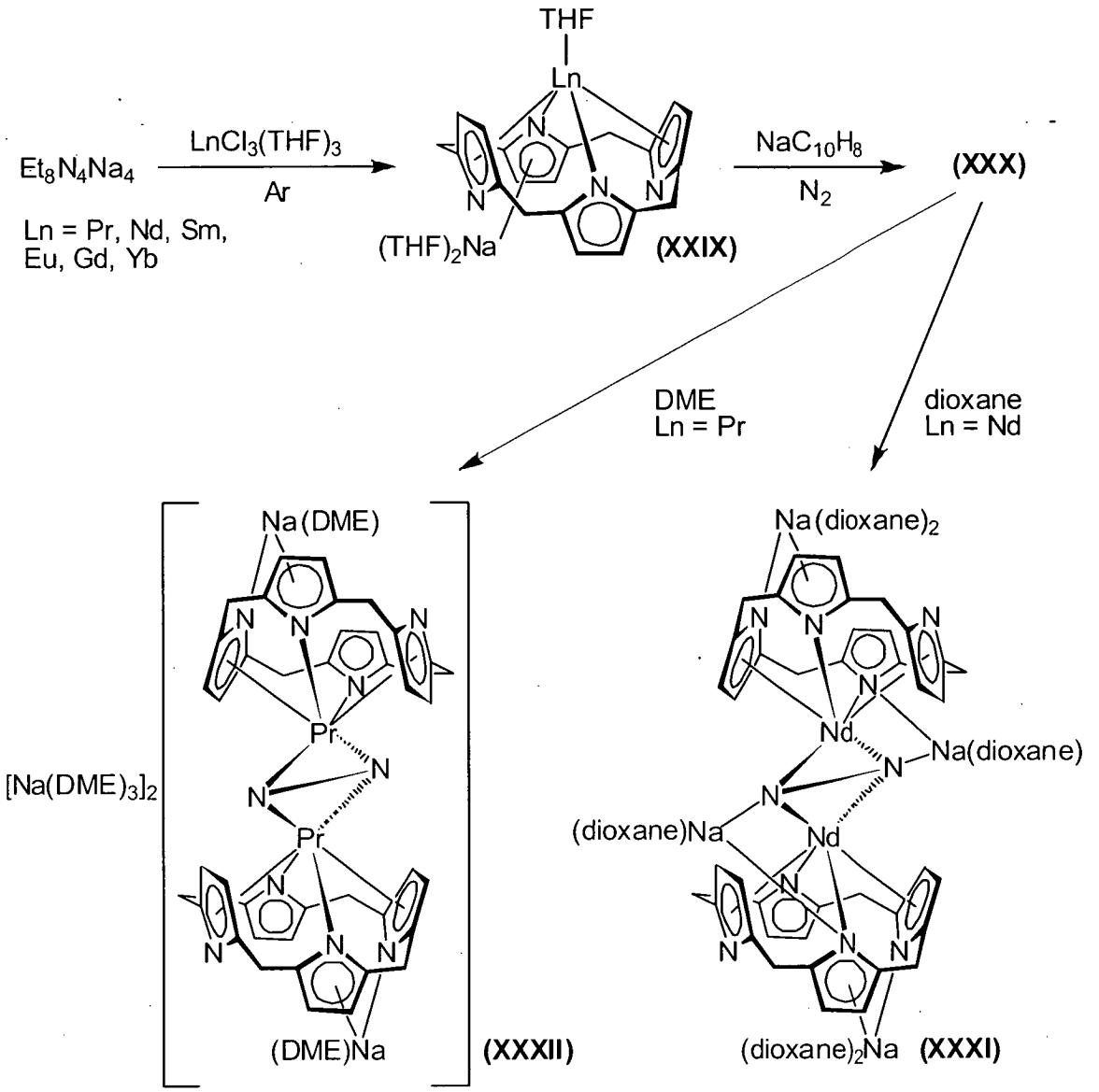

Scheme 7: Reactions of $(Et_8N_4)Na_4$.

Complex **(XXIX)** also displayed reactivity with ethylene and acetylene, Scheme 8.[25] Reaction of **(XXIX)** with sodium napthalenide in the presence of 18-crown-6 and ethylene produced the ionic complex $[\{(THF)_2Na(Et_8N_4)Ln\}_2(\mu:\eta^2:\eta^2\text{-}C_2H_4)][\{Na(THF)(18\text{-crown-}6)\}_2(\mu\text{-dioxane})]$, **(XXXIII)**. The ethylene unit is side-bound and was determined to be reduced on the basis of the C-C distance (1.49(2) Å) in its molecular structure. Reaction of **(XXIX)** with sodium in the presence of acetylene produced the neutral complex $[\{(Et_8N_4)Ln\}_2\{(\mu\text{-}C_2)\text{-}(\mu\text{-}Na)_4]$, **(XXXIV)**, in which the deprotonated acetylide moeity is bound end-on.

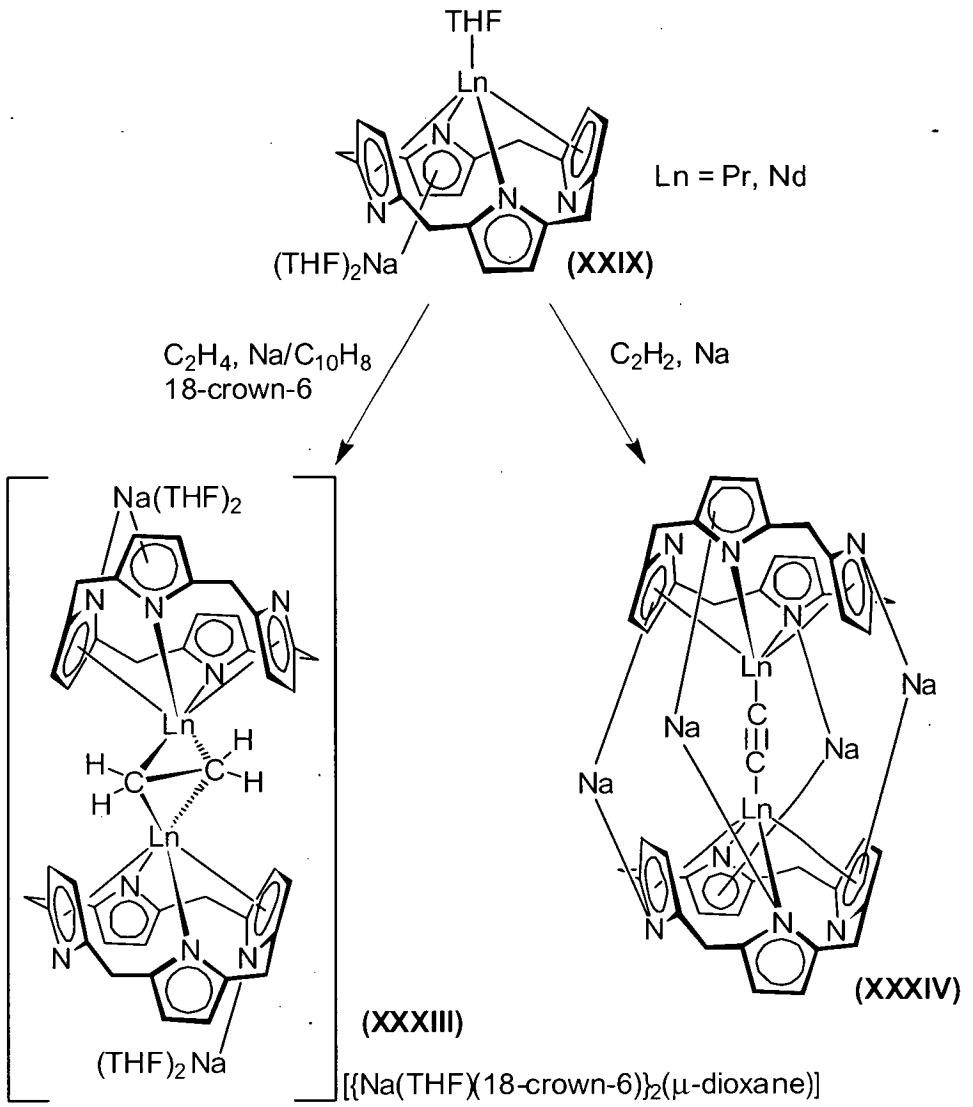

Scheme 8: Reactivity with ethylene and acetylene.

It can be generalised from the above discussions that lanthanide complexes of tetradeprotonated porphyrinogens are polynuclear and often heteronuclear due to the tetraanionicity of the ligand. Although a wide range of reactivities have been established for this class of ligand, the presence of more than one metal centre can lead to uncertainty in establishing mechanisms for observed reactivity. The presence of potential σ-donors on each side of the macrocyclic plane creates a wide range of possible binding modes, making reaction outcomes difficult to predict. Modification of the porphyrinogen ligand to provide a better defined coordination environment and reduced anionicity has been investigated to promote the synthesis of monomeric, homonuclear lanthanide complexes.

1.5 Lanthanide dianionic porphyrinogen chemistry

Modified porphyrinogens have been investigated as non-participative ligands suited to the stabilisation of divalent and trivalent lanthanides. A reduction in anionicity from -4 to -2 promotes the synthesis of mononuclear lanthanide complexes whilst retaining the high degree of control over the lanthanide coordination sphere offered by a bulky, macrocyclic ligand. Two systems have been used by our research group: *meso*-octaethyl-*trans*-dioxaporphyrinogen ($Et_8N_2O_2H_2$), **(XXXV)**, and *trans*-*N*,*N'*-dimethyl-*meso*-octaethylporphyrinogen ($Et_8N_4Me_2H_2$), **(XXXVI)**, Figure 11. The 'O_2' in the abbreviated form of **(XXXV)** refers to the two furanyl oxygen centres, whilst the 'Me_2' in the abbreviated form of **(XXXVI)** refers to the *N*-methyl substituents.

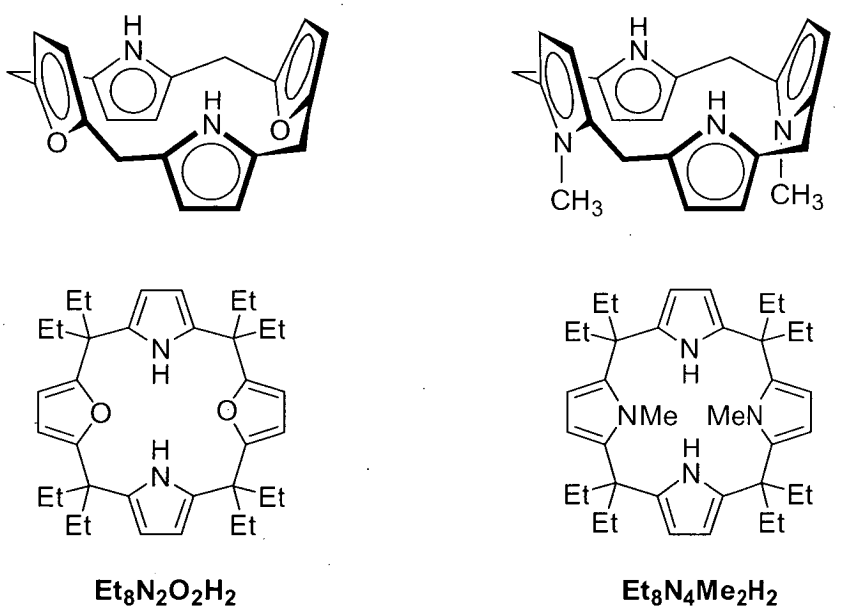

Figure 11: Modified porphyrinogens.

The bis-(furanyl) functionalised porphyrinogen **(XXXV)** contains two pyrrolyl and two furanyl rings in a 1,3-alternate arrangement.[26] Following deprotonation, the two anionic pyrrolide nitrogens face one side of the macrocycle and the two furanyl oxygens face the other. Although the formal anionicity of the deprotonated ligand is -2, the furanyl oxygens are observed to act as Lewis base donors in a number of lanthanide complexes.

The *trans*-dimethyl functionalised porphyrinogen **(XXXVI)** also adopts a 1,3-alternate conformation.[27] It differs from **(XXXV)** in that the two opposite *N*-Me

functionalities block access to the other side of the cavity and are not Lewis basic. Further, *trans*-annular interactions between the *N*-Me substituents severly restrict the conformational freedom of the rest of the macroycle. The result is a rigid "bowl" shaped porphyrinogen, with a single cavity bearing two pyrrolide nitrogens capable of deprotonation and subsequent coordination.

The dilithium complex **(XXXVII)** and dipotassium complex **(XXXVIII)** were prepared by deprotonation of $Et_8N_2O_2H_2$ with *n*-butyllithium or potassium metal, Scheme 9.[28,29] The potassium salt was structurally characterised as the TMEDA adduct $[(Et_8N_2O_2)K_2(TMEDA)_2]$, **(XXXIX)**. The molecular structure of **(XXXIX)** is monomeric, with a potassium centre bound in an $\eta^1{:}\eta^5{:}\eta^1{:}\eta^5$ fashion within the macrocyclic cavity, with the macrocycle adopting an alternate conformation. Therefore one potassium centre is η^5-bound to the furanyl rings and η^1-bound to the pyrrolide rings, whilst the reverse occurs for the other potassium centre. One TMEDA molecule completes the coordination sphere of each potassium.

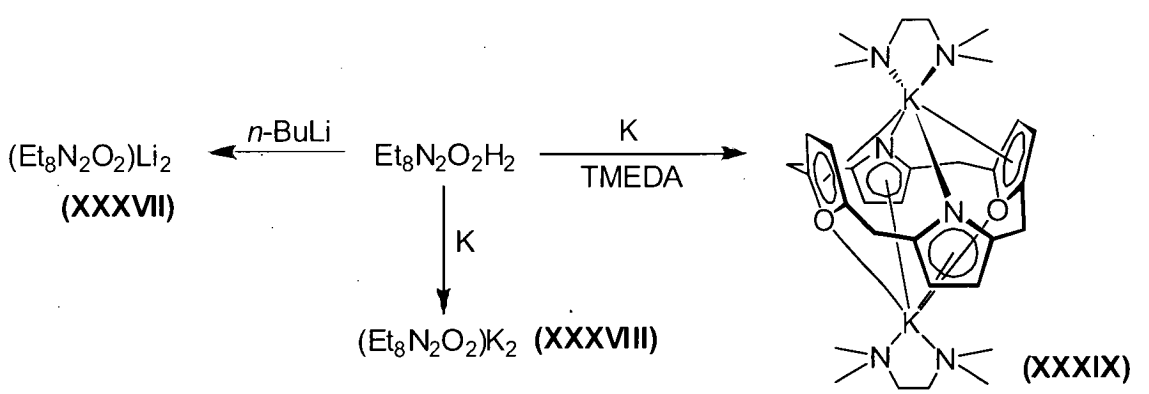

Scheme 9: Lithium and potassium salts of $(Et_8N_2O_2)^{2-}$.

The structurally characterised samarium(II) complex $[\{(THF)_2K(Et_8N_2O_2)Sm(\mu\text{-}I)\}_2]$, **(XL)**, was prepared by reaction of the potassium salt **(XXXVIII)** with SmI_2, Equation 2.[29] The molecular structure of **(XL)** is dimeric, with each samarium centre bound to the macrocycle *via* $\eta^1{:}\eta^5{:}\eta^1{:}\eta^5$ interactions. The samarium centres are each η^1-bound to the furanyl oxygens, and η^5-bound to the pyrrolide rings, with two iodide anions bridging the samarium centres. Two solvated potassium cations are bound to the rear of each macrocycle with η^1-binding to the pyrrolide nitrogens and η^5-binding to the furanyl rings.

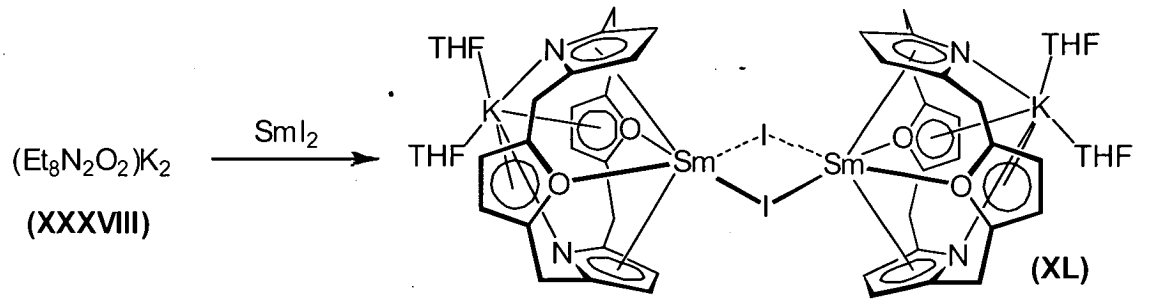

Equation 2

The samarium(II) complex **(XL)** underwent oxidation with I_2 to give the dimeric samarium(III) iodide complex $[\{(Et_8N_2O_2)SmI\}_2]$, **(XLI)**, Scheme 10.[29,30] Complex **(XLI)** underwent salt metathesis with sodium bis(trimethylsilyl)amide to give the monomeric amide $[(Et_8N_2O_2)SmN(SiMe_3)_2]$, **(XLII)**. Both **(XLI)** and **(XLII)** contain a single samarium centre, and no incorporated alkali metals. Reaction of complex **(XLII)** with an additional equivalent of sodium bis(trimethylsilyl)amide resulted in deprotonation of a trimethylsilyl group to give $[(THF)_2Na(Et_8N_2O_2)SmN(SiMe_3)Si(Me)_2CH_2]$, **(XLIII)**. Complex **(XLIII)** contains a single samarium centre and a sodium counterion bound to the base of the cavity. Reaction with an excess of sodium bis(trimethylsilyl)amide results in displacement of samarium from the macrocycle and formation of the disodium salt $[(Et_8N_2O_2)Na_2(THF)_4]$, **(XLIV)**. Analogous reactions were obtained using potassium bis(trimethylsilyl)amide in place of the sodium reagent.

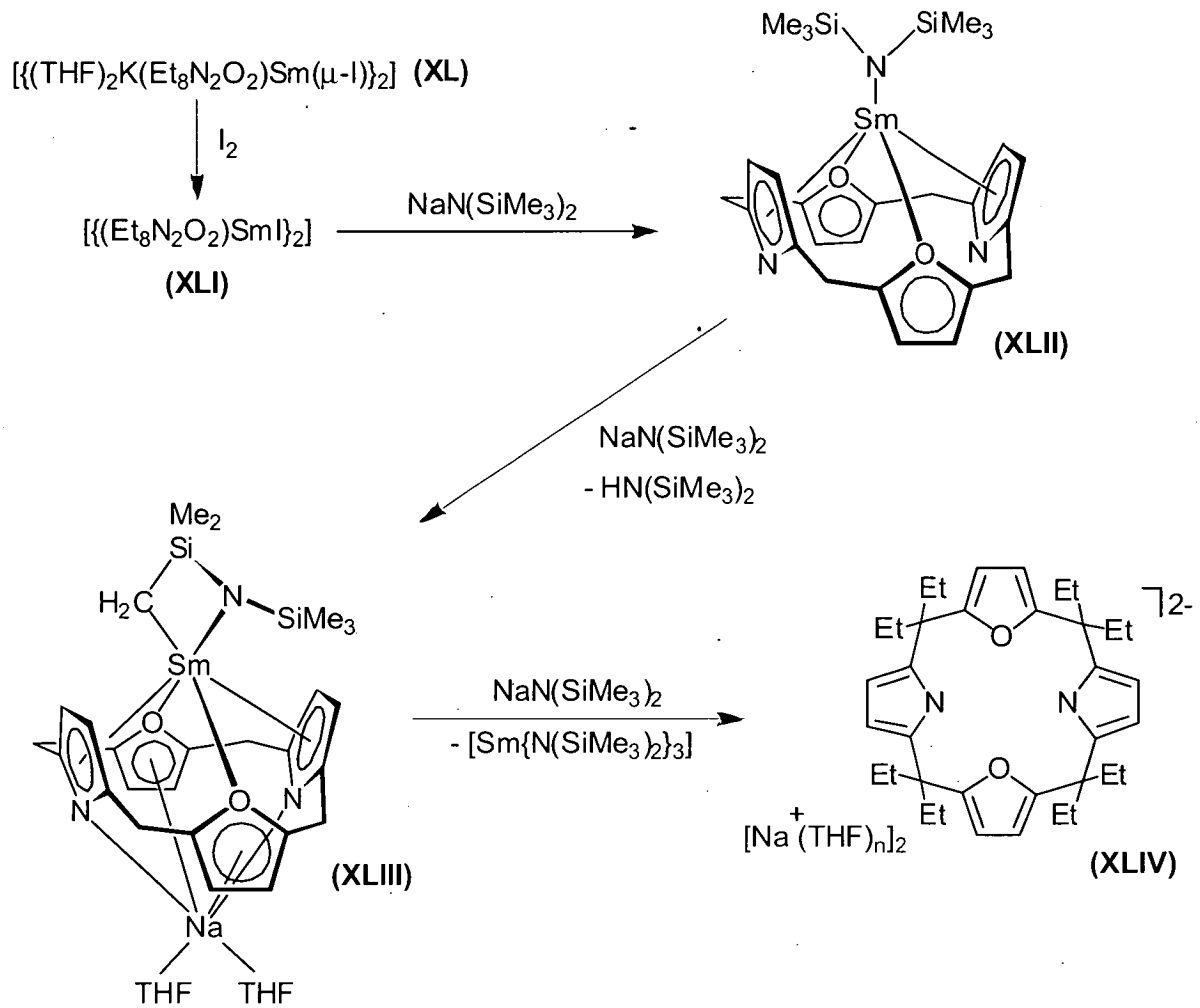

Scheme 10: Synthesis of Sm(III) complexes of $(Et_8N_2O_2)^{2-}$.

Group 1 metal salts of $(Et_8N_2Me_2)^{2-}$ were prepared by deprotonation with *n*-butyllithium, sodium hydride or potassium metal to give $[(Et_8N_4Me_2)Li_2(THF)]$, **(XLV)**, $[(Et_8N_4Me_2)Na_2(THF)_2]$, **(XLVI)**, and $[(Et_8N_4Me_2)K_2(THF)_2]_n$, **(XLVII)**, respectively (Scheme 11).[28,29] The potassium salt **(XLVII)** was structurally authenticated, showing a single potassium cation bound within the cavity, with the usual alternate $\eta^1{:}\eta^5{:}\eta^1{:}\eta^5$ arrangement consisting of η^1-binding to the anionic pyrrolide nitrogens, and η^5-binding to the *N*-methylpyrrolyl rings. The remaining potassium centre is forced to bind *exo*-, thus bridging adjacent macrocycles to form a polymeric chain. The polymeric structure of **(XLVII)** contrasts with monomeric $[(Et_8N_2O_2)K_2(TMEDA)_2]$, **(XXXIX)**, in which a potassium centre is accomodated on each side of the macrocyclic plane.

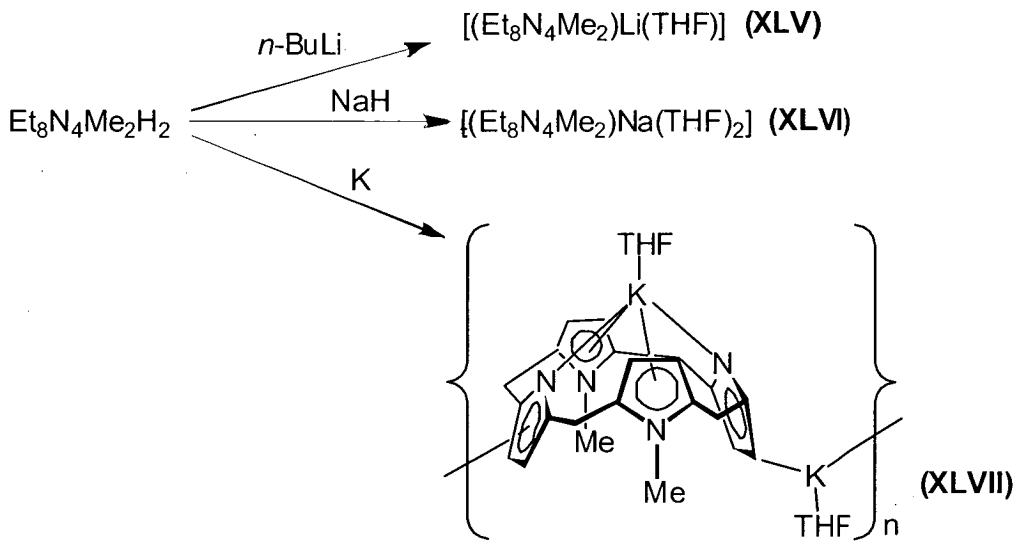

Scheme 11: Synthesis of Group 1 metal salts of $(Et_8N_4Me_2)^{2-}$.

The potassium salt $[(Et_8N_4Me_2)K_2(THF)_2]_n$, **(XLVII)**, was used as a precursor for the synthesis of samarium(II) and ytterbium(II) complexes of $(Et_8N_4Me_2)^{2-}$.[31] Reaction of the potassium salt **(XLVII)** with SmI_2 or YbI_2 in THF gave the monomeric, alkali metal-free lanthanide(II) complexes $[(Et_8N_4Me_2)Sm(THF)_2]$, **(XLVIII)**, and $[(Et_8N_4Me_2)Yb(THF)]$, **(XLIX)**, Scheme 12. The molecular structure of both complexes contain single lanthanide metal centres bound in alternate $\eta^1{:}\eta^5{:}\eta^1{:}\eta^5$ fashion with η^1-binding to the anionic pyrrolide nitrogens and η^5-binding to the *N*-methylpyrrolyl rings. In the case of **(XLVIII)** two THF molecules occupy the binding groove to complete the samarium coordination sphere, whilst the ytterbium(II) centre in **(XLIX)** posesses only one THF molecule. The lesser degree of solvation observed in the ytterbium(II) complex is due to the smaller ytterbium(II) centre residing deeper within the macrocycle, thereby presenting less coordination sphere for solvation at the top of the cavity.

The steric bulk of the macrocycle restricts coordination of auxiliary ligands or solvating molecules to a relatively narrow strip of coordination sphere exposed between the top of the *N*-methylpyrrolide rings, referred to as the "binding groove", as shown in the space filling diagram of complex **(XLVIII)**, Figure 11 (left). On the underside of the macrocycle the lanthanide centre is completely shielded by the two *N*-Me groups, Figurre 11 (right). In addition, steric abuttal between the two opposite *N*-Me groups severely limits the ability of the *N*-methylpyrrolyl rings to tilt back towards the macrocyclic plane

to increase the size of the binding groove. Thus coordination is restricted to the binding groove, the size of which is governed by the rigidity of the macrocyclic framework. The role of this steric restriction in determining the outcome of subsequent reduction chemistry at the binding groove is a recurring theme throughout this thesis.

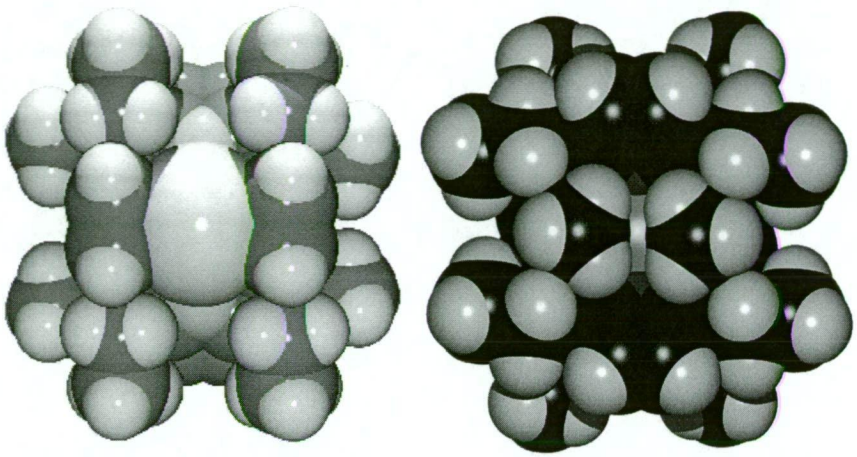

Figure 11: Space-filling representation of the top (binding groove, right) and bottom (left) of complex **(XLVIII)** (THF molecules omitted for clarity).

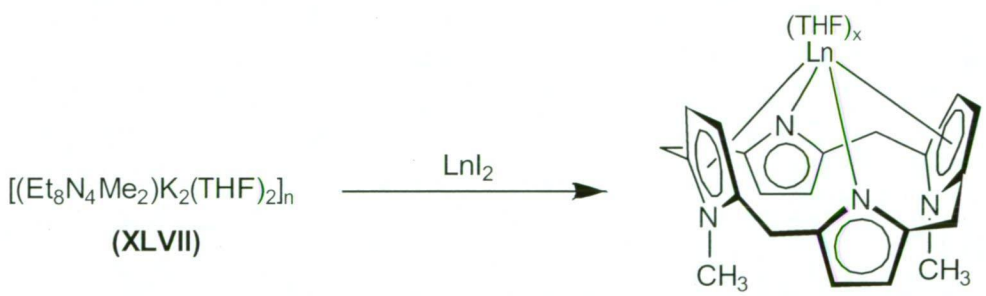

Scheme 12: Synthesis of Sm(II) and Yb(II) complexes of $(Et_8N_4Me_2)^{2-}$.

The samarium(III) halides $[(Et_8N_4Me_2)SmI]$, **(L)**, $[\{(Et_8N_4Me_2)SmBr\}_2]$, **(LI)**, and $[\{(Et_8N_4Me_2)SmCl\}_2]$, **(LII)**, were prepared *via* oxidation of the samarium(II) precursor **(XLVIII)**, Scheme 13.[29,32] The iodide was structurally authenticated as a monomeric complex, whilst the bromide and chloride were structurally authenticated as the dimers. Their molecular structures show a single samarium centre bound inside each macrocyclic cavity in an alternate $\eta^1:\eta^5:\eta^1:\eta^5$ fashion, with no species bound to the sterically hindered underside.

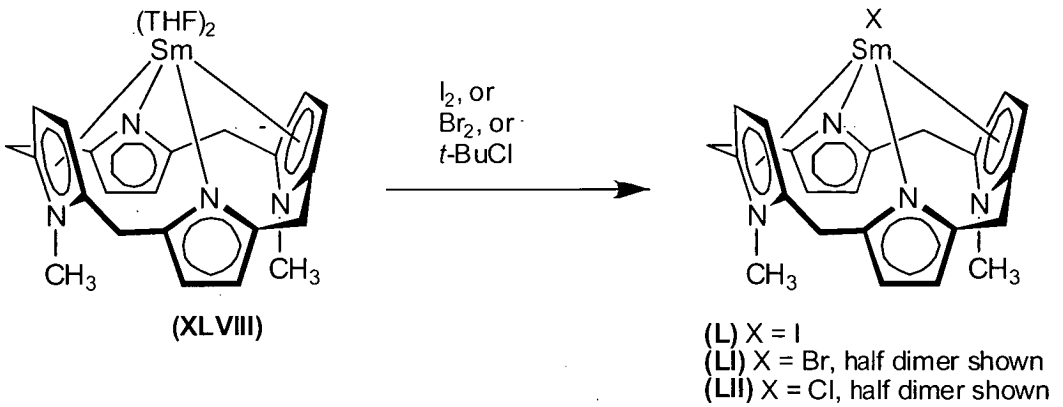

(XLVIII)

(L) X = I
(LI) X = Br, half dimer shown
(LII) X = Cl, half dimer shown

Scheme 13: Synthesis of $(Et_8N_4Me_2)Sm(III)$ halides.

The chloride complex **(LII)** has been used in the synthesis of other samarium(III) complexes *via* metathesis reactions, Scheme 14. The samarium(III) methyl derivative $[(Et_8N_4Me_2)SmMe]$, **(LIII)**, and the (trimethylsilyl)methyl derivative $[(Et_8N_4Me_2)SmCH_2SiMe_3]$, **(LIV)**, were prepared by reaction of **(LII)** with methyllithium and (trimethylsilyl)methyl sodium, respectively.[33] Each of the alkyl complexes are monomeric, with a single samarium centre bound within the macrocycle cavity in alternate $\eta^1:\eta^5:\eta^1:\eta^5$ fashion. The samarium centres are unsolvated and only bound to the alkyl ligands at the binding groove, highlighting the steric restrictions placed upon the metal centre by the bulky porphyrinogen skeleton. The alkali metal and halide-free nature of the complexes can be attributed to the lack of Lewis base donors and dianionicity of the ligand.

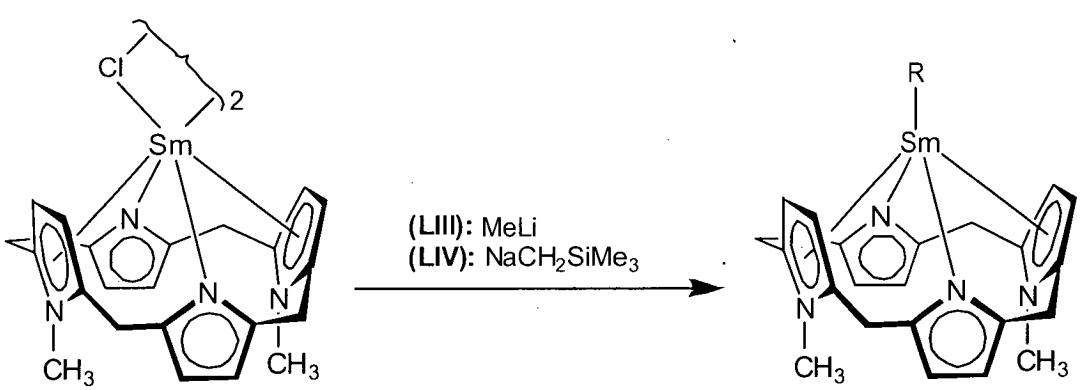

(LII)

(LIII) R = Me
(LIV) R = CH_2SiMe_3

Scheme 14: Synthesis of Sm(III) alkyl complexes.

1.6 References

1. Chemistry of the elements, N.W. Greenwood and A. Earnshaw, Pergamon Press, 1984.

2. Shorter Oxford english dictionary, Oxford Press, 3rd edition, 1944.

3. L.R. Morss, *Chem. Rev.*, 1976, **76**, 827.

4. Chemistry of the f-Block elements, H. C. Aspinall, Gordon and Breach, 2001.

5. G. Wilkinson, J.M. Birmingham, *J. Am. Chem. Soc.,* 1954, **76**, 6210.

6. **a**. G. Wilkinson, J.M. Birmingham, *J. Am. Chem. Soc.*, 1954, **76**, 6210.
b. W.J. Evans, I. Bloom, W.E. Hunter, J.L. Atwood,
J. Am. Chem. Soc., 1981, **103**, 6507.
c. W.J. Evans, R.A. Keyer, J.W. Ziller, *J. Organomet. Chem.*, 1990, **394**, 87.
d. S.D. Stults, R.A. Anderson, A. Zalkin, *Organometallics*, 1990, **9**, 115.
e. W.A. Herrmann, R. Anwander, F. Munck, W. Scherer,
Chem. Ber., 1993, **126**, 331.
f. G. Jeske, L.E. Schock, P.N. Swepston, H. Schumann, T. J. Marks,
J. Am. Chem. Soc., 1985, **107**, 8103.

7. **a**. R.G. Hayes, J.L. Thomas, *J. Am. Chem. Soc.*, 1969, **91**, 6876.
b. A.L. Wayda, I. Mukerji, J.L. Dye, R.D. Rogers,
Organometallics, 1987, **6**, 1328.
c. S.R. Ely, T.E. Hopkins, C.W. DeKock, *J. Am. Chem. Soc.*, 1976, **98**, 1624.
d. W.J. Evans, G.W. Nyce, J.W. Ziller, *Angew. Chem. Int. Ed.*, 1994, **39**, 240.
e.I. Bach, K.-R. Pörschke, B. Proft, R. Goddard, C. Kopiske, C. Krüger,
A. Rufińska, K. Seevogel,
J. Am. Chem. Soc., 1997, **119**, 3773.
f. F. Schager, K.-J. Haack, R. Mynott, A. Rufińska, K.-R. Pörschke,
Organometallics, 1998, **17**, 807.
g. F. Mares, K. Hodgson, A. Streitwieser, *J. Organomet. Chem.*, 1970, **24**, C68.
h. K.O. Hodgson, K.N. Raymond, *Inorg. Chem.*, 1972, **11**, 3030.

i. U. Kilimann, F.T. Edelmann, *J. Organomet. Chem.*, 1994, **469**, C5.

j. U. Kilimann, F.T. Edelmann, *J. Organomet. Chem.*, 1993, **444**, C15.

k. U. Reissmann, P. Poremba, M. Noltemeyer, H.-G. Schmidt, F.T. Edelmann, *Inorg. Chim. Acta*, 2000, **303**, 156.

l. H. Schumann, J. Winterfeld, H. Hemling, F.E. Hahn, P. Reich, K.-W. Brzezinka, F.T. Edelmann, U. Kilimann, M. Schäfer, R. Herbst-Irmer, *Chem. Ber.*, 1995, **128**, 395.

m. P. Poremba, F.T. Edelmann, *J. Organomet. Chem.*, 1997, **549**, 101.

n. P.W. Roesky, *J. Organomet. Chem.*, 2001, **621**, 277.

o. P.W. Roesky, *Eu. J. Inorg. Chem.*, 2001, **7**, 1653.

p. T.G. Wetzel, P.W. Roesky, *Organometallics*, 1998, **17**, 4009.

q. T.G. Wetzel, S. Dehnen, P.W. Roesky, *Organometallics*, 1999, **18**, 3835.

r. W.J. Evans, S.L. Gonzales, J.W. Ziller, *J. Am. Chem. Soc.*, 1991, **113**, 7423.

8. M. Ganesan, C.D. Berube, S. Gambarotta, G.P.A. Yap, *Organometallics*, 2002, **21**, 1707.

9. H. Schumann, E.C.E. Rosenthal, J. Winterfeld, G. Kociok-Kohn, *J. Organomet. Chem.*, 1995, **495**, C12.

10. H. Schumann, E.C.E. Rosenthal, J. Winterfeld, R. Weimann, J. Demtschuk, *J. Organomet. Chem.*, 1996, **507**, 287.

11. M. Westerhausen, M. Wieneke, H. Nöth, T. Seifert, A. Pfitzner, W. Schwarz, O. Schwarz, J. Weidlein, *Eur. J. Inorg. Chem.*, 1998, 1175.

12. H.-D. Hausen, J. Tödtmann, J. Weidlein, *J. Organomet. Chem.*, 1994, **466**, C1.

13. M. Ganesan, S. Gambarotta, G.P.A. Yap, *Angew. Chem. Int. Ed.*, 2001, **40**, 766.

14. T. Dubé, S. Conoci, S. Gambarotta, G.P.A. Yap, G. Vasapollo, *Angew. Chem. Int. Ed.*, 1999, **38**, 3657.

15. T. Dubé, M. Ganesan, S. Conoci, S. Gambarotta, G.P.A. Yap, *Organometallics*, 2000, **19**, 3716.

16. M. Ganesan, M.P. Lalonde, S. Gambarotta, G.P.A. Yap, *Organometallics*, 2001, **20**, 2443.

17. J.-I. Song, S. Gambarotta, *Angew. Chem. Int. Ed. Engl.*, 1995, **34**, 2141.

18. T. Dubé, S. Gambarotta, G.P.A. Yap, *Angew. Chem. Int. Ed.*, 1999, **38**, 1432.

19. T. Dubé, S. Gambarotta, G.P.A. Yap, *Organometallics*, 2000, **19**, 817.

20. T. Dubé, S. Gambarotta, G. Yap, *Organometallics,* 2000, **19**, 121.

21. J. Jubb, S. Gambarotta, *J. Am. Chem. Soc.*, 1994, **116**, 4477.

22. J. Guan, T. Dubé, S. Gambarotta, G.P.A. Yap, *Organometallics*, 2000, **19**, 4820.

23. E. Campazzi, E. Solari, R. Scopelliti, C. Floriani, *Inorg. Chem.*, 1999, **38**, 6240.

24. E. Campazzi, E. Solari, C. Floriani, R. Scopelliti, *Chem. Commun.*, 1998, 2603.

25. E. Campazzi, E. Solari, R. Scopelliti, C. Floriani, *Chem. Commun.*, 1999, 1617.

26. **a**. Y.S. Jang, H.J. Kim, P.H. Lee, C.H. Lee, *Tetrahedron Letters*, 2000, **41**, 2919.
b. R. Crescenzi, E. Solari, C. Floriani, A. Chiesi-Villa, C. Rizzoli, *Inorg. Chem.*, 1996, **35**, 2413.

27. Y. Furusho, H. Kawasaki, S. Nakanishi, T. Aida, T. Takata, *Tetrahedron Letters*, 1998, **39**, 3537.

28. J. Wang, M.G. Gardiner, E.J. Peacock, B.W. Skelton, A.H. White, *Dalton Trans.*, 2003, 161.

29. J. Wang, Ph.D. Thesis, University of Tasmania, 2003.

30. J. Wang, M.G. Gardiner, *Chem. Commun.*, 2005, 1589.

31. **a**. Ref: J. Wang, A.K.J. Dick, M.G. Gardiner, B.F. Yates, E.J. Peacock, B.W. Skelton, A.H. White, *Eur. J. Inorg. Chem.*, 2004, 1992.
b. S. Powanusorn, M.Appl.Sci. Thesis, University of Tasmania, 2004.

32. J. Wang, Unpublished results, University of Tasmania, 2003.

33. J. Wang, M.G. Gardiner, *Organometallics*, 2005, **24**, 815.

Chapter 2

Synthesis of Modified Porphyrinogens

2.1 Introduction

The condensation of four equivalents of pyrrole with four equivalents of ketone in an alcohol solvent to give the symmetrical, unmodified porphyrinogen, **(I)**, was first reported by Baeyer in 1886, Equation 1.[1] Yields of *meso*-octaalkylporphyrinogen are typically good, for example *meso*-octamethylporphyrinogen is obtained in 88 % yield by the methanesulfonic acid catalysed reaction of pyrrole with acetone.[2]

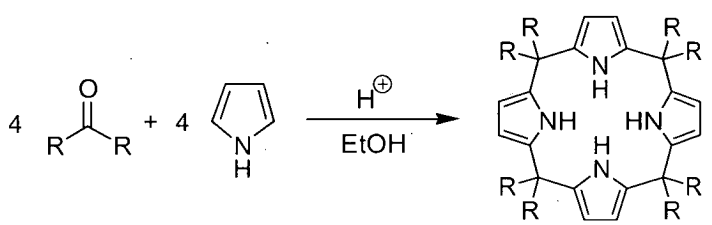

(I)

Equation 1

The term "modified porphyrinogen" refers to a functionalised version of the basic porphyrinogen skeleton **(I)**. An existing porphyrinogen skeleton can be modified by substitution at the pyrrole β-carbons ("*C*-rim" modification), pyrrole nitrogens ("*N*-rim" modification), or at the *meso*-carbons. Further, a modified porphyrinogen can be prepared by the synthesis of the porphyrinogen skeleton using functionalised reagents. The latter approach includes stepwise procedures, where the final modified porphyrinogen is built up by a number of individual reactions. Examples of each type are reviewed below.

Pyrroles bearing β-substituents have been condensed with ketones to give *C*-rim modified porphyrinogens. For example, the condensation of 3,4-dimethoxypyrrole with cyclohexanone gave β-octamethoxy-*meso*-tetraspirocyclohexylporphyrinogen, **(II)**, in a yield of 8 % after chromatographic separation, Equation 2.[3]

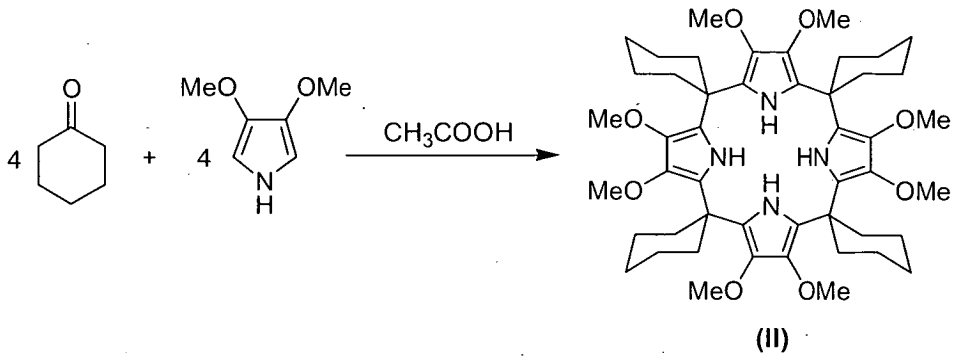

Equation 2

C-rim modification of an existing porphyrinogen skeleton was reported[3] by reaction of *meso*-octamethylcalix[4]pyrrole with 4 equivalents of *n*-butyllithium in THF at -78 °C followed by 4 equivalents of ethyl bromoacetate (Equation 3). The reaction produced the mono-β-alkylated product ((**III**), 26 %) in addition to a di-β-alkylated product ((**IV**), 3 %) upon hydrolytic workup.

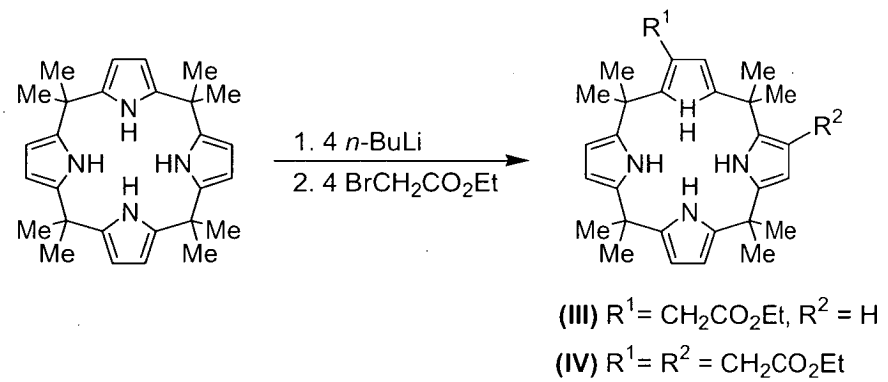

Equation 3

Related to *C*-rim modification is the synthesis of calix[1]pyridino[3]pyrrole derivative (**V**) *via* a ring expansion reaction. Macrocycle (**V**) was obtained in 45 % yield on treating a 1,2-dimethoxyethane solution of calix[4]pyrrole with 15 equivalents of sodium trichloroacetate (Equation 4).[4] The trichloroacetate salt acts as an *in situ* source of dichlorocarbene ($:CCl_2$), the insertion of which into a pyrrole ring gives the product after elimination of HCl and rearrangement. As a result of multiple dichlorocarbene insertions, (**V**) was accompanied by a mixture of di- tri- and tetra-pyridine containing macrocycles.

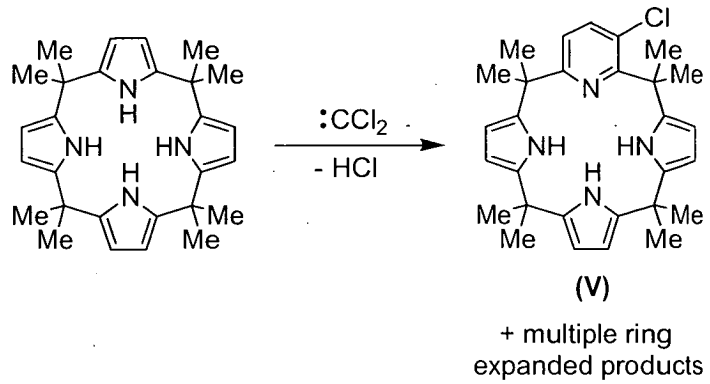

Equation 4

A phenylene-containing modified porphyrinogen, *trans*-calix[2]benzene[2]pyrrole, **(VI)**, was prepared by condensation of pyrrole with α,α,α',α'-tetramethylbenzene-1,3-dimethanol in acetonitrile using $BF_3.OEt_2$ catalyst.[5] The yield was 16 % after chromatographic separation. Functionalisation of **(VI)** was carried out by treatment with sodium trichloroacetate to give the chloropyridine-containing *trans*-calix[2]benzene[1]-3-chloropyridine[1]pyrrole, **(VII)**, in a 36 % yield from **(VI)**, (Scheme 1).

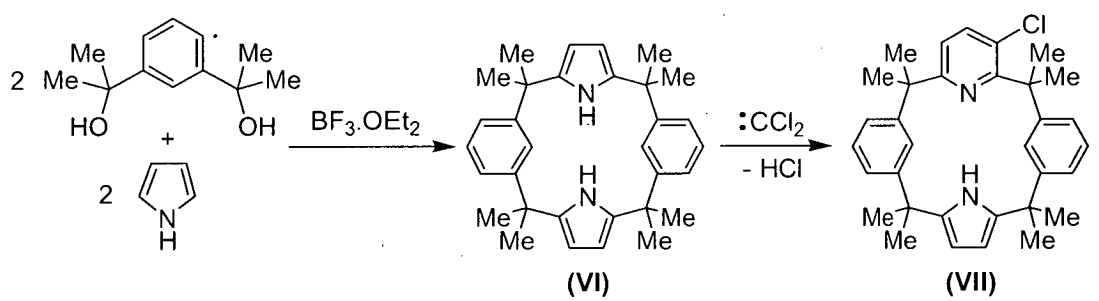

Scheme 1: Synthesis of *trans*-calix[2]benzene[2]pyrrole using functionalised reagents followed by *C*-rim modification.

A functionalised porphyrinogen **(VIII)** containing *meso*-aryl substituents was prepared by the methanesulfonic acid catalysed condensation of equimolar amounts of 4-hydroxyacetophenone and pyrrole in methanol, Equation 5. The product was obtained as three chromatographically separable products, each bearing different conformations: full cone (42 % yield), partial cone (12 % yield) and 1,2-alternate (6 %). The full cone conformer displays *meso*-aryl substituents lying exclusively on one face of the macrocycle. This opened up the possiblity of discrimination between the faces of the

macrocycle in subsequent binding studies. Figure 1 shows the *meso*-groups of the full cone conformer directing the binding of four dimethylformamide molecules to one face of the macrocycle.[6]

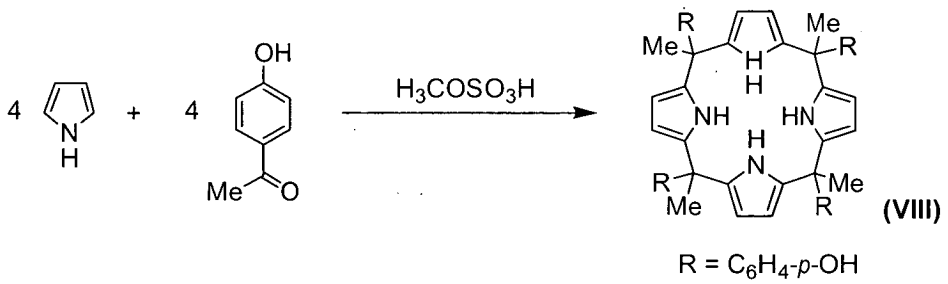

Equation 5

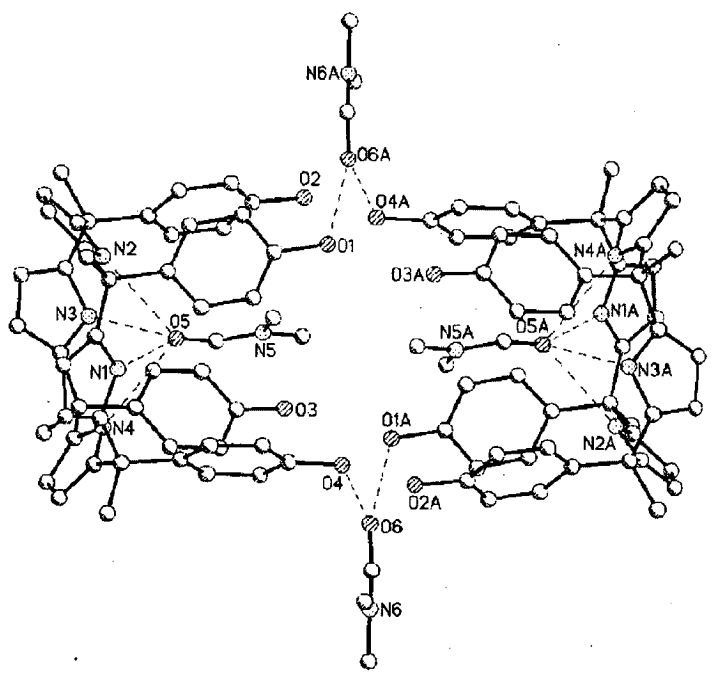

Figure 1: Porphyrinogen **(VIII)** with *exo*- and *endo*-bound dimethylformamide.[6]

The choice of ketone in the general porphyrinogen synthesis determines the *meso*-substituents present in the final porphyrinogen (Equation 1). Preparation of the mono-*meso*-functionalised porphyrinogen **(IX)** was achieved by reaction of pyrrole with a mixture of cyclohexanone and methyl 4-acetylbutyrate (Equation 6).[7] Porphyrinogen **(IX)** was obtained in 12 % yield after the chromatographic separation of di-, tri- and tetra-*meso*-substituted products. Subsequent hydrolysis of the ester functionality gave a carboxylic acid which was used in molecular self-assembly investigations.

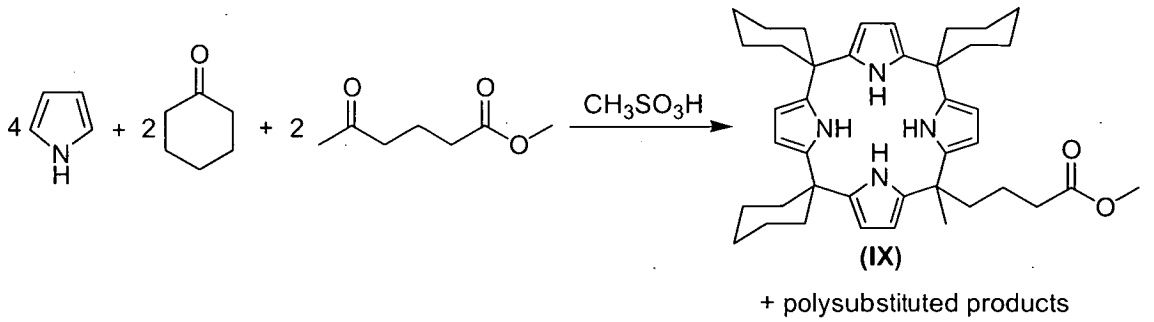

Equation 6

N-rim modification of a porphyrinogen was reported in 1998 by Takata *et al.*[8] Deprotonation of *meso*-octaethylporphyrinogen with 4 equivalents of sodium hydride in the presence of 4 equivalents of 18-crown-6 was followed by the addition of methyl iodide to give a statistical distribution of mono-, di-, tri- and tetra-*N*-methylated isomers, **(X)**, Scheme 2. The distribution of isomers was determined by the ratio of methyl iodide to deprotonated porphyrinogen, more equivalents of methyl iodide favouring formation of the highly substituted products. Takata found that 2 equivalents of methyl iodide per 1 equivalent of tetradeprotonated porphyrinogen gave a product distribution of 22 % *N,N',N'',N'''*-tetramethylated, 23 % *N,N',N''*-trimethylated, 37 % *trans-N,N'*-dimethylated, 0.8 % *cis-N,N'*-dimethylated and 0.6 % *N*-methylated porphyrinogen (17 % of unreacted porphyrinogen recovered). The two dimethylated isomers are differentiated by the position of the *N*-methylpyrroles within the macrocycle; *cis*: $R^1 = R^2$ = Me, *trans*: $R^1 = R^3$ = Me, Scheme 2. Earlier work by our research group found the yield of *trans-N,N'*-dimethyl-*meso*-octaethylporphyrinogen was increased to 56 % by using 2.5 equivalents of methyl iodide.[9] The preparation of doubly deprotonated *trans-N,N'*-dimethyl-*meso*-octaethylporphyrinogen lanthanide(II) and (III) complexes and their subsequent chemistry is covered in later chapters of this thesis.

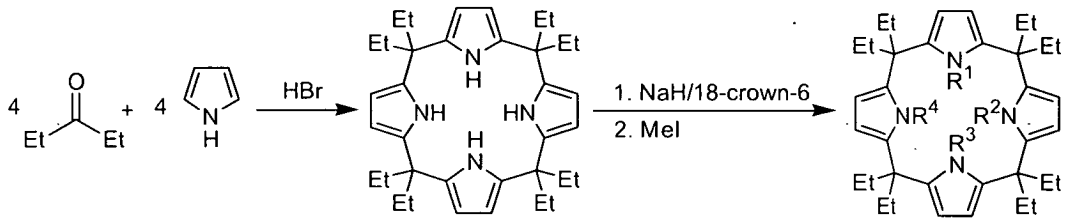

(X)

R^1 = Me, R^2 = R^3 = R^4 = H;
R^1 = R^2 = Me, R^3 = R^4 = H;
R^1 = R^3 = Me, R^2 = R^4 = H;
R^1 = R^2 = R^3 = Me, R^4 = H;
R^1 = R^2 = R^3 = R^4 = Me.

Scheme 2: *N*-rim modification of $Et_8N_4H_4$.

Attempts to effect *N*-substitution in the absence of 18-crown-6 were not successful, resulting in complicated mixtures of β-methylated isomers regardless of the deprotonating agent used.[8] *n*-Butyllithium, sodium hydride, potassium hydride and potassium metal were trialled but failed to give *N*-substituted products in the absence of the crown ether (*cf.* β-carbon functionalisation of a tetradeprotonated intermediate in the absence of crown ether, Equation 3). The preference for *N*-rim methylation in the presence of 18-crown-6 was attributed by the authors to sequestration of the Group 1 metal cations by the crown ether, thus breaking up the ion-pair existing between the deprotonated pyrrole nitrogens and their Group 1 metal counterions to allow reaction with the methyl electrophile. The electrophile was found to influence reaction outcome, with ethyl iodide forming the monosubstituted *N*-ethyl-*meso*-octaethylporphyrinogen as the sole product, even in the presence of excess iodide.

Functionalisation of *N*-rim, *C*-rim and *meso*-positions can, in principle, be effected selectively by a stepwise approach, incorporating discrete units into a linear chain and cyclising to afford the target macrocycle. Such a procedure was exploited in the first synthesis of the bis(furanyl), **(XI)**, and bis(thiophenyl), **(XII)**, functionalised porphyrinogens, Scheme 3.[10] The final porphyrinogens were obtained in overall yields of 29 % from furan (X = O), and 15 % from thiophene (X = S).

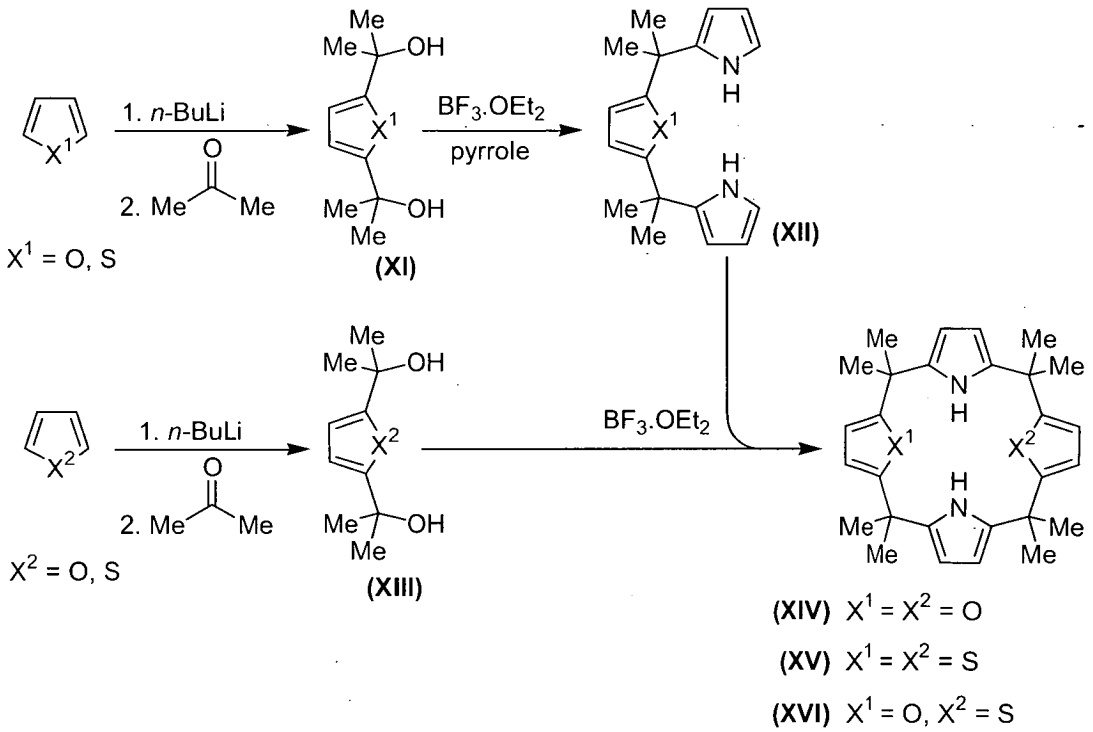

Scheme 3: Stepwise synthesis of furanyl and thiophenyl functionalised porphyrinogens.

The stepwise procedure shown in Scheme 3 allows for a high degree of control over the functionalities present at individual parts of the final molecule. The choice of starting heterocycle determines the final *N*-rim functionality whilst the starting ketone determines the final *meso*-substituents. *C*-rim functionalisation might also be possible by the incorporation of β-substituents into the starting heterocycle and/or pyrrole. Use of a suitably functionalised dialcohol, **(XIII)**, in the final "3+1" cyclisation step allows inclusion of a functionality on a single heterocyclic ring at the N-rim or C-rim. The use of a furanyl dialcohol **(XI)** (X^1 = O), and dialcohol **(XIII)** bearing a sulfur heteroatom (X^2 = S) allowed the asymmetric porphyrinogen **(XVI)** to be prepared in an overall yield of 20 % from furan.

2.2 Research aim

We wished to exploit the advantages of a stepwise approach in the synthesis of the new porphyrinogen $Me_8N_4Me_2H_2$, **(3)**, containing *trans-N,N'*-dimethylpyrrolyl and *meso*-octamethyl functionalities. This target molecule was chosen as it is a close analogue of the well-studied *trans-N,N'*-dimethyl-*meso*-octaethylporphyrinogen. Demonstration of a stepwise procedure would also conceivably allow the synthesis of

new, mono-functionalised porphyrinogens to be considered for future lanthanide coordination studies. Such mono-functionalisation might include a "tether" at a *N*-methylpyrrolyl 3-position bearing an alkene or other Lewis basic functionality capable of reversibly binding to the lanthanide metal centre to provide a further means of controlling access to the metal centre and possibly influencing the outcome of subsequent reactions.

2.3 Results and discussion

2.3.1 Synthesis of *trans*-*N*,*N*-dimethyl-*meso*-octamethylporphyrinogen, (3)

The proposed synthetic pathway for the synthesis of modified porphyrinogen $Me_8N_4Me_2H_2$, **(3)**, is shown in Scheme 4.

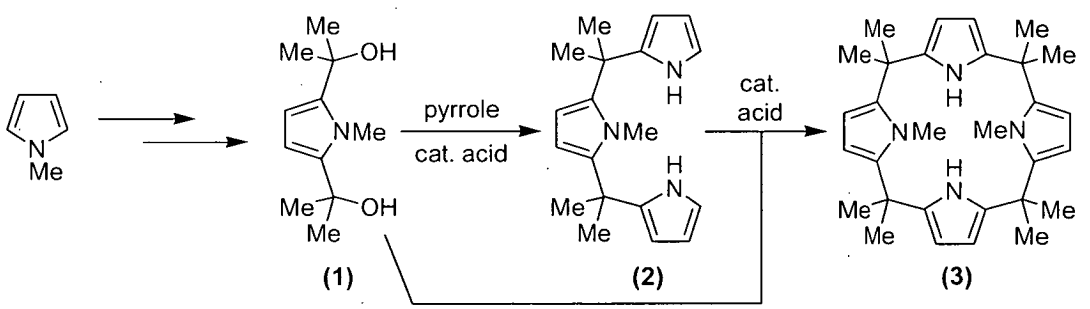

Scheme 4: Proposed synthesis of *trans*-*N*,*N*'-dimethyl-*meso*-octamethylporphyrinogen *via* convergent "3+1" procedure.

The initial dilithiation conditions were chosen according to the results of investigations into the lithiation of 1-methylpyrrole by Chadwick.[11] Using 4.5 equivalents of *n*-butyllithium in the presence of 4.5 equivalents of TMEDA Chadwick obtained a 90 % yield of 2,5-dilithio-1-methylpyrrole. TMEDA increases the efficacy of the lithiation reagent by coordinating to lithium centres and reducing the aggregated state of *n*-butyllithium as well as increasing the nucleophilicity of the alkyl carbon centre by donating electron density through the lithium centre. The same researchers undertook a comparative reaction using no TMEDA under otherwise identical conditions, which produced 2,5-dilithio-1-methylpyrrole in 1.1 % yield, in addition to 1.5 % of other mono- and di-lithiated isomers.

Using the published conditions, 1-methylpyrrole in hexane solution was refluxed for 1 h with 4.5 equivalents of *n*-butyllithium in the presence of 4.5 equivalents of TMEDA. The entire reaction mixture was added to an excess of dried acetone without isolation of the 2,5-dilithiated intermediate, **(4)**, followed by hydrolytic workup (Scheme 5).

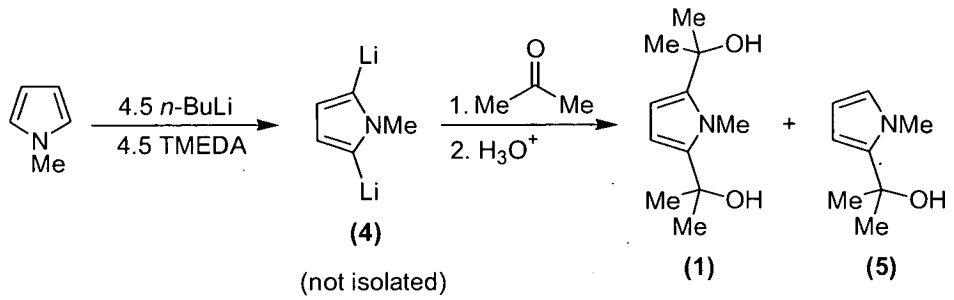

Scheme 5: Lithiation of 1-methylpyrrole with *n*-butyllithium, reaction with acetone.

Analysis of the crude product by ^{1}H NMR spectroscopy showed it to consist of the desired 1-methyl-2,5-bis(1,1'-dimethylhydroxymethyl)pyrrole **(1)** (10 % yield) accompanied by a larger amount of monosubstituted 1-methyl-2-hydroxydimethylmethylpyrrole **(5)** (24 % yield). No other mono- or di-substituted isomers were observed in the ^{1}H NMR spectrum of the crude product. Both **(1)** and **(5)** were analysed by ^{1}H, ^{13}C, gHMQC and gHMBC NMR spectroscopy, and returned satisfactory microanalyses. Crystals of **(1)**, Figure 2, suitable for X-ray structure determination were obtained from a hot hexane/acetone solution (20:1 v/v), and crystals of **(5)**, Figure 3, were obtained by vacuum sublimation (3 h at 65 °C / 1 x 10^{-2} mmHg).

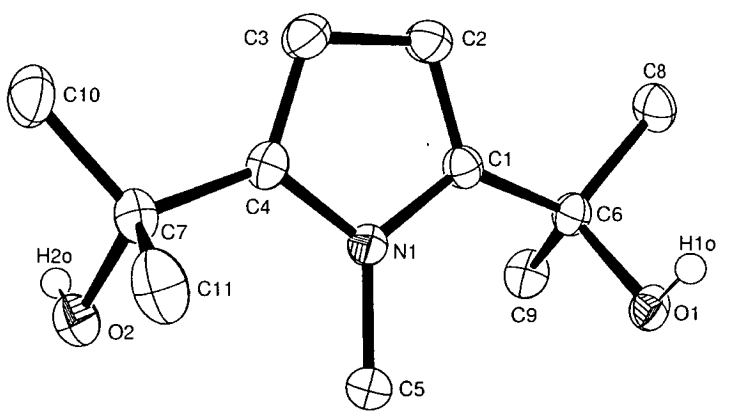

Figure 2: Molecular structure of 1-methyl-2,5-bis(1,1'-dimethylhydroxymethyl)pyrrole, **(1)**, with thermal ellipsoids drawn at the level of 50 % probability (protons removed for clarity, except OH).

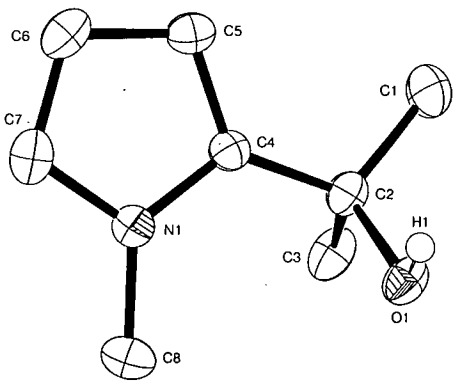

Figure 3: Molecular structure of 1-methyl-2-hydroxydimethylmethylpyrrole **(5)**, with thermal ellipsoids drawn at the level of 50 % probability (protons removed for clarity, except OH).

Both **(1)** and **(5)** display hydrogen bonding between alcohol groups in the solid state resulting in hexameric units. Hexameric hydrogen bonded assemblies have been structurally authenticated in the solid state in methanol units bound to a Ga complex [Ref: F.N. Penkert, T. Weyhermüller, K. Wieghardt, *Chem. Commun.*, 1998, 557.] and also in a functionalised benzyl alcohol.[12] Hexameric clusters have also been postulated to be the dominant species present in liquid methanol at room temperaure, in contrast to the molecular structure (-110 °C) of solid methanol which consists of infinite zigzag chains.[13] The solid state molecular structure of the monoalcohol **(5)** shows 6 molecules arranged *via* alternate O-H and H···O bonds into a 12-membered ring which adopts a pseudo-chair conformation, Figure 3.

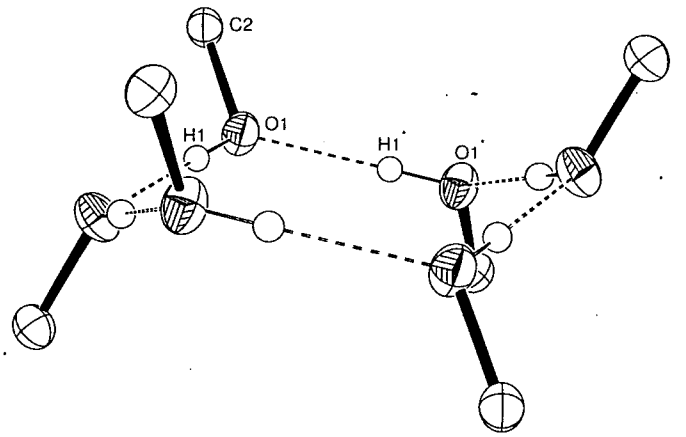

Figure 4: Detail of the molecular structure of 1-methyl-2-hydroxydimethylmethylpyrrole **(5)**, showing the hexameric hydrogen bonded unit with thermal ellipsoids drawn at the level of 50 % probability.

Dialcohol **(1)** forms an approximately planar hexamer though one of the -OH groups, (O1), Figure 5, whilst the second -OH group participates in a 3-fold helical structure, (O2), Figure 6, perpendicular to the plane of the (O1) hexamer. The molecules are thus arranged *via* hydrogen bonds in a three dimensional polymeric lattice, space group *R*-3, Figure 7. The network structure is shown in Figure 8, in which each dialcohol O(1) is modelled in light grey and each O(2) is modelled in dark grey.

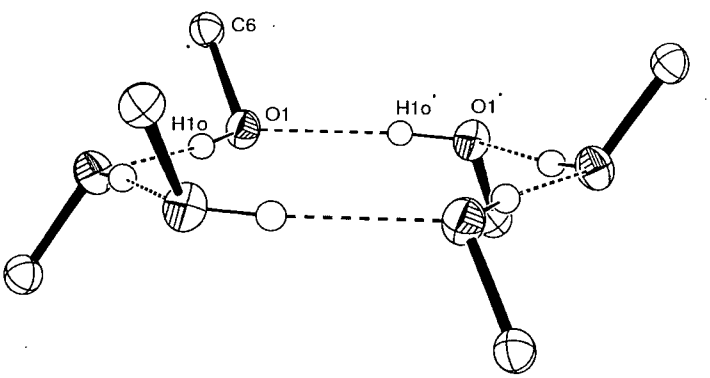

Figure 5: Detail of the molecular structure of 1-methyl-2,5-bis(1,1'-dimethylhydroxymethyl)pyrrole, **(1)**, showing the hexameric hydrogen bonded unit with thermal ellipsoids drawn at the level of 50 % probability.

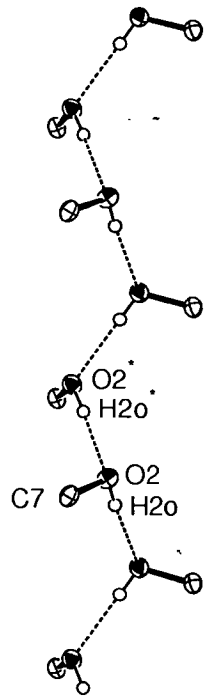

Figure 6: Detail of the molecular structure of 1-methyl-2,5-bis(1,1'-dimethylhydroxymethyl)pyrrole, **(1)**, showing the helical hydrogen bonded unit with thermal ellipsoids drawn at the level of 50 % probability.

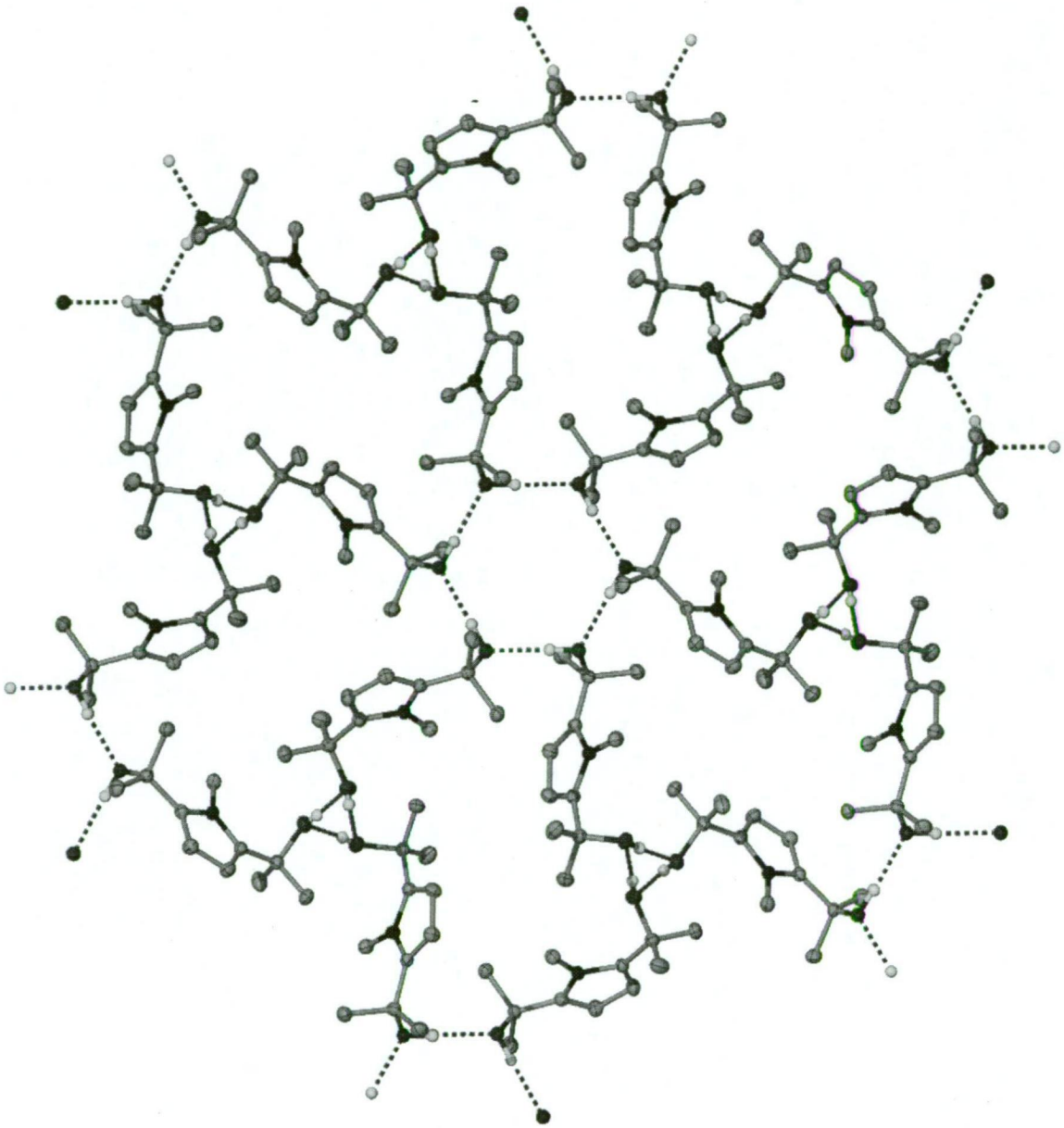

Figure 7: Molecular structure of 1-methyl-2,5-bis(1,1'-dimethylhydroxymethyl)pyrrole, **(1)**, showing hexameric and 3-fold helical hydrogen bonding interactions.

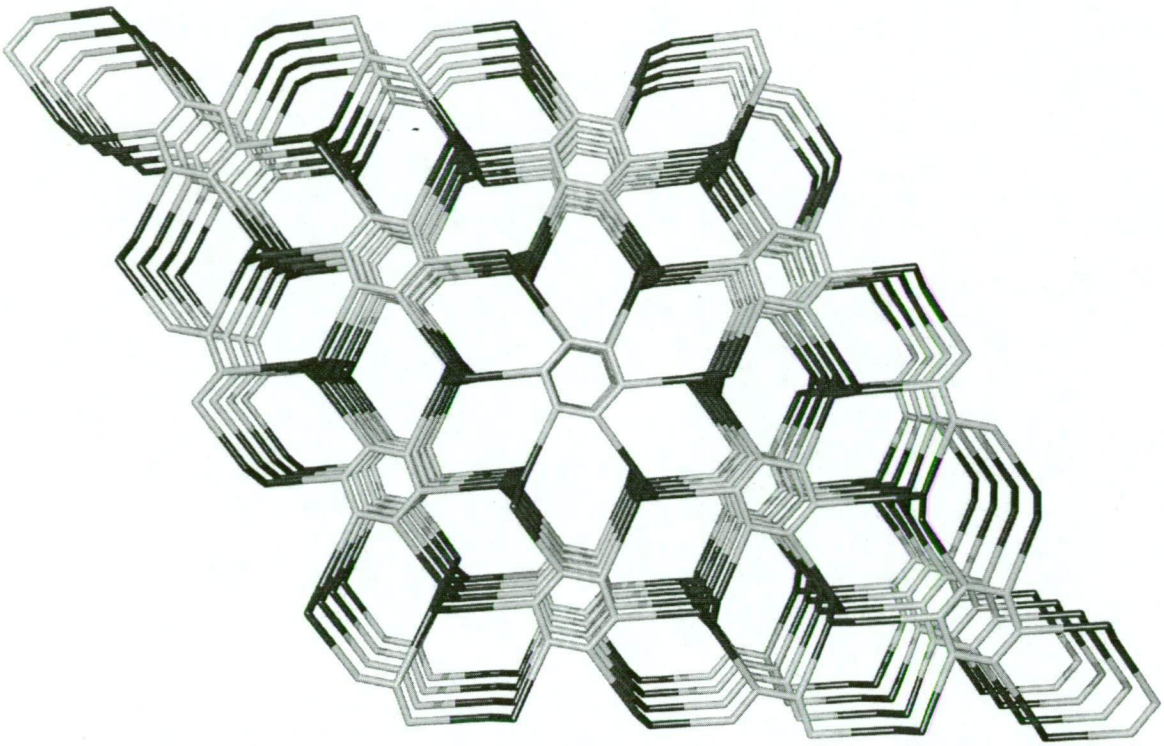

Figure 8: Network structure of 1-methyl-2,5-bis(1,1'-dimethylhydroxymethyl)pyrrole, **(1)**, showing hexameric (O(1), topology 6.8^2, light grey) and 3-fold helical (O(2), topology $8^2.10$, dark grey) hydrogen bonding interactions. Overall the topology of the supramolecular network is $(6.8^2)(8^2.10)$.

Reasons considered for the poor yield of **(1)** and relatively large ratio of **(5)** included the presence of water in solvent or starting material(s), incomplete lithiation of 1-methylpyrrole and/or abstraction of the relatively acidic acetone α-protons by the strongly basic lithiated intermediate.[14] The presence of water was excluded due to the air-sensitive techniques employed. Solvent and reagents were dried immediately prior to distillation and Schlenk techniques employed to prevent subsequent contact with air. Acetone was deaerated and dried by stirring over sequential portions of B_2O_3 whilst TMEDA and hexane were refluxed over sodium wire. *n*-Butyllithium concentration was determined by titration against air- and water-free *t*-butanol (1,10-phenanthroline indicator) immediately before use.

The possibility of incomplete lithiation of 1-methylpyrrole was circumvented by preparing the dilithiated intermediate **(4)** *via* a different route. Bromination of 1-methylpyrrole with 2 equivalents of NBS in THF was reported to give the 2,5-dibromo-1-methylpyrrole, **(6)**, with 99 % regioselectivity and in yields around 90 %

(Equation 7).[15] Halogen-lithium exchange of **(6)** was expected to proceed under mild conditions to afford **(4)** in high yield.

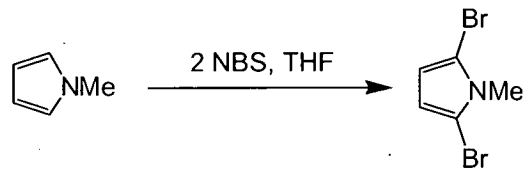

(6)

Equation 7

Dibromination of 1-methylpyrrole was carried out using 2 equivalents of NBS. Consistent results were obtained using recrystallised NBS (colourless platelets from boiling water; after drying *in vacuo* over KOH and storage at -20 °C there was no discolouration after 2 months). The reaction was carried out at -78 °C in THF and allowed to warm to room temperature. The dibromopyrrole was separated from succinimide by-product by removal of THF *in vacuo* and extraction with Et_2O. The resulting Et_2O solution of 2,5-dibromopyrrole was used in subsequent lithiation reactions without further purification. The absence of succinimide byproduct or brominated products other than **(6)** was confirmed by ^1H NMR spectroscopy.

2,5-Dibromo-1-methylpyrrole, **(6)**, is stable as a solution in Et_2O or THF, and as such was stored at -20 °C under air for days without visible decomposition. The solid is stable at -78 °C in air (moist with Et_2O), and at RT under vacuum. In air at RT the solid decomposes within minutes to a black polymeric mass, nearly insoluble in organic solvents and concentrated acids.

Halogen-lithium exchange was attempted by adding a solution of 2,5-dibromo-1-methylpyrrole, **(6)**, in Et_2O to a suspension of excess lithium metal in refluxing Et_2O; however analysis of the reaction mixture by ^1H NMR spectroscopy indicated no reaction had taken place. Instead, halogen-lithium exchange was effected by adding a solution of 2,5-dibromo-1-methylpyrrole **(4)** in Et_2O to excess *n*-BuLi in hexane at -78 °C (Scheme 6). Warming to RT was followed by addition to excess acetone and hydrolysis. ^1H NMR spectra showed the existence of three disubstituted 1-methylpyrrolyl alcohols and a monosubstituted alcohol, the distribution being 61 % 2-monosubstituted **(5)**, 15 % 2,3-disubstituted, 13 % 2,4-disubstituted and 11 % of the desired 2,5-disubstituted

product **(1)**. Analysis by GC showed two new species with retention times close to that of the 2,5-diol, confirming the spectroscopic interpretation.

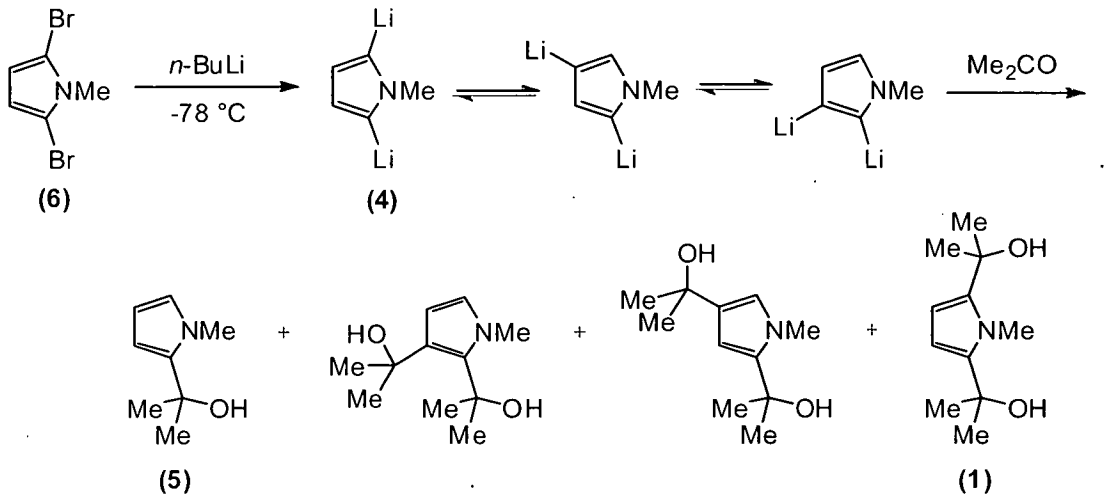

Scheme 6: Lithiation of 1-methylpyrrole *via* 2,5-dibromo-1-methylpyrrole, isomerisation leading to mixture of products upon addition to acetone.

Isomerisation between lithiated pyrroles has been noted in the literature[11] relating to the lithiation of 1-methylpyrrole with excess *n*-BuLi and TMEDA, in which 2,4-dilithio-1-methylpyrrole was formed in addition to the expected 2,5-dilithio-1-methylpyrrole. The mechanism proposed related to the interchange of lithium between various mono- and di-lithiated species. A similar process may be responsible for the isomeric product distribution noted in this halogen exchange reaction.

The presence of monoalcohol in both directly dilithiated (*n*-butyllithium / TMEDA) and indirectly dilithiated (dibromination followed by lithium-halogen exchange) 1-methylpyrrole suggested abstraction of acetone α-protons as a common cause. The acetone carbonyl oxygen of the ketone draws electron density away from the hydrogens α- to the carbonyl group, making them relatively acidic. α-Deprotonation competes with nucleophilic attack at the acetone carbonyl and leads to reduced yields of the desired product, Scheme 7. Single substitution followed by proton exchange is also possible.

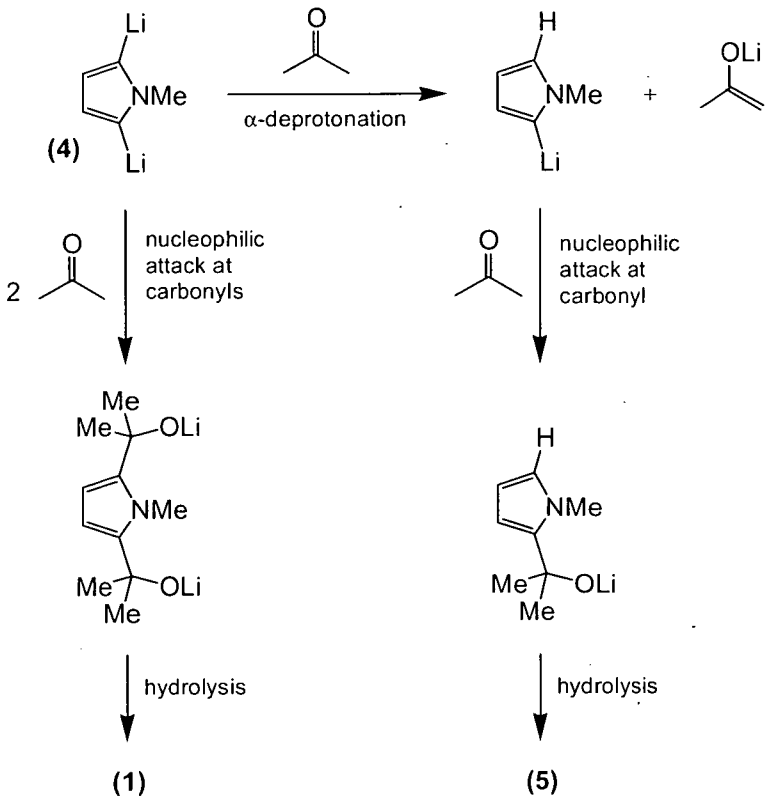

Scheme 7: Competition between acetone proton abstraction and nucleophilic attack.

Abstraction of acetone α-protons by 2,5-dilithiofuran has been investigated previously.[9] The reaction of 2,5-dilithiofuran with acetone-d_6 gave 2-(dimethylhydroxymethyl)-5-deutero-furan-d_6 in *ca.* 50 % yield, in addition to the dialcohol-d_{12}. The incorporation of deuterium in the 5-position of the monoalcohol indicates deuterium abstraction by the strongly basic dilithiated furan and does indeed prove the mechanism for monoalcohol formation in that case.

An alternative, two-step procedure for the preparation of the dialcohol **(1)** was developed to allow the preparation of **(1)** in improved yield over direct addition to a ketone. Dialkyl carbonates contain no hydrogens α- to a carbonyl group and are not enolisable, hence proton abstraction should be a less facile process than in a ketone. An improved yield of dialcohol was secured *via* a diester intermediate, Scheme 8.

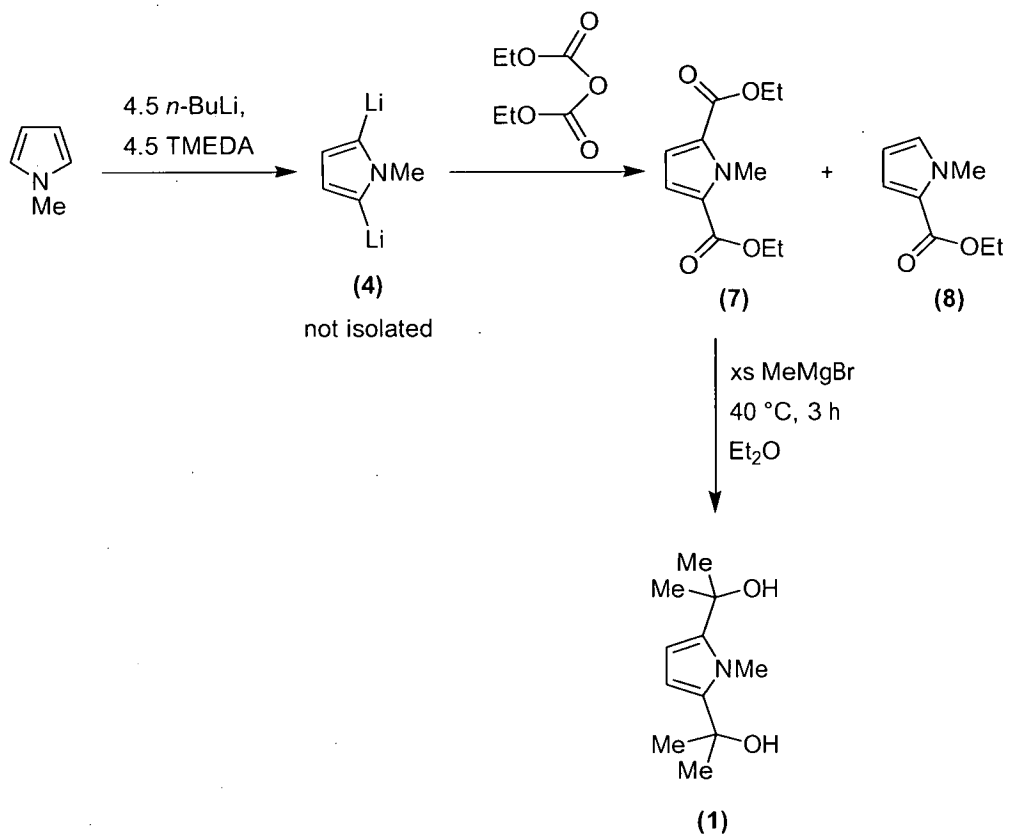

Scheme 8: Synthesis of 1-methyl-2,5-bis(1,1'-dimethylhydroxymethyl)pyrrole *via* diester intermediate.

The dilithiated intermediate **(4)** was prepared *via* deprotonation of 1-methylpyrrole with *n*-butyllithium to avoid the isomerisation observed with the halogen exchange route. 1-methylpyrrole-2,5-dicarboxylic acid diethyl ester **(7)** was prepared by the addition of 2,5-dilithio-1-methylpyrrole, **(4)**, to diethyl carbonate. Diester **(7)** was obtained as a pale yellow crystalline solid in 44 % yield, accompanied by 10 % of the monosubstituted 1-methylpyrrole-2-carboxylic acid ethyl ester, **(8)**, determined by ^{1}H NMR spectroscopy. The monoester was separated by column chromatography (eluent dichloromethane/hexane 60:40), or by fractional vacuum distillation in a Kugelrohr oven (0.04 mmHg, 55 - 70 °C); the yield of monoester was not recorded. Compound **(7)** was characterised by microanalysis, ^{1}H, ^{13}C, gHMQC and gHMBC NMR spectroscopy. The low melting point of **(7)** (*ca.* 30 °C) frustrated efforts to grow crystals suitable for X-ray crystal structure determination. Compound **(8)** was obtained as a fragrant, pale yellow oil, and characterised by ^{1}H NMR spectroscopy alone. The presence of the monoester **(8)** may be due to incomplete dilithiation of the 1-methylpyrrole starting material resulting in the formation of 2-lithio-1-methylpyrrole along with **(4)**.

Diester **(7)** underwent subsequent reaction with excess MeMgI to give the 1-methyl-2,5-bis(1,1'-dimethylhydroxymethyl)pyrrole, **(1)**, in a yield of 93 %. The overall yield of **(1)** based on 1-methylpyrrole was 41 %. Compound **(1)** was purified by recrystallisation from a hot hexane/acetone solution (20:1 v/v), and characterised by ^{1}H, ^{13}C, gHMQC and gHMBC NMR spectroscopy, and microanalysis, in addition to X-ray crystal structure determination (*vide supra*).

The dialcohol **(1)** was expected to undergo an acid-catalysed condensation reaction with excess (40 equivalents per OH) pyrrole to give 1-methyl-2,5-bis{(2'-pyrrolyl)dimethylmethyl}pyrrole **(2)**. $BF_3.OEt_2$ was used as a Lewis acid catalyst in the reaction of the furan analogue of **(3)** with excess pyrrole, Scheme 3.[10] However $BF_3.OEt_2$ was found to react directly with **(1)** to produce a brown mass from which the starting dialcohol could not be recovered upon hydrolysis and extraction. Less reactive Lewis acid catalysts were used in an attempt to avoid the side reactions and/or decomposition encountered with $BF_3.OEt_2$. $HgCl_2$ and $ZnCl_2$ were trialled but failed to catalyse the reaction.

Use of a Brønstead acid was found to effect reaction. 48% hydrobromic acid (150 mol %) in methanol solvent was found to produce **(2)** at temperatures below -20 °C, Scheme 9. After treatment with aqueous Na_2CO_3 and extraction with Et_2O the resulting transparent, brown oil was placed under vacuum (5 h at 20 °C / 1 x 10^{-2} mmHg, then 7 h at 55 °C / 20 mmHg) to ensure complete removal of excess pyrrole. This afforded 1-methyl-2,5-bis{(2'-pyrrolyl)dimethylmethyl}pyrrole, **(2)**, as a brown crystalline mass in a yield of 98 % based on the starting dialcohol **(1)**, or 40 % overall based on 1-methylpyrrole. This compares favourably to the yield of 34 % reported for the published one-pot synthesis of 1-methyl-2,5-bis{(2'-pyrrolyl)diphenylmethyl}pyrrole from the reaction of dilithiated 1-methylpyrrole[16] with benzophenone. (Reaction with the phenyl substituted ketone would be expected to proceed in higher yield due to the lack of acidic α-protons). The brown crystalline product was determined to be free of impurities by ^{1}H NMR spectroscopy and GC analysis, and was used in subsequent reactions without further purification. No investigation was undertaken to determine the reaction outcome using a lesser excess of pyrrole.

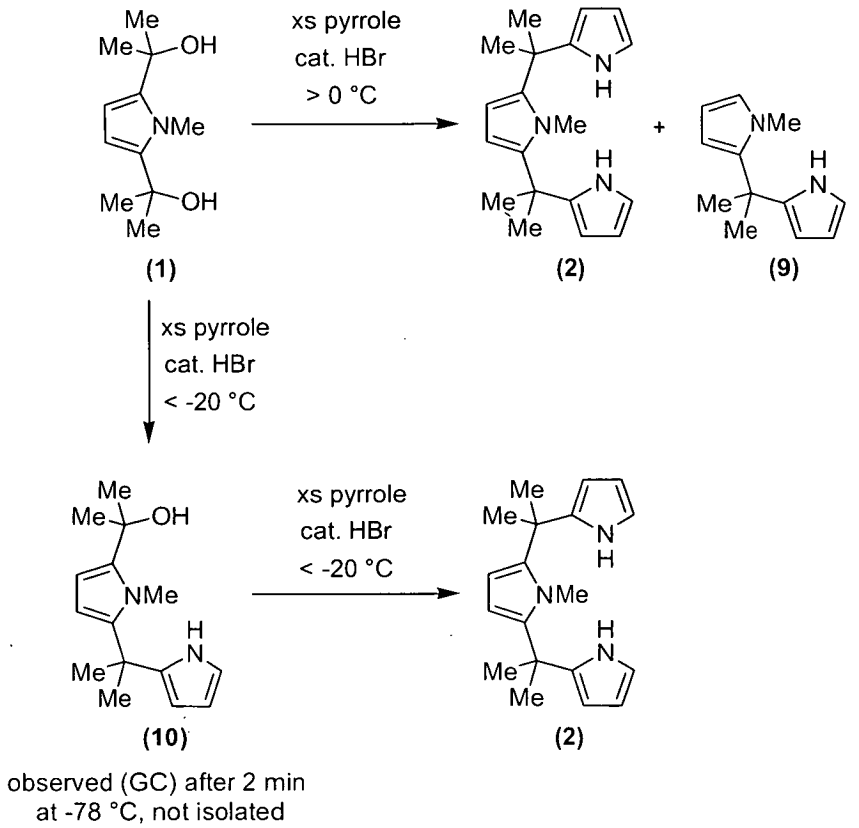

Scheme 9: Temperature dependent reaction of **(1)** with pyrrole.

The product distribution of the reaction was found to be dependent on temperature. Reaction at 0 °C or above resulted in reduced yields of **(2)** and increased production of the side-product dipyrromethane **(9)**, observed by GC/MS. The proportion of **(2)** fell to 0 % at reaction temperatures above 60 °C.

At temperatures below -20 °C the reaction required more time to reach completion. GC analysis of a reaction at -78 °C for 1 min showed 57 % of **(2)** in addition to 35 % of the starting dialcohol **(1)** and 18 % of a product with an intermediate retention time, presumed to be the singly-substituted intermediate **(10)**. Complete conversion of **(1)** to **(2)** was achieved after 2 minutes at -20 °C and 30 min at -78 °C. Compound **(2)** returned satisfactory microanalysis, and was also analysed by ^{1}H, ^{13}C, gCOSY, gHMQC and gHMBC NMR spectroscopy. Crystals of **(2)** suitable for X-ray crystal structure determination and microanalysis were obtained by sublimation of the crude crystalline material at 100 – 140 °C / 2 x 10^{-2} mmHg, Figure 9.

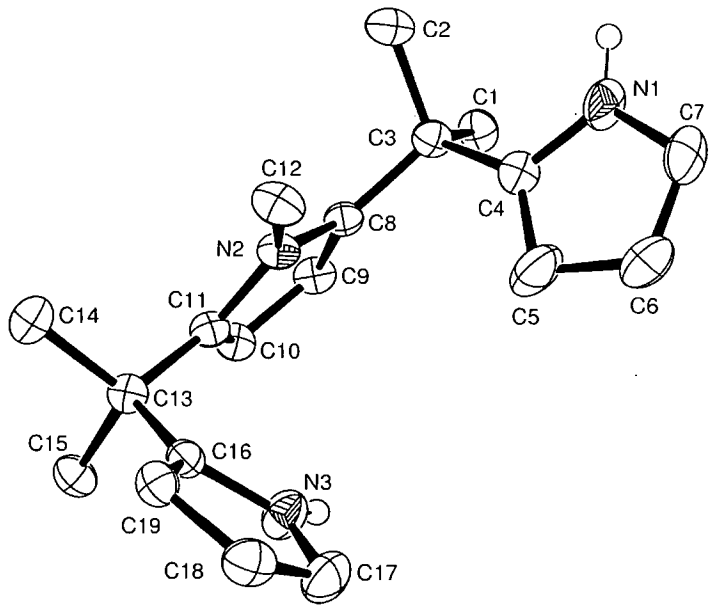

Figure 9: Molecular structure of 1-methyl-2,5-bis{(2'-pyrrolyl)dimethylmethyl}pyrrole, **(2)**, with thermal ellipsoids drawn at the level of 50 % probability (protons removed for clarity, except N-H).

Compounds **(1)** and **(2)** were cyclised in a "3+1" condensation reaction to provide the target macrocycle **(3)** (Equation 8). Since the 3+1 condensation reaction involves nucleophilic attack by pyrrole at a tertiary alcohol centre, initial attempts used the same Brønstead acid catalyst, solvent and concentrations used in the synthesis of **(2)** from **(1)**. However, trial reactions employing 48 % hydrobromic acid (150 mol %) added to a solution of equimolar amounts of **(1)** and **(2)** in methanol at -78, -20, and -20 → 20 °C failed to produce reaction.

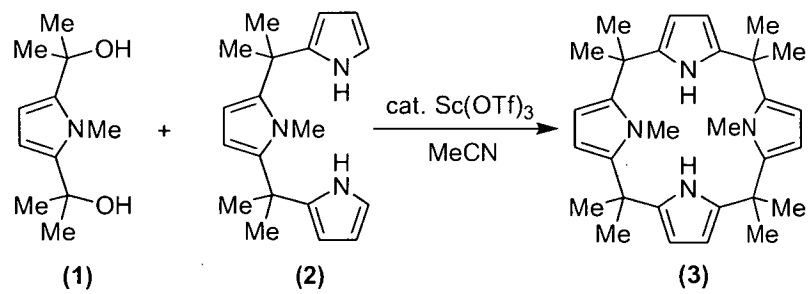

Equation 8

Scandium trifluoromethanesulfonate, $Sc(OTf)_3$, is a water tolerant Lewis acid which has been used to catalyse a range of carbon-carbon bond forming reactions.[17] $Sc(OTf)_3$ was trialled in the 3+1 reaction on NMR scale at 10 mol % using MeOH and

MeCN as solvents. Analysis of the crude reaction mixtures by ^{1}H NMR spectroscopy showed the presence of the target macrocycle in each of the reactions, and the presence of fewer side-products with MeCN as solvent. A preparative scale reaction (2.2 mmol of **(1)** and **(2)**) using 10 mol % of $Sc(OTf)_3$ gave a 37 % yield of **(3)** as an off-white solid. No attempt was made to optimise the yield of **(3)** through the use of high-dilution conditions. Macrocycle **(3)** was analysed by ^{1}H, ^{13}C, gHMQC and gHMBC NMR spectroscopy. Crystals of **(3)** suitable for X-ray crystal structure determination and microanalysis were obtained by evaporation of a pentane/dichloromethane solution (4:1). Figure 10.

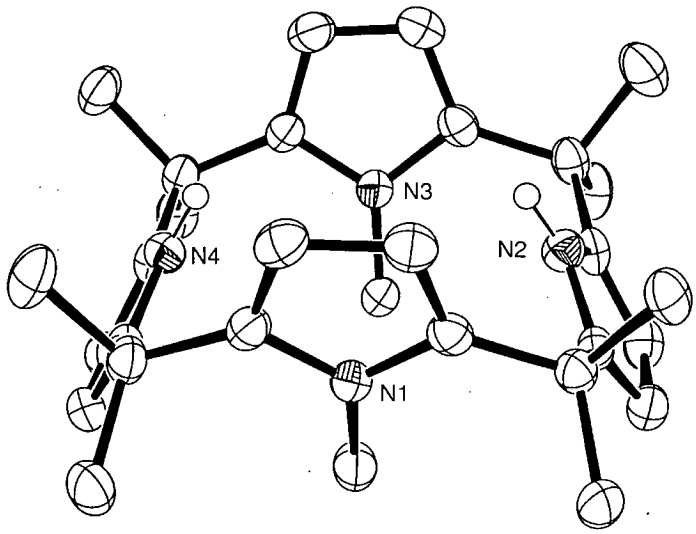

Figure 10: Molecular structure of *trans-N,N'*-dimethyl-*meso*-octamethylporphyrinogen, $Me_8N_4Me_2H_2$, **(3)**, with thermal ellipsoids drawn at the level of 50 % probability (protons removed for clarity).

The molecular structure of the target *trans-N,N'*-dimethyl-*meso*-octamethylporphyrinogen, $Me_8N_4Me_2H_2$, **(3)**, displays alternate pyrrolyl and *N*-methylpyrrolyl rings joined by dimethyl-substituted sp^3 carbons. Similarly to the octaethyl analogue $Et_8N_4Me_2H_2$, **(XXXVI)**, the *N*-CH_3 substituents both point to the same side of the macrocyclic plane, whilst the pyrrolyl *N*-H groups face the opposite side. Given the similarity between the two macrocycles it is anticipated that the Group 1 and lanthanide coordination chemistry developed for **(XXXVI)** will be broadly applicable to **(3)**. In addition, the stepwise nature of the synthesis of **(3)** will allow selective functionalisation of the macrocyclic ring (*e.g.* incorporation of pendant groups on the *N*-methylpyrrolyl C-3).

The synthesis, from *N*-methylpyrrole to the target $Me_8N_2Me_2H_2$, **(3)**, takes place over four steps with an overall yield of 15 %. In contrast, the yield of $Et_8N_2Me_2H_2$ obtained *via* methylation of $Et_4N_4H_4$ with 2.5 equivalents of MeI and separation from the statistical mixture of methylated isomers is 56 %, so direct methylation is currently the favoured means of producing *trans-N,N'*-dimethyloctaalkylporphyrinogens. The yield of diester **(7)** might be optimised *via* use of a coordinating solvent such as THF in place of hexane to further assist in breaking up the *n*-BuLi aggregate, and/or the use of a different lithiating agent. The yield of the ultimate 3+1 cyclisation step might be improved from the current 37% by use of higher dilution conditions to prevent intermolecular side reactions, and by trialling other group 3 and f-block triflates as Lewis acid catalysts.

2.4 Experimental

Synthesis of 1-methyl-2,5-bis(1,1'-dimethylhydroxymethyl)pyrrole, (1), by lithiation of 1-methylpyrrole and addition to acetone

1-methylpyrrole (0.01 mol, 0.81 g), TMEDA (0.045 mol, 5.23 g, 6.8 mL), *n*-butyllithium in hexanes (2.3 M, 20 mL) and hexane (20 mL) were refluxed with stirring for 18.5 h. The brown, heterogeneous reaction mixture was allowed to cool to room temperature and added *via* cannula to vigorously stirred acetone (50 mL) over the course of 1 h. Stirring was continued for 1.5 h before addition to saturated NH_4Cl solution and extraction with Et_2O (3 x 60 mL). The organic extracts were dried over $MgSO_4$ overnight. Solvents and TMEDA were removed by rotary evaporation (3.5 h at 60 °C, overnight at room temperature, 3 h at 60 °C) resulting in a yellow oil which formed white solids upon cooling. The solids were rinsed with hexane and collected at the pump to give a crude product (0.17 g). The product was shown by ^1H NMR analysis to consist of a mixture of 1-methyl-2,5-bis(1,1'-dimethylhydroxymethyl)pyrrole and 1-methyl-2-hydroxydimethylmethylpyrrole.

A sample (0.08 g) of the crude product was added to refluxing hexane/acetone (19:1 v/v, 40 mL) followed by further addition of acetone until complete dissolution had occured (2.6 mL required). Slow cooling gave pale yellow, transparent crystals of 1-methyl-2,5-bis(1,1'-dimethylhydroxymethyl)pyrrole suitable for X-ray crystal structure determination.

^{1}H NMR (400 MHz, $(CD_3)_2CO$, 25 °C): δ = 1.54 (s, 12H, C-CH_3), 3.76 (s, 2H, OH), 4.07 (s, 3H, N-CH_3), 5.72 (s, 2H, =CH).

^{13}C NMR (75 MHz, $(CD_3)_2CO$, 25 °C): δ = 31.2 (C-CH_3), 34.7 (N-CH_3), 69.3 (COH), 103.9 (=CH), 140.1 (=CR).

Anal. Calcd.: C, 66.97; H, 9.71; N, 7.10 ($C_{11}H_{19}NO_2$, MW 197.27)
Found: C, 66.98; H, 9.50; N, 7.04

Synthesis of 1-methyl-2,5-bis(1,1'-dimethylhydroxymethyl)pyrrole, (1), by lithium-halogen exchange of of 1-methyl-2,5-dibromopyrrole and addition to acetone

Freshly recrystallised *N*-bromosuccinimide (0.04 mol, 7.2 g) was added with stirring to 1-methylpyrrole (0.02 mol, 1.62 g) in THF (80 mL) at -78 °C. The reaction was stirred for 2 min and allowed to warm to room temperature. Solvent was removed *in vacuo* leaving off-white solids which were dissolved in Et_2O (50 mL). The solution was filtered *via* cannula dropwise into a flask containing 1.6 M *n*-butyllithium in hexane (0.04 mol, 25 mL) at -78 °C. Once addition was complete a further portion of Et_2O was added (20 mL) and the mixture allowed to warm to room temperature. The off-white suspension was added dropwise to acetone (80 mL) with stirring at 0 °C. The light brown reaction mixture was added to saturated NH_4Cl solution (250 mL) and the organic layer separated. The aqueous layer was extracted with Et_2O (2 x 60 mL) and the combined organics dried over $MgSO_4$ and solvent removed *in vacuo* to give an orange solid. The crude product was not weighed. Analysis by ^{1}H NMR spectroscopy showed the presence of more than one disubstituted isomer in addition to **(1)** and **(5)**.

Synthesis of 1-methyl-2,5-bis(1,1'-dimethylhydroxymethyl)pyrrole, (1), by reaction of 1-methylpyrrole 2,5-dicarboxylic acid diethyl ester with excess MeMgI

Iodomethane (17.8 mmol, 1.1 mL) was added dropwise *via* syringe to Mg turnings (22 mmol, 0.54 g) in Et_2O (10 mL). A crystal of I_2 was used to intiate reaction and addition performed at a rate which maintained a gentle reflux. A further portion of Et_2O (20 mL) was added once reaction had commenced. A solution of 1-methylpyrrole-2,5-dicarboxylic acid diethyl ester (2.22 mmol, 0.50 g) in Et_2O (10 mL) was added *via* cannula to the stirred solution and the reaction held at 40 - 45 °C for 25 h with the flask kept sealed to prevent solvent loss. Reaction was quenched by addition to 10 % w/v

NH_4Cl solution (30 mL) and the organic layer separated. The aqueous layer was extracted with Et_2O (2 x 20 mL) and the combined organics dried over $MgSO_4$. Solvent was removed *in vacuo* to give the product as a yellow solid (407 mg, 93 %).

Synthesis of 1-methyl-2,5-bis{(2'-pyrrolyl)dimethylmethyl}pyrrole, (2)

1-methyl-2,5-bis(1,1'-dimethylhydroxymethyl)pyrrole (6 mmol, 1.18 g) and pyrrole (0.252 mol, 17.5 mL) were dissolved in MeOH (150 mL). The mixture was cooled to -32 °C and stirred for 5 min. 48 % Hydrobromic acid (1.5 mL), precooled to -32 °C was added dropwise with vigorous stirring over 30 s, and the reaction mixture changed from yellow to dark orange. The stirred mixture was allowed to warm to -21 °C over 50 min before being quenched by the addition of 5 % w/v Na_2CO_3 solution (100 mL). The mixture was extracted with Et_2O (2 x 60 mL) and the extracts washed with brine (2 x 40 mL), dried over $MgSO_4$ and stripped of solvent *in vacuo* to give a brown viscous oil. The crude oil was placed under vacuum (5 h at 20 °C / 1 x 10^{-2} mmHg then 7 h at 55 °C / 20 mmHg) during which time it spontaneously crystallised to form a brown solid (1.73 g, 98 %). The crude solid was used in subsequent reactions without further purification.

^{1}H NMR (300 MHz, $(CD_3)_2CO$, 25 °C): δ = 1.57 (s, 12H, C-CH_3), 2.68 (s, 3H, N-CH_3), 5.87 (m, 2H, N-CH=CH-C*H*), 5.92 (m, 2H, N-CH=C*H*), 5.98 (s, 2H, =CH, pyrMe), 6.54 (m, 2H, N-CH), 9.18 (s, 2H, NH).

^{13}C NMR (75 MHz, $(CD_3)_2CO$, 25 °C): δ = 30.4 (C-*C*H_3), 31.8 (N-CH_3), 36.4 (*C*-CH_3), 103.6 (N-CH=CH-*C*H), 105.0 (=CH, pyrMe), 108.1 (N-CH=*C*H), 117.2 (N-CH), 139.9 (=CR, pyr), 140.0 (=CR, pyrMe).

Anal. Calcd.: C, 77.24; H, 8.53; N, 14.23 ($C_{19}H_{25}N_4$, MW 295.42)
Found: C, 77.17; H, 8.54; N, 14.05

Synthesis of *trans*-*N*,*N'*-dimethyl-*meso*-octamethylporphyrinogen, $Me_8N_4Me_2H_2$, (3)

1-methyl-2,5-bis{(2'-pyrrolyl)dimethylmethyl}pyrrole (2.2 mmol, 0.65 g) was dissolved in MeCN (250 mL). 1-methyl-2,5-bis(1,1'-dimethylhydroxymethyl)pyrrole (2.2 mmol, 0.434 g) was added as a solution in MeCN (50 mL) and the mixture warmed to 45 °C. Scandium trifluoromethanesulfonate (0.22 mmol, 108 mg) was added as a

solution in MeCN (10 mL). There was an immediate colour change from yellow to pink, and reaction was continued for 19 h before being cooled in an ice bath and filtered at the pump. The off-white solid product was washed with MeCN and dried. A second crop of product was obtained by removing solvent from the filtrate *in vacuo*, adding Et_2O (10 mL) and hexane (0.5 mL), collecting the off-white solid product, rinsing with MeCN and drying. Total mass of product was 372 mg (37 %). Crystals suitable for X-ray structure determination were grown by evaporation of a solution in pentane/ dichloromethane (4:1).

^{1}H NMR (300 MHz, C_6D_6, 25 °C): δ = 1.50 (s, 12H, C-CH_3), 1.54 (s, 12H, C-CH_3), 2.84 (s, 6H, N-CH_3), 5.99 (d, 4H, pyr =CH), 6.03 (s, 4H, NMepyr =CH), NH not observed.

^{13}C NMR (75 MHz, C_6D_6, 25 °C): δ = 26.2 (C-*C*H_3), 32.6 (N-CH_3), 33.6 (C-*C*H_3), 36.2 (*C*-CH_3), 103.3 (=CH, pyr), 105.2 (=CH, pyrMe), 138.8 (=CR, pyr), 139.5 (=CR, pyrMe).

Anal. Calcd.: C, 78.90; H, 8.83; N, 12.27 ($C_{30}H_{40}N_4$, MW 456.66)
Found: C, 78.97; H, 9.04; N, 12.42

Synthesis of 1-methyl-2-(hydroxydimethylmethyl)pyrrole, (5), by lithiation of 1-methylpyrrole and addition to acetone

1-methylpyrrole (0.071 mol, 5.85 g, 6.4 mL), TMEDA (0.321 mol, 37.3 g, 48.5 mL) and *n*-butyllithium in hexanes (1.6 M, 200 mL) were refluxed with stirring for 70 min then stirred for 3 d at ambient temperature, producing a brown suspension. A portion of the suspension (10 mL) was added *via* cannula to acetone (15 mmol, 0.87 g, 1.1 mL; distilled from B_2O_3) in hexanes (10 mL) heated to reflux. A further portion of acetone (13.6 mmol, 0.79 g, 1.0 mL) was added dropwise *via* syringe. Heating was continued for 15 min then the mixture cooled to ambient temperature. Volatiles were removed *in vacuo* and the beige solids treated with NH_4Cl (20 mL, 25 % w/v) and extracted with Et_2O (1 x 20 mL). The organic extracts were rinsed with brine, dried over $MgSO_4$ and reduced *in vacuo* to yield a transparent brown oil. The oil was placed under vacuum (1 x 10^{-2} mmHg) at 65 °C for 3 h during which time the product formed as a colourless crystalline sublimate above the oil (not weighed). Single crystals suitable for X-ray crystal structure determination were obtained from the sublimate.

^{1}H NMR (400 MHz, $(CD_3)_2CO$, 25 °C): δ = 1.53 (s, 6H, C-CH_3), 3.77 (br s, 1H, OH), 3.81 (s, 3H, N-CH_3), 5.81 (q, 1H, =CH), 5.84 (q, 1H, =CH), 6.50 (t, 1H, =CH).

^{13}C NMR (75 MHz, $(CD_3)_2CO$, 25 °C): δ = 31.1 (C-*C*H_3), 36.2 (N-CH_3), 69.2 (*C*-CH_3), 105.8 (N-CH=*C*H), 106.3 (N-CH=CH-*C*H), 124.2 (N-*C*H), 139.3 (C-OH).

Synthesis of 1-methylpyrrole 2,5-dicarboxylic acid diethyl ester, (7)

1.6 M *n*-butyllithium (0.321 mol, 200 mL) was added to TMEDA (0.321 mol, 48.5 mL) with stirring. 1-methylpyrrole (0.071 mol, 6.4 mL) was added by syringe and the mixture refluxed with stirring for 70 min before being cooled to room temperature. 200 mL of this mixture was added dropwise *via* cannula to diethyl carbonate (0.66 mol, 78 g) in hexane (100 mL) at -70 °C with stirring. The reaction mixture was allowed to warm to room temperature, and added to 20% w/v NH_4Cl solution (400 mL). The layers were separated and the aqueous layer extracted with Et_2O (2 x 80 mL). The combined organic layers were washed with 20 % w/v NH_4Cl soluion (2 x 100 mL), brine (1 x 50 mL), and stripped of solvent *in vacuo* to give a dark brown oil containing 1-methylpyrrole 2-carboxylic acid ethyl ester as a siginificant side product. The mixture was separated by vacuum distillation in a Kugelrohr oven. The first fraction (0.3 mmHg; 2.5 h at 55°C, 2 h at 70 °C) was 1-methylpyrrole 2-carboxylic acid ethyl ester, followed by 1-methylpyrrole 2,5-dicarboxylic acid diethyl ester (0.04 mmHg; 3 h at 100 °C, 2 h at 140 °C, 2 h at 160 °C) as a transparent yellow oil which crystallised spontaneously upon standing (5.47 g, 44 %). Pure 1-methylpyrrole 2,5-dicarboxylic acid diethyl ester was also obtained from the crude oil by chromatography over silica gel (dichloromethane/hexane 60:40).

^{1}H NMR (400 MHz, $(CD_3)_2CO$, 25 °C): δ = 1.33 (t, 3H, C-CH_3), 4.24 (s, 3H, N-CH_3), 4.29 (q, 2H, CH_2), 6.87 (s, 2H, =CH).

^{13}C NMR (100 MHz, $(CD_3)_2CO$, 25 °C): δ = 13.7 (C-*C*H_3), 33.9 (N-CH_3), 60.2 (CH_2), 115.8 (=CH), 128.1 (*C*-CO), 160.5 (C=O).

Anal. Calcd.: C, 58.65; H, 6.71; N, 6.22 ($C_{11}H_{15}NO_4$, MW 225.24)

Found: C, 58.56; H, 6.88; N, 6.13

Synthesis of 1-methylpyrrole 2-carboxylic acid ethyl ester, (8)

Following the same procedure as for the synthesis of 1-methylpyrrole 2,5-dicarboxylic acid diethyl ester, the product was obtained from the initial vacuum distillation fraction as a pale yellow oil (not weighed).

^{1}H NMR (400 MHz, $(CD_3)_2CO$, 25 °C): δ = 1.29 (t, 3H, C-CH_3), 3.90 (s, 3H, N-CH_3), 4.23 (q, 2H, CH_2), 6.06 (m, 1H, =CH), 6.85 (m, 1H, =CH), 6.96 (m, 1H,=CH).

2.5 References

1. A. Baeyer, *Ber. Dtsch. Chem. Ges.*, 1886, **19**, 2184.

2. P. Rothemund, C.L. Gage, *J. Am. Chem. Soc.*, 1955, **77**, 3340.

3. P.A. Gale, J.L. Sessler, W.E. Allen, N.A. Tvermoes, V. Lynch, *Chem Commun.*, 1997, 665.

4. V. Král, P.A. Gale, P. Anzenbacher Jr., K. Jursíková, V. Lynch, J.L. Sessler, *Chem. Commun.*, 1998, 9.

5. J.L. Sessler, W.-S. Cho, V. Lynch, V. Král, *Chem. Eur. J.*, 2002, **8**, 1134.

6. L. Bonomo, E. Solari, G. Toraman, R. Scopelliti, M. Latronico, C. Floriani, *Chem. Commun.*, 1999, 2413.

7. J.L. Sessler, A. Andrievsky, P.A. Gale, V. Lynch, *Angew. Chem. Int. Ed. Engl.*, 1996, **35**, 2782.

8. Y. Furusho, H. Kawasaki, S. Nakanishi, T. Aida, T. Takata, *Tetrahedron Lett.*, 1998, 3537.

9. J. Wang, Ph.D. Thesis, University of Tasmania, 2003.

10. Y.-S. Jang, H.-J. Kim, P.-H. Lee and C.-H. Lee, *Tetrahedron Lett.*, 2000, **41**, 2919.

11. D.J. Chadwick, C. Willbe, *J. Chem. Soc., Perkin Trans. 1*, 1977, 887.

12. Ref: F.T. Edelmann, P. Poremba, F.M. Bohnen, R. Herbst-Irmer, *Z. Anorg. Allg. Chem.*, 2004, **630**, 1671.

13. **a**. J.K. Tauer, W.N. Lipscomb, *Acta Crystallogr.*, 1952, **5**, 606.
b. S. Sarkar, R.N. Joarder, *J. Chem. Phys.*, 1993, **99**, 2032.
c. L. Benisvy, I. Mutikanien, M. Quesada, U. Turpeinen, P. Gamez, J. Reedijk, *Chem. Commun.*, 2006, 3723.

14. J. Wang, D.N. Stringer, M.G. Gardiner, B.W. Skelton, A.H. White, *J. Organomet. Chem.*, 2005, **690**, 220.

15. **a.** H.M. Gilow, D.E. Burton, *J. Org. Chem.*, 1982, **46**, 2221.
b. G.A. Cordell, *J. Org. Chem.*, 1975, **40**, 3161.

16. A. Arunachalampillai, P. Crewdson, I. Korobkov, S. Gambarotta, *Organometallics*, 2006, **25**, 3856.

17. S. Kobayashi, *Eur. J. Org. Chem.*, 1999, 15.

Chapter 3

1,4-Diazabuta-1,3-diene Reduction Chemistry

3.1 Introduction

Metal complexes of 1,4-diaza-1,3-butadiene (≡ RDAB) ligand were first reported by Krumholz in 1953 by the reaction of methylamine and glyoxal or 2,3-butanedione in the presence of iron(II) chloride and potassium iodide, giving the *tris*(MeDAB) iron(II) complexes $[Fe(MeDAB)_3]I_2$ and $[Fe(MeDAB\{Me\})_3]I_2$.[1] Throughout this thesis the abbreviation "RDAB" is used, where R ≡ *N*-substituents, whilst 1,4-diazabuta-1,3-dienes featuring substitution at the imine carbons are abbreviated RDAB{R'}, where R ≡ *N*-substituents, and R' ≡ *C*-substituents. DAB complexes of s-, p-, d- and f-block elements have been prepared that feature the DAB ligand in a wide range of binding modes and various states of reduction.[2]

RDAB ligands posess two potential N σ- and C=N π-donors, each capable of supplying 2 electrons to a metal centre. The number of electrons donated is dependant on the conformation of the RDAB, the coordination environment of the metal centre and the nature of the metal itself. Thus in the planar *E-s-trans-E* conformation the RDAB can bind to a single metal centre (Figure 1(A)) or bridge two metal centres (Figure 1(B)), resulting in donation of 2 or 4 electrons, respectively. The *E-s-cis-E* conformation allows a chelating arrangement (Figure 1(C)) where both N donors are bound to the same metal centre with the donation of 4 electrons. In addition, the *E-s-cis-E* conformation allows one or both C=N double bonds to π-bond to metal centres, resulting in donation of up to 8 electrons (Figure 1(D)) whilst the conformation shown in Figure 1(E) represents the donation of 6 electrons from two N donors and a single π-interaction.[2]

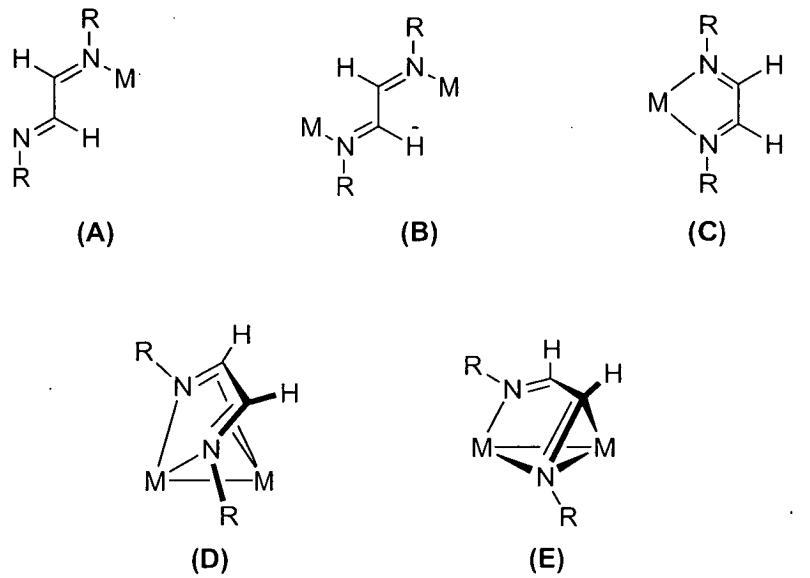

Figure 1: Binding modes of DAB ligands.

In addition to acting as a σ- and π-donor ligand, RDAB can accept one or two electrons to form a radical anion or dianion, Scheme 1. Representative examples of anionic binding modes are discussed below, as well as lanthanide complexes displaying unusual redox reactivity.

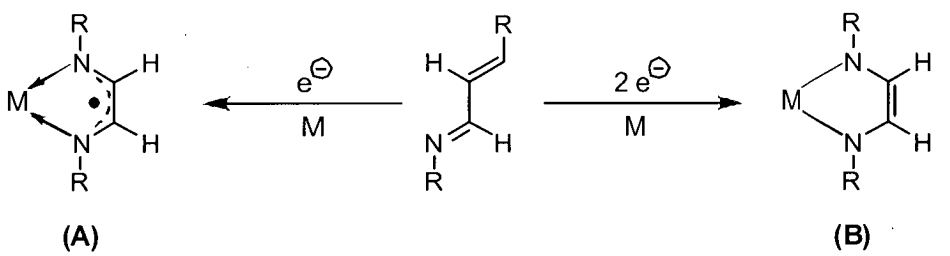

Scheme 1: DAB radical anion **(A)**, and dianion **(B)**.

The reaction of 1,4-di-*t*-butyl-1,4-diazabuta-1,3-diene (*t*-BuDAB) with lithium metal in hexane gives the neutral complex [Li(*t*-BuDAB)$_2$], **(I)**.[3] The lithium centre is bound to two chelating *t*-BuDAB ligands, one acting as a radical anion and the other as a neutral Lewis base donor, Figure 2. The different formal charges of the two chelating 1,4-diazabuta-1,3-dienes result in disparate bond lengths within the NCCN subunits of the respective ligands. The bond lengths witin the *t*-BuDAB unit acting as a Lewis base adduct correspond to those expected for alternating C=N, C-C and C=N double bonds (as observed in the neutral ligand). In contrast, the NC and CC bond lengths observed in the

radical anion are more uniform, reflecting distribution of the anionic charge through the conjugated system, Figure 1. The Li-N(radical *t*-BuDAB) bond distances (1.993(7), 1.996(8) Å) are shorter than the Li-N(neutral *t*-BuDAB) distances (2.134(7), 2.148(6) Å) due to the formal charge present on the radical anion. Satisfactory simulation of of the EPR spectrum confirmed the radical anion / neutral *t*-BuDAB arrangements.

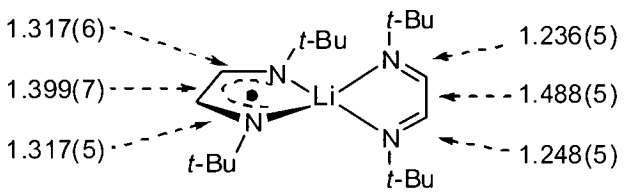

(I)

Figure 2: Lewis base and radical anion binding of *t*-BuDAB in [Li(*t*-BuDAB)$_2$], **(I)**, bond lengths of the central *t*-BuDAB NCCN units marked in Ångströms.

The reaction of beryllium chloride with sodium metal and 1,4-di-*o*-tolyl-2,3-diphenyl-1,4-diazabuta-1,3-diene (*o*-tolDAB{Ph}) in toluene gives the mononuclear beryllium complex [Be(*o*-tolDAB{Ph})$_2$], **(II)**, Equation 1.[4]

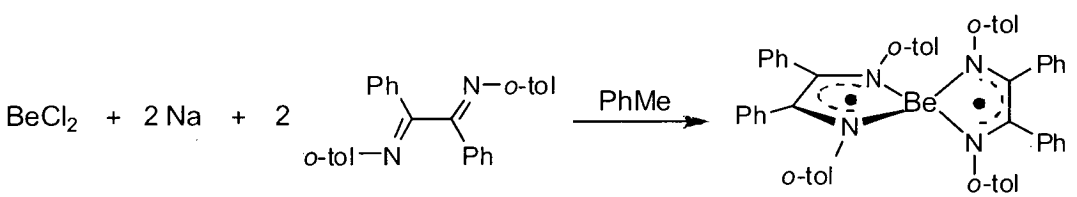

(II)

Equation 1

The molecular structure of **(II)** contains two singly reduced DAB radical anions in a planar *cis*-conformation with the four ligating N atoms occupying the verticies of a distorted tetrahedron around the beryllium centre. Comparison of bond lengths within the central DAB NCCN units with those in the neutral ligand confirmed a delocalisation of charge in both of the DAB ligands. EPR spectroscopic observations confirmed the existence of two independent radical anions. Addition of THF to **(II)** causes intramolecular disproportionation and transfer of an electron at the metal centre. Subsequent loss of one neutral DAB ligand and dimerisation gives [{(*o*-tolDAB{Ph})Be(THF)}$_2$], **(III)**, containing one dianionic DAB ligand per beryllium centre, Equation 2.

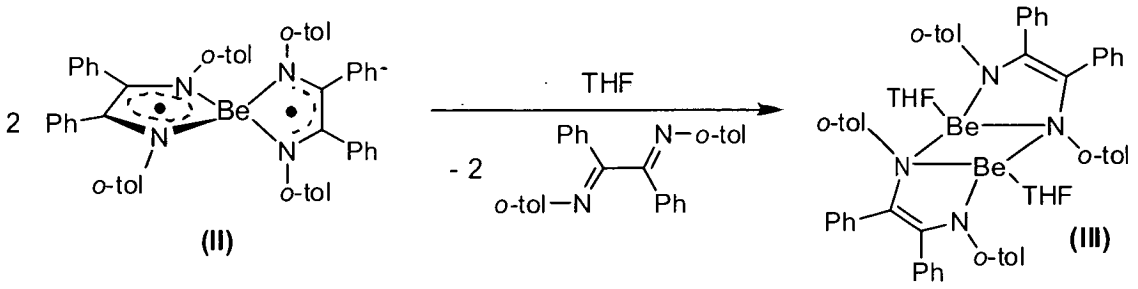

Equation 2

RDAB ligands in both singly and doubly deprotonated states are most commonly observed in chelating binding modes. The only report of a complex containing an anionic DAB bridging two metal centres is the binuclear niobium(V) complex **(IV)**.[5] Complex **(IV)** was formed by the reaction of $NbCl_5$ with lithium metal and *t*-BuDAB in diethyl ether, Equation 3. In addition to chelating DAB dianions, the complex features a *t*-BuDAB ligand η^2-bound to each niobium centre through a C=N group and a dianionic *t*-BuDAB bridging the two metal centres to form a *syn* oriented Nb-N-C-C fragment. The bond distances within the bridging DAB NCCN unit (1.409(5), 1.323(5) and 1.406(4) Å, respectively) confirm the dianionic nature of the bridging ligand.

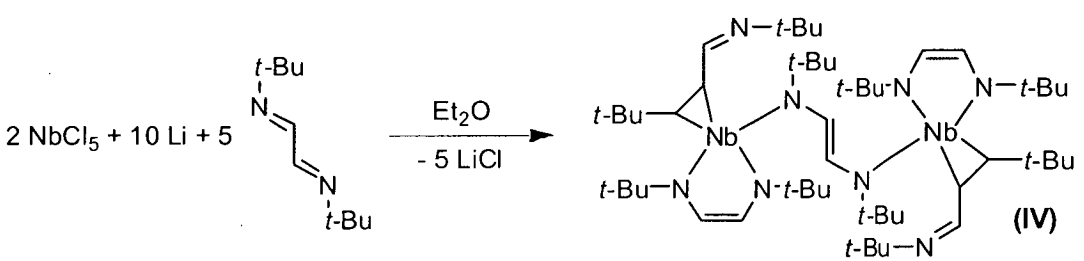

Equation 3

Amongst the first lanthanide complexes incorporating DAB ligands were the homoleptic [Ln(*t*-BuDAB)$_3$] complexes of yttrium, neodymium, samarium and ytterbium, Figure 3.[6] The compounds were preprared by cocondensing the respective lanthanide metal vapour with excess *t*-BuDAB at 77 K. The oxidation state of the lanthanide centre was assigned as Ln(0) on the basis of ESR and NMR spectra. Later, solid state magnetic susceptibility studies of the ytterbium complex over a 5 to 300 K

temperature range indicated that the ytterbium centre was divalent at low temperatures (5 K), and trivalent at higher temperatures.[7]

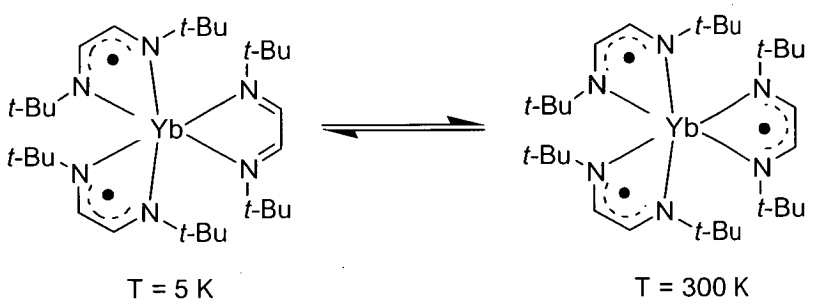

Figure 3: Temperature dependant ytterbium(II)/(III) interconversion.

Heteroleptic samarium and ytterbium RDAB complexes with the 1,4-bis(trimethylsilyl)cyclooctatetraenediyl dianion ($(C_8H_6(SiMe_3)_2)^{2-}$) were prepared by reaction of the powdered lanthanide metal with $C_8H_8(SiMe_3)_2$ and DAB in THF, Scheme 2.[8] The samarium(III) complexes of *t*-BuDAB and PhDAB{Me}, $[(C_8H_6(SiMe_3)_2)Sm(RDAB\{R'\})(THF)]$ (R = *t*-Bu, R' = H **(V)**; R = Ph, R' = Me **(VI)**) were prepared, each featuring chelating radical DAB anions. Reaction between ytterbium and PhDAB{Me} gave the ytterbium(II) complex $[(C_8H_6(SiMe_3)_2)Yb(PhDAB\{Me\})(THF)]$, **(VII)**, whilst *t*-BuDAB failed to react. The difference in oxidation state of the samarium and ytterbium compounds was attributed to the electronic porperties of the Ln^{2+} ions. Perhaps the most obvious rationale for the failure of *t*-BuDAB to react with the smaller ytterbium centre is steric hindrance between the bulky $(C_8H_6(SiMe_3)_2)^{2-}$ and *t*-butyl groups. However, the presence of THF in the formulation of complex **(VII)** suggests that the *t*-BuDAB could have obtained better access to the metal centre by loss of THF, and steric factors alone are not responsible for the observed +2 ytterbium oxidation state. The oxidation state of the lanthanides was ascertained by ^1H and ^{171}Yb NMR spectroscopy.

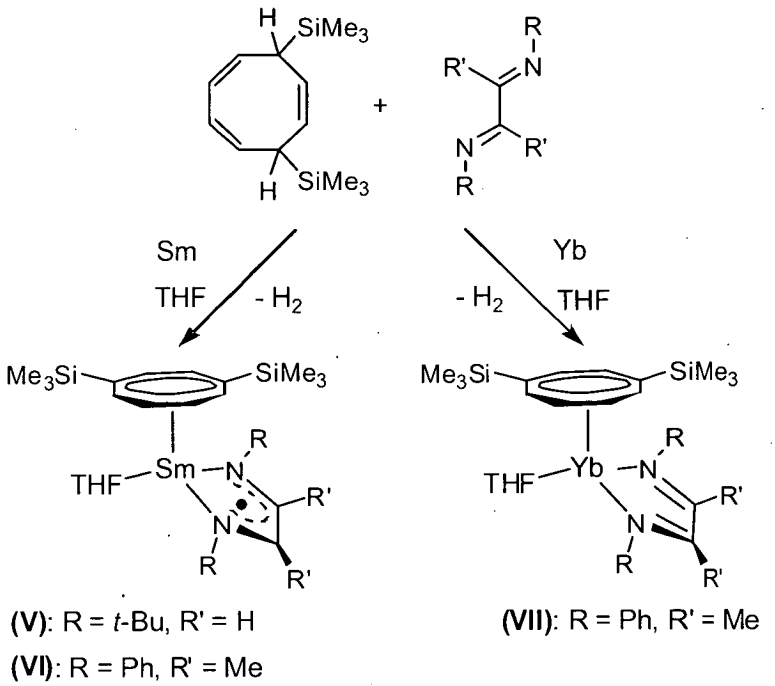

(V): R = *t*-Bu, R' = H

(VI): R = Ph, R' = Me

(VII): R = Ph, R' = Me

Scheme 2: Synthesis of samarium(III) and ytterbium(II) COT* complexes.

Steric interaction between DAB and other ligands has been implicated in novel reversible redox reactions of ytterbium DAB complexes. The reaction of $[(C_5Me_5)_2Yb(THF)_2]$, **(VIII)**, with *t*-BuDAB in toluene gives the ytterbium(III) complex $[(C_5Me_5)_2Yb(t\text{-BuDAB})]$, **(IX)**, featuring a chelating radical anionic DAB ligand.[9] Addition of THF reverses this reaction, giving the ytterbium(II) starting material and free *t*-BuDAB. The analogous ytterbium(II) non-methylated cyclopentadienyl complex, $[(C_5H_5)_2Yb(THF)_2]$, **(X)**, reacts with *t*-BuDAB to form $[(C_5H_5)_2Yb(t\text{-BuDAB})]$, **(XI)**, which does not revert to **(X)** in THF solution, but persists as the ytterbium(III) complex, Scheme 3.[10] This reversible redox behaviour is discussed in more detail in Chapter 5.

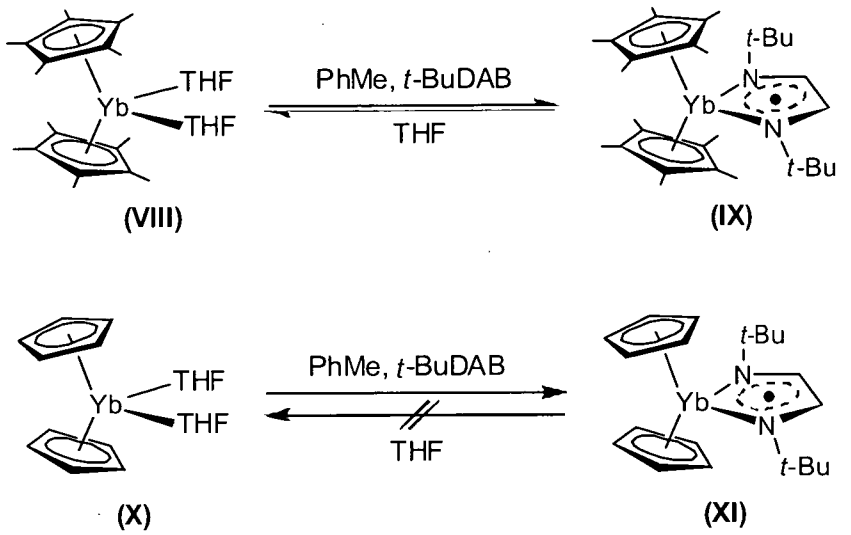

Scheme 3: Solvent mediated reversible redox behaviour in Yb *t*-BuDAB complexes.

The reversible redox chemistry displayed in Scheme 3 was attributed by the authors to the steric bulk of the C_5Me_5 rings restricting interaction between the DAB radical anion and ytterbium centre. The non-reversible nature of the $(C_5H_5)^-$-based system was thus rationalised as being due to better DAB-ytterbium interaction making replacement of the DAB ligand by THF unfavourable. Comparison of bond lengths between the two complexes reflect a weaker DAB-Yb interaction in the bulkier $(C_5Me_5)^-$ system, *viz.* Yb-N = 2.385(3) and 2.394(3) Å in $[(C_5Me_5)_2Yb(t\text{-BuDAB})]$, **(IX)** vs. 2.306(9) and 2.309(9) Å in $[(C_5H_5)_2Yb(t\text{-BuDAB})]$, **(XI)**.

Solvent-mediated reversible redox chemistry has also been reported in ytterbium DAB complexes containing indenyl and *ansa*-indenyl ligands.[11] The ytterbium(III) complexes $[(C_9H_7)_2Yb(t\text{-BuDAB})]$, **(XII)**, and $[(C_9H_7)_2Yb(2,6\text{-di-}i\text{-}PrC_6H_3DAB)]$, **(XIII)**, were prepared by reaction of $[(C_9H_7)_2Yb(THF)_2]$, **(XIV)**, with the respective DAB in toluene. The CH_2CH_2 bridged *ansa*-metallocene ytterbium(III) complex $[rac\text{-}(CH_2\text{-}1\text{-}C_9H_6)_2Yb(t\text{-BuDAB})]$, **(XV)**, was also prepared from the corresponding ytterbium(II) starting precursor **(XVI)** and *t*-BuDAB, Scheme 4.

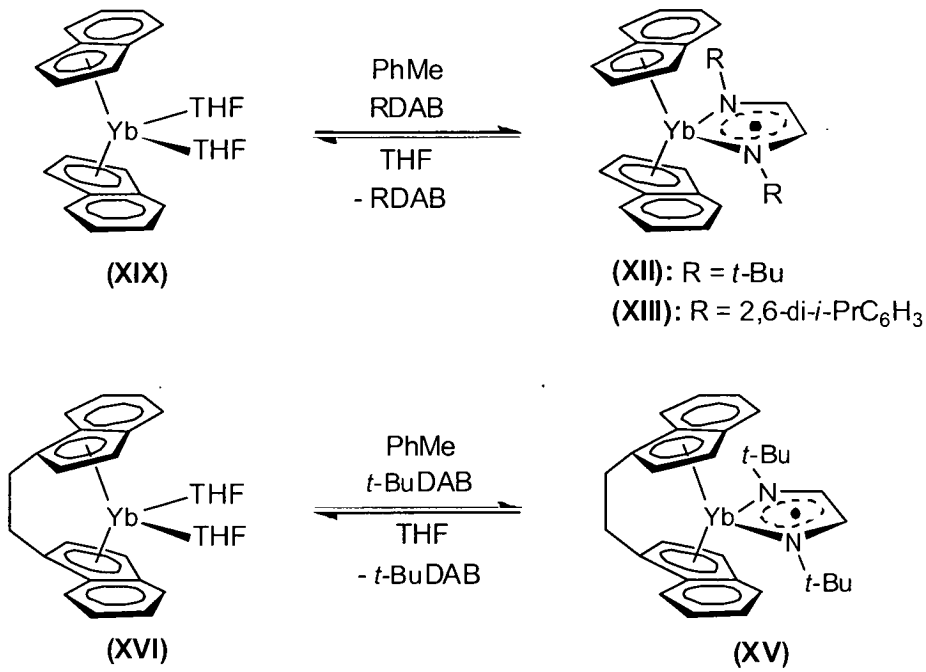

(XIX)

(XII): R = *t*-Bu
(XIII): R = 2,6-di-*i*-PrC_6H_3

(XVI)

(XV)

Scheme 4: Solvent-mediated reversible redox behaviour in Yb indenyl complexes.

Addition of THF to the ytterbium(III) complexes **(XII)**, **(XIII)** and **(XV)** resulted in reversion to the respective ytterbium(II) precursor and free DAB. Ytterbium-nitrogen bond distances in these three complexes can be compared with those in the $(C_5H_5)^-$ analog **(XI)**, *viz.* Yb-N = 2.318(5) and 2.335(5) Å in [$(C_9H_7)_2$Yb(*t*-BuDAB)], **(XII)**; 2.381(3) Å in [$(C_9H_7)_2$Yb(2,6-di-*i*-PrC_6H_3DAB)], **(XIII)**; 2.321(4) and 2.343(5) Å in [*rac*-(CH_2-1-$C_9H_6)_2$Yb(*t*-BuDAB)] **(XV)** vs. 2.306(9) and 2.309(9) Å in [$(C_5H_5)_2$Yb(*t*-BuDAB)], **(XI)**. The relatively modest increase in ytterbium-nitrogen bond lengths observed in **(XII)**, **(XIII)** and **(XV)** over those observed in **(XI)** make steric factors a less convincing rationale for reversible redox chemistry than in the pentamethylcyclopentadienyl complex **(IX)**.

The europocene complex [$(C_5Me_5)_2$Eu$(THF)_2$], **(XVII)**, was reported to react with *t*-BuDAB in toluene to give the Eu(II) complex [$(C_5Me_5)_2$Eu(*t*-BuDAB)], **(XVIII)**, in which the *t*-BuDAB fragment bears no formal charge, Scheme 5.[12] Treatment of complex **(XVIII)** with THF did not result in substitution of the chelating *t*-BuDAB unit by THF, in contrast to the Yb(III) complex **(IX)**. Reaction of [$(C_5Me_5)_2$Eu$(THF)_2$] with C_6F_5DAB{Me} in toluene resulted in oxidation of the Eu centre to form the Eu(III) complex [$(C_5Me_5)_2$Eu(C_6F_5DAB{Me})], **(XIX)**. Treatment of **(XIX)** with THF resulted in electron transfer from the radical anionic C_6F_5DAB{Me} unit back to the metal to give the THF solvated Eu(II) europocene [$(C_5Me_5)_2$Eu$(THF)_2$], **(XX)**, and free

$C_6F_5DAB\{Me\}$ (by ^1H NMR spectroscopy). The authors implicated the weak electron donating characteristics of the perfluorophenyl subsituted $C_6F_5DAB\{Me\}$ ligand as a cause of the reversible redox chemistry displayed by $[(C_5Me_5)_2Eu(C_6F_5DAB\{Me\})]$, **(XIX)**.

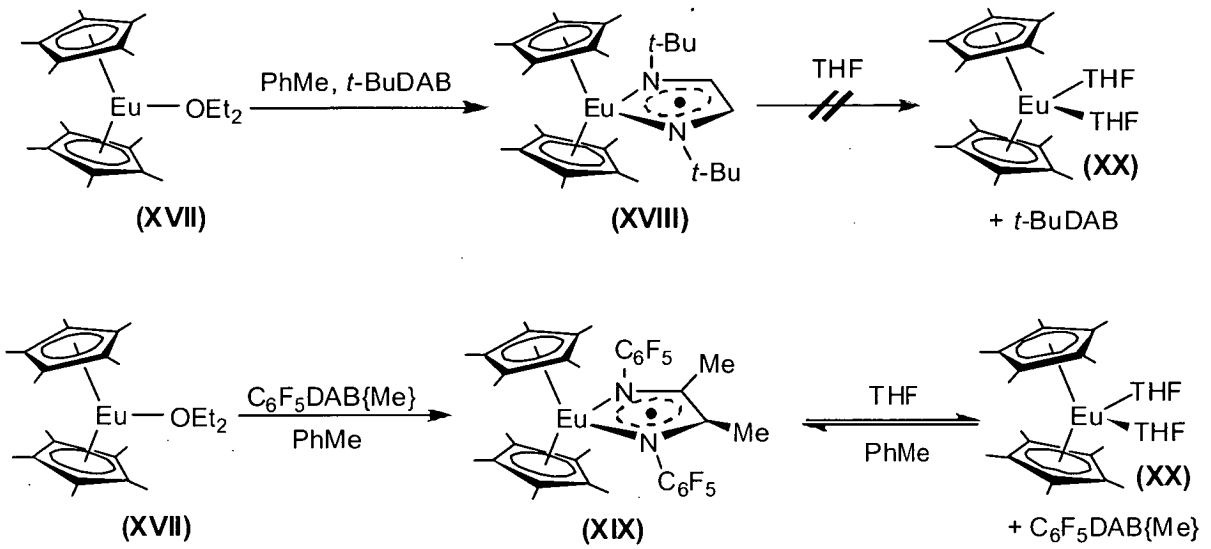

Scheme 5: Solvent mediated reversible redox behaviour in Eu RDAB complexes.

The solvent mediated reversible redox chemistry discussed above is represented by complexes of europium and ytterbium, the two most readily reduced lanthanide metals. Analogous reversible redox chemistry in RDAB complexes of other lanthanides is not known, presumably due to the greater reduction potential involved in accessing the Ln(II) oxidation state.

3.2 Research aim

Reduction of RDAB (R = *t*-Bu, *i*-Pr, *n*-Bu) by Sm(II), Eu(II) and Yb(II) complexes of the sterically demanding $(Et_8N_4Me_2)^{2-}$ ligand was to be undertaken to give Ln(III) complexes featuring anionic RDAB auxiliary ligands. Lanthanide ionic radius (Sm(II) > Eu(II) >> Yb (II)) and the RDAB *N*-alkyl substituent (*t*-Bu > *i*-Pr > *n*-Bu) were expected to influence the binding modes observed in the resultant complexes.

3.3 Results and discussion

3.3.1 Complex syntheses

3.3.1.1 Synthesis of lanthanide(II) complexes

The dipotassium, samarium(II) and ytterbium(II) complexes $[[(Et_8N_4Me_2)K_2(THF)_2]_n$ **(11)**, $[(Et_8N_4Me_2)Sm(THF)_2]$, **(12)**, and $[(Et_8N_4Me_2)Yb(THF)]$, **(13)**, were prepared by modifications of the literature procedures.[13]

The starting material used in the synthesis of the deprotonated complex **(11)** was the crude mixture obtained by methylation of $(Et_8N_4)^{4-}$ with methyl iodide, containing neutral porphyrinogen **(14)** as well as *N*-methyl-*meso*-octaethylporphyrinogen, *cis*-*N*,*N'*-dimethyl-*meso*-octaethylporphyrinogen, *N*,*N'*,*N''*-trimethyl-*meso*-octaethylporphyrinogen and *N*,*N'*,*N''*,*N'''*-tetramethyl-*meso*-octaethylporphyrinogen, Scheme 6. The crude product obtained from the methylation reaction was suspended in CH_2Cl_2:hexanes 1:5 and flashed through a plug of silica gel to remove any unreacted $Et_8N_4H_4$. The filtrate was evaporated *in vacuo* and the mixture of methylated isomers deprotonated with potassium metal at 75 °C in THF/PhMe to give the dipotassium salt, **(11)**, as an insoluble white solid. The other deprotonated methylated porphyrinogens remained in the supernatant which was filtered away from **(11)** *via* cannula.

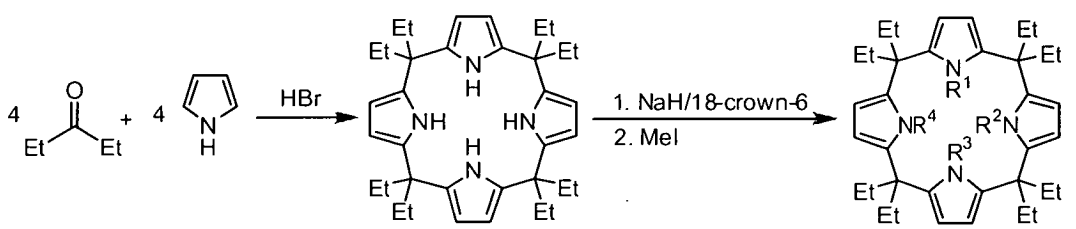

R^1 = Me, R^2 = R^3 = R^4 = H;
R^1 = R^2 = Me, R^3 = R^4 = H;
R^1 = R^3 = Me, R^2 = R^4 = H **(14)**;
R^1 = R^2 = R^3 = Me, R^4 = H;
R^1 = R^2 = R^3 = R^4 = Me.

Scheme 6: Methylation of $Et_8N_4H_4$ to give **(14)** and methylated isomers.

Subsequent metathetical exchange with the lanthanide(II) iodide in THF at room temperature gave the respective lanthanide(II) complexes and two equivalents of potassium iodide (Scheme 7). Removal of potassium iodide was effected by reducing the metathesis reaction mixture to dryness *in vacuo* and extraction of the lanthanide(II) complexes as a solution in toluene. Removal of toluene *in vacuo* and crystallisation from hot THF gave the lanthanide(II) complexes as crystalline solids (Ln = Sm, **(12)**, dark purple-black; Ln = Yb, **(13)**, orange-yellow).

The methodology was extended to synthesise $[(Et_8N_4Me_2)Eu(THF)_2]$, **(15)**. Europium(II) iodide was prepared as the bis(THF) adduct according to the literature procedure[14] by reacting a slight excess of europium powder with 1,2-diiodoethane in THF followed by filtration, partial removal of solvent and crystallisation at -20 °C. A solution of $EuI_2(THF)_2$ in THF was added to a suspension of **(11)** in THF which caused a change in colour from beige to yellow.

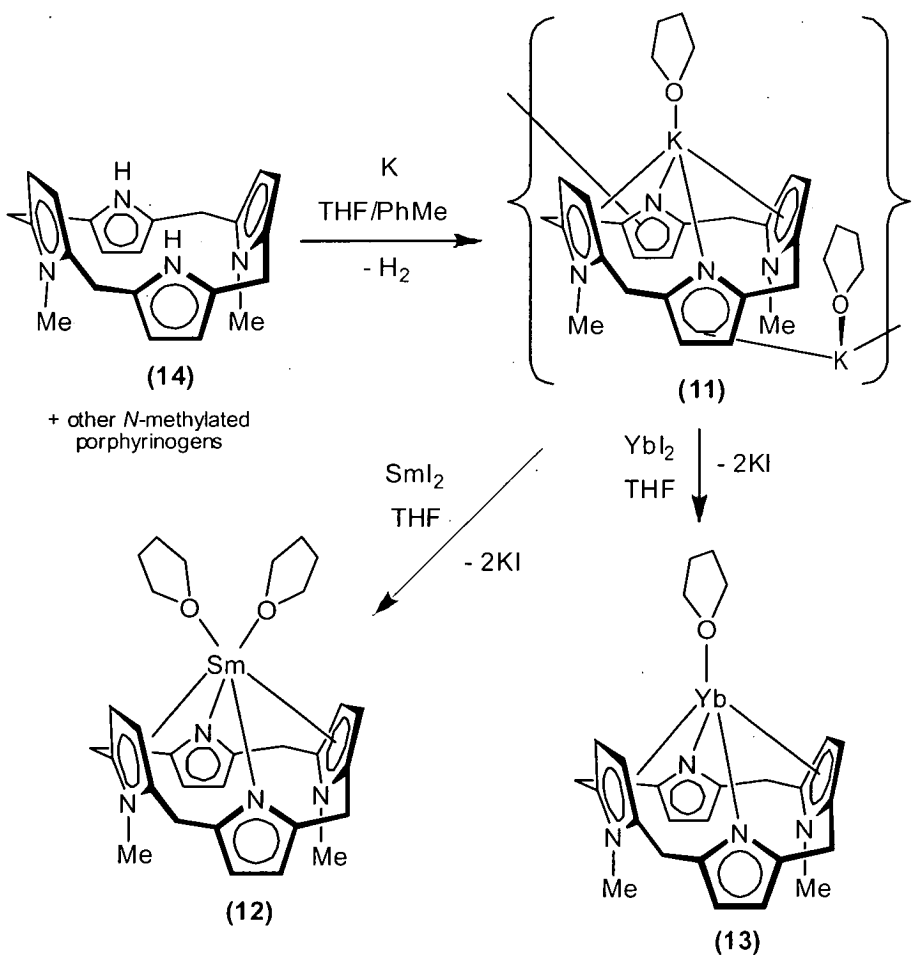

Scheme 7: Synthesis of $[(Et_8N_4Me_2)Sm(THF)_2]$, **(12)**, and $[(Et_8N_4Me_2)Yb(THF)]$, **(13)**.

The molecular structure of **(11)** contains one *endo-* bound potassium within the macrocyclic cavity, and the other bridging potassium binding *exo-* between macrocycles. The polymeric structure of **(11)** results in low solubility in organic solvents, and the reaction between **(11)** and $EuI_2(THF)_2$ is therefore heterogeneous. Even though the change in colour suggested reaction was complete within 10 minutes, stirring was maintained overnight to ensure complete reaction. After settling, the reaction mixture was a transparent yellow solution over pale solids, presumably potassium iodide. THF was removed *in vacuo* and toluene used to dissolve the soluble **(15)**. The solution was filtered *via* cannula from the insoluble potassium iodide, toluene removed *in vacuo*, and the yellow residue dissolved in hot THF and allowed to cool overnight. The mixture was left at -20 °C for 24 h to complete the crystallisation, and removal of the supernatant *via* cannula afforded $[(Et_8N_4Me_2)Eu(THF)_2]$, **(15)** as yellow prisms suitable for X-ray crystal structure determination in 75 % yield, Equation 4.

$$^1/_n\,[\{(Et_8N_4Me_2)K_2(THF)_2\}_n] \xrightarrow[THF]{EuI_2(THF)_2} [(Et_8N_4Me_2)Eu(THF)_2] + 2KI$$

(11) **(15)**

Equation 4

The toluene extraction step was found to be necessary to ensure complete separation of $[(Et_8N_4Me_2)Eu(THF)_2]$, **(15)** from potassium iodide. Attempts to filter **(15)** from the metathesis reaction as a solution in THF, concentration and subsequent crystallisation resulted in the precipitation of potassium iodide along with **(15)**, thus implying that potassium iodide was partially dissolved in the THF metathesis reaction mixture. Toluene extraction was also found to improve the previously reported isolations of **(12)** and **(13)**, resulting in less contamination by potassium iodide.

A number of features of the $(Et_8N_4Me_2)^{2-}$ ligand system are qualitatively shown by the three-dimensional representations of **(12)** and **(13)** in Scheme 7. The macrocycle adopts the same 1,3-alternate conformation as the neutral ligand, and the two anionic pyrrolide nitrogens act as a σ donors. The metal is bound within the cavity, and displays η^5-interactions with the two *N*-methylpyrrolyl rings. The *N*-methyl groups extend towards the other side of the macrocyclic plane, blocking access to the metal centre from the underside of the complex.

THF solvent molecules are coordinated to the metal centres at the binding groove. Complexes **(12)** and **(15)** bear two THF molecules, whilst the metal centre in **(13)** accomodates only one THF molecule. The differing numbers of coordinated THF molecules are due to the interplay of macrocycle bulk and the difference in ionic radius of the metal centres. The similarly sized Sm(II) and Eu(II) centres in **(12)** and **(15)** expose sufficient coordination sphere at the binding groove to allow coordination of two THF molecules. Due to the increased effective nuclear charge, Yb(II) has a smaller ionic radius than the earlier lanthanides, and the smaller Yb(II) centre in **(13)** resides further within the macrocyclic cavity. This reduces the coordination sphere available for coordination at the binding groove, hence allowing only one THF molecule to bind to the metal. Metal size and macrocycle bulk recur as important factors in determining coordination and reactivity of the macrocyclic Ln(II) and Ln(III) complexes discussed later in this and subsequent chapters.

Complex **(15)** is soluble in THF, toluene and benzene, and partially desolvates in the latter two solvents. Solutions of **(15)** in benzene or toluene deposited yellow crystals of the mono-THF adduct, $[(Et_8N_4Me_2)Eu(THF)]$, **(16)**, upon standing at RT for 6 days, Equation 5.

$$\underset{\textbf{(15)}}{[(Et_8N_4Me_2)Eu(THF)_2]} \xrightarrow{PhMe} \underset{\textbf{(16)}}{[(Et_8N_4Me_2)Eu(THF)]} + THF$$

Equation 5

Complexes **(15)** and **(16)** have been characterised by X-ray crystal structure determination. NMR spectroscopy was not informative due to the extreme line-broadening effect of the paramagnetic Eu(II) centre. Satisfactory microanalytical data were obtained for **(15)** and **(16)**. The molecular structure of **(15)** is isostructural and isomorphous with $[(Et_8N_4Me_2)Sm(THF)_2]$, **(12)**, whilst **(16)** is isostructural and isomorphous with both $[(Et_8N_4Me_2)Yb(THF)]$, **(13)**, and the Sm(II) mono-THF adduct $[(Et_8N_4Me_2)Sm(THF)]$, **(17)**.[15]

3.3.1.2 Synthesis of samarium(III) DAB complexes and Sm(II) derivative

The *t*-BuDAB Sm(III) complex was prepared by addition of a solution of *t*-BuDAB in toluene to two equivalents of the Sm(II) precursor $[(Et_8N_4Me_2)Sm(THF)_2]$, **(12)**, in toluene at room temperature, Equation 6. Reaction was indicated by an immediate change of colour from purple to bright green. Removal of solvent *in vacuo* gave the product, $[\{(Et_8N_4Me_2)Sm\}_2(t\text{-BuDAB})]$, **(18)**, as a bright green crystalline powder in 86 % yield (Equation 3). Reaction of *t*-BuDAB with **(12)** in a 1:1 ratio resulted in isolation of the same product.

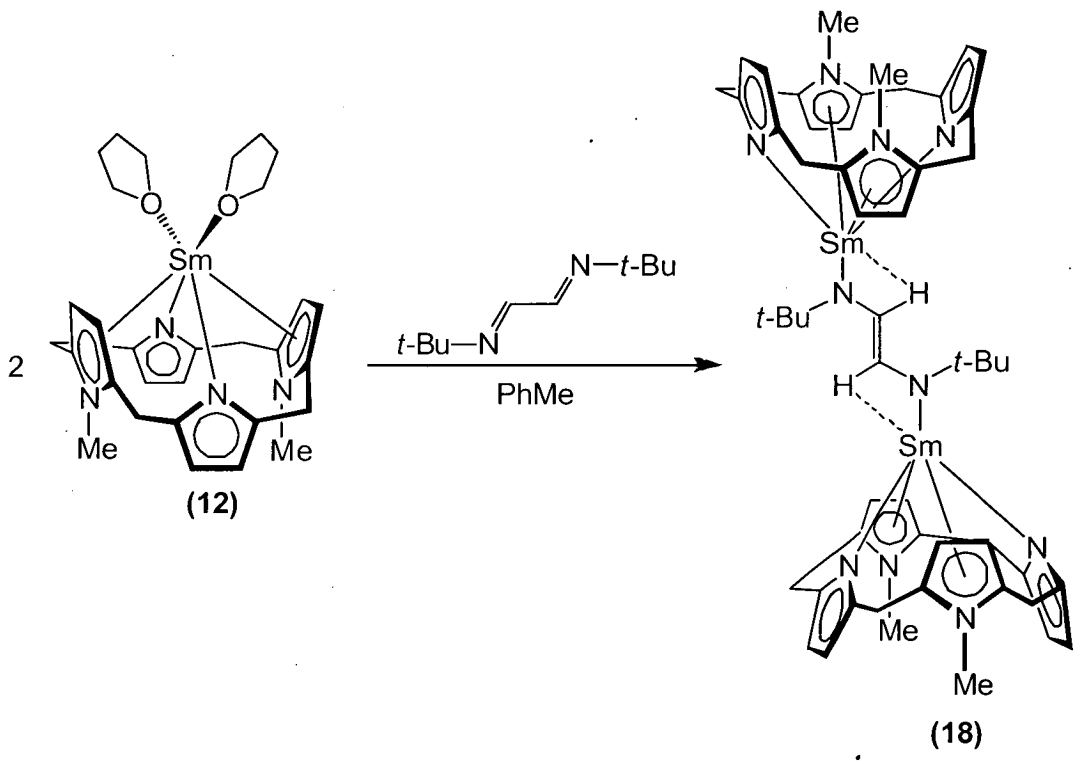

Equation 6

Complex **(18)** was characterised by X-ray crystal structure determination, ^1H, ^{13}C, gHMQC and gHMBC NMR spectroscopy, magnetic moment measurement and microanalysis. The molecular structure of the complex is binuclear, with a two-electron reduced 1,4-diaza-1,3-diene anion bridging the samarium centres. The long-short-long bond distances within the bridging 1,4-diaza-1,3-diene NCCN fragment are consistent with a dianionic formulation, Figure 4, and are similar to those in **(IV)**, *viz* 1.409(5)-1.323(5)-1.406(4) Å. The observed Sm-N distances (2.241(3)-2.251(3) Å) are shorter than those reported for Sm(III) amides (*e.g.* $[(Et_8N_4Me_2)SmN(SiMe_3)_2]$, 2.306(2)-

2.314(2) Å.)[13] NMR spectra confirmed that the overall symmetry present in solution was C_{2h}.

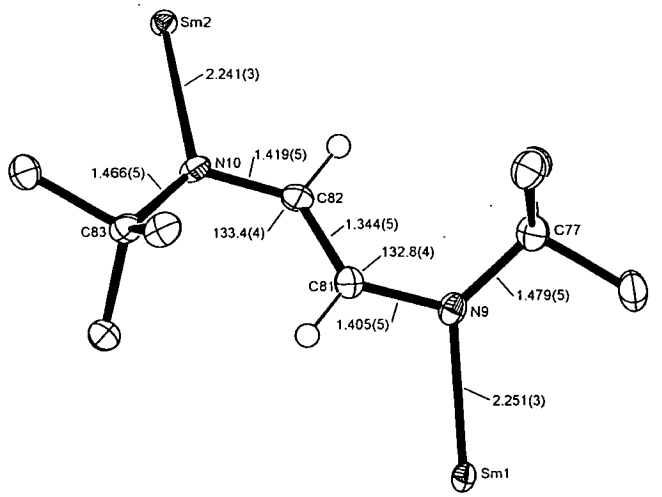

Figure 4: Bond lengths (Å) of the *t*-BuDAB fragment of **(18)**.

The +3 oxidation state of the samarium centres in **(18)** was determined by measuring the magnetic moment and by comparison of the DAB ligand geometry, samarium(III)-macrocycle contacts and the macrocyclic conformation in the solid state. Magnetic moment was measured in C_6D_6 at 25 °C (Evans' method) to be 2.74 μ_B (1.94 μ_B per Sm for noncommunicating metal centres), which is typical for Sm(III).[16] The Sm-centroid(*N*-methylpyrrolyl) distances of 2.64-2.69 Å are comparable to those in $[(Et_8N_4Me_2)SmN(SiMe_3)_2]$ (2.645-2.667 Å) and are considerably shorter than in the Sm(II) starting material $[(Et_8N_4Me_2)Sm(THF)_2]$, **(12)**, (2.756 Å).

Complex **(18)** dissolves in toluene, benzene or hexanes to form green solutions from which it can be isolated by cooling of hot solutions or removal of solvent *in vacuo*. However, dissolution in THF causes the complex to revert to the Sm(II) precursor and free 1,4-diazabuta-1,3-diene, Equation 7. Subsequent removal of solvent *in vacuo* forces the equilibrium back towards the green Sm(III) derivative **(18)**, which can be crystallised from toluene as before. Complex **(18)** does not react further upon addition of an extra equivalent of 1,4-diazabuta-1,3-diene, and is stable under vacuum at 100 °C for 2 h (well above the sublimation conditions for the free *t*-BuDAB ligand).

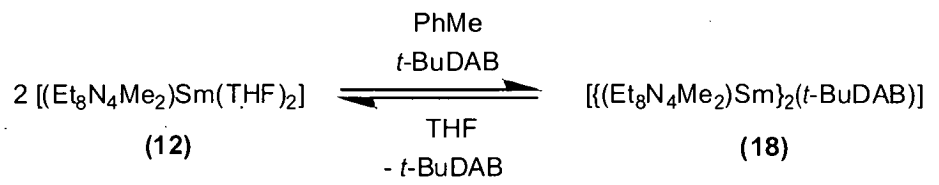

Equation 4

This reversible, solvent-mediated Sm(II)/Sm(III) system is extremely unusual. Reports of reversible Sm(II)/Sm(III) chemistry in the literature are restricted to (i) dinitrogen and substituted alkene and butadiene complexes of decamethylsamarocene[17] and (ii) dinitrogen and ethylene complexes of tetrametallated porphyrinogens.[18] Solvent-mediated reversible equilibria also exist in Yb(III) bis(pentamethylcyclopentadienyl), bis(indenyl) and *ansa*-indenyl RDAB complexes,[9-11] and a Eu(III) bis(pentamethylcyclopentadienyl) RDAB complex[12] (see Section 3.1).

The oxidation of Sm(II) to Sm(III) introduces a further subtlety that may be responsible for the reversible redox chemistry displayed here. The ionic radius of the samarium centre decreases with the removal of an electron from Sm(II) to Sm(III), as the effective nuclear charge increases. The smaller Sm(III) centre then resides slightly further within the macrocyclic cavity, making less coordination sphere available for binding at the top of the macrocycle and resulting in increased steric strain between the reduced 1,4-diazabuta-1,3-diene and the macrocycle. This implies a balance whereby the forward reaction (oxidation of Sm(II) to Sm(III)) is favoured on electronic grounds, whilst the reverse reaction is favoured on steric grounds (relief of strain between the deeper bound Sm(III) centre and the reduced 1,4-diazabuta-1,3-diene). The deeper position of the Sm(III) centre in **(18)** relative to the starting Sm(II) complex [$(Et_8N_4Me_2)Sm(THF)_2$], **(12)**, is reflected in the respective metallocene bend angles (defined below, see Section 3.3.3.1), *viz.* $154.4_4°$ in **(12)**, $161.5_3°$ in **(18)**.

Close contacts (of the length observed for Sm-C/H agostic interactions) to the C_2H_2 portion of the 1,4-diazabuta-1,3-diene were observed (Sm1-C81,H81 = 3.050(4), 2.8_7 Å; Sm2-C82,H82 = 3.007(4), 2.8_5 Å). The only other reported example of a bridging $(RDAB)^{2-}$ ligand is the Nb(V) complex **(IV)** which exhibits no close contacts between the Nd centre and the C_2H_2 section due to a *syn* arrangement of the Nb-N-C-C fragment.

In addition to solvent-mediated reversible redox chemistry, the ease by which the Sm(III) complex **(18)** reverted to starting Sm(II) suggested the possibility of the complex **(18)** participating directly as a Sm(III) reducing agent. Such reactivity was explored with a number of organic substrates, and is expanded upon in Chapter 5.

If steric restriction is responsible for the reversible redox behaviour shown in Equation 4, smaller 1,4-diazabuta-1,3-diene substituents should allow increased interaction with the deeply bound Sm(III) centre and thus be less liable to undergo the reverse reaction on steric grounds. This was investigated by making Sm(III) derivatives of less bulky 1,4-diazabuta-1,3-dienes featuring *i*-propyl and *n*-butyl groups in place of the *t*-butyl groups in **(18)**.

The *i*-PrDAB Sm(III) complex (1:1) was prepared by the addition of a toluene solution of *i*-PrDAB to one equivalent of the Sm(II) precursor $[(Et_8N_4Me_2)Sm(THF)_2]$, **(12)**, in toluene at room temperature. Reaction was accompanied by an immediate change of colour from dark purple to orange. Crystallisation at -80 °C overnight gave the product, $[(Et_8N_4Me_2)Sm(i\text{-PrDAB})]$, **(19)**, as an orange-brown crystalline powder in 52 % yield (Equation 8).

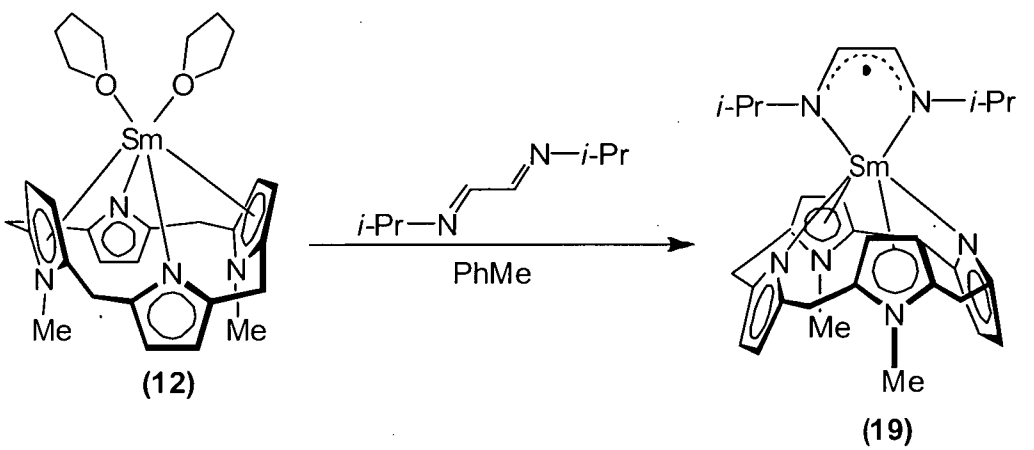

Equation 8

Complex **(19)** is mononuclear, containing a singly reduced *i*-PrDAB moiety. The chelating 1,4-diazabuta-1,3-diene radical anion is σ-bound through both nitrogen centres to the samarium center, giving an overall symmetry approximating to C_{2v} in the solid state and in solution. This is in contrast to the binuclear *t*-butyl analogue **(18)**, which features a doubly reduced 1,4-diazabuta-1,3-diene unit bridging two Sm centres.

Complex **(19)** was characterised by ^{1}H, ^{13}C, gHMQC and gHMBC NMR spectroscopy and X-ray crystal structure determination. Satisfactory microanalytical data were obtained.

The bond lengths of the 1,4-diazabuta-1,3-diene unit are indicative of its singly reduced nature, being intermediate in length between those of the neutral and dianionic ligand. The C-N and C-C distances within the NCCN unit of **(19)** (1.331(12)-1.384(14)-1.305(12) Å) are similar to those in other complexes featuring the radical anion, *e.g.* [Li(*t*-BuDAB)$_2$], **(I)**, (1.317(6)-1.399(7)-1.317(5) Å in the radical anion instance). The singly reduced nature of the 1,4-diazabuta-1,3-diene in the mononuclear **(19)** is congruent with the assignment of a +3 oxidation state to the Sm centre.

Complex **(19)** dissolves in benzene, toluene and hexanes to give orange solutions from which the complex can be isolated by cooling of a hot solution or removal of solvent *in vacuo*. Dissolution of **(19)** in THF does not produce a change in colour indicative of the Sm(II) precursor, and ^{1}H NMR spectra of **(19)** in THF-d_8 are identical to those obtained in benzene-d_6. Thus complex **(19)** does not undergo solvent-mediated reversible redox chemistry, in contrast to the 1:2 *t*-BuDAB complex **(18)**.

Complex **(19)** reacts with another equivalent of Sm(II) precursor **(12)** over the course of 5 minutes in toluene at 110 °C to form a green 1:2 binuclear complex [{($Et_8N_4Me_2$)Sm}$_2$(*i*-PrDAB)], **(20)**, Equation 9. Complex **(20)** was characterised by X-ray crystal structure determination and microanalysis. Low solubility in benzene-d_6 and THF-d_8 prevented characterisation by NMR spectroscopy.

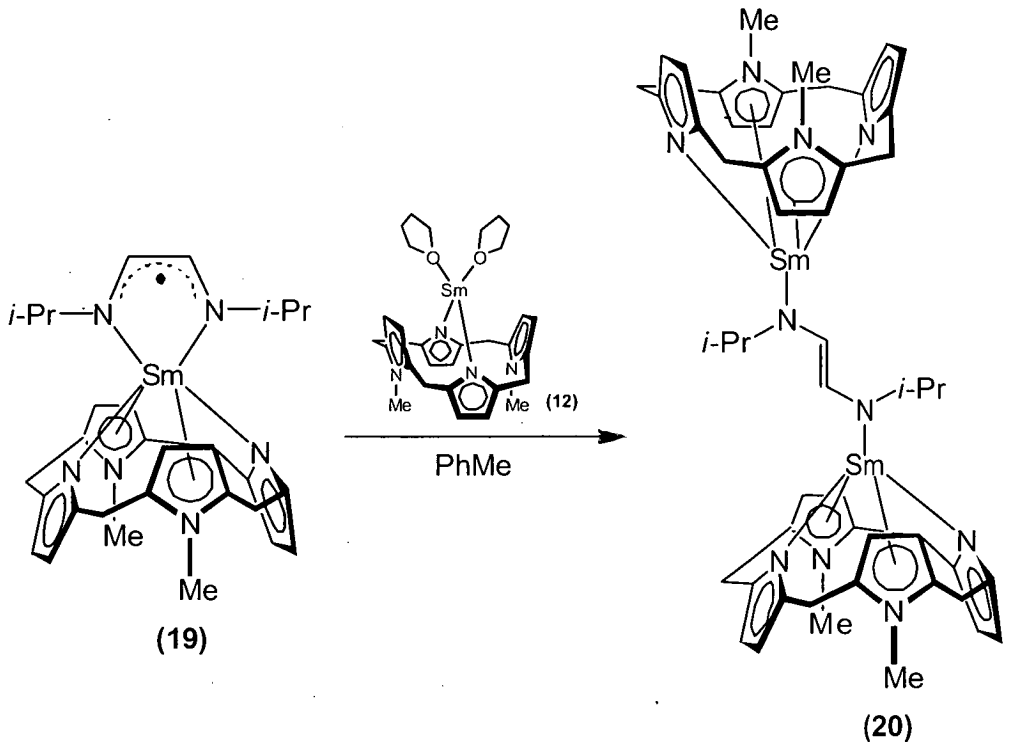

Equation 9

The bridging DAB in **(20)** adopts the same *anti* conformation with regards to the Sm centres as observed in the 1:2 *t*-butyl analogue **(18)**. The NCCN bond lengths (1.385(9)-1.339(11)-1.399(9) Å) are similar to those observed in **(18)** (1.405(5)-1.344(5)-1.419(5) Å), thereby confirming the dianionicity of the DAB.

The binuclear complex **(20)** was demonstrated to be stable in THF and not undergo the solvent-mediated reversible redox reactivity displayed by [{($Et_8N_4Me_2$)Sm}$_2$(*t*-BuDAB)], **(18)**. However, **(20)** did act as a Sm(III) reducing agent towards benzil, a reaction covered in Chapter 5.

A further reduction in 1,4-diazabuta-1,3-diene bulk was achieved by the use of *n*-butyl substituted 1,4-diazabuta-1,3-diene. Addition of one equivalent of *n*-BuDAB in toluene to a solution of two equivalents of the Sm(II) precursor [($Et_8N_4Me_2$)Sm($THF)_2$], **(12)**, in toluene at room temperature led to the precipitation of green solids under a brown supernatant. The solids redissolved upon heating and subsequent cooling to room temperature led to the crystallisation of the Sm(III) complex [{($Et_8N_4Me_2$)Sm}$_2$(*n*-BuDAB)], **(21)** as green crystals, which were separated from the reaction mixture and analysed by X-ray crystal structure determination, Equation 10.

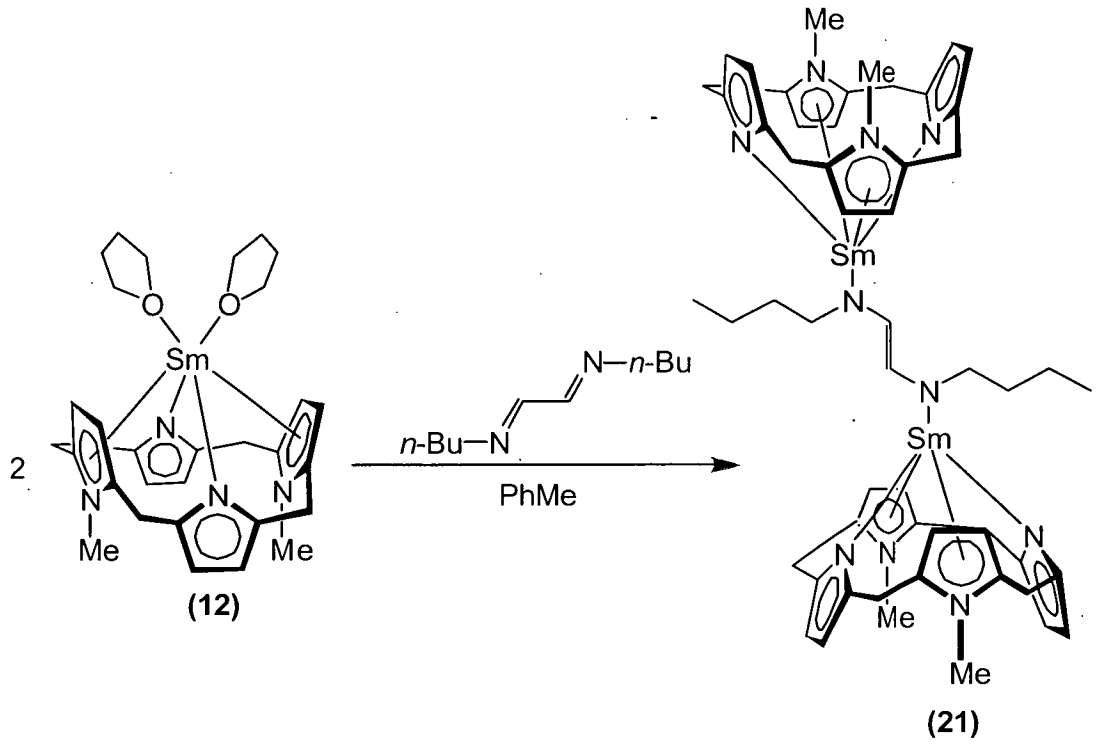

Equation 10

Different crystallisation conditions resulted in a different product being obtained from the above reaction of *n*-BuDAB and $[(Et_8N_4Me_2)Sm(THF)_2]$, **(12)**. One equivalent of *n*-BuDAB in benzene-d_6 was added to a solution of two equivalents of $[(Et_8N_4Me_2)Sm(THF)_2]$, **(12)**, in toluene at room temperature, with the formation of green solids under a brown supernatant which was decanted away from the green solids. Benzene-d_6 was added to the green solids and the mixture heated to effect dissolution, forming a transparent green solution. Upon cooling small green-brown dichroic crystals of an unsolvated, dimeric Sm(II) complex, $[\{(Et_8N_4Me_2)Sm\}_2]$, **(22)**, formed. These crystals were suitable for X-ray crystal structure determination.

The above mentioned *n*-BuDAB reactions yielding complexes **(21)** and **(22)** were run on small (3×10^{-5} mole Sm(II) precursor) scale in deuterated solvents, and attempts to repeat reactions on increased scales were unsuccessful. As a result yields of product were not recorded and microanalyses not performed. ^{1}H NMR spectroscopy was undertaken in each case but the presence of multiple species prevented assignment or inference of structural information.

The molecular structure of [{($Et_8N_4Me_2$)Sm}$_2$(*n*-BuDAB)], **(21)**, is similar to the *t*-butyl analogue **(18)** in that it is binuclear with a dianionic 1,4-diazabuta-1,3-diene unit bridging the two Sm centres. As in the case of the bridging *t*-BuDAB **(18)** and bridging *i*-PrDAB **(20)** complexes, the Sm-N-C-C moiety in **(21)** displays an *anti* conformation, allowing short contact between the Sm centre and the C_2H_2 hydrogens (Sm1-C43,H43 = 2.99_8, 2.82_5 Å; Sm2-C44,H44 = 3.02_6, 2.86_5 Å). The overall molecular symmetry is again C_2.

A possible rationalisation for the unexpected formation of complex **(22)** is the presence of an equilibrium between the binuclear Sm(III) complex **(21)**, and an unobserved mononuclear Sm(III) complex **(23)**, Scheme 8. A solubility-driven equilibrium may explain the subsequent crystallisation of **(22)** from the reaction mixture. A reaction using equimolar amounts of [($Et_8N_4Me_2$)Sm(THF)$_2$], **(12)**, and *n*-BuDAB to target a possible 1:1 chelating complex was not undertaken.

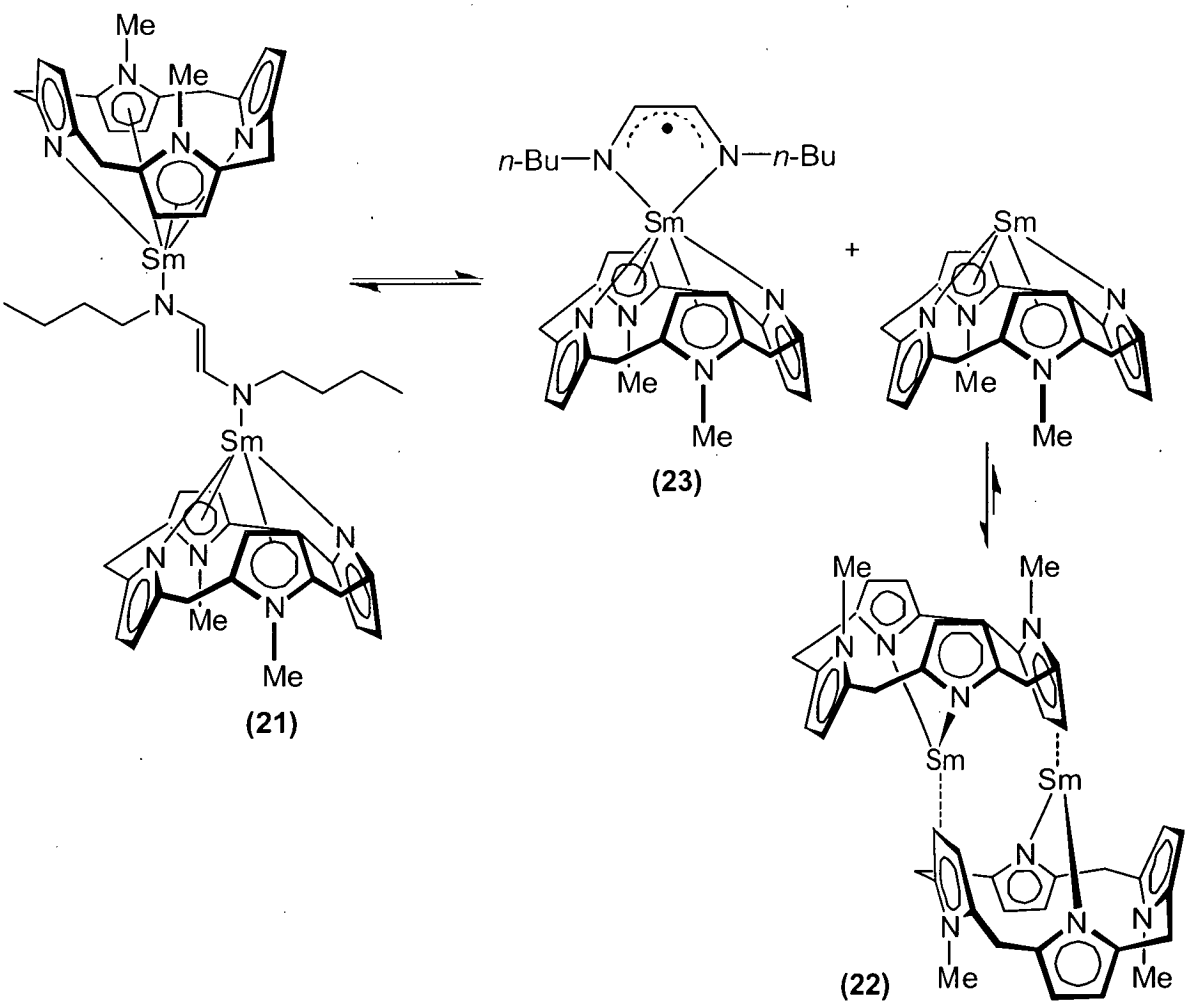

Scheme 8: Proposed mechanism for the formation of unsolvated dimer **(22)**.

Dissolution of crystals of [{($Et_8N_4Me_2$)Sm}$_2$(*n*-BuDAB)], **(21)**, in THF did not produce a colour change from green to the deep purple-black of the Sm(II) precursor **(12)**, suggesting that they do not undergo the solvent-mediated reversible redox reactivity noted for the *t*-butyl analogue **(18)**. Studies into the reducing ability of **(21)** and **(22)** were not carried out due to inability to obtain large amounts of the pure complexes.

The failure of the less bulky *i*-propyl and *n*-butyl substituted 1,4-diazabuta-1,3-diene complexes to undergo reversible redox chemistry upon addition to THF may be the result of improved 1,4-diazabuta-1,3-diene access to the Sm(III) centre. This will be expanded upon by reference to quantitative molecular structure data in Section 3.3.3.2. ^{1}H and ^{13}C NMR spectra for the Sm(III) complexes will be discussed further in Section 3.3.2.

3.3.1.3 Synthesis of ytterbium(II) DAB complexes

Due to the increased effective nuclear charge, the ionic radius of Yb(II) is smaller than Sm(II). Therefore a Yb(II) centre is expected to reside further within the macrocyclic cavity than a Sm(II) centre. This results in less coordination sphere available for subsequent reaction in the case of a Yb(II) complex (*viz.* Sm(II) complex [($Et_8N_4Me_2$)Sm(THF)$_2$], **(12)**, contains two THF molecules, whilst the Yb(II) complex [($Et_8N_4Me_2$)Yb(THF)], **(13)**, is observed with only one THF). Yb(II) is also less strongly reducing than Sm(II) (Yb(II) reduction potential -1.15 V compared with -1.55 V for Sm(II) vs NHE, respectively).[19] Therefore a given 1,4-diazabuta-1,3-diene substrate is less likely to be reduced by a Yb(II) complex than an analogous Sm(II) complex both on electronic and steric grounds.

Reactions between [($Et_8N_4Me_2$)Yb(THF)], **(13)**, and 1,4-diazabuta-1,3-dienes of differing bulk were carried out to further investigate the role of steric bulk and lanthanide reducing power, allowing comparison with the outcomes of the samarium reactions. The same 1,4-diazabuta-1,3-dienes were used as in the previously described samarium section: *t*-BuDAB, *i*-PrDAB and *n*-BuDAB (in order of decreasing bulk).

Attempted reaction between the Yb(II) precursor [($Et_8N_4Me_2$)Yb(THF)], **(13)**, and *t*-BuDAB in toluene was unsuccessful, with no colour change upon addition, and starting **(13)** recovered upon removal of solvent *in vacuo*. This is in contrast to the

reaction of $[(Et_8N_4Me_2)Sm(THF)_2]$, **(12)**, with *t*-BuDAB in toluene to give the binuclear Sm(III) complex $[\{(Et_8N_4Me_2)Sm\}_2(t\text{-BuDAB})]$, **(18)**. The difference in reactivity is accounted for by the smaller Yb(II) residing further within the macrocyclic cavity, thus exposing less coordination sphere and/or less reducing nature of Yb(II) precluding redox reaction, and resulting in competition between THF and (*t*-BuDAB) Lewis bases for the metal centre.

The less bulky *i*-PrDAB was used in an attempt to bring about reaction by allowing better access to the ytterbium centre. Addition of 1 equivalent of *i*-PrDAB in toluene solution to a solution of $[(Et_8N_4Me_2)Yb(THF)]$, **(13)**, in toluene produced an immediate change in colour from yellow to green. Removal of solvent *in vacuo* gave $[(Et_8N_4Me_2)Yb(i\text{-PrDAB})]$, **(24)**, as a green crystalline solid in 88 % yield, Equation 11. The same product was obtained when 2 equivalents of $[(Et_8N_4Me_2)Yb(THF)]$, **(13)**, were used. Complex **(24)** was characterised by X-ray crystal structure determination and ^1H NMR spectroscopy. Satisfactory microanalytical results were obtained.

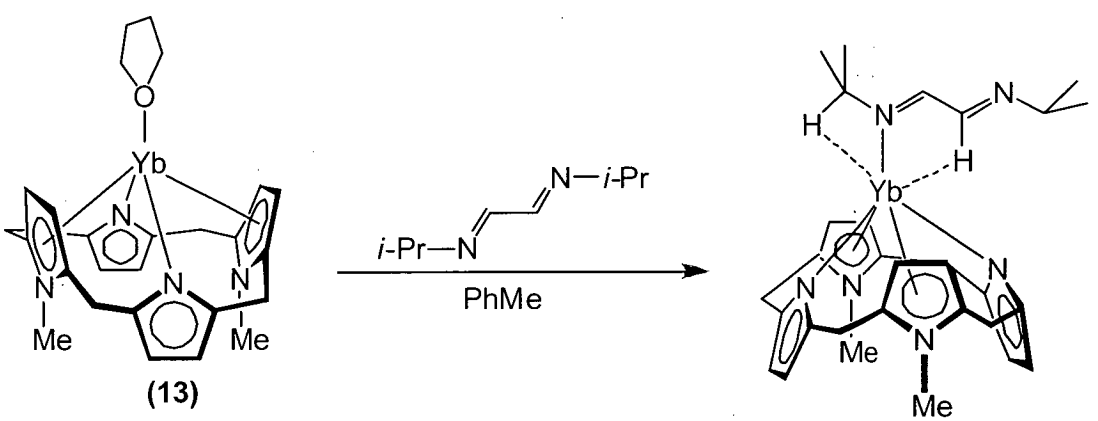

(13) **(24)**

Equation 11

Complex **(24)** is mononuclear, with one 1,4-diazabuta-1,3-diene nitrogen σ-bound to the ytterbium centre as a Lewis basic donor and the other nitrogen remaining uncoordinated. The *i*-propyl group furthest from the ytterbium centre points away from the macrocycle, and the steric bulk of this group reduces access to the adjacent nitrogen centre. Thus the nitrogen furthest from the Yb centre is prevented from binding to a second $(Et_8N_4Me_2)Yb$ unit, and the mononuclear structure observed in **(24)** results. This is expanded on further in the molecular structure section.

The bond distances within the 1,4-diazabuta-1,3-diene NCCN unit of **(24)** indicate the ligand is neutral and the ytterbium centre is therefore assigned an oxidation state of +2. This is congruent with the Yb-N(pyrrolide) bond distances in **(24)**, which differ from those of the starting Yb(II) complex **(13)** by no more than 0.036 Å (*viz.* 2.497(12) and 2.507(12) Å in **(24)**, 2.485(2) and 2.471(2) Å in **(13)**). Close contacts were observed between the ytterbium centre and the proximal *i*-propyl CH hydrogen and the proximal DAB C_2H_2 hydrogen (Yb1-C41,H41 = 3.42_0, 3.13_2 Å; Yb1-C40,H40 = 3.73_4, 3.23_6 Å). The ^{1}H NMR spectrum of **(24)** in benzene-d_6 is essentially unchanged from that of the individual starting materials. The similarity between the ^{1}H NMR spectra of **(24)** and the starting materials confirmed the non-reduced nature of the 1,4-diazabuta-1,3-diene.

Complex **(24)** is soluble in toluene and benzene, forming green solutions from which the complex can be recovered by crystallisation from a hot solution or removal of solvent *in vacuo*. Dissolution in THF causes an immediate colour change from green to yellow, implying the reversal of Equation 7 and the formation of the starting Yb(II) complex **(13)**. This is best described as a non-redox based solvation equilibrium being forced back towards the mono-THF adduct starting material.

The effect of a further reduction in 1,4-diazabuta-1,3-diene bulk was investigated by reaction of *n*-BuDAB with [($Et_8N_4Me_2$)Yb(THF)], **(13)**. The addition of *n*-BuDAB in benzene-d_6 to two equivalents of **(13)** in toluene produced an immediate change in colour from yellow to green-brown. Evaporation of the solvent mixture under an inert atmosphere over 2 weeks gave brown crystals of [{($Et_8N_4Me_2$)Yb}$_2$(*n*-BuDAB)], **(25)**, suitable for X-ray crystal structure determination (Equation 12). No attempt was made to react [($Et_8N_4Me_2$)Yb(THF)], **(13)** and *n*-BuDAB in equimolar amounts to prepare the chelating 1:1 complex.

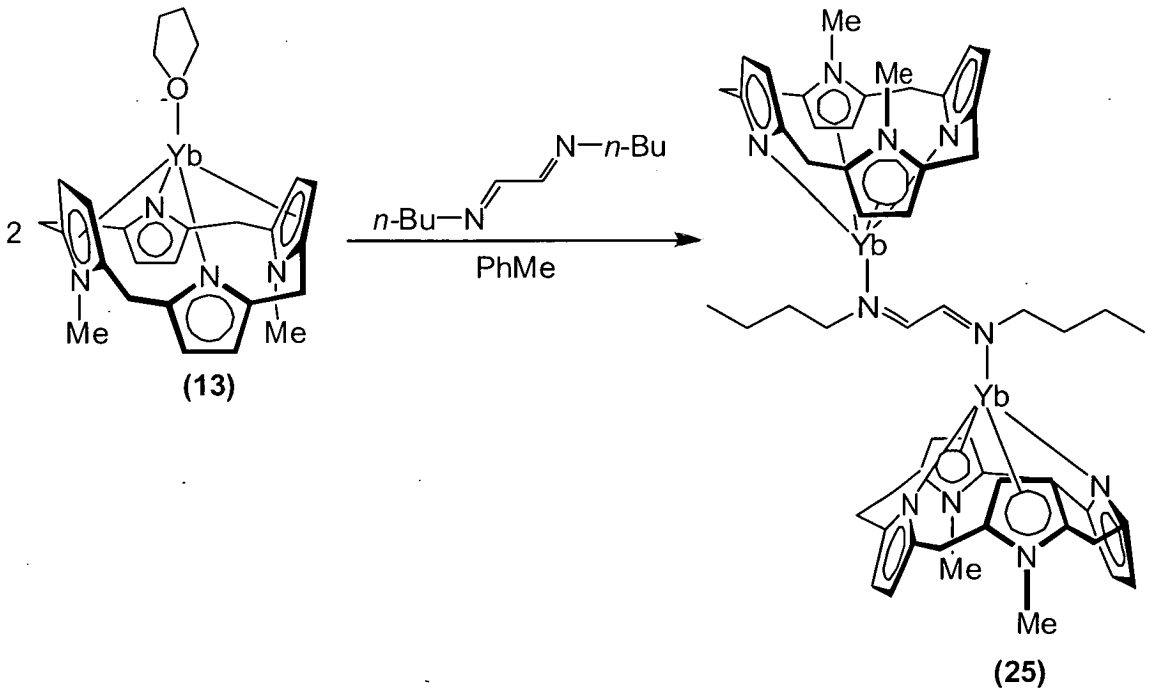

Equation 12

Attempts to repeat the reaction on large scale resulted in the formation of a crude product which resisted attempts at recrystallisation. As a result no yield was recorded, and the product was characterised by X-ray crystal structure determination alone. Analysis of the reaction mixture by ^{1}H NMR spectroscopy produced a spectrum containing very broadened resonances which roughly corresponded to the starting materials.

Similarly to [($Et_8N_4Me_2$)Yb(*i*-PrDAB)], **(24)**, the bond lengths within the *n*-BuDAB NCCN unit indicate it is bound as a neutral ligand, with each nitrogen σ-bound to a ytterbium centre as a Lewis basic donor. Unlike complex **(24)**, both nitrogens of the *n*-BuDAB ligand participate in coordination to a ($Et_8N_4Me_2$)Yb unit. The resulting binuclear complex contains Yb-N-C-C fragments which adopt *syn* arrangements, in contrast to the bridging Sm(III) complexes **(18)**, **(20)** and **(21)** featuring doubly reduced RDAB ligands, all of which feature *anti* arrangements of the corresponding Sm-N-C-C fragments.

Complex **(21)** is soluble in benzene-d_6 and toluene. Similarly to complex **(24)**, addition of THF to a toluene solution of complex **(25)** resulted in an immediate colour

change from green-brown to yellow, representing a reversal of the non-redox based solvation equilibrium (Equation 12).

3.3.1.4 Attempted synthesis of europium RDAB complexes

Europium lies directly beside samarium in the lanthanides and Eu(II) has an ionic radius very similar to that of Sm(II). Thus [($Et_8N_4Me_2$)Eu(THF)$_2$], **(15)**, would be expected to present effectively the same amount of coordination sphere to an incoming DAB molecule as the equivalent Sm(II) complex [($Et_8N_4Me_2$)Sm(THF)$_2$], **(12)**. However, Eu(II) is a much weaker reducing agent than Sm(II) (reduction potentials -0.35 V and -1.55 V vs NHE, respectively).[19] An attempted reaction between the Eu(II) precursor [($Et_8N_4Me_2$)Eu(THF)$_2$], **(15)**, and *t*-BuDAB was thus undertaken.

A solution of [($Et_8N_4Me_2$)Eu(THF)$_2$], **(15)**, in benzene-d_6 was added to a solution of *t*-BuDAB in benzene-d_6 on an NMR scale, producing no immediate visible sign of reaction. Partial removal of solvent *in vacuo* and standing at room temperature for 2 weeks produced yellow crystals of the mono-THF adduct [($Et_8N_4Me_2$)Eu(THF)], **(16)**, characterised by X-ray crystal structure determination. Resonances in the ^{1}H NMR spectrum of **(16)** were extremely broadened due to the paramagnetic Eu(II) centre, making assignment impossible; only free *t*-BuDAB was clearly identifiable in the ^{1}H NMR spectrum of the reaction mixture. The similarity between the ^{1}H NMR spectra of the starting materials and the reaction mixture also suggested no reaction had taken place.

Failure of *t*-BuDAB to react with the Eu(II) precursor constrasts with the formation of the Sm(III) complex [{($Et_8N_4Me_2$)Sm}$_2${*t*-BuDAB}], **(18)**, from the analogous Sm(II) precursor and *t*-BuDAB. The crystallisation of the mono-THF adduct **(16)** from the reaction mixture in preference to a *t*-BuDAB Lewis base adduct may be due to a solubility-driven equilibrium.

Addition of *i*-PrDAB to a solution of [($Et_8N_4Me_2$)Eu(THF)$_2$], **(15)**, in benzene-d_6 also produced no visible change in colour. ^{1}H NMR spectroscopy identified free *i*-PrDAB in the reaction mixture, indicating that reduction had not taken place. Similarly to *t*-BuDAB and *i*-PrDAB, addition of *n*-BuDAB to a solution of [($Et_8N_4Me_2$)Eu(THF)$_2$],

(15), resulted in no change in colour, and was presumed to indicate no reaction had taken place.

3.3.2 NMR spectroscopic characterisation of Sm(III) RDAB complexes

All resonances in the ^{1}H NMR spectra of [{($Et_8N_4Me_2$)Sm}$_2$(*t*-BuDAB)], **(18)**, and [($Et_8N_4Me_2$)Sm(*i*-PrDAB)], **(19)**, have been assigned *via* gCOSY, gHMQC and gHMBC experiments, Table 1. The bridging *i*-propyl complex [{($Et_8N_4Me_2$)Sm}$_2$(*i*-PrDAB)], **(20)**, had limited solubility in benzene-d_6 or THF-d_8 at room temperature, and a ^{1}H NMR spectrum collected over 14 h was too complex to allow confident assignment of macrocyclic or *i*-PrDAB protons. ^{13}C, gHMQC and gHMBC NMR experiments were attempted with complex **(20)** but provided no useful information due to low solubility. ^{1}H NMR spectroscopic analysis of reaction mixtures containing [{($Et_8N_4Me_2$)Sm}$_2$(*n*-BuDAB)], **(21)**, and the unsolvated Sm(II) dimer [{($Et_8N_4Me_2$)Sm}$_2$], **(22)**, did not allow confident assignment of resonances due to the presence of multiple species.

	pyrrolide CH	*N*-Me pyrrolyl CH	*N*-CH_3	CH_2 (*meso*-Et)	CH_3 (*meso*-Et)	RDAB =CH	RDAB R protons
(18)	6.12, 6.72	4.29, 5.66	7.00	0.51, 0.70 (2xCH_2), 1.13, 1.34, 1.87, 2.15 (2xCH_2)	-0.03, 0.05, 0.41, 0.61	11.06	2.54
(19)	6.68	12.58	13.42	1.52 (2xCH_2), 1.89, 4.25	-0.46, 1.95	-395.6	-19.26 (CH_3), 36.64 (CH)

Table 1: ^{1}H NMR spectroscopic data of [{($Et_8N_4Me_2$)Sm}$_2$(*t*-BuDAB)], **(18)** and [($Et_8N_4Me_2$)Sm(*i*-PrDAB)], **(19)** (benzene-d_6, 300 MHz, 298 K, ppm).

The ^{1}H and ^{13}C NMR spectra of **(18)** contain a greater number of macrocyclic resonances compared with **(19)**, consistent with a C_{2h} symmetric conformation. Thus the overall molecular conformation with respect to the *t*-BuDAB and macrocyclic units

observed in the solid state molecular structure of **(18)** persists in solution, and rotation about the Sm-N bonds in solution at room temperature can be excluded. The chelating complex **(19)** displays the more typical C_{2v} symmetry in solution.

The range of chemical shifts observed in the ^{1}H NMR spectrum of **(18)** (11.06 to -0.03 ppm) indicate the presence of only minimal paramagnetic effects, typical of those noted for other Sm(III) complexes of the $(Et_8N_4Me_2)^{2-}$ ligand system (*c.f.* chemical shift range of 42.19 to -21.07 ppm for the Sm(II) precursor $[(Et_8N_4Me_2)Sm(THF)_2]$, **(12)**). The wider range of chemical shifts for the macrocyclic protons of complex **(19)** (13.42 and -0.46 ppm) compared with **(18)** (7.00 to -0.03 ppm) is attributed to the presence of the radical anion in **(19)**.

The pyrrolide CH protons in each complex appeared as singlets in the region typical for aromatic protons (6.12 and 6.72 ppm in **(18)**, 6.68 ppm in **(19)**). However, the radical anionic nature of the *i*-PrDAB ligand in **(19)** causes the resonances of certain protons of the macrocyclic unit (including some not directly proximal) to appear at chemical shifts significantly different to those normally observed. The *N*-methylpyrrolyl CH singlets in complex **(18)** appear at 4.29 and 5.66 ppm, whilst the same protons in **(19)** appear further downfield at 12.58 ppm. Similarly, the *N*-CH_3 protons in **(19)** appeared at 13.42 ppm, compared with 7.00 ppm observed in the spectrum of **(18)**. The effect is less marked in the case of the *meso*-ethyl protons. The *meso*-ethyl CH_2 protons appeared as multiplets or broadened resonances within the range of 0.51 - 2.15 ppm in **(18)**, and were observed within the range 1.52 - 4.25 ppm in **(19)**. The *meso*-ethyl CH_3 triplets in **(18)** appear over the region of -0.03 to 0.61 ppm whilst those in **(19)** were observed at -0.46 and 1.95 ppm.

The DAB =CH protons in complex **(18)** were observed as a singlet at 11.06 ppm, whilst the *t*-butyl CH_3 protons were observed as a broadened singlet at 2.54 ppm. The presence of the radical anion in **(19)** resulted in a paramagnetic shift of the DAB =CH protons, which were observed as a singlet at -395.6 ppm (integration = 2H). The chemical shift of this resonance is in keeping with extreme upfield shifts associated with radical anionic DAB =CH protons reported for other Ln(III) complexes, *e.g.* $[(C_5Me_5)Yb(i\text{-PrDAB})]$ (-28.3 ppm),[20] $[(t\text{-BuDAB})_3Nd]$ (-171.6 ppm), $[(t\text{-BuDAB})_3Sm]$ (-222.3 ppm)[6] and $[(C_8H_6(SiMe_3)_2)Sm(t\text{-BuDAB})(THF)]$ (-182, -226 ppm).[8]

The paramagnetic shifts of the *i*-propyl CH and CH_3 protons in **(19)** were less extreme, appearing as singlets at 36.64 and -19.26 ppm, respectively.

^{13}C NMR spectra were collected for complexes **(18)** and **(19)**, but not for complex **(20)**, again due to its poor solubility in benzene-d_6 and THF-d_8. The data is summarised in Table 2. The four sets of chemically inequivalent *meso*-CH_3 carbons in **(18)** appear as two resonaces at 8.0 and 8.3 ppm, whilst the two sets of inequivalent *meso*-CH_3 carbons appear at 8.6 and 10.0 ppm in **(19)**. The pyrrolide =CH resonances were observed at 101.1, 101.9 ppm **(18)** and 100.0 ppm **(19)**, whilst the pyrrolide quaternary carbons appear at 148.1, 149.4 ppm **(18)** and 149.5 ppm **(19)**.

There are significant differences in ^{13}C chemical shifts of carbons within the *N*-methylpyrrolyl units and *meso*-CH_2 groups of the two complexes which can be attributed to the effect of the radical anion in the chelating 1:1 complex **(19)**. The *N*-methylpyrrolyl and upper *meso*-CH_2 groups are in the vicinity of the radical anion, and their chemical shifts therefore experience the greatest changes. Resonances corresponding to carbons of the *i*-PrDAB radical anion in **(19)** were not observed in either wide sweep width ^{13}C or heteronuclear 2D NMR experiments, presumably due to paramagnetic line broadening caused by the radical anion.

The ^{13}C NMR spectra of complexes **(18)** and **(19)** were partially assigned (except for *i*-PrDAB resonances) by gHMQC and gHMBC NMR spectroscopy. The *N*-methylpyrrolyl aromatic protons were distinguished from pyrrolide aromatic protons by observation of a $^3J_{CH}$ correlation from the *N*-CH_3 carbon to the *N*-methylpyrrolyl quaternary carbon and a $^2J_{CH}$ correlation between the aromatic protons and the same carbon. The *meso*-ethyl quaternary carbon was assigned according to $^2J_{CH}$ and $^3J_{CH}$ coupling to the *meso*-CH_2 and *meso*-CH_3 groups, respectively.

	Pyrrolide =CH	Pyrrolide quaternary C	*N*-MePyrrolyl =CH	*N*-MePyrrolyl quaternary C	*N*-CH_3
(18)	101.1, 101.9	148.1, 149.4	99.7, 100.8	136.5, 138.7	38.2
(19)	100.0	149.5	159.6	107.4	14.4

	meso-CH_2	*meso*-CH_3	*meso*-CH_3 quaternary C	RDAB =CH	RDAB R
(18)	22.0, 22.5, 28.9, 29.4	8.0, 8.3	43.5, 44.5	125.6	7.4, 69.6
(19)	18.2, 37.6	8.6, 10.0	47.9	Not observed	Not observed

Table 2: ^{13}C NMR spectroscopic data of [{($Et_8N_4Me_2$)Sm}$_2$(*t*-BuDAB)], **(18)** and [($Et_8N_4Me_2$)Sm(*i*-PrDAB)], **(19)** (benzene-d_6, 75 MHz, 298 K, ppm).

3.3.3 Molecular structures

3.3.3.1 Molecular structures of [($Et_8N_4Me_2$)Eu(THF)$_2$], (15), and [($Et_8N_4Me_2$)Eu(THF)], (16)

Yellow crystals of [($Et_8N_4Me_2$)Eu(THF)$_2$], **(15)**, suitable for X-ray crystal structure determination were grown by slow cooling of a hot, concentrated THF solution to ambient temperature which was then allowed to stand at -20 °C overnight. The crystals belong to the orthorhombic space group *Pbcn* (No. 60), a = 21.422(4), b = 10.646(2), c = 18.569(4) Å, with 4 molecules in the unit cell, the asymmetric unit consisting of half a molecule of [($Et_8N_4Me_2$)Eu(THF)$_2$], **(15)**, residing on a crystallographic C_2 axis. The molecule has approximate C_{2v} symmetry, except for the orientations of the THF molecules and a minor twist in the macrocycle. The structure of **(15)** is shown in Figure 5.

Yellow crystals of [($Et_8N_4Me_2$)Eu(THF)], **(16)**, suitable for X-ray crystal structure determination were grown by standing a concentrated solution of **(15)** in

benzene-d_6 for 2 weeks at room temperature. The crystals belong to the monoclinic space group *C2/c* (No. 15), a = 39.698(8), b = 11.060(2), c = 21.190(4) Å, β = 118.21(3) °, with 8 molecules in the unit cell, the asymmetric unit consisting of one molecule of [($Et_8N_4Me_2$)Eu(THF)], **(16)**, and one half of a molecule of benzene residing on a crystallographic C_2 axis. The molecule has approximate C_{2v} symmetry, except for the orientation of the THF molecule. The molecular structures are shown in Figure 5.

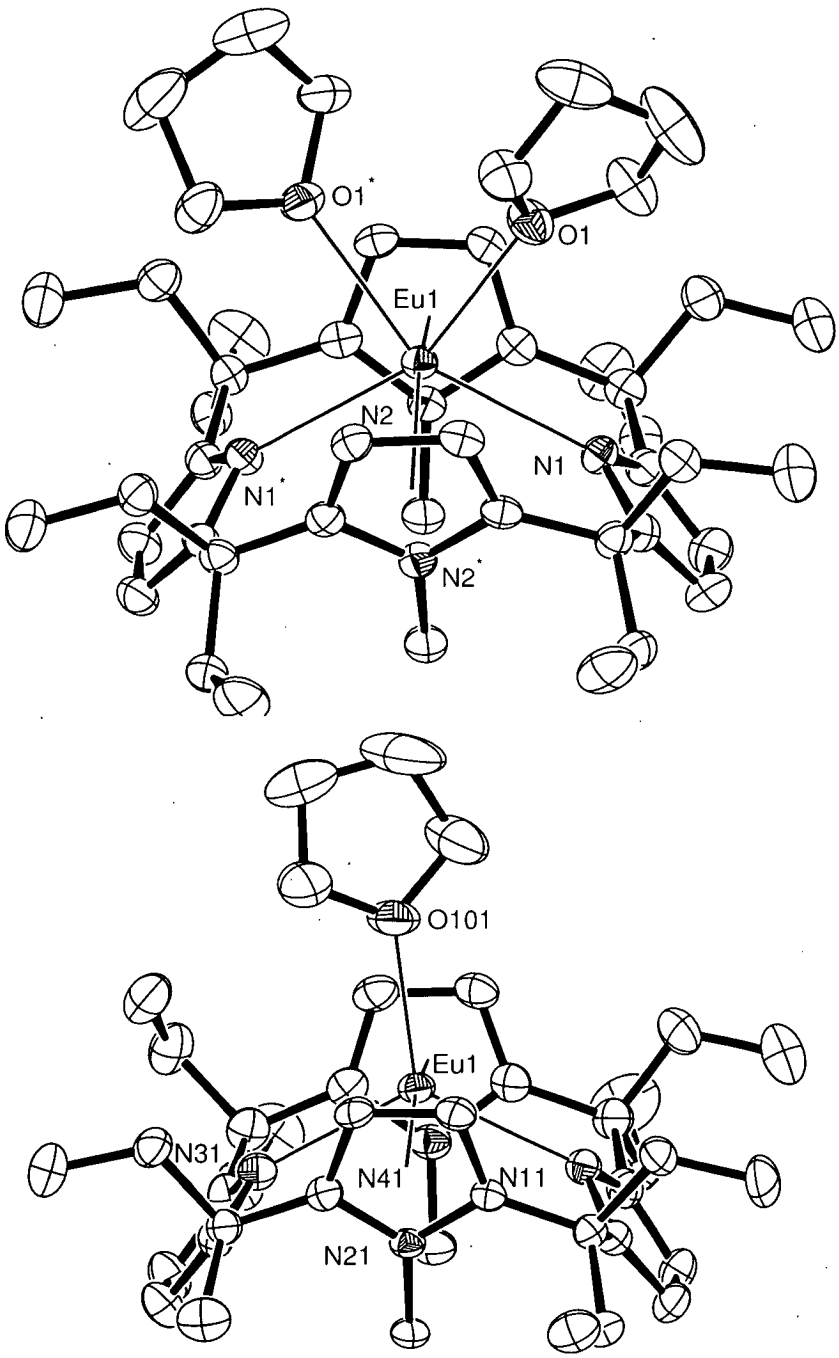

Figure 5: Molecular structure of [($Et_8N_4Me_2$)Eu($THF)_2$], **(15)** (above) and [($Et_8N_4Me_2$)Eu(THF)], **(16)** (below) with thermal ellipsoids drawn at the level of 50% probability (protons removed for clarity).

The macrocyclic units in both **(15)** and **(16)** adopt 1,3-alternate conformations, and the Eu centres display $\eta^1:\eta^5:\eta^1:\eta^5$ binding modes to the pyrrolide and *N*-methylpyrrolyl units alternately. The *N*-methyl groups extend downwards and block access to the metal from the bottom of the cavity, Figure 6(a)), and THF molecules bind to the remaining coordination sphere at the top, Figure 6(b).

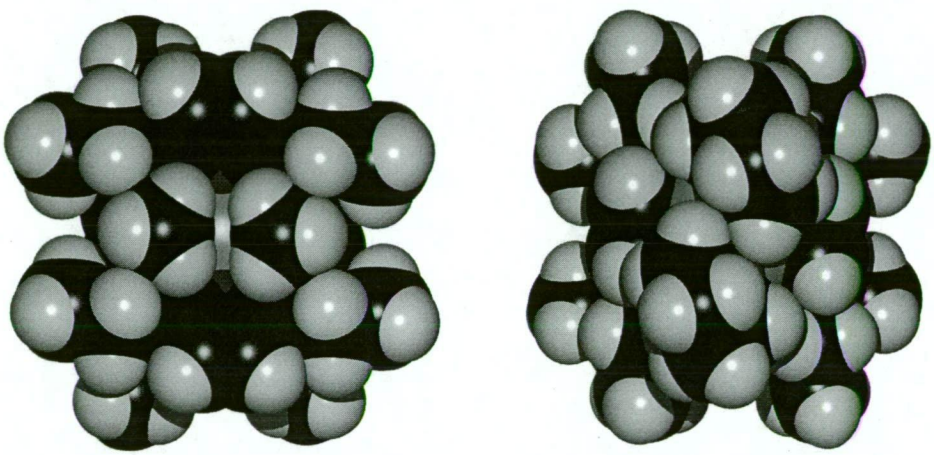

(a) (b)

Figure 6: Space filling representations of the molecular structure of $[(Et_8N_4Me_2)Eu(THF)_2]$, **(15)**, (a) viewed from the direction of two *N*-methylpyrrole groups; (b) viewed down the bisector of the O-Sm-O angle.

Complex **(15)** contains two coordinated THF molecules, and **(16)** only one. The degree of solvation bears only minor influence on the conformation of the macrocyclic skeleton. The quantitative differences in the molecular structures of the two complexes are attributable to the steric interaction between coordinated THF molecule(s) and the macrocycle, and also to the difference in electronic saturation around the Sm centre. The decrease in ionic radius for a reduction of 1 coordination number has been determined in a crystallographic survey of Eu(II) compounds to be *ca.* 3.7% (1.35 Å to 1.30 Å from coordination number 10 to 9).[21] The Eu-N(pyrrolide) and Eu-O bond lengths in **(15)** are longer than those observed in **(16)** by 3.1 – 5.2 %, consistent with a reduction in coordination number from 10 in the bis(THF) adduct **(15)** to 9 in mono(THF) adduct **(16)**.

The Eu centres in **(15)** and **(16)** are σ-bound to the pyrrolide nitrogen centres with Eu-N distances of 2.665(3) Å **(15)** and 2.561(2) Å, 2.584(2) Å **(16)**. The distance between the Eu centre and *N*-methylpyrrolyl ring centroid is longer in **(15)** (2.75_7 Å) than **(16)** (2.69_8 Å and 2.70_3 Å). Likewise, the Eu-O(THF) bond distances in **(15)** (2.659(2) Å) are longer than than **(16)** (2.528(2) Å). The consistently shorter Eu-C/N/O bond lengths observed in the mono-THF adduct, **(16)**, are consistent with the lesser degree of electronic saturation in the less ligated complex.

The metallocene bend angle of modified porphyrinogen complexes is defined as the angle between the lanthanide centre and the *N*-methypyrrolyl centroids. The bend angle in the bis-(THF) adduct **(15)** ($154.1_8°$) is more acute compared to that observed in the mono-THF adduct **(16)** ($162.7_0°$). The N(pyrrolide)-Eu-N(pyrrolide) angle of 119.20(11)° in **(15)** increases to $124.8_0°$ with the removal of one THF in **(16)**, indicating that the Eu centre sits further down inside the cavity in **(16)**. This corroborates with the decreased Sm-N bond lengths observed in the mono-THF adduct **(16)**.

The position of the europium centre deeper within the cavity in **(16)** is also demonstrated by the tilt angles of the pyrrolide and *N*-methylpyrrolyl rings with respect to the macrocyclic plane. The tilt angle is defined as the angle between a heterocycle ring plane and the macrocyclic plane (the macrocyclic plane being defined as the least-squares fit to the four *meso*- carbons of the macrocycle). These terms are displayed graphically in Figure 7.

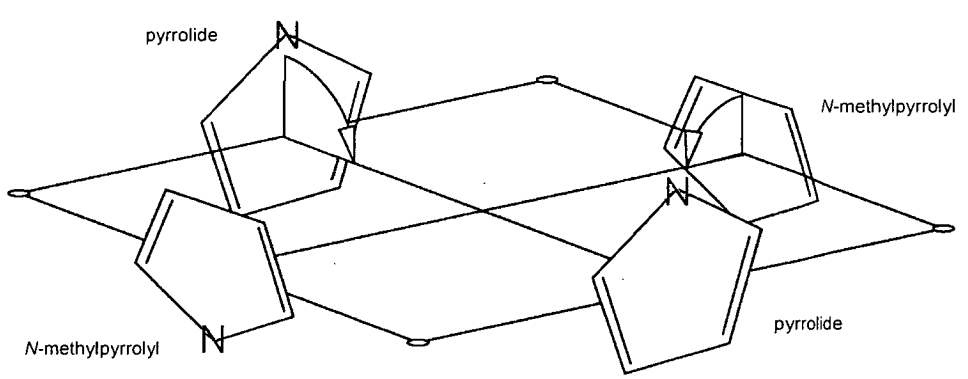

Figure 7: Graphical representation of macrocyclic ring tilt angles in $(Et_8N_4Me_2)^{2-}$ macrocycle.[15]

Compared to the tilt angles in the mono-THF adduct **(16)**, the *N*-methylpyrrolyl rings in the bis-(THF) adduct **(15)** are splayed slightly further backwards towards the macrocyclic plane. The *N*-methylpyrrolyl ring tilt angles in **(15)** are $73.2_6°$, whilst those in **(16)** are $75.7_0°$ and $77.2_1°$. The europium centre in **(15)** lies slightly further out of the macrocyclic plane, hence requiring the *N*-methylpyrrolyl rings to splay backwards to optimise the η^5 interaction between the metal and the ring π-electrons. The deeper position of the europium centre with respect to the macrocyclic cavity in the mono-(THF) adduct **(16)** is also reflected in the tilt angle of the pyrrolide rings. The pyrrolide ring tilt angles in **(15)** are $50.4_4°$, whilst those in **(16)** are $52.9_4°$ and $55.5_5°$. The tilt angles in **(16)** are larger as the pyrrolide rings splay away from the deeper residing metal centre.

Similar trends are observed in the isostructural and isomorphous Sm(II) complexes $[(Et_8N_4Me_2)Sm(THF)]$, **(17)**, and $[(Et_8N_4Me_2)Sm(THF)_2]$, **(12)**.[15,22] The bond lengths and ring tilt angles are very similar between each analogous complex. The data presented above for **(15)** and **(16)** are listed in Table 3 alongside the Sm(II) complexes **(12)** and **(17)**.

	(12)	**(17)**	**(15)**	**(16)**
Ln-N(pyrrolide)	2.6671(16)	2.556(3), 2.565(2)	2.665(3)	2.561(2), 2.584(2)
Ln-centroid(*N*-Mepyrrolyl)	2.75_6	2.66_8, 2.66_8	2.75_7	2.69_8, 2.70_3
Ln-O(THF)	2.6552(14)	2.543(3)	2.659(2)	2.528(2)
N(pyrrolide)-Ln-N(pyrrolide) angle	120.03(7)	125.48(9)	119.20(11)	124.8_0
Metallocene bend angle	154.4_4	163.7_0	154.1_8	162.7_0
Pyrrolide ring tilt angle	50.3_7	49.4_7, 55.5_9	50.4_4	52.9_4, 55.5_5
N-Mepyrrolyl ring tilt angle	70.0_3	77.8_4, 78.2_8	73.2_6	75.7_0, 77.2_1

Table 3: Selected bond lengths (Å) and angles (°) for $[(Et_8N_4Me_2)Sm(THF)_2]$, **(12)**, $[(Et_8N_4Me_2)Sm(THF)]$, **(17)**, $[(Et_8N_4Me_2)Eu(THF)_2]$, **(15)**, and $[(Et_8N_4Me_2)Eu(THF)]$, **(16)**.

3.3.3.2 Molecular structures of [{($Et_8N_4Me_2$)Sm}$_2$(*t*-BuDAB)], (18), [($Et_8N_4Me_2$)Sm(*i*-PrDAB)], (19), [{($Et_8N_4Me_2$)Sm}$_2$(*i*-PrDAB)], (20), and [{($Et_8N_4Me_2$)Sm}$_2$(*n*-BuDAB)], (21)

Green crystals of [{($Et_8N_4Me_2$)Sm}$_2$(*t*-BuDAB)], **(18)**, suitable for X-ray crystal structure determination were grown by slow cooling of a hot, concentrated toluene solution to ambient temperature. The crystals belong to the triclinic space group *P*1 (No. 2), a = 14.6994(4), b = 17.0733(5), c = 18.7037(6) Å, α = 113.7890(10) °, β = 93.1120(10) °, γ = 95.3020(10) °, with 2 molecules in the unit cell, the asymmetric unit consisting of 1 molecule of [{($Et_8N_4Me_2$)Sm}$_2${*t*-BuDAB}], **(18)**. The molecule has approximate C_{2h} symmetry. The structure of **(18)** is shown in Figure 8.

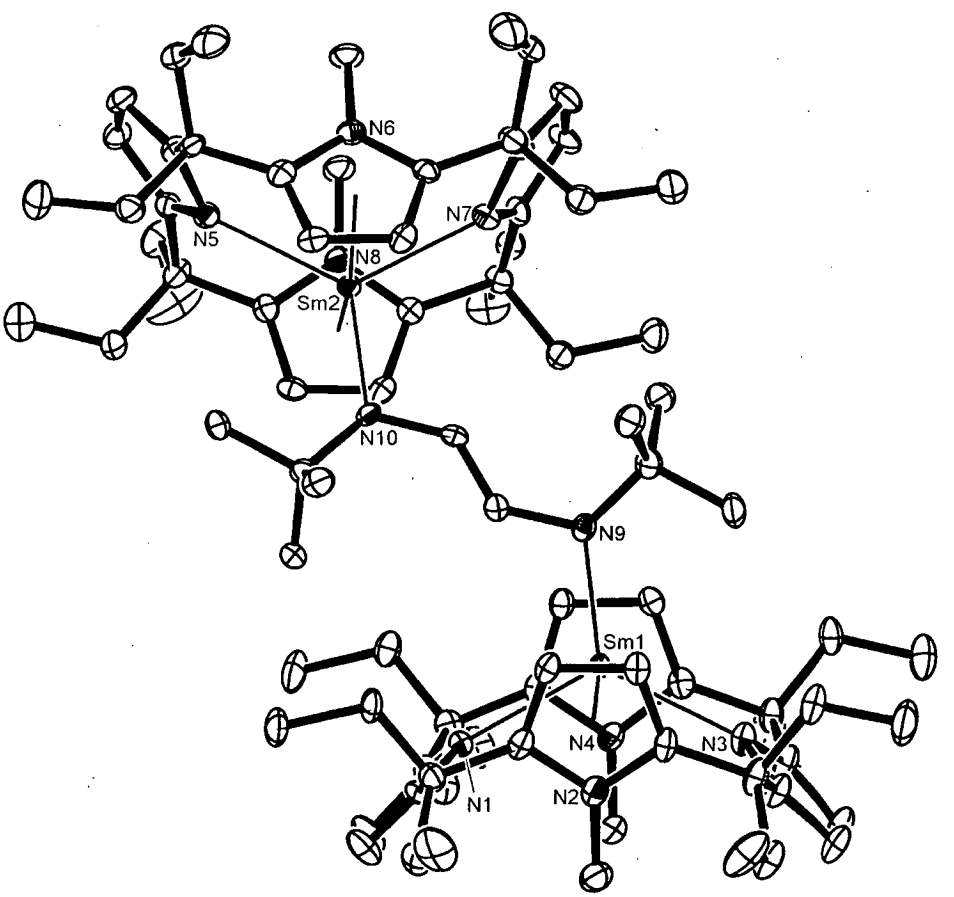

Figure 8: Molecular structure of [{($Et_8N_4Me_2$)Sm}$_2${*t*-BuDAB}], **(18)**, with thermal ellipsoids drawn at the level of 50% probability (protons removed for clarity).

Orange-brown crystals of [($Et_8N_4Me_2$)Sm(*i*-PrDAB)], **(19)**, suitable for X-ray crystal structure determination were grown by evaporation of a concentrated solution in benzene-d_6 over 8 days. The crystals belong to the triclinic space group *P*1 (No. 2), a = 9.933(2), b = 12.573(3), c = 19.020(4) Å, α = 85.53(3) °, β = 84.48(3) °, γ = 67.26(3) °, with 2 molecules in the unit cell, the asymmetric unit consisting of 1 molecule of [($Et_8N_4Me_2$)Sm(*i*-PrDAB)], **(19)**. The molecule has approximate C_{2v} symmetry. The structure of **(19)** is shown in Figure 9.

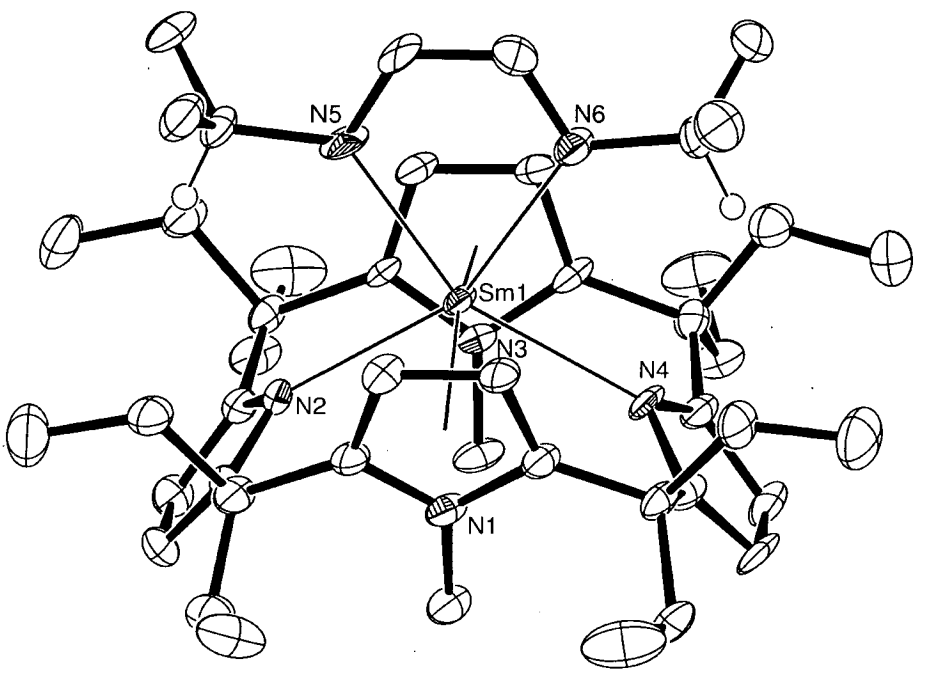

Figure 9: Molecular structure of [($Et_8N_4Me_2$)Sm(*i*-PrDAB)], **(19)**, with thermal ellipsoids drawn at the level of 50% probability (all except *i*-propyl methine protons removed for clarity).

Green crystals of [{($Et_8N_4Me_2$)Sm}$_2$(*i*-PrDAB)], **(20)**, suitable for X-ray crystal structure determination were grown directly from the reaction of [($Et_8N_4Me_2$)Sm(*i*-PrDAB)], **(19)**, with [($Et_8N_4Me_2$)Sm(THF)$_2$], **(12)**, in toluene solution by slow cooling of the reaction mixture from 110 °C to ambient temperature. The crystals belong to the triclinic space group *P*1 (No. 2), a = 14.8664(5), b = 16.5364(5), c = 18.7793(5) Å, α = 114.512(2) °, β = 91.984(2) °, γ = 94.824(2) °, with 2 molecules in the unit cell, the asymmetric unit consisting of 1 molecule of [{($Et_8N_4Me_2$)Sm}$_2$(*i*-PrDAB)], **(20)**. The molecule has approximate C_{2h} symmetry and the structure of **(20)** is shown in Figure 10.

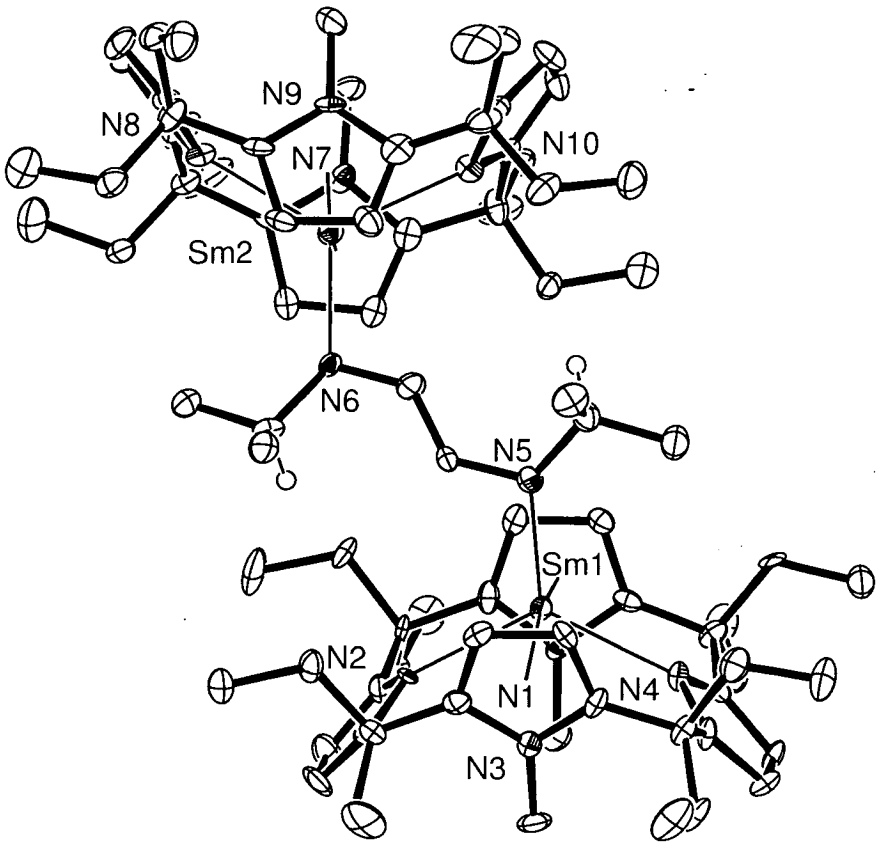

Figure 10: Molecular structure of [{($Et_8N_4Me_2$)Sm}$_2$(*i*-PrDAB)], **(20)**, with thermal ellipsoids drawn at the level of 50% probability (all except *i*-propyl methine protons removed for clarity).

Green crystals of [{($Et_8N_4Me_2$)Sm}$_2$(*n*-BuDAB)], **(21)**, suitable for X-ray crystal structure determination were grown directly from the reaction of *n*-BuDAB with [($Et_8N_4Me_2$)Sm(THF)$_2$], **(12)**, in a toluene/benzene-d_6 solution by slow cooling of the reaction mixture from 110 °C and standing at room temperature for 2 d. The crystals belong to the monoclinic space group $P2_1/n$ (No. 14), a = 12.1546(4), b = 21.8141(8), c = 32.6673(12) Å, β = 95.273(2) °, with 4 molecules in the unit cell, the asymmetric unit consisting of 1 molecule of [{($Et_8N_4Me_2$)Sm}$_2$(*n*-BuDAB)], **(18)**. The molecule has approximate C_{2h} symmetry. The structure of **(21)** is shown in Figure 11.

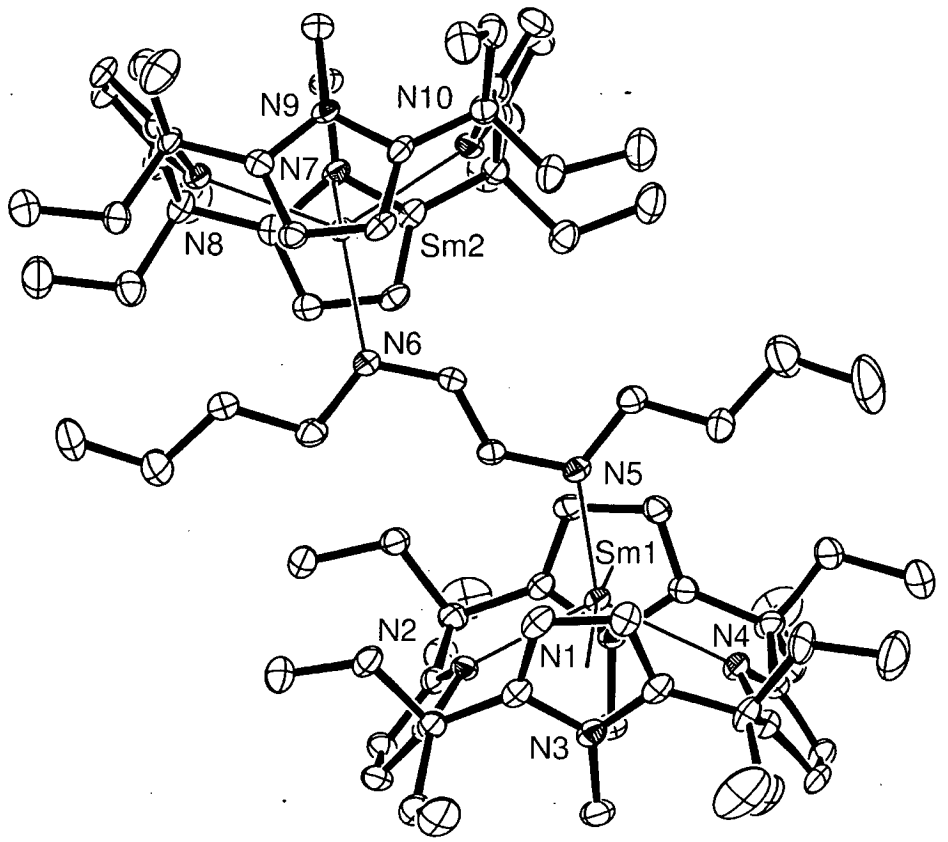

Figure 11: Molecular structure of [{($Et_8N_4Me_2$)Sm}$_2$(*n*-BuDAB)], **(21)**, with thermal ellipsoids drawn at the level of 50% probability (protons removed for clarity).

The macrocyclic units in each of the complexes **(18)**, **(19)**, **(20)** and **(21)** display 1,3-alternate conformations with the Sm centres bound to the macrocycle in η^1:η^5:η^1:η^5-fashion. The structures of the three binuclear DAB complexes **(18)**, **(20)** and **(21)** are very similar, featuring bridging dianionic DAB ligands binding through each nitrogen to a Sm centre. The DAB Sm-N-C-C fragments in complexes **(18)**, **(20)** and **(21)** display *anti* arrangements. The mononuclear *i*-PrDAB complex **(19)** contains a single radical anionic *i*-PrDAB unit bound through both nitrogens to a single Sm centre.

The Sm-N(pyrrolide) bond lengths of the three bridging RDAB complexes decrease with decrease in R bulk, *viz.* R = *t*-Bu **(18)**: 2.504(3)-2.545(3) Å, R = *i*-Pr **(20)**: 2.503(6)-2.511(6) Å, R = *n*-Bu **(21)**: 2.466(3)-2.500(3) Å. The Sm-centroid(pyrrolyl) bond distances follow a similar trend: **(18)**: 2.64_0-2.69_6 Å, **(20)**: 2.64_4-2.66_9 Å, **(21)**: 2.62_6-2.64_7 Å. The Sm-N(pyrrolide) bond lengths in the mononuclear chelating *i*-Pr complex **(19)** are 2.588(7) and 2.590(7) Å, whilst the Sm-centroid(pyrrolyl) bond

distances are 2.68_0 and 2.69_7 Å. The longer bond lengths observed in complex **(19)** are due to the chelating binding mode of the DAB ligand.

The metallocene bend angles of the bridging RDAB complexes increase with decreasing R bulk, *viz.* R = *t*-Bu **(18)**: 161.5_3, 161.5_4 °, R = *i*-Pr **(20)**: 163.2_6, 163.2_8 °, R = *n*-Bu **(21)**: 165.5_2, 166.3_6 °. Similarly, N(pyrrolide)-Sm-N(pyrrolide) angles increase with decreasing R bulk across the bridging complexes, *viz.* R = *t*-Bu **(18)**: 121.71(10), 123.12(11) °, R = *i*-Pr **(20)**: 122.9(2), 123.9(2) °, R = *n*-Bu **(21)**: 124.05(8), 125.24(8) °. The chelating *i*-PrDAB complex **(19)** displays a more acute metallocene bend angle (156.7_3 °) than the analogous bridging complex **(20)**. The N(pyrrolide)-Sm-N(pyrrolide) angle in complex **(19)** (117.4(2) °) is also more acute than that observed in **(20)**. The longer bond lengths and more acute metallocene and N(pyrrolide)-Sm-N(pyrrolide) bend angles observed in the chelating complex **(19)** imply the samarium centre resides less deep within the macrocyclic cavity than in the bridging complexes **(18)**, **(20)** and **(21)**, due to the effect of the DAB ligand attempting to attain its ideal chelating geometry. The abovementioned bond lengths and angles are summarised in Table 4.

	(18)	**(20)**	**(21)**	**(19)**
Sm-N(pyrrolide) bond lengths	2.504(3), 2.520(3), 2.542(3), 2.545(3)	2.503(6), 2.508(5), 2.508(6), 2.511(6)	2.466(3), 2.472(3), 2.490(3), 2.500(3)	2.588(7), 2.590(7)
Sm-centroid(pyrrolyl) bond lengths	2.64_0, 2.65_4, 2.66_6, 2.69_6	2.64_4, 2.64_8, 2.65_6, 2.66_9	2.62_6, 2.63_0, 2.63_9, 2.64_7	2.68_0, 2.69_7
Metallocene bend angles	161.5_3, 161.5_4	163.2_6, 163.2_8	165.5_2, 166.3_6	156.7_3
N(pyrrolide)-Sm-N(pyrrolide) angles	121.71(10), 123.12(11)	122.9(2), 123.9(2)	124.05(8), 125.24(8)	117.4(2)

Table 4: Selected bond lengths (Å) and angles (°) for complexes [{($Et_8N_4Me_2$)Sm}$_2$(*t*-BuDAB)], **(18)**, [($Et_8N_4Me_2$)Sm(*i*-PrDAB)], **(19)**, [{($Et_8N_4Me_2$)Sm}$_2$(*i*-PrDAB)], **(20)**, and [{($Et_8N_4Me_2$)Sm}$_2$(*n*-BuDAB)], **(21)**.

The tilt angles of the macrocyclic pyrrolide rings in bridging DAB complexes **(18)**, **(20)** and **(21)** tend to increase with decreasing RDAB bulk, *viz.* R = *t*-Bu **(18)**: 45.1_0-53.8_2 °, R = *i*-Pr **(20)**: 47.8_0-54.7_1 °, R = *n*-Bu **(21)**: 49.0_9-54.6_5 °. Similarly, the tilt angles of the *N*-methylpyrrolyl rings of the bridging complexes tend to increase with decreasing R size, *viz.* R = *t*-Bu **(18)**: 77.0_5-78.9_5 °, R = *i*-Pr **(20)**: 78.1_0-79.3_7 °, R = *n*-Bu **(21)**: 79.1_3-81.6_7 °. The chelating *i*-PrDAB complex **(19)** displays pyrrolide ring tilt angles of 51.2_3 and 51.4_1 °; these fall within the same range observed for the bridging *i*-PrDAB complex **(20)**. The *N*-methylpyrrolyl ring tilt angles of 77.5_6 and 77.6_9 ° in **(19)** are slightly lower than those observed in the analogous bridging complex. The ring tilt angles of the four complexes are listed in Table 5.

	(18)	**(20)**	**(21)**	**(19)**
Pyrrolyl ring tilt angles	45.1_0, 46.9_3, 52.1_5, 53.8_2	47.8_0, 48.0_5, 50.4_0, 54.7_1	49.0_9, 52.6_2, 52.7_9, 54.6_5	51.2_3, 51.4_1
N-methylpyrrolyl ring tilt angles	77.0_5, 78.1_5, 78.4_7, 78.9_5	78.1_0, 78.5_0, 79.1_8, 79.3_7	78.1_0, 78.5_4, 79.1_8, 79.3_7	77.5_6, 77.6_9

Table 5: Pyrrolide and *N*-methylpyrrolyl ring tilt angles (°) for complexes [{($Et_8N_4Me_2$)Sm}$_2$(*t*-BuDAB)], **(18)**, [($Et_8N_4Me_2$)Sm(*i*-PrDAB)], **(19)**, [{($Et_8N_4Me_2$)Sm}$_2$(*i*-PrDAB)], **(20)**, and [{($Et_8N_4Me_2$)Sm}$_2$(*n*-BuDAB)], **(21)**.

3.3.3.3 Molecular structure of [{($Et_8N_4Me_2$)Sm}$_2$], (22)

Green crystals of [{($Et_8N_4Me_2$)Sm}$_2$], **(22)**, suitable for X-ray crystal structure determination were grown from the reaction of *n*-BuDAB with [($Et_8N_4Me_2$)Sm(THF)$_2$], **(12)** (see Section 3.3.1.2 for details). The crystals belong to the triclinic space group *P*1 (No. 2), a = 12.0933(7), b = 12.9794(9), c = 13.0864(12), α = 63.691(3) °, β = 85.002(5) °, γ = 67.565(4) °, with 1 molecule in the unit cell, the asymmetric unit consisting of half a molecule of **(22)**. The molecular symmetry is crystallographically C_i and the structure of **(22)** is shown in Figure 12.

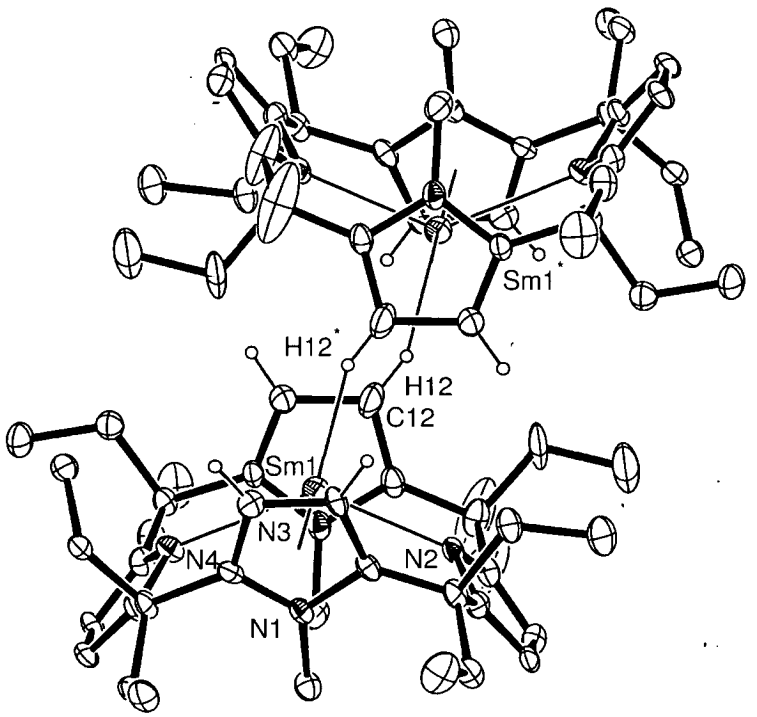

Figure 12: Molecular structure of $[\{(Et_8N_4Me_2)Sm\}_2]$, **(22)**, with thermal ellipsoids drawn at the level of 50% probability (all except *N*-methylpyrrolyl β-hydrogens removed for clarity).

Although the poor quality of the refined structure precludes a detailed quantitative analysis of the molecular structure of **(22)**, the connectivity has been established and a qualitative discussion of the structure is presented below. The samarium centres in the molecular structure of $[\{(Et_8N_4Me_2)Sm\}_2]$, **(22)**, are bound within the macrocycle cavity in the usual $\eta^1:\eta^5:\eta^1:\eta^5$ binding bode. Each samarium centre is bound to an *N*-methylpyrrolyl β-hydrogen on the facing macrocycle, and the binding grooves of each $(Et_8N_4Me_2)Sm$ fragment are interlocked, Figure 13. Critically, the possibility of metallation of the *N*-methylpyrrolyl groups by the Sm centre is ruled out by the distance between each Sm centre and the facing *N*-methylpyrrolyl β-hydrogen (Sm···H = 2.2_0 Å) and β-carbon (Sm···C = 3.0_7 Å). These long distances also exclude the possibility of "*N*-confusion" in the macrocyclic skeleton giving rise to Sm···N(pyrrolide) interactions (see Chapter 7.3.1).

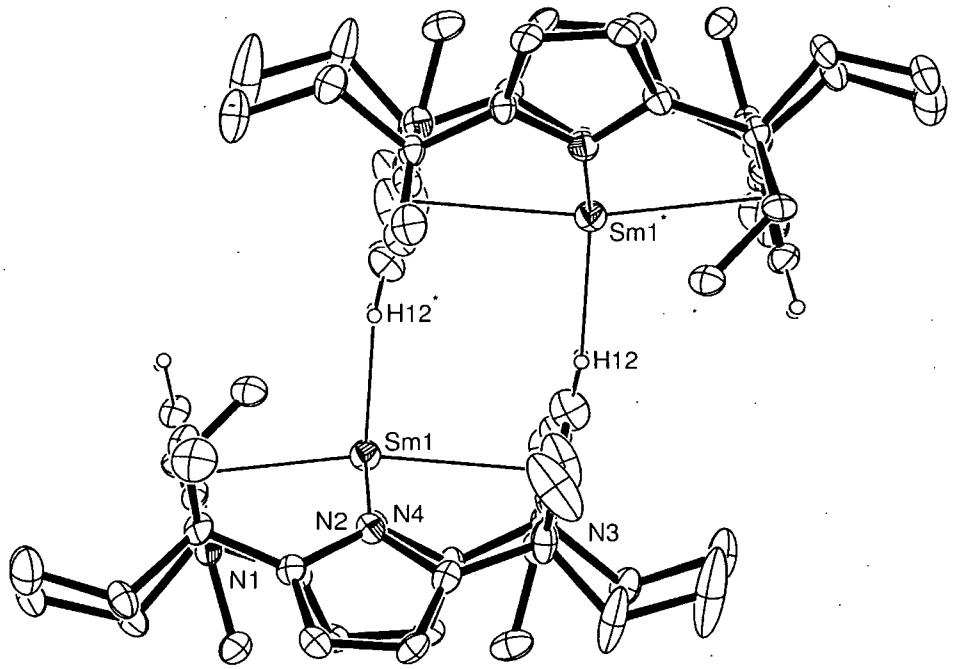

Figure 13: Molecular structure of [{($Et_8N_4Me_2$)Sm}$_2$], **(22)**, looking along the interlocked binding grooves. Thermal ellipsoids drawn at the level of 50% probability (all except *N*-methylpyrrolyl β-hydrogens removed for clarity).

3.3.3.4 Molecular structures of [($Et_8N_4Me_2$)Yb(*i*-PrDAB)], (24), and [{($Et_8N_4Me_2$)Yb}$_2$(*n*-BuDAB)], (25)

Emerald green crystals of [($Et_8N_4Me_2$)Yb(*i*-PrDAB)], **(24)**, suitable for X-ray crystal structure determination were grown by evaporation of a solution of the title compound in benzene-d_6 over 11 days. The crystals belong to the triclinic space group *P*1 (No. 2), a = 10.743(2), b = 11.817(2), c = 18.106(4) Å, α = 77.47(3) °, β = 84.82(3) °, γ = 79.56(3) °, with 2 molecules in the unit cell, the asymmetric unit consisting of 1 molecule of [($Et_8N_4Me_2$)Yb(*i*-PrDAB)], **(24)**. The molecule has approximate C_s symmetry. The structure of **(24)** is shown in Figure 14.

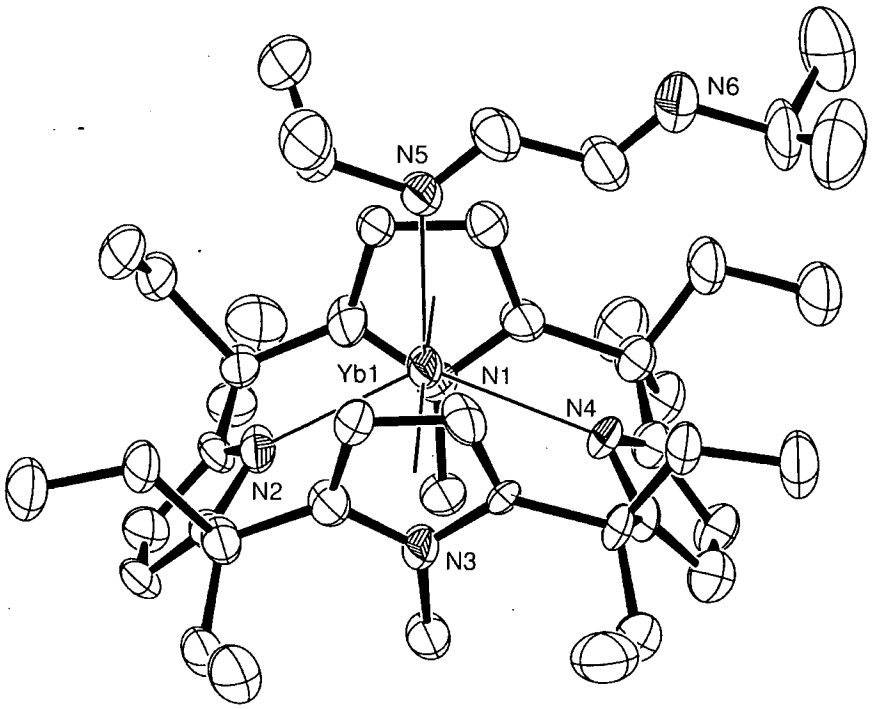

Figure 14: Molecular structure of [($Et_8N_4Me_2$)Yb(*i*-PrDAB)], **(24)**, with thermal ellipsoids drawn at the level of 50% probability (protons removed for clarity).

Brown crystals of [{($Et_8N_4Me_2$)Yb}$_2$(*n*-BuDAB)], **(25)**, suitable for X-ray crystal structure determination were grown by evaporation of a solution of the title compound in toluene/benzene-d_6 over 11 days. The crystals belong to the monoclinic space group *C*2/*c* (No. 15), a = 55.0910(4), b = 16.1262(2), c = 22.4357(4) Å, β = 103.9370(10) °, with 8 molecules in the unit cell, the asymmetric unit consisting of 2 half molecules of [{($Et_8N_4Me_2$)Yb}$_2$(*n*-BuDAB)], **(25)** lying on inversion centres. The molecule has approximate C_{2h} symmetry. The structures of each of the two crystallographically independent molecules of **(25)** are shown in Figure 15.

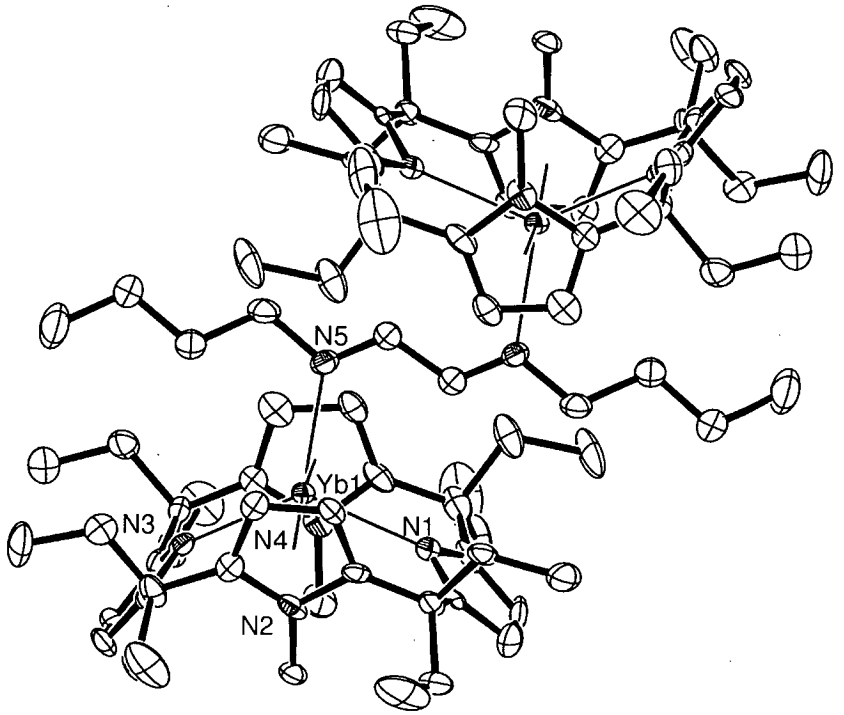

(1)

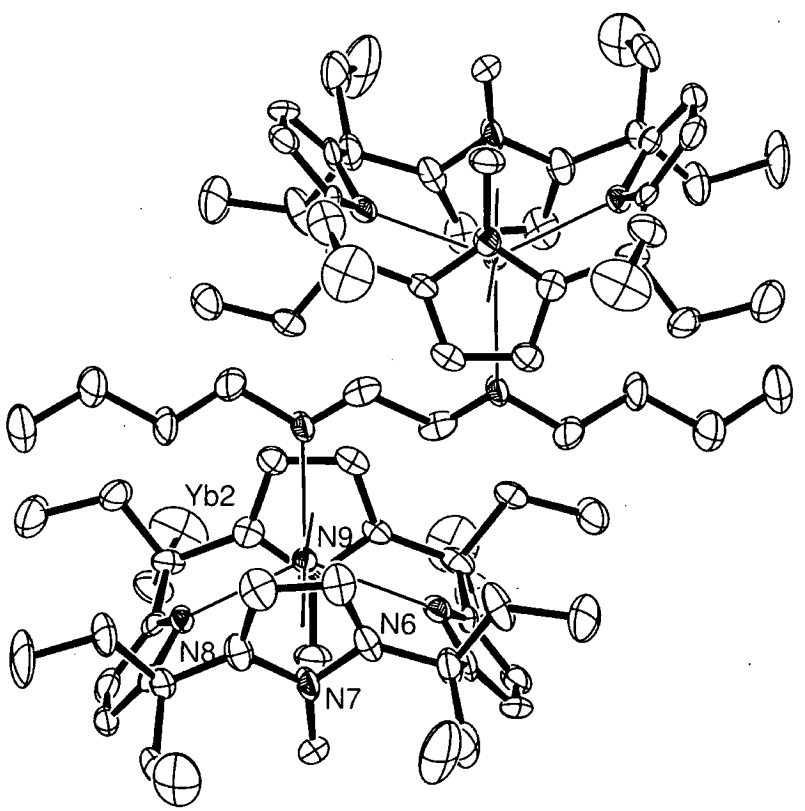

(2)

Figure 15: Molecular structure of $[(Et_8N_4Me_2)Yb(n\text{-BuDAB})]$, **(25)**, with thermal ellipsoids drawn at the level of 50% probability (protons removed for clarity). The two crystallographically independent molecules are shown.

The *i*-PrDAB complex [$(Et_8N_4Me_2)$Yb(*i*-PrDAB)], **(24)**, is mononuclear whilst the *n*-BuDAB complex [$\{(Et_8N_4Me_2)Yb\}_2$(*n*-BuDAB)], **(25)**, contains a DAB unit bridging two Yb centres. The Yb centres in **(24)** and **(25)** are bound to the $(Et_8N_4Me_2)^{2-}$ macrocycle *via* the same $\eta^1{:}\eta^5{:}\eta^1{:}\eta^5$ binding mode observed in the Sm RDAB complexes **(18)**, **(19)**, **(20)** and **(21)**.

The *i*-PrDAB ligand in complex **(24)** is bound to the Yb centre through one nitrogen centre of the *i*-PrDAB ligand (Yb(1)-N(5) = 2.529(12) Å), the second DAB nitrogen remaining uncoordinated. This is in marked contrast to the Sm *i*-PrDAB chelating complex [$(Et_8N_4Me_2)$Sm(*i*-PrDAB)], **(19)**, and bridging complex [$\{(Et_8N_4Me_2)Sm\}_2$(*i*-PrDAB)], **(20)**, in which both *i*-PrDAB nitrogen centres are involved in bonding to a Sm centre. The Yb-N-C-C fragment of the *i*-PrDAB ligand in complex **(24)** displays a *syn* arrangement, whilst the corresponding Sm-N-C-C fragment in the bridging Sm *i*-PrDAB complex **(20)** is present in an *anti* arrangement. The *syn* arrangement in complex **(24)** results in N6 remaining uncoordinated due to the steric influence of the methyl groups of the proximal *i*-Pr group. In contrast, the *anti* arrangement in the Sm bridging complex **(20)** results in neither DAB nitrogen centre being blocked by the adjacent *i*-Pr group, and coordination to both nitrogen centres is observed. The *i*-PrDAB N-C-C-N bond lengths in complex **(24)** (1.28(2), 1.47(2), 1.28(2) Å) are consistent with those expected for a neutral DAB ligand.

The Yb centre in complex **(24)** is bound to the macrocyclic pyrrolide nitrogen centres with Yb-N distances of 2.497(12) and 2.507(12) Å whilst the distances between the Yb centre and the macrocyclic *N*-methylpyrrolyl ring centroids are 2.68_6 and 2.67_9 Å. These lengths are similar to those observed in the starting Yb(II) complex [$(Et_8N_4Me_2)$Yb(THF)], **(13)**, (Yb-N(pyrrolide) distance = 2.471(2), 2.485(2) Å, Yb-N(*N*-methylpyrrolyl) centroid distance = 2.61_6, 2.64_4 Å), consistent with the Yb centre in complex **(24)** being in a +2 oxidation state.

The metallocene bend angle in complex **(24)** is 167.8_5 °, whilst the N(pyrrolide)-Yb-N(pyrrolide) angle is 127.8(4) °. The pyrrolide ring tilt angles are 43.4_6 and 52.8_4 °, and the *N*-methylpyrrolyl ring tilt angles are 78.2_9 and 78.4_8 °. Again, these are similar to the respective values observed in [$(Et_8N_4Me_2)$Yb(THF)], **(13)**: metallocene bend angle

= 169.4_5 °, N(pyrrolide)-Yb-N(pyrrolide) angle = 128.82(8) °, pyrrolide ring tilt angles = 46.7_6 and 52.6_2 °, *N*-methylpyrrolyl ring tilt angles = 80.1_2 and 80.1_3 °.

Complex [{($Et_8N_4Me_2$)Yb}$_2$(*n*-BuDAB)], **(25)**, features a neutral *n*-BuDAB ligand bound through each nitrogen to a Yb centre. Both of the crystallographically independent molecules will be discussed together below. The Yb-N-C-C fragment of the *n*-BuDAB ligand displays a *syn* arrangement; this contrasts with the respective Sm-N-C-C fragment in the bridging Sm complexes [{($Et_8N_4Me_2$)Sm}$_2$(*t*-BuDAB)], **(18)**, [{($Et_8N_4Me_2$)Sm}$_2$(*i*-PrDAB)], **(20)**, and [{($Et_8N_4Me_2$)Sm}$_2$(*n*-BuDAB)], **(21)**, which feature *anti* arrangements.

The Yb-N(DAB) bond lengths in complex **(25)** (2.531(6), 2.534(7) Å) are similar to that observed in [($Et_8N_4Me_2$)Yb(*i*-PrDAB)], **(24)**, (2.529(12) Å). The *n*-BuDAB N-C-C-N bond lengths in complex **(25)** (1.265(10), 1.463(16), 1.265(10) Å and 1.282(10), 1.440(16), 1.282(10) Å) are indicative of a neutral DAB ligand.

The Yb centre in **(25)** is bound to the macrocyclic pyrrolide nitrogen centres with Yb-N distances in the range 2.472(7) to 2.511(6) Å whilst the distances between the Yb centre and the macrocyclic *N*-methylpyrrolyl ring centroids range over 2.60_9 to 2.65_1 Å. The metallocene bend angles are 169.1_6, 169.8_6 ° and the N(pyrrolide)-Yb-N(pyrrolide) angles are 130.4_2, 130.7_2 °. The pyrrolide ring tilt angles vary over 44.3_7 to 51.4_5 ° and the *N*-methylpyrrolyl ring tilt angles over 76.7_4 to 79.4_1 °. These bond lengths and angles are similar to those observed in the Yb(II) complexes [($Et_8N_4Me_2$)Yb(*i*-PrDAB)], **(24)**, and [($Et_8N_4Me_2$)Yb(THF)], **(13)** (see above discussion of complex **(24)**).

3.4 Experimental

Synthesis of $\{(Et_8N_4Me_2)K_2(THF)_2\}_n$, (11), modified literature procedure[23]

Crude $Et_8N_4Me_2H_2$ (3.60 g), containing amounts of $Et_8N_4H_4$, $Et_8N_4MeH_3$, *cis*-$Et_8N_4Me_2H_2$, $Et_8N_4Me_3H$ and $Et_8N_4Me_4$ impurities (combined *ca.* 25 %) from the methylation of $Et_8N_4H_4$ was suspended in 1:5 CH_2Cl_2:hexanes and flashed though a plug of silica gel to remove any unreacted $Et_8N_4H_4$. The filtrate was evaporated *in vacuo* and dried by heating at 110 °C/2 x 10^{-2} mmHg for 2 h before being dissolved in a mixture of THF (75 mL) and toluene (75 mL). To this was added potassium metal (2.6 x 10^{-2} mol, 1.0 g) and the mixture heated at 75 °C for 1 d with gentle stirring. The turbid reaction mixture was decanted away from excess potassium metal, allowed to settle, and the transparent brown supernatant removed *via* cannula. The beige solid thus obtained was rinsed with toluene (3 x 30 mL) and dried *in vacuo* to furnish the title compound as a pale beige powder (3.2 g, 4.1 x 10^{-3} mol). The ^{1}H NMR spectrum of a hydrolysed sample in benzene-d_6 showed no traces of other *N*-methylated porphyrinogens.

Synthesis of $[(Et_8N_4Me_2)Sm(THF)_2]$, (12), modified literature procedure[24]

A solution of $SmI_2(THF)_2$ in THF (0.1 M, 48 mL, 4.8 x 10^{-3} mol) was added *via* cannula to a suspension of $\{(Et_8N_4Me_2)K_2(THF)_2\}_n$, **(11)**, (4.81 x 10^{-3} mol, 3.80 g) in THF (30 mL) with stirring. The colour changed from beige to dark purple with the formation of pale solids. Stirring was continued overnight, solvent was removed *in vacuo* and the solids extracted twice *via* filter cannula with toluene (40 and 20 mL). The solvent was removed *in vacuo*, THF (20 mL) added and the mixture warmed to effect dissolution. The warm solution was cooled to ambient temperature overnight, then stood overnight at -20 °C to complete crystallisation. Removal of the supernatant and drying *in vacuo* afforded the product as dark purple-black prisms (3.2 g, 77 %). ^{1}H NMR spectroscopic data matched those previously reported.

Synthesis of $[(Et_8N_4Me_2)Eu(THF)_2]$, (15)

A solution of $EuI_2(THF)_2$ (6.3 x 10^{-4} mol, 0.35 g) in THF (15 mL) was added *via* cannula to a suspension of $\{(Et_8N_4Me_2)K_2(THF)_2\}_n$, **(11)**, (6.3 x 10^{-4} mol, 0.50 g) in THF (15 mL) with stirring. The colour changed from beige to yellow with the formation of

pale solids. Stirring was continued overnight, solvent was removed *in vacuo* and the solids extracted twice *via* filter cannula with toluene (20 and 10 mL). The solvent was removed *in vacuo*, THF (15 mL) added and the mixture warmed to effect dissolution. The warm solution was cooled to ambient temperature overnight, then stood overnight at -20 °C to complete crystallisation. Removal of the supernatant and drying *in vacuo* afforded the product as bright yellow prisms which were suitable for X-ray crystal structure determination (0.41 g, 75 %).

Anal. Calcd.: C, 64.02; H, 8.18; N, 6.49 ($C_{46}H_{70}N_4O_2Eu$, MW 863.01)
Found: C, 63.85; H, 8.25; N, 6.51

Synthesis of [($Et_8N_4Me_2$)Eu(THF)], (16)

[($Et_8N_4Me_2$)Eu(THF)$_2$], **(15)**, (2.4 x 10^{-4} mol, 0.21 g) was dissolved in toluene (3 mL) and allowed to stand at ambient temperature for 6 days, during which time large yellow prisms of the title compound suitable for X-ray crystal structure determination formed. Supernatant was removed *via* cannula and the product dried *in vacuo* (0.17 g, 90 %).

Synthesis of [{($Et_8N_4Me_2$)Sm}$_2$(*t*-BuDAB)], (18)

A solution of 1,4-di-*t*-butyl-1,4-diazabuta-1,3-diene (2.9 x 10^{-4} mol, 49 mg) in toluene (1 mL) was added to a solution of [($Et_8N_4Me_2$)Sm(THF)$_2$], **(12)**, (5.8 x 10^{-4} mol, 0.50 g) in toluene (5 mL) with stirring. There was an immediate colour change from dark purple to green, and the reaction stood overnight. Solvent was removed *in vacuo* to produce the title compound as a bright green crystalline powder (0.47 g, 86 %).

^{1}H NMR (300 MHz, C_6D_6, 25 °C): δ = -0.51 (b, 4H, CH_2), -0.03 (t, 12H, CH_3), 0.05 (t, 12H, CH_3), 0.41 (t, 12H, CH_3), 0.55-0.90 (m, 20H, CH_3 + 2xCH_2), 1.13 (b, 4H, CH_2), 1.34 (b, 4H, CH_2), 1.87 (b, 4H, CH_2), 2.15 (m, 8H, 2xCH_2), 2.54 (b, 18H, CH_3, *t*-BuDAB), 4.29 (s, 4H, =CH, *N*-CH_3pyr), 5.66 (s, 4H, =CH, *N*-CH_3pyr), 6.12 (s, 4H, =CH, pyr), 6.72 (s, 4H, =CH, pyr), 7.00 (s, 12H, NCH_3), 11.06 (s, 2H, =CH, *t*-BuDAB).

^{13}C NMR (75 MHz, C_6D_6, 25 °C): δ=7.4 (CH_3, *t*-BuDAB), 8.0 (2 x CH_3), 8.3 (2 x CH_3), 22.0 (CH_2), 22.5 (CH_2), 28.9 (CH_2), 29.4 (CH_2), 38.2 (N-CH_3), 43.5,

44.5 (*C*-Et_2), 69.6 (*C*-Me_3), 99.7, 100.8 (=CH, *N*-CH_3pyr), 101.1, 101.9 (=CH, pyr), 125.6 (=CH, *t*-BuDAB), 136.5, 138.7 (C, *N*-CH_3pyr), 148.1, 149.4 (C, pyr).

Anal. Calcd.: C, 64.45; H, 8.05; N, 8.74 ($C_{86}H_{128}N_{10}Sm_2$, MW 1602.75)
Found: C, 64.51; H, 8.15; N, 8.72.

Synthesis of [($Et_8N_4Me_2$)Sm(*i*-PrDAB)], (19)

A solution of 1,4-di-*i*-propyl-1,4-diazabuta-1,3-diene (5.8×10^{-4} mol, 81 mg) in toluene (5 mL) was added to a solution of [($Et_8N_4Me_2$)Sm(THF)$_2$], **(12)**, (5.8×10^{-4} mol, 0.50 g) in toluene (15 mL) with stirring. There was an immediate colour change from dark purple to light brown, and the reaction stood at -80 °C overnight. The supernatant was decanted from the cold mixture *via* cannula and the solids dried *in vacuo* to afford the title compound as a brick red crystalline powder (0.26 g, 52 %).

^{1}H NMR (300 MHz, C_6D_6, 25 °C): δ = -395.6 (br s, 2H, =CH, *i*-PrDAB), -19.26 (s, 12H, CH_3, *i*-PrDAB), -0.46 (t, 12H, CH_3), 1.52 (m, 8H, 2xCH_2), 1.89 (m, 4H, CH_2), 1.95 (t, 12H, CH_3), 4.25 (br, 4H, CH_2), 6.68 (s, 4H, =CH, pyr), 12.58 (s, 4H, =CH, *N*-CH_3pyr), 13.42 (s, 6H, N-CH_3), 36.64 (s, 2H, CH, *i*-PrDAB).

^{13}C NMR (75 MHz, C_6D_6, 25 °C): δ = 8.6, 10.0 (CH_3), 14.4 (N-CH_3), 18.2 (CH_2), 37.6 (CH_2), 47.9 (*C*-Et_2), 100.0 (=CH, pyr), 107.4 (C, *N*-CH_3pyr), 149.5 (C, pyr), 159.6 (=CH, *N*-CH_3pyr).

Anal. Calcd.: C, 64.43; H, 8.23; N, 9.80 ($C_{46}H_{70}N_6Sm$, MW 857.47)
Found: C, 63.78; H, 7.88; N, 9.51.

Synthesis of [{($Et_8N_4Me_2$)Sm}$_2$(*i*-PrDAB)], (20)

A solution of [($Et_8N_4Me_2$)Sm(*i*-PrDAB)], **(19)**, (2×10^{-5} mol, 17 mg) in toluene (0.5 mL) was added to a solution of [($Et_8N_4Me_2$)Sm(THF)$_2$], **(12)**, (2×10^{-5} mol, 17 mg) in toluene (0.5 mL) in a sealed tube. The mixture was heated to 110 °C for 5 minutes and allowed to cool to ambient temperature, whereupon the title compound formed as green crystals suitable for X-ray crystal structure determination (29 mg, 92 %).

Anal. Calcd.: C, 65.57; H, 7.98; N, 8.41 ($C_{84}H_{124}N_{10}Sm.C_7H_8$, MW 1666.85)
Found: C, 65.56; H, 8.06; N, 8.13

Synthesis of [{($Et_8N_4Me_2$)Sm}$_2$(*n*-BuDAB)], (21)

A solution of 1,4-di-*n*-butyl-1,4-diazabuta-1,3-diene (3.0×10^{-5} mol, 5 mg) in benzene-d_6 (50 μL) was added to a solution of [($Et_8N_4Me_2$)Sm(THF)$_2$], **(12)**, (6.0×10^{-5} mol, 52 mg) in toluene (0.4 mL). The mixture was briefly heated to reflux and allowed to stand for 2 d at ambient temperature, over which time green crystals of the title compound suitable for X-ray crystal structure determination formed.

Synthesis of [{($Et_8N_4Me_2$)Sm}$_2$], (22)

A solution of 1,4-di-*n*-butyl-1,4-diazabuta-1,3-diene (1.5×10^{-5} mol, 2.5 mg) in benzene-d_6 (25 μL) was added to a solution of [($Et_8N_4Me_2$)Sm(THF)$_2$], **(12)**, (3.0×10^{-5} mol, 26 mg) in benzene-d_6 (0.5 mL) and stood overnight. The yellow-brown supernatant was decanted away from a green precipitate and toluene (0.4 mL) was added. The mixture was briefly heated to reflux to effect dissolution and cooled to ambient temperature to give green crystals of the title compound suitable for X-ray crystal structure determination.

Synthesis of [($Et_8N_4Me_2$)Yb(*i*-PrDAB)], (24)

A solution of 1,4-di-*i*-propyl-1,4-diazabuta-1,3-diene (5.3×10^{-4} mol, 74 mg) in toluene (5 mL) was added to a solution of [($Et_8N_4Me_2$)Yb(THF)], **(13)**, (5.3×10^{-4} mol, 0.43 g) in toluene (20 mL) with stirring. There was an immediate colour change from yellow to emerald green, and stirring continued overnight. Removal of solvent *in vacuo* gave the product as a bright green crystalline powder (0.41 g, 88 %).

Anal. Calcd.: C, 62.77; H, 8.02; N, 9.55 ($C_{46}H_{70}N_6Yb$, MW 880.11)
Found: C, 62.82; H, 7.40; N, 8.51

Synthesis of [{($Et_8N_4Me_2$)Yb}$_2$(*n*-BuDAB)], (25)

A solution of 1,4-di-*n*-butyl-1,4-diazabuta-1,3-diene (1.5×10^{-5} mol, 2.5 mg) in benzene-d_6 (25 μL) was added to a solution of [($Et_8N_4Me_2$)Yb(THF)], **(13)**, (3.0×10^{-5} mol, 24 mg) in toluene (0.5 mL) and stood overnight. There was an immediate change in colour from yellow to green-brown. The solution was allowed to evaporate at ambient temperature over the course of 2 weeks to produce the title compound as brown crystals suitable for X-ray crystal structure determination.

3.5 References

1. P. Krumholz, *J. Am. Chem. Soc.*, 1953, **75**, 2163.

2. G. van Koten, K. Vreize, *Adv. Organomet. Chem.*, 1982, **21**, 151.

3. **a**. M.G. Gardiner, G.R. Hanson, M.J. Henderson, F.C. Lee, C.L. Raston, *Inorg. Chem.*, 1994, **33**, 2456.
b. J. Scholz, B. Richter, R. Goddard, C. Krüger, *Chem. Ber.*, 1993, **126**, 57.

4. K.-H. Thiele, V. Lorenz, G. Thiele, P. Zönnchen, J. Scholz, *Angew. Chem. Int. Ed. Engl.*, 1994, **33**, 1372.

5. B. Richter, J. Scholz, J. Sieler, K.-H. Thiele, *Angew. Chem. Int. Ed. Engl.*, 1995, **34**, 2649.

6. F.G.N. Cloke, H.C. de Lemos, A.A. Sameh, *J. Chem. Soc., Chem. Commun.*, 1986, 1344.

7. M.N. Bochkarev, A.A. Trifonov, F.G.N. Cloke, C.I. Dalby, P.T. Matsunaga, R.A. Anderson, H. Schumann, J. Loebel, H. Hemling, *J. Organomet. Chem.*, 1995, **486**, 177.

8. P. Poremba, F.T. Edelmann, *J. Organomet. Chem.*, 1997, **549**, 101.

9. A.A. Trifonov, Y.A. Kurskii, M.N. Bochkarev, S. Muehle, S. Dechert, H. Schumann, *Russ. Chem. Bull., Int Ed.*, 2003, **52**, 601.

10. A.A. Trifonov, E.N. Kirillov, M.N. Bochkarev, H. Schumann, S. Muehle, *Russ. Chem. Bull.*, 1999, **48**, 384.

11. **a**. A.A. Trifonov, E.A. Fedorova, G.K. Fukin, V.N. Ikorskii, Y.A. Kurskii, S. Dechert, H. Schumann, M.N. Bochkarev, *Russ. Chem. Bull., Int. Ed.*, 2004, **53**, 2736.

b. A.A. Trifonov, E.A. Fedorova, V.N. Ikorskii, S. Dechert, H. Schumann, M.N. Bochkarev, *Eu. J. Inorg. Chem.*, 2005, 2812.

12. J.A. Moore, A.H. Cowley, J.C. Gordon, *Organometallics*, 2006, **25**, 5207.

13. **a**. J. Wang, M.G. Gardiner, E.J. Peacock, B.W. Skelton, A.H. White, *Dalton Trans.*, 2003, 161.
b. J. Wang, Ph.D. Thesis, University of Tasmania, 2003. **c**. S. Powanusorn, M.Appl.Sci. Thesis, University of Tasmania, 2004.

14. P.L. Watson, T.H. Tulip, I. Williams, *Organometallics*, 1990, **9**, 1999.

15. A. Dick, B.Sc.(Hons.) Thesis, University of Tasmania, 2003.

16. W.J. Evans, M.A. Hozbor, *J. Organomet. Chem.*, 1987, **326**, 299.

17. **a**. W.J. Evans, T.A. Ulibarri, J.W. Ziller, *J. Am. Chem. Soc.*, 1988, **110**, 6877.
b. W.J. Evans, T.A. Ulibarri, J.W. Ziller, *J. Am. Chem. Soc.*, 1990, **112**, 219.
c. W.J. Evans, D.G. Giarikos, C.B. Robledo, V.S. Leong, J.W. Ziller, *Organometallics*, 2001, **20**, 5648.

18. **a**. T. Dubé, S. Gambarotta, G.P.A. Yap, *Angew. Chem. Int. Ed.*, 1999, **38**, 1432.
b. J. Guan, T. Dubé, S. Gambarotta, G.P.A. Yap, *Organometallics*, 2000, **19**, 4820.

19. L.R. Morss, *Chem. Rev.*, 1976, **76**, 827.

20. M.D. Walter, D.J. Berg, R.A. Anderson, *Organometallics*, 2007, **26**, 2296.

21. R.D. Shannon, *Acta Crystallogr.*, 1976, **A32**, 751.

22. J. Wang, M. G. Gardiner, B. W. Skelton, A. H. White, *Organometallics*, 2005, **24**, 815.

23. **a**. Y. Furusho, H. Kawasaki, S. Nakanishi, T. Aida, T. Takata,

Tetrahedron Letters, 1998, **39**, 3537.

b. J. Wang, M.G. Gardiner, E.J. Peacock, B.W. Skelton, A.H. White, *Dalton Trans.*, 2003, 161.

24. J. Wang, A. K. J. Dick, M. G. Gardiner, B. F. Yates, E. J. Peacock, B.W. Skelton, A. H. White, *Eur. J. Inorg. Chem.*, 2004, 1992.

Chapter 4

Cyclopentadienyl and Cyclooctatetraenediyl Complexes

4.1 Introduction

Deprotonation of cyclopentadiene results in the planar, aromatic cyclopentadienide anion, Equation 1. Reaction of cyclopentadiene with a suitable lanthanide precursor is a synthetically useful entry to lanthanide cyclopentadienide chemistry, although salt metathesis and redox transmetallation reactions are also commonly used.

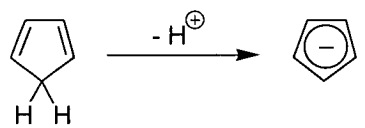

Equation 1

The cyclopentadienyl anion ($(C_5H_5)^-$ ≡ Cp) has remained ubiquitous in organolanthanide chemistry, in both homoleptic and heteroleptic complexes, since the first tris(cyclopentadienyl)lanthanide(III) complexes were reported in 1954.[1] Functionalised cyclopentadienyl ligands were subsequently employed to allow greater saturation of the lanthanide coordination sphere and to improve the solubility and crystallinity of the resultant complexes. Early work using pentamethyl- and bis(trimethylsilyl)- functionalised cyclopentadienyl ligands resulted in the synthesis of soluble, structurally characterisable $[(C_5Me_5)_2Sm(THF)_2]$[2] and $[\{(Me_3Si)_2C_5H_3\}_3Sm]$.[3]

Beyond a simple increase in size to block the coordination sphere, the hapticity of the cyclopentadienyl ligand can be increased by incorporating "pendant" substituents bearing donor atoms. An example is the neodymium complex $[(Me_2NCH_2CH_2C_5H_4)_2NdCl]$, **(I)**, which features a tertiary nitrogen σ-bound to the metal centre in addition to the η^5-bound cyclopentadienyl ligand, Figure 1.[4]

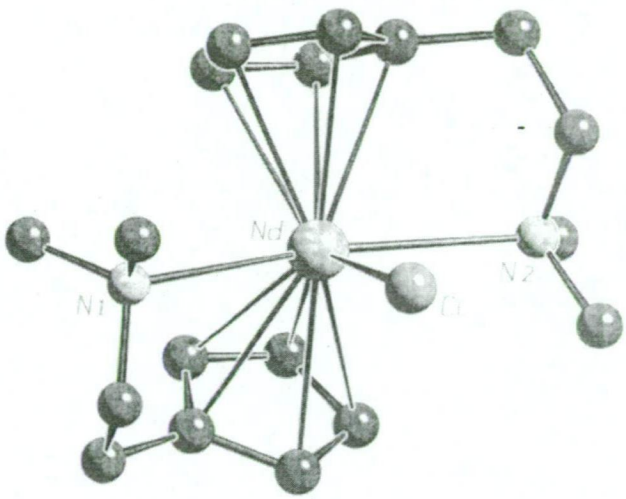

Figure 1: Pendant-substituted cyclopentadienyl complex **(I)**.[4]

The pendant arm of a cyclopentadienyl ligand can also be functionalised with another cyclopentadienyl ring resulting in "*ansa*-metallocenes" upon subsequent coordination to a lanthanide metal centre. The length of the alkylene chain linking the two rings can be altered or entirely replaced by a bridging heteroatom. Such an approach was used to advantage in developing catalytically active complexes such as $[\{Me_2Si(C_5Me_4)_2\}NdCH(SiMe_3)_2]$, **(II)**, Figure 2.[5] The complex features two tetramethylcyclopentadienyl rings joined by a silicon atom. The single bridging silicon forces the complex to adopt a decreased centroid-Nd-centroid angle (metallocene "bend angle"), thereby increasing access to the metal centre and promoting catalytic activity.

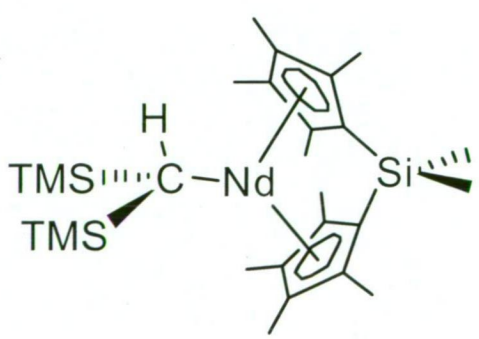

Figure 2: *Ansa*-metallocene **(II)** with -Si(Me_2)- bridge.

Other π-bound species have been examined as potential organolanthanide ligands. Cyclooctatetraene can accept two electrons to form a planar, aromatic dianion, Equation 2. The bulky nature of the cyclooctatetraenediyl dianion (≡ COT) has led to its use as a

ligand in a wide range of homoleptic and heteroleptic lanthanide complexes. More recently this has been extended to include cyclooctatetraenediyl derivatives incorporating additional bulky substituents, *e.g.* 1,4-bis(trimethylsilyl) and 1,3,6-tris(trimethylsilyl) functionalities.

Equation 2

The lanthanide(II) cyclooctatetraenediyl complexes $[Eu(COT)]_n$ and $[Yb(COT)]_n$ were obtained by the addition of cyclooctatetraene to solutions of Eu or Yb in liquid ammonia.[6] The insolubility of the compounds in hydrocarbon and ether solvents was attributed to a polymeric structure resulting from the ability of the cyclooctatetraenediyl dianion to satisfy only one side of a coordinated lanthanide(II) centre. The polymeric aggregate can be broken into mononuclear solvates by strongly basic solvents such as pyridine or dimethylformamide, which allowed the structure of the monomeric Ln-COT unit to be determined by X-ray crystal structure determination, *e.g.* $[(C_5H_5N)_3Yb(COT)]$, **(III)**, Figure 3.[7]

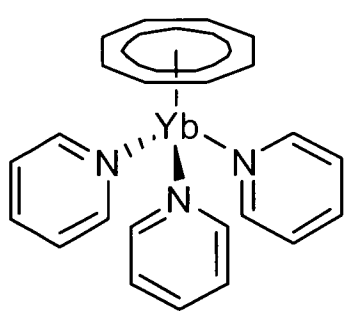

Figure 3: Mononuclear Yb(II) COT complex **(III)** as the tris-pyridine Lewis base adduct.

Homoleptic lanthanide cyclooctatetraenediyl complexes often adopt binuclear "decker" structures due to the dianionicity of the cyclooctatetraenediyl ligand. The neodymium(III) complex $[Nd_2(COT)_3]$ was reported in 1976 and structurally characterised as the asymmetrical bis(THF) adduct, $[(COT)Nd(\mu{:}\eta^8{:}\eta^3{:}COT)Nd(COT)(THF)_2]$, **(IV)**, Figure 4.[8] Related to this example is $[\{(C_5Me_5)(COT)U\}_2(COT)]$, **(V)**, the only other structurally authenticated f-element

complex containing a cyclooctatetraenediyl dianion bound with a hapticity other than η^8, Figure 5.[9] The bridging COT ring in **(V)** is non-planar and bound η^3- to each U centre. Complexes **(IV)** and **(V)** are notable in that the coordination sphere of one of the metal centres is saturated, which leads to a reduction in hapticity.

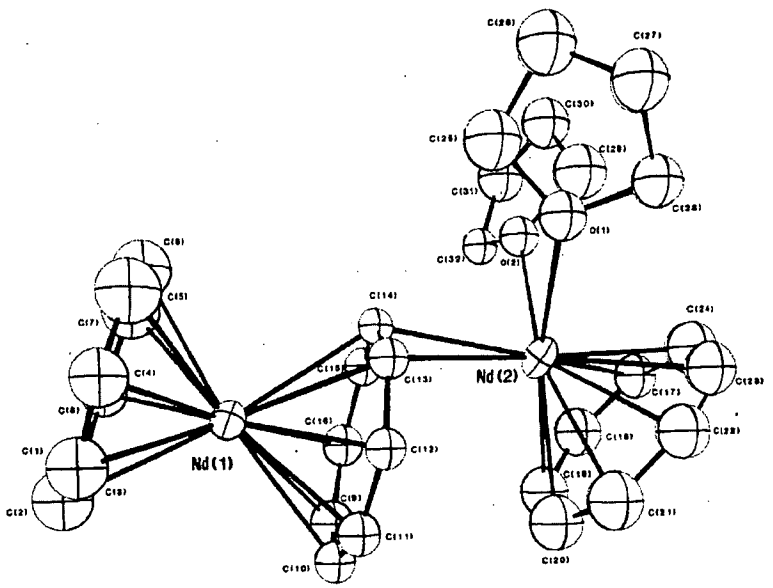

Figure 4: Cyclooctatetraenediyl Nd complex **(IV)** featuring η^3 and η^8 hapticities.[8]

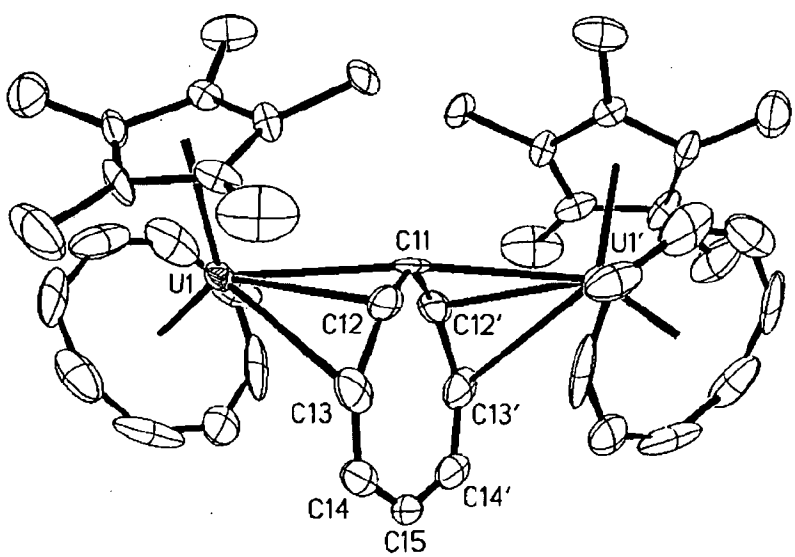

Figure 5: Cyclooctatetraenediyl U complex **(V)** featuring η^3 and η^8 hapticities.[9]

Cyclooctatetraenediyl ligands with hapticities less than η^8 are also known in transition metal chemistry. The Ni(0) complex [{(*t*-$Bu_2PCH_2CH_2P$-*t*-Bu_2)Ni}$_2$(μ-η^2:η^2-C_8H_8)], **(VI)**, displays η^2-binding to a planar C_8H_8 ring which is described as semiaromatic (*ie.* singly anionic) due to backbonding from the Ni centre, Figure 6. The low hapticity of the C_8H_8 ring in this case is due to the coordination mode imposed by the chelating ligand, in addition to steric effects.[10]

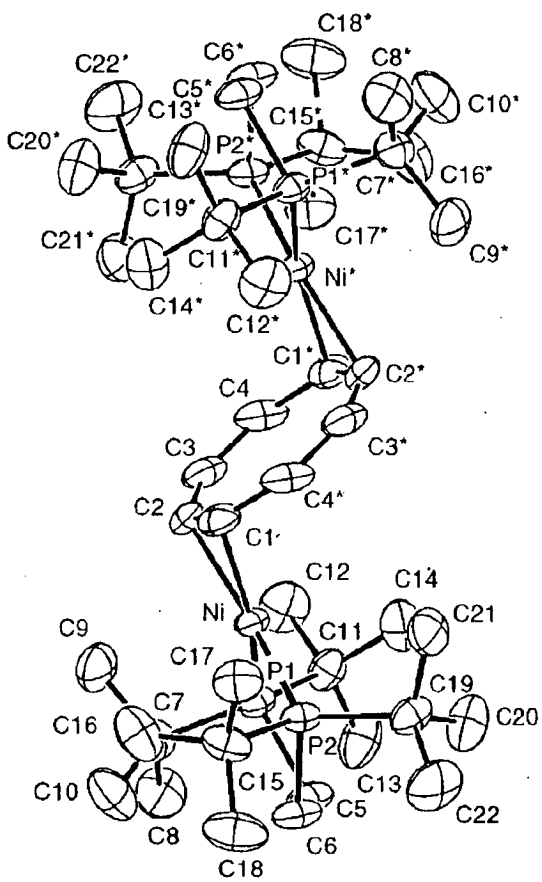

Figure 6: Ni(0) complex **(VI)** featuring η^2 COT hapticity.[10]

Symmetrical sandwich complexes containing the $[Ln(COT)_2]^-$ anion were first reported in 1970 (Ln = Ce, Pr, Nd, Sm, Tb),[11] and structurally authenticated in 1972 (Ln = Ce), **(VII)**.[12] Complex **(VII)**, [(COT)Ce(μ-COT)K(O{CH_2CH_2OMe}$_2$)], contains a cerium centre η^8-bound to two COT rings, with a solvated potassium cation η^8-bound to the bridging COT, Figure 7.

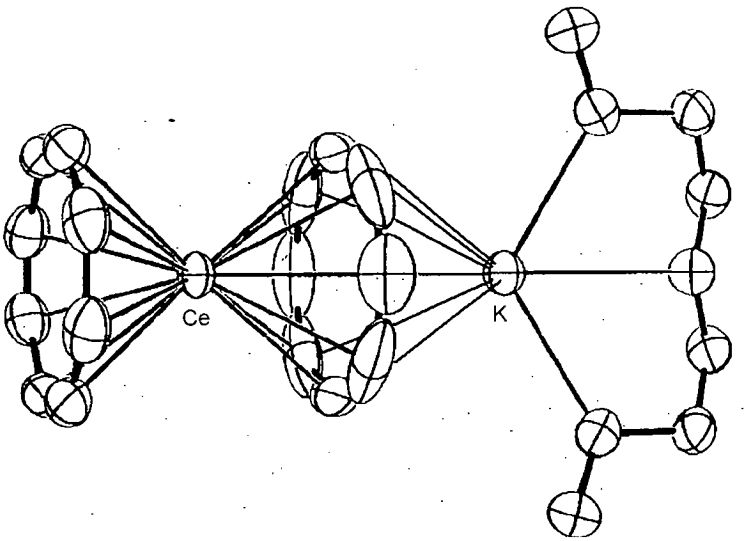

Figure 7: Heterometallic Ce(III) sandwich complex.[12]

More than half the coordination sphere of a cyclooctatetraenediyl-bound lanthanide centre is left open to further ligation due to the planar nature of the cyclooctatetraenediyl dianion. To facilitate the development of mononuclear cyclooctatetraenediyl complexes, the cyclooctatetraenediyl ligand has most frequently been employed as a component of heteroleptic complexes. Recent efforts to provide better coordination sphere control have resulted in the use of chelating ligands (especially those featuring nitrogen donors) in addition to cyclooctatetraene derivatives functionalised with bulky and/or pendant substituents.

Chelating ligands used in heteroleptic lanthanide cyclooctatetraenediyl complexes include silylated benzamidinates,[13,14] silylated diiminophosphinates,[14,15] pyrazolylborates,[14,16] 1,4-diazabuta-1,3-dienes[17] and substituted aminotroponiminate ligands.[18] A representative example is the pyrazolyl complex **(VIII)**, which features a tridentate pyrazolylborate ligand σ-bound through each of three nitrogen atoms to the lanthanide centre, which binds in the usual η^8 fashion to the cyclooctatetraenediyl dianion, Figure 8.[14]

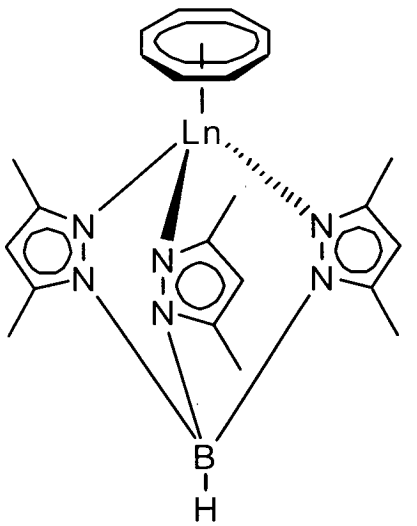

Figure 8: COT / pyrazolylborate complex **(VIII)**, (Ln = Ce, Pr, Nd, Sm)

Substituted cyclooctatetraene offers a means of satisfying a larger portion of the lanthanide coordination sphere.[15,19] Complex **(IX)**, $[Li(diglyme)_2]^+[Ln(1,4\text{-}R_2C_8H_6)_2]^-$ (R = *o*-(dimethylsilyl)-*N*,*N*-dimethylaniline, Ln = Nd, Sm) features a pendant functionalised cyclooctatetraenediyl ligand to increase the steric bulk of the ligand. The presence of a tertiary amine on the aryl pendant raised the possibility of a Lewis basic interaction to the Ln centre, however no coordination to the Ln centre was observed in the solid state molecular structure (Ln = Nd, figure 9). This was investigated further by spin-lattice relaxation NMR studies of the Sm complex, which showed minimal interaction in solution.[20]

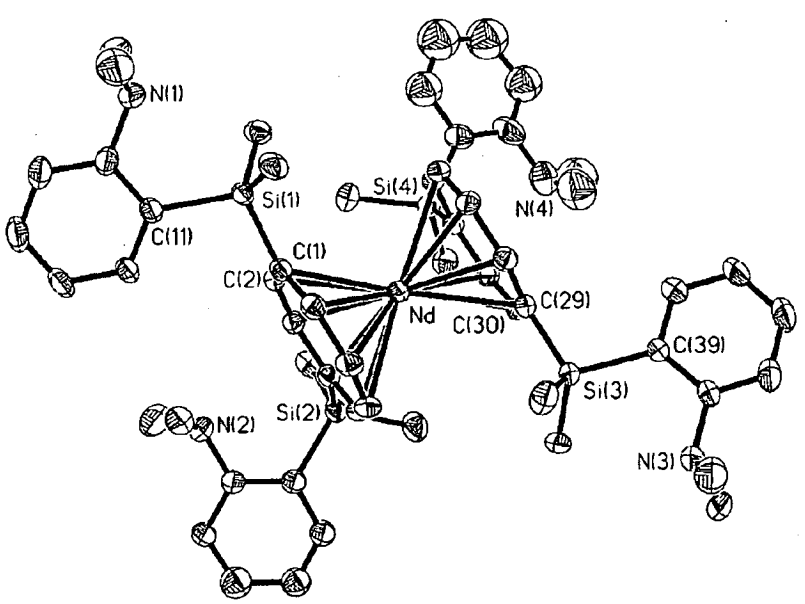

Figure 9: Pendant functionalised COT complex **(IX)**.[20]

Attempts to synthesise complexes with saturated coordination spheres can result in steric interaction between ligands forcing unexpected outcomes. The reaction between $[(C_5Me_5)_2Sm]$; **(X)**, and cyclooctatetraene was undertaken with the intention of producing the bimetallic species $[(C_5Me_5)_2Sm(\mu\text{-COT})Sm(C_5Me_5)_2]$, **(XI)**, where the bridging COT might plausibly adopt a non-planar conformation owing to congestion around the samarium centres.[21] Instead, ligand redistribution took place and the extremely crowded $[(C_5Me_5)_3Sm]$, **(XII)**, was produced along with $[(COT)Sm(C_5Me_5)]$, **(XIII)**, Scheme 1. The crowded tris(pentamethylcyclopentadienyl)samarium(III) proved to be a highly reactive compound displaying alkyl-like reactivity and reductive behaviour, a topic which will be revisited in Chapter 5.

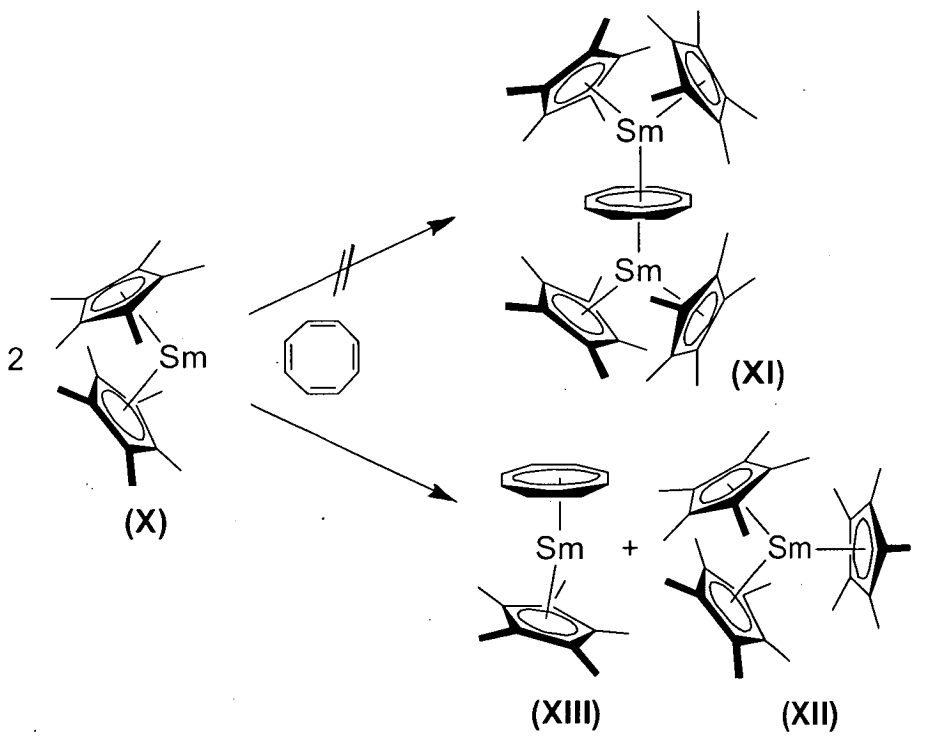

Scheme 1: Ligand disproportionation in the attempted synthesis of $(C_5Me_5)_3Sm$.

4.2 Research aim

The preparation of heteroleptic complexes containing Cp (or substituted Cp) ligands and the $(Et_8N_4Me_2)^{2-}$ porphyrinogen system was undertaken to examine the result of the anticipated interaction between the two ligands. The lack of mononuclear lanthanide complexes featuring Cp with a hapticity other than five made this a natural target for the sterically demanding porphyrinogen. Lack of space across the narrow binding groove of the macrocyclic complexes was expected to result in unusual binding modes for the cyclopentadienyl ligand and/or the macrocycle.

Related to this, reduction of cyclooctatetraene by two $[(Et_8N_4Me_2)Sm(THF)_2]$ molecules was expected to result in a binuclear Sm(III) complex. Steric abuttal at the binding groove of the macrocyclic complexes was expected to preclude η^8-binding between the cyclooctatetraenediyl ligand and samarium centres. Ligand disproportionation was deemed unlikely due to the macrocyclic modified porphyrinogen, so the reaction was thought likely to force the COT to deviate from its normal η^8-binding mode, and/or lose planarity.

4.3 Results and discussion

4.3.1 Complex syntheses

The samarium(III) cyclopentadienyl complex $[(Et_8N_4Me_2)Sm(C_5H_5)]$, **(26)**, was prepared by the metathetical exchange reaction of $[\{(Et_8N_4Me_2)SmCl\}_2]$, **(27)**, with $Na(C_5H_5)$ in THF, Equation 3. Complex **(26)** is soluble in THF, toluene and hexanes, and was obtained in 46 % yield as air and moisture sensitive orange-red crystals suitable for X-ray structure determination by crystallisation from a hot, saturated solution in hexanes.

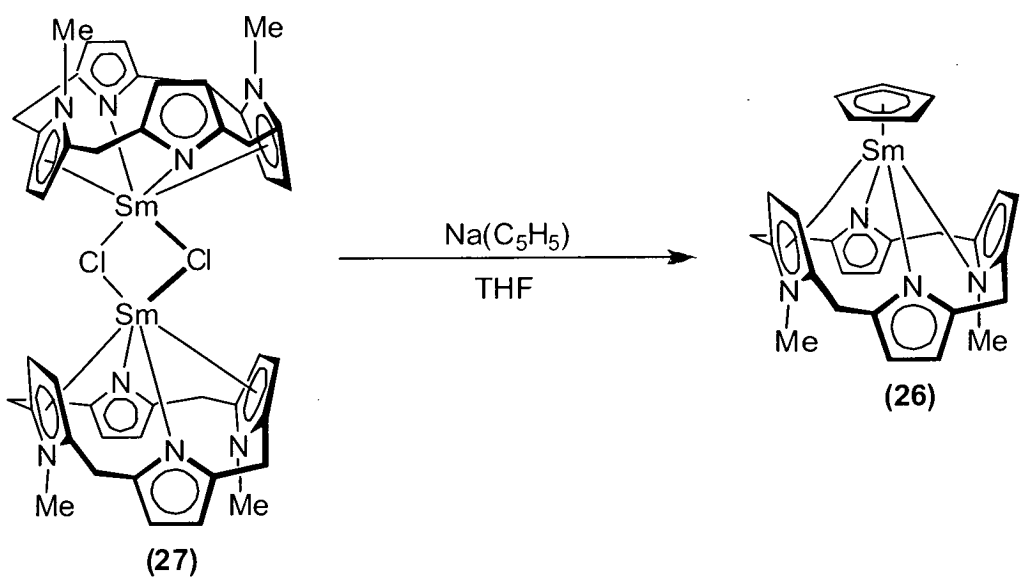

(27) **(26)**

Equation 3

During reaction the colour changed from the brown-pink of the starting $[\{(Et_8N_4Me_2)SmCl\}_2]$, **(27)**, to orange and a pale precipitate (presumably NaCl) formed. The reaction mixture was filtered and the product recovered by removal of solvent from the filtrate. The synthesis can be carried out at ambient temperature in THF or hexanes,

however solutions of **(26)** in toluene, THF, hexanes and benzene-d_6 were observed to deposit a pale yellow, powdery solid upon standing at room temperature. This was presumed to be a decomposition product, and was not observed in solutions held at –20 °C or below. As a result, preparative syntheses of **(26)** were carried out at low temperature, using THF as solvent to maximise the solubility of the starting materials.

The low solubility of the decomposition product in benzene-d_6 or THF-d_8 prevented direct characterisation by NMR spectroscopy. Hydrolysis of the decomposition product and analysis by ^{1}H NMR and mass spectroscopy showed the presence of $Et_8N_4Me_2H_2$ and C_5H_6, with no other species visible (such as $C_{10}H_{10}$ from $(C_5H_5)^{\bullet}$ coupling, or alkenes formed by THF ring opening or THF ring opening and addition to C_5H_5 as observed for the chemistry of the strained $(C_5Me_5)_3Sm$). Complex **(26)** has been characterised by ^{1}H, ^{13}C, gCOSY, gHMQC, gHMBC and gNOESY NMR spectroscopy, and single crystal X-ray structure determination. Satisfactory microanalytical data were obtained.

The molecular structure of **(26)** features a η^5-bound cyclopentadienyl ligand. The two pyrrolide nitrogens are σ-bound to the samarium centre, and one *N*-methylpyrrolyl ring is η^5-bound. The remaining macrocyclic *N*-methylpyrrolyl unit is bent back towards the macrocyclic plane due to interactions caused by the presence of the C_5H_5 ligand, and binds to the samarium centre with reduced η^1 hapticity. Lack of space along the binding groove results in the retention of no THF molecules. The macrocyclic strain introduced by the $(C_5H_5)^-$ group suggested the possibility of reductive reactivity, as reported for highly strained $[(C_5Me_5)_3Ln]$ complexes ("Sterically Induced Reduction").[22] This was investigated by attempted reactions with a number of reducible substrates, and is expanded on in Chapter 5. A similar deformation of a *N*-methylpyrrolyl methyl group from its usual coplanar conformation was reported in a Cr(II) complex of 2,5-bis(diphenyl-(pyrrol-2yl)methyl)-1-methylpyrrole.[23] The deformation in this case appears to be the result of an optimised contact between the two anionic pyrrolide *N* centres and the Cr(II) centre in an otherwise sterically unrestricted system, implying that the energy penalty for the loss of *N*-methyl coplanarity in the *N*-methylyrrolyl group was not significant.

The samarium(III) complex $[\{(Et_8N_4Me_2)Sm\}_2(COT)]$, **(28)**, was prepared by the

reduction of cyclooctatetraene by two equivalents of $[(Et_8N_4Me_2)Sm(THF)_2]$, **(12)**, in toluene, Equation 4. Addition of a solution of cyclooctatetraene in toluene to a dark purple solution of the Sm(II) precursor in toluene resulted in an immediate change in colour to deep green, and a green precipitate slowly formed over 5 minutes. The colourless supernatant was decanted away and the green solids rinsed with toluene. The solids were dried *in vacuo* to give **(28)** as an emerald green powder in 82 % yield.

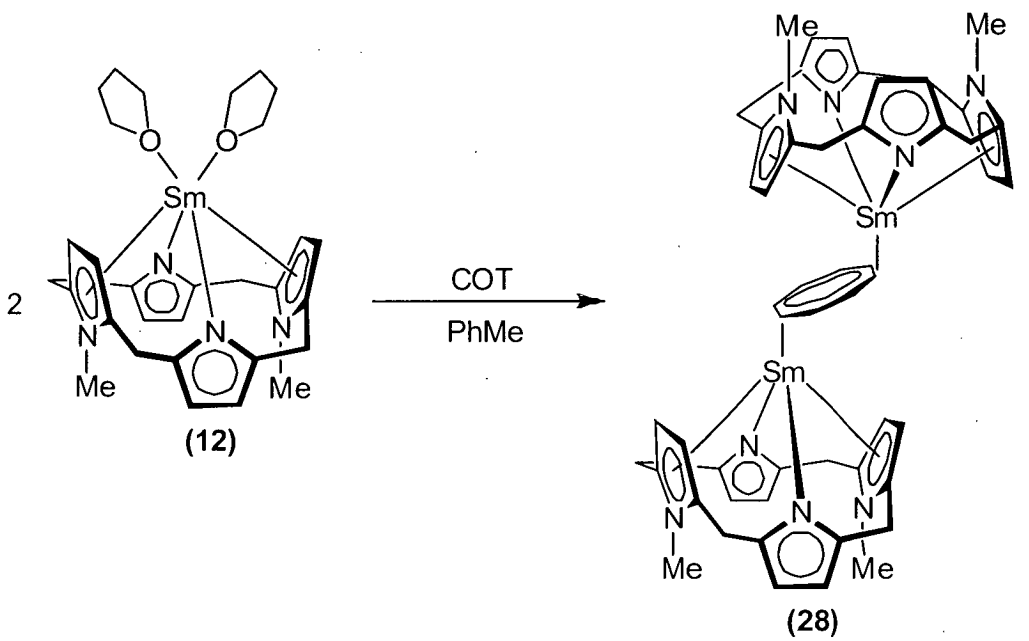

Equation 4

Complex **(28)** is insoluble in hexanes, diethyl ether, benzene-d_6 and toluene. It is slightly soluble in 1,4-dioxane and THF, its solubility in these solvents increasing at elevated temperature. The complex can be recrystallised from hot, saturated THF solutions to give transparent emerald green needles which readily lose solvent upon removal from the mother liquor. Complex **(28)** has been characterised by microanalysis and single crystal X-ray structure determination. NMR spectroscopy was not informative due to low solubility of **(28)** in THF-d_8 and 1,4-dioxane-d_8.

With the samarium bound within the macrocyclic cavity, the upward projecting 3- and 4- postions of the *N*-methylpyrrolyl groups and the *meso*-ethyl groups do not allow a possible η^8 interaction between the metal and the face of the large, oblate COT ligand. To achieve η^8 binding it is likely that both *N*-methylpyrrolyl groups would need

to splay backwards towards the macrocyclic plane, but are prevented from doing so by *trans*-annular interactions between the two *N*-methyl groups. The *meso*-ethyl groups would also be required to shift considerably to allow full access to the metal coordination sphere, further increasing the strain within the macrocyclic skeleton. It seems as though such deformation can only occur to a single *N*-methylpyrrolyl unit, as observed in $[(Et_8N_4Me_2)Sm(C_5H_5)]$, **(26)**.

Another possible route *via* which η^8-(COT) binding to samarium might be achieved is ligand disproportionation. This was the observed outcome in the reaction between two equivalents of $[Sm(C_5Me_5)_2(THF)_2]$ and cyclooctatetraene with the formation of $[(C_5Me_5)_3Sm]$ resulting, leaving the other samarium centre able to bind η^8- to COT in the sterically unhindered species $[(C_5Me_5)Sm(COT)]$.[21] The driving force of such a disproportionation reaction would be the increased hapticity of the COT ligand. However, in the case of the macrocyclic ligand set being studied here, this would require one of the samarium(III) centres to bind to only *one* macrocyclic pyrrolide/ *N*-methylpyrrolyl *N* donor in η^1- or η^5- fashion. Instead the COT hapticity is reduced by ring slippage to η^2, allowing the macrocyclic conformation in **(28)** to remain essentially unchanged from that observed in other $[(Et_8N_4Me_2)Sm(L)]$ complexes featuring non-bulky auxiliary ligands.

4.3.2 NMR spectroscopic characterisation

Low solubility in deuterated solvents prevented characterisation of $[\{(Et_8N_4Me_2)Sm\}_2(COT)]$, **(28)**, by NMR spectroscopy, however all resonances in the ^{1}H NMR spectrum of $[(Et_8N_4Me_2)Sm(C_5H_5)]$, **(26)**, (benzene-$d_6$ solution) were assigned by ^{1}H, ^{13}C, gCOSY, gHMQC, gHMBC and gNOESY NMR spectroscopy, Table 1. The $(C_5H_5)^-$ protons appear as a sharp singlet at 9.27 ppm, and the aromatic pyrrolide protons appear as a singlet at 7.05 ppm. The *N*-methylpyrrolyl aromatic protons appear much further upfield at 1.31 ppm. The chemically equivalent *N*-methyl protons appear as a singlet at 3.88 pm whilst four separate *meso*-ethyl CH_2 multiplets are found at 1.08, 1.46, 2.11 and 2.80 ppm. The two *meso*-ethyl CH_3 triplets are at -0.49 and 1.60 ppm.

	Pyrrole CH	*N*-MePyrrole CH	*N*-CH_3	*meso*-Et CH_2	*meso*-Et CH_3	C_5H_5
(26)	7.05	1.31	3.88	1.08, 1.46, 2.11, 2.80	-0.49, 1.60	9.27

Table 1: ^{1}H NMR spectroscopic data for $[(Et_8N_4Me_2)Sm(C_5H_5)]$, **(26)** (benzene-$d_6$, 300 MHz, 298 K, ppm).

The room temperature ^{1}H NMR spectroscopic data implies an averaged C_{2v} symmetry for the molecule in solution resulting from free rotation of the $(C_5H_5)^-$ ring about the Sm-(C_5H_5) bond at a rate faster than the timescale of the NMR experiment. This was investigated further *via* low temperature ^{1}H NMR spectroscopic studies. Spectra were collected at 10 °C increments between 20 °C and -60 °C in a toluene-d_8 solution of **(26)**. Over this range of temperatures some changes in chemical shifts were noted, in keeping with the Curie-Weiss Law. However, no significant line broadening or coalescences giving rise to changes in multiplicity were observed over the range of temperatures. This indicated that the $(C_5H_5)^-$ fluctionality remained fast enough to preserve approximate C_{2v} symmetry, even at -60 °C. In addition to free rotation of the $(C_5H_5)^-$ ligand, the chemical equivalence of the two *N*-methylpyrrolyl rings indicates the Sm-(*N*-methylpyrrolyl) interactions are also fluctional in solution over the range of temperatures investigated (the *N*-methylpyrrolyl groups display η^1- and η^5- binding to Sm in the solid state molecular structure, see Section 4.3.3.1). Similar studies performed on the (presently unsynthesised) monomethyl derivative $[(Et_8N_4Me_2)Sm(C_5H_4Me)]$ would be of interest, as the asymmetry introduced by the monosubstitution might be expected to cause the $(C_5H_4Me)^-$ ring to "lock in" to the macrocycle binding groove, resulting in loss of fluctionality. Beyond monomethyl substitution further steric interferences would be apparent.

The *N*-methylpyrrolyl aromatic proton resonances in the ^{1}H NMR spectrum of $[(Et_8N_4Me_2)Sm(C_5H_5)]$, **(26)**, were distinguished from the pyrrolide aromatic protons *via* gHMBC and NOESY spectra. In the gHMBC spectrum the *N*-CH_3 protons showed a $^3J_{CH}$ correlation to the *N*-methylpyrrolyl quaternary carbon, and the *N*-methylpyrrolyl aromatic protons a $^2J_{CH}$ correlation to the same carbon. In the NOESY spectrum the

N-methylpyrrolyl protons showed a weak through-space correlation to the protons of the nearby $(C_5H_5)^-$ ring, thus confirming the gHMBC assignment. The ^1H NMR chemical shift of the pyrrolide and *N*-methylpyrrolyl aromatic proton resonances differ markedly (7.05 and 1.31 ppm, respectively). Disparity in pyrrolide and *N*-methylpyrrolyl aromatic proton chemical shifts has been observed in other Sm(III) complexes of the $(Et_8N_4Me_2)^{2-}$ macrocycle, *e.g.* $[(Et_8N_4H_2)SmMe]$, 6.76 and 2.98 ppm, respectively; $[(Et_8N_4H_2)Sm(CH_2SiMe_3)]$, 6.77 and 2.94 ppm, respectively.[24] The difference in chemical shifts between the two sets of protons may be due to paramagnetic effects of the Sm centre, although the even greater upfield chemical shift of the aromatic *N*-methylpyrrolyl protons in **(26)** (1.31 ppm) may be due to the shielding influence of the proximal aromatic $(C_5H_5)^-$ ring.

gCOSY, NOESY, gHMQC and gHMBC NMR spectroscopy were used to assign all ^{13}C resonances using a toluene-d_8 solution of **(26)**, Table 2. Resonances at 104.6 and 154.5 ppm were assigned to aromatic carbons in the pyrrolide rings, whilst those at 102.0 and 134.8 ppm were assigned to carbons in the *N*-methylpyrrolyl rings. The $(C_5H_5)^-$ carbon resonances appeared at 111.5 ppm and the signal at 35.0 was assigned to the *N*-methyl carbon. The signal at 45.0 ppm was assigned to the *meso*-carbons, signals at 23.9 and 32.3 ppm were assigned to CH_2 carbons, and the methyl groups appeared at 8.2 and 9.7 ppm.

	Pyrrolide =CH	**Pyrrolide quaternary C**	***N*-MePyrrolyl =CH**	***N*-MePyrrolyl quaternary C**	***N*-CH_3**
(26)	104.6	154.5	102.0	134.8	35.0

	***meso*-CH_2**	***meso*-CH_3**	***meso*-CH_3 quaternary C**	**C_5H_5**
(26)	23.9, 32.3	8.2, 9.7	45.0	111.5

Table 2: ^{13}C NMR spectroscopic data for $[(Et_8N_4Me_2)Sm(C_5H_5)]$, **(26)** (toluene-$d_8$, 75 MHz, 298 K, ppm).

4.3.3 Molecular structures

4.3.3.1 Molecular structure of $[(Et_8N_4Me_2)Sm(C_5H_5)]$, (26)

Orange crystals of **(26)** suitable for X-ray crystal structure determination were grown from a hot saturated solution in hexanes which was allowed to cool slowly to ambient temperature overnight. The crystals belong to the orthorhombic space group *Pbcn* (No. 60), a = 16.794(3), b = 30.921(5), c = 15.991(3) Å, with 8 molecules in the unit cell. The asymmetric unit consists of 1 molecule of **(26)** in addition to ¼ badly disordered hexane molecule residing on a crystallographic C_2 axis. The disordered hexane molecule was removed from the final refinement using the SQUEEZE routine.[25] The overall solid state molecular symmetry of **(26)** approximates to C_s.

Complex **(26)** adopts a monomeric structural form in the solid state. The complex contains an η^5 bound $(C_5H_5)^-$ ligand, and σ-bound pyrrolide units. Strain introduced by the oblate, π-bound $(C_5H_5)^-$ ligand results in a unique $\eta^5{:}\eta^1{:}\eta^1{:}\eta^1$ binding mode for the macrocycle, with one of the *N*-methylpyrrolyl units bending back towards the macrocyclic plane. *Trans*-annular interaction between the *N*-methyl substituents restricts the consequent movement of the *N*-Me substituents of this ring and results in displacement of the *N*-CH_3 group of 27.4(2) ° (0.674(6) Å) from the plane of the heterocycle. The bending of the *N*-methylpyrrolyl methyl group from the heterocyclic plane indicates a high degree of strain present within the molecule, Figure 10.

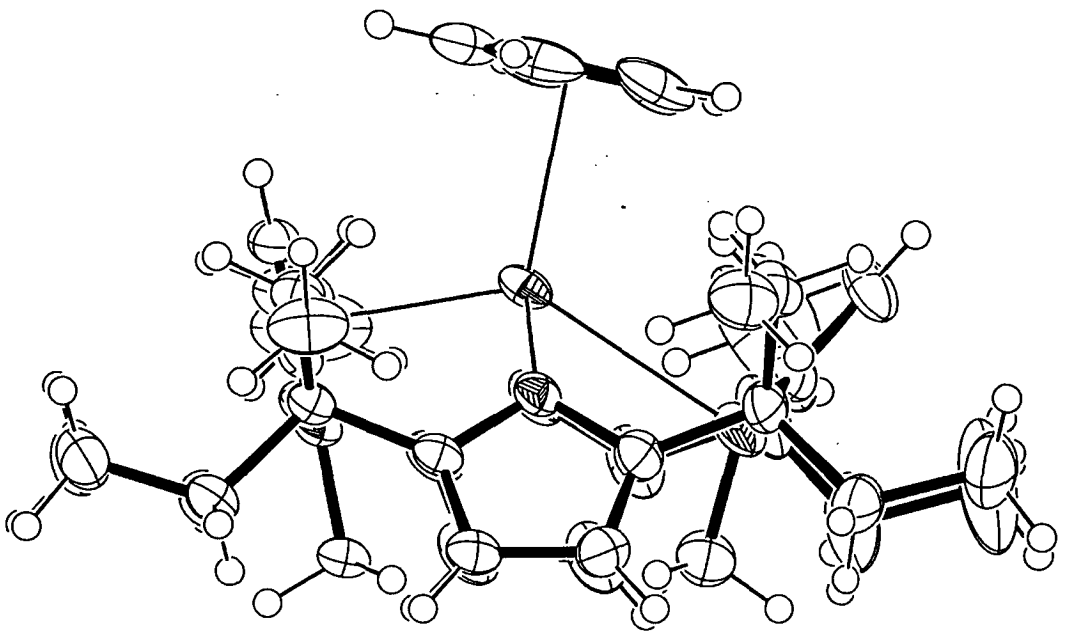

Figure 10: Molecular structure of $[(Et_8N_4Me_2)Sm(C_5H_5)]$, **(26)**, with thermal ellipsoids drawn at the level of 50% probability.

The Sm centre in **(26)** is σ-bound to the pyrrolide nitrogen centres with Sm-N distances of 2.489(3) and 2.529(2) Å. The η^1-bound *N*-methylpyrrolyl unit is bound *via* the nitrogen to the Sm centre with a Sm-N distance of 2.838(3) Å, whilst the *N*-methylpyrrolyl centroid-Sm distance of the η^5-bound *N*-methylpyrrolyl ring is 2.58_5 Å. The macrocyclic distortion is also reflected in the disparate ring tilt angles of the two *N*-methylpyrrolyl rings, *viz.* 48.8(2) ° (η^1-bound), 75.7(1) ° (η^5-bound).

The presence of the ubiquitous cyclopentadienyl ligand allows comparison to be made between the modified porphyrinogen macrocycle and other common ligand systems, such as the $\{(C_5Me_5)_2\}^{2-}$ ligand set. The macrocyclic deformation observed in **(26)** contrasts with $[(C_5Me_5)_2Sm(C_5H_5)]$, in which the three cyclopentadienyl ligands are η^5-bound with only minor steric deformations, and typical Sm-C distances.[26] Severe steric distortions are noted, however, in the more congested $[(C_5Me_5)_3Sm]$, which features lengthened Sm-C distances (up to ~0.14 Å) and large Me displacements from the ligand planes (up to 0.52 Å).[21,27] These comparisons indicate that the $(Et_8N_4Me_2)^{2-}$ modified porphyrinogen is more sterically demanding than the $\{(C_5Me_5)_2\}^{2-}$ ligand set, at least in this context.

The energy of a 0.67 Å *N*-Me displacement from the pyrrolyl plane of *N*-methylpyrrole was calculated at a modest 11.5 $kJmol^{-1}$, which is greater than that required for a 0.52 Å methyl displacement in $(C_5Me_5)^-$ (9.6 $kJmol^{-1}$).[27] $[(C_5Me_5)_3Sm]$ features a number of methyl displacements, but an additive effect is still unlikely to account for its high reactivity. The high reactivity of $[(C_5Me_5)_3Sm]$ is likely due to elongated Sm-C distances, and thus the large methyl displacements in these systems are an indicator of steric congestion rather than the primary energetic cause for high reactivity.[28] Studies to determine if the steric strain in **(26)** leads to increased reactivity are discussed in Chapter 5.

4.3.3.2 Molecular structure of $[\{(Et_8N_4Me_2)Sm\}_2(COT)]$, (28)

Green crystals of **(28)** suitable for X-ray diffraction were grown over the course of 2 weeks by diffusing cyclooctatetraene vapour into a toluene solution of the Sm(II) precursor $[(Et_8N_4Me_2)Sm(THF)_2]$, **(12)**. The crystals belong to the monoclinic space group *C2/c* (No. 15), a = 19.8414(3), b = 13.6819(2), c = 31.6735(5) Å, β = 99.8610(10) °, with 4 molecules in the unit cell. The asymmetric unit consists of one half of the dimeric unit residing on an inversion centre and one toluene molecule. The overall solid state molecular symmetry approximates to C_{2h}, Figure 11.

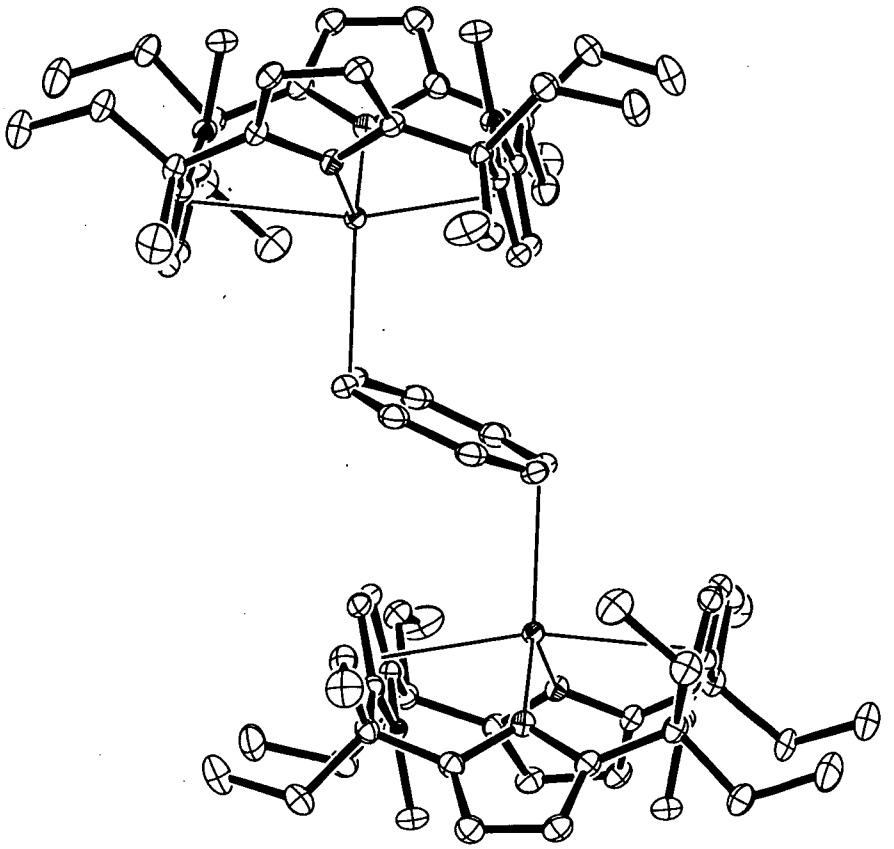

Figure 11: Molecular structure of $[\{(Et_8N_4Me_2)Sm\}_2(COT)]$, **(28)**, with thermal ellipsoids drawn at the level of 50% probability (protons removed for clarity).

Two macrocyclic units assume a centrosymmetric bimetallic arrangement with an η^2-slipped planar COT bridging the two samarium centres. The preferred binding mode for the large COT ligand is η^8, with only two f-element complexes published to date featuring COT binding without this maximum hapticity. The remarkable reduction in hapticity from the preferred η^8 binding mode to η^2 observed in **(28)** is a result of steric competition between the macrocycle and COT ligand, and a lack of alternate reaction pathways in avoiding such structural change.

The two macrocyclic pyrrolide *N* donors are σ-bound to the Sm centre with bond distances of 2.4841(11) and 2.4983(11) Å. The *N*-methylpyrrolyl ring centroid-Sm distances are 2.55_8 and 2.73_0 Å. These distances are comparable to those in $[(Et_8N_4Me_2)SmMe]$ (Sm-N distance 2.478(3) Å; Sm-(*N*-methylpyrrolyl) centroid distances 2.59_3 and 2.60_9 Å), a complex which would be expected to display little steric stain between the macrocycle and the small methyl ligand. The similarity in bond

distances between **(28)** and [$(Et_8N_4Me_2)$SmMe] indicates a similar lack of strain introduced by the slipped COT ring in **(28)**.

The metallocene bend angle in **(28)** is 165.2_4 °, which is in the range typical of other sterically unhindered [$(Et_8N_4Me_2)$Sm(III)] complexes, such as [$(Et_8N_4Me_2)$SmMe] (168.8_6 °). The tilt angles of the *N*-methylpyrrolyl rings vary according to their proximity to the slipped COT ring. The tilt angle of the *N*-methylpyrrolyl ring proximal to the face of the COT is 78.7_9 °, whilst the *N*-methylpyrrolyl ring further from the COT is 73.8_5 °. The small disparity in the two angles reflects the influence of the neighbouring COT ring and accounts for the earlier noted difference in Sm-centroid distances to these heterocyclic rings.

The closest Sm-C distances to the COT ligand are 2.704(1) and 2.751(1) Å, the next closest being 3.523(2) Å, Figure 12. In consequence of the large ring slippage there are close contacts between the Sm centres and hydrogens of the COT attached to the Sm-bound carbons (Sm···H 2.75(2), 2.78(2) Å, isotropically refined H positions). There are also close contacts between the COT and hydrogens in the 3,4-positions of a *N*-methylpyrrolyl unit (C···H 2.53, 2.55 Å, calculated H positions).

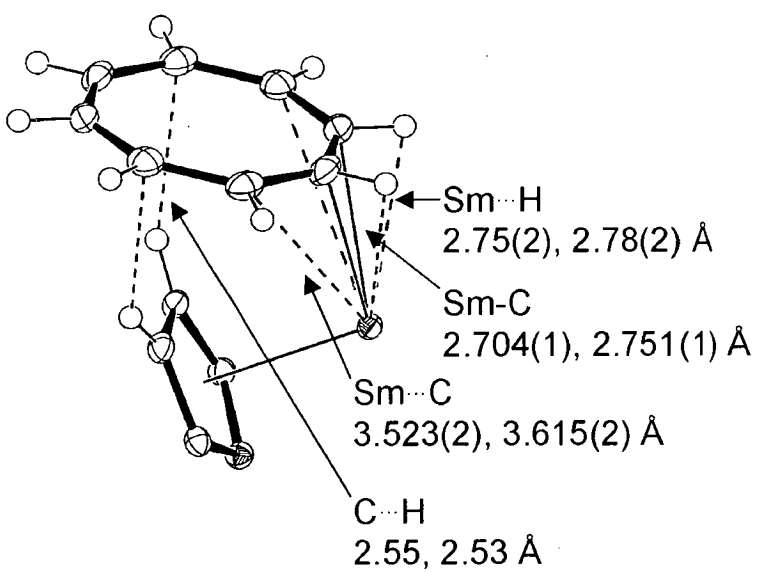

Figure 12: Detail of the COT bonding mode in [$\{(Et_8N_4Me_2)Sm\}_2$(COT)], **(28)** (Sm/macrocycle interactions on one face of the COT shown only).

4.4 Experimental

Synthesis of $[(Et_8N_4Me_2)Sm(C_5H_5)]$, (26)

2-Chloro-2-methylpropane (5.8×10^{-4} mol, 1.25 mL of 4.3 % w/v solution in THF) was added to a solution of $Et_8N_4Me_2Sm(THF)_2$ (5.8×10^{-4} mol, 0.50 g) in toluene (20 mL) at 0 °C. The mixture was stirred for 1 h then cooled to -35 °C. A suspension of $Na(C_5H_5)$ (5.8×10^{-4} mol, 0.051 g) in toluene (5 mL) was cooled to -35 °C and added *via* cannula to the cold reaction mixure with stirring. The mixture was warmed to room temperature for 1.5 h during which time the colour changed from pale brown to orange, before being cooled to -50 °C and filtered *via* cannula. Solvent was removed from the filtrate *in vacuo* at -20 °C to give an orange solid. Hexanes (5 mL) were added and the flask briefly warmed to room temperature to form a uniform suspension. Overnight cooling to -80 °C, removal of the supernatant *via* cannula and drying *in vacuo* afforded the product as an orange powder (0.21 g, 46 %). Crystals suitable for X-ray diffraction analysis were obtained by cooling a hot, saturated hexane solution.

^{1}H NMR (300 MHz, C_6D_6, 25 °C): δ = -0.49 (t, 12H, CH_3), 1.08 (m, 4H, CH_2),1.31 (s, 4H, =CH, *N*-CH_3pyr), 1.46 (m, 4H, CH_2), 1.60 (t, 12H, CH_3), 2.11 (m, 4H, CH_2), 2.80 (m, 4H, CH_2), 3.88 (s, 6H, N-CH_3), 7.05 (s, 4H, =CH, pyr), 9.27 (s, 5H, C_5H_5).

^{13}C NMR (75 MHz, $C_6D_5CD_3$, 25 °C): δ= 8.2 (CH_3), 9.7 (CH_3), 23.9 (CH_2), 32.3 (CH_2), 35.0 (N-CH_3), 45.0 (CEt_2), 102.0 (=CH, *N*-CH_3pyr), 104.6 (=CH, pyr), 111.5 (C_5H_5), 134.8 (C, *N*-CH_3pyr), 154.5 (C, pyr).

Anal. Calcd.: C, 66.01; H, 7.60; N, 7.16 ($C_{43}H_{59}N_4Sm$, MW = 782.34)
Found: C, 66.06; H, 7.55; N, 6.77.

Synthesis of $[\{(Et_8N_4Me_2)Sm\}_2(COT)]$, (28)

Cyclooctatetraene (1.15×10^{-4} mol, 60 µL of 20 % w/v solution in toluene) was added to a solution of $Et_8N_4Me_2Sm(THF)_2$ (2.3×10^{-4} mol, 198 mg) in toluene (15 mL). There was an immediate colour change from dark purple to green, and green solids formed over the course of 5 minutes. The mixture was allowed to settle and the colourless supernatant

decanted away. The precipitate was rinsed with toluene (10 mL) and dried *in vacuo* to give the product as a bright green crystalline powder (153 mg, 82 %).

Anal. Calcd.: C, 65.57; H, 7.60; N, 7.28 ($C_{84}H_{116}N_8Sm_2$, MW 1538.64)
Found: C, 65.07; H, 7.32; N, 7.04.

4.5 References

1. G. Wilkinson, J.M. Birmingham, *J. Am. Chem. Soc.*, 1954, **76**, 6210.

2. W.J. Evans, I. Bloom, W.E. Hunter, J.L. Atwood, *J. Am. Chem. Soc.*, 1981, **103**, 6507.

3. **a**. W.J. Evans, R.A. Keyer, J.W. Ziller, *J. Organomet. Chem.*, 1990, **394**, 87.
   b. S.D. Stults, R.A. Anderson, A. Zalkin, *Organometallics*, 1990, **9**, 115.

4. W.A. Herrmann, R. Anwander, F. Munck, W. Scherer, *Chem. Ber.*, 1993, **126**, 331.

5. G. Jeske, L.E. Schock, P.N. Swepston, H. Schumann, T. J. Marks, *J. Am. Chem. Soc.*, 1985, **107**, 8103.

6. R.G. Hayes, J.L. Thomas, *J. Am. Chem. Soc.*, 1969, **91**, 6876.

7. A.L. Wayda, I. Mukerji, J.L. Dye, R.D. Rogers, *Organometallics*, 1987, **6**, 1328.

8. S.R. Ely, T.E. Hopkins, C.W. DeKock, *J. Am. Chem. Soc.*, 1976, **98**, 1624.

9. W.J. Evans, G.W. Nyce, J.W. Ziller, *Angew. Chem. Int. Ed.*, 1994, **39**, 240.

10. **a**. I. Bach, K.-R. Pörschke, B. Proft, R. Goddard, C. Kopiske, C. Krüger, A. Rufińska, K. Seevogel, *J. Am. Chem. Soc.*, 1997, **119**, 3773.
    b. F. Schager, K.-J. Haack, R. Mynott, A. Rufińska, K.-R. Pörschke, *Organometallics*, 1998, **17**, 807.

11. F. Mares, K. Hodgson, A. Streitwieser, *J. Organomet. Chem.*, 1970, **24**, C68.

12. K.O. Hodgson, K.N. Raymond, *Inorg. Chem.*, 1972, **11**, 3030.

13. U. Kilimann, F.T. Edelmann, *J. Organomet. Chem.*, 1994, **469**, C5.

14. U. Kilimann, F.T. Edelmann, *J. Organomet. Chem.*, 1993, **444**, C15.

15. U. Reissmann, P. Poremba, M. Noltemeyer, H.-G. Schmidt, F.T. Edelmann, *Inorg. Chim. Acta*, 2000, **303**, 156.

16. H. Schumann, J. Winterfeld, H. Hemling, F.E. Hahn, P. Reich, K.-W. Brzezinka, F.T. Edelmann, U. Kilimann, M. Schäfer, R. Herbst-Irmer, *Chem. Ber.*, 1995, **128**, 395.

17. P. Poremba, F.T. Edelmann, *J. Organomet. Chem.*, 1997, **549**, 101.

18. P.W. Roesky, *J. Organomet. Chem.*, 2001, **621**, 277.

19. P.W. Roesky, *Eu. J. Inorg. Chem.*, 2001, **7**, 1653.

20. **a**. T.G. Wetzel, P.W. Roesky, *Organometallics*, 1998, **17**, 4009.
b. T.G. Wetzel, S. Dehnen, P.W. Roesky, *Organometallics*, 1999, **18**, 3835.

21. W.J. Evans, S.L. Gonzales, J.W. Ziller, *J. Am. Chem. Soc.*, 1991, **113**, 7423.

22. W.J. Evans, *Coord. Chem. Rev.*, 2000, **206**, 263.

23. P. Crewdson, S. Gambarotta, M.-C. Djoman, I. Korobkov, R. Duchateau, *Organometallics*, 2005, **24**, 5214.

24. J. Wang, M.G. Gardiner, *Organometallics*, 2005, **24**, 815.

25. **a**. A.L. Spek, *J. Appl. Cryst.*, 2003, **36**, 7.
b. P. v.d. Sluis, A.L. Spek, *Acta Cryst.*, 1990, **A46**, 194.

26. W. J. Evans, T. A. Ulibarri, *J. Am. Chem. Soc.* **1987**, *109*, 4292.

27. B3LYP/6-311+G(2d,p)//B3LYP/6-31G(d): Gaussian 03 (Revision D.01), M. J. Frisch et al.

28. W. J. Evans, S. A. Kozimor, J. W. Ziller, *Inorg. Chem.* **2005**, *44*, 7960.

Chapter 5

Ligand Based Reduction Chemistry of Strained Sm(III) Complexes

5.1 Introduction

The reduction potential of most accessible lanthanide(II) centres allows them to participate in a wide range of reduction chemistry. This is routinely exploited in the synthesis of new organometallic complexes by reductive routes (*e.g.* electron transfer to reducible auxiliary ligands, redox transmetallation), and has also led to the increasingly important use of stoichiometric samarium(II) reducing agents in organic syntheses *e.g.* SmI_2, SmI_2/HMPA.[1]

In addition to electron transfer from a low-valent lanthanide metal centre, reduction chemistry can be facilitated *via* electron transfer from a ligand, and ligand-based reduction chemistry has been established in a number of lanthanide systems. The extremely strained $[(C_5Me_5)_3Ln]$ complexes contain three $(C_5Me_5)^-$ ligands which are η^5-bound to the samarium centre with Ln-$(C_5Me_5)^-$ centroid distances considerably longer than typically observed in Sm(III) complexes containing the $(C_5Me_5)^-$ ligand.[2,3] The cone angle of the $(C_5Me_5)^-$ ligand in sterically unhindered lanthanide complexes is typically 130 - 138 °.[4] The presence of three $(C_5Me_5)^-$ ligands around the one lanthanide centre results in an increase in Ln-C bond lengths (up to 2.910(3) Å in the case of Sm) to achieve a cone angle of 120° for each ligand. The resultant strain is also evident in out-of-plane bending of some methyl groups of the $(C_5Me_5)^-$ ligands (θ = 6.7 - 20.7 ° in the case of Sm) due to abutting with adjacent $(C_5Me_5)^-$ rings.[5]

$[(C_5Me_5)_3Sm]$, **(I)**, was found to be highly reactive, undergoing reactions normally associated with lanthanide alkyl complexes such as insertion chemistry with small molecules (*e.g.* CO, H_2, C_2H_4), suggesting that the complex was behaving as though one of the $(C_5Me_5)^-$ ligands was an η^1-bound, alkyl-like group.[6] In addition to alkyl-like reactivity, $[(C_5Me_5)_3Ln]$ (Ln = La **(II)**, Nd **(III)**, Sm **(I)**) complexes were found to be active reductants, behaving in some reactions like a lanthanide(II) synthon. The reductive properties were found to be due to strain between ligands within the $[(C_5Me_5)_3Ln]$ molecule, and this sub-set of ligand based reductive chemistry has been

termed *Sterically Induced Reduction* (≡ SIR).[7] Reduction by $[(C_5Me_5)_3Ln]$ complexes is accompanied by oxidative coupling of the $(C_5Me_5)^-$ rings, Scheme 1.

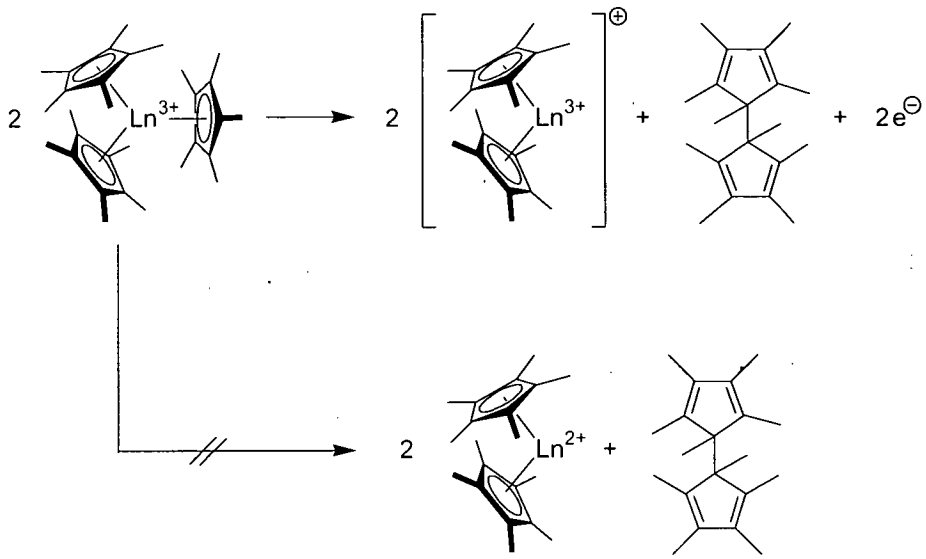

Scheme 1: Reductive reactivity in $[(C_5Me_5)_3Ln]$ complexes.

An example of SIR chemistry is the reduction of $Ph_3P{=}Se$ by $[(C_5Me_5)_3Ln]$, **(I)** - **(III)**, to give $[\{(C_5Me_5)_2Ln\}_2(\mu{:}Se_2)]$, **(IV)**, Scheme 2.[6,8,9] The less sterically crowded product **(IV)** forms in the case of all three lanthanides, with the concomittant formation of $(C_5Me_5)_2$. Using a different reaction stoichiometry, only the Sm complex gave the more reduced product $[\{(C_5Me_5)_2Sm(THF)\}_2(\mu{:}Se)]$, **(V)**. The variation in SIR reactivity between lanthanides is due to variations in ionic radius and the consequent degree of steric crowding present in the $[(C_5Me_5)_3Ln]$ molecules, thus allowing the potential to fine tune reducing reactivity by choice of Ln.[5]

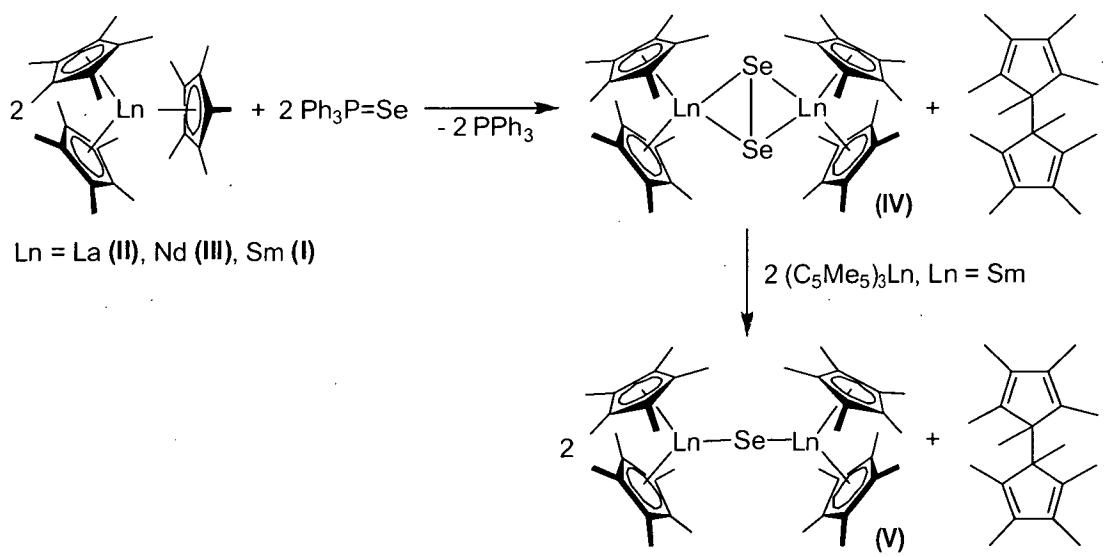

Scheme 2: SIR reduction by $[(C_5Me_5)_3Ln]$.

Sterically induced reduction of some substrates by $[(C_5Me_5)_3Ln]$ produces reaction outcomes different to those obtained by samarium(II) complexes.[6,10] For example, $[(C_5Me_5)_2Sm]$ reduces anthracene (Scheme 3) and pyrene to give the Sm(III) complexes $[\{(C_5Me_5)_2Sm\}_2(\mu\text{-}C_{14}H_{10})]$ and $[\{(C_5Me_5)_2Sm\}_2(\mu\text{-}C_{16}H_{10})]$[11] whilst $[(C_5Me_5)_3Sm]$ fails to react with either substrate. Such examples indicate that the SIR reductive pathway does not progress *via* a Sm(II) intermediate, an assertion which was conclusively demonstrated by the recent synthesis of $[(C_5Me_5)_3Sm]$, **(I)**, from the reaction of $(C_5Me_5)_2Sm$ with $(C_5Me_5)_2$.[9] The availability of $[(C_5Me_5)_3Ln]$ for Ln other than Sm makes reductive chemistry feasible even for lanthanides which are not known to form stable or even transient Ln(II) species.

A type of SIR reactivity was implicated in the formation of the crystallographically characterised bis(imino)acenaphthene Sm(III) complex **(VI)** from $[(C_5Me_5)_2Sm(OEt_2)]$, **(VII)**, Equation 1. The presence of $(C_5Me_5)_2$ in the reaction mixture confirmed that electron transfer from a $(C_5Me_5)^-$ ligand had taken place resulting in coordination of the dianionic acenaphthene ligand to a Sm(III) centre.[12]

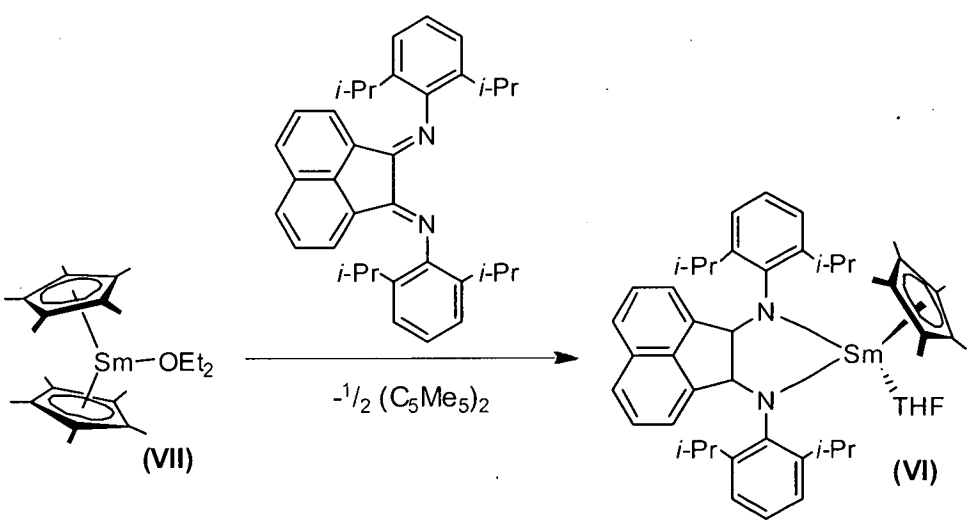

Equation 1

Solvent-mediated Sm(III)-Sm(II) reactivity has been reported for samarium(III) complexes of anthracene, pyrene, stilbene and styrene.[11,13] For example, anthracene was reacted with $[(C_5Me_5)_2Sm]$, **(VIII)**, to give $[\{(C_5Me_5)_2Sm\}_2\{\mu:\eta^3:\eta^3\text{-}(C_{14}H_{10})\}]$, **(IX)**, Scheme 3. The +3 oxidation state of the samarium centres in **(IX)** was determined by ^{13}C NMR spectroscopic chemical shifts and Sm-C bond lengths in the solid state molecular structure. Addition of THF to **(IX)** gave anthracene and the samarium(II) complex

$[(C_5Me_5)_2Sm(THF)_2]$, **(X)**; the solvated nature of **(X)** prevented regeneration of **(IX)** by removal of THF and addition of a non-polar solvent, thus rendering the transformation irreversible. However, complex **(IX)** might be expected to act as a source of Sm(II) and thus facilitate reductive chemistry in the presence of THF.

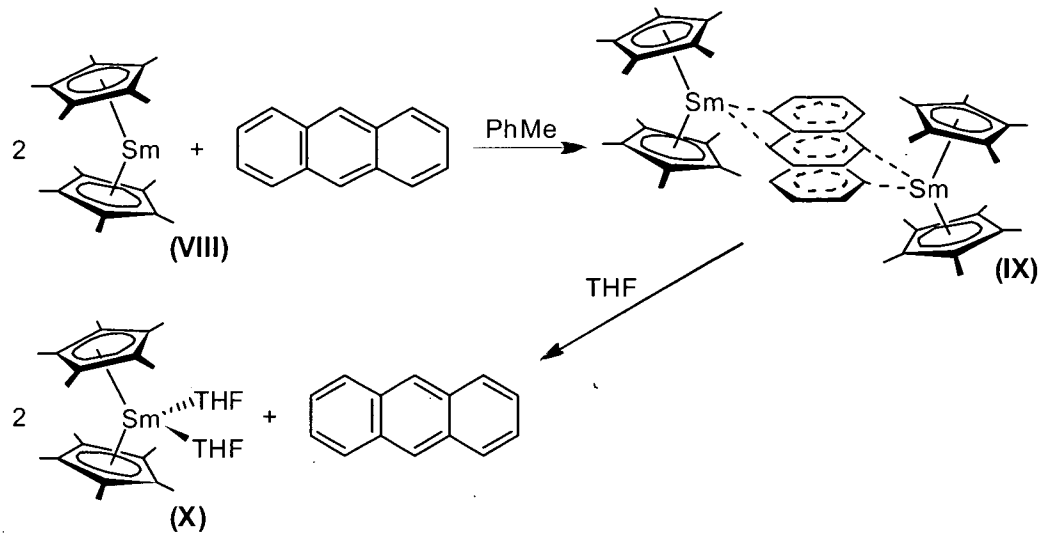

Scheme 3: THF-mediated Sm(III)-Sm(II) redox chemistry.

Solvent-mediated redox reversal has been observed in ytterbium(III) complexes of indenyl, *ansa*-indenyl and $(C_5Me_5)^-$ ligands with *t*-BuDAB (see Chapter 3.1).[14] Addition of THF to the ytterbium(III) complexes resulted in formation of the respective THF-solvated ytterbium(II) complex and loss of neutral *t*-BuDAB. It was noted that the ytterbium *t*-BuDAB complex of the less bulky $(C_5H_5)^-$ ligand, $[(C_5H_5)_2Yb(t\text{-BuDAB})]$, **(XI),** did not revert to the ytterbium(II) starting material upon addition of THF.[15] The difference in reactivity was attributed to the smaller $(C_5H_5)^-$ ligand allowing better interaction between the ytterbium and nitrogen centres of the *t*-BuDAB ligand, making replacement by THF and the concomitant Yb(III) reduction to Yb(II) a less facile process. However, complex **(XI)** reacted directly with 9-fluorenone in a ligand-replacement reaction involving electron transfer from the DAB radical anion to the ketone, Equation 2. Reaction of equimolar amounts of 9-fluorenone and **(XI)** gave the dimeric ytterbium(III) complex **(XII)** which contains two CpYb(THF) units linked through two 9,9-difluorenyl dioxide fragments. In addition to electron transfer from the *t*-BuDAB radical to 9-fluorenone, a pinacol condensation had taken place with loss of two $(C_5H_5)^-$ ligands. A perfluorophenyl-substituted DAB ligand is implicated in the solvent mediated reversible redox chemistry observed in complex $[(C_5Me_5)_2Eu(C_6F_5DAB\{Me\})]$, which reverts to the THF-solvated europocene and free DAB upon addition of THF (see Chapter 3.1).[16]

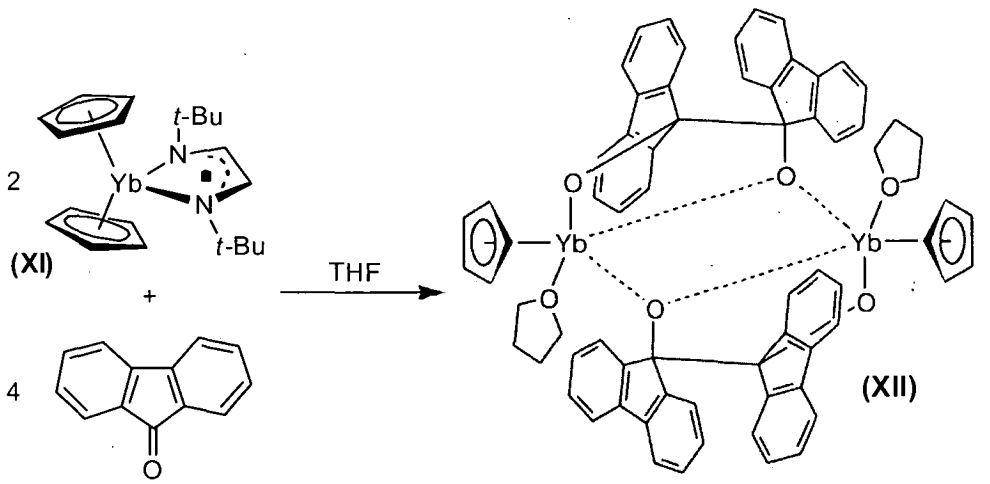

Equation 2 [15]

Ligand participation in redox chemistry has been reported for phenylchalcogenolate lanthanide complexes. $Ln(SPh)_3$ (Ln = Ce, Pr, Nd, Sm, Gd, Tb, Dy, Ho, Er) are found to reduce elemental sulfur giving octanuclear lanthanide sulfido clusters and an oxidatively coupled byproduct according to Equation 3.[17]

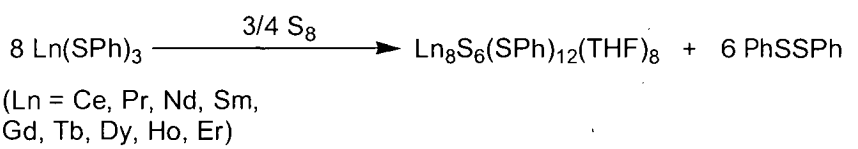

Equation 3

Phenylchalcogenolate reduction chemistry was explored further in the context of the $\{(C_5Me_5)_2\}^{2-}$ ligand set with the preparation of $[(C_5Me_5)_2Sm(EPh)(THF)]$, **(XIII)**, and $[\{(C_5Me_5)_2Sm(EPh)\}_2]$, **(XIV)**, for E = S, Se and Te.[18] Complex **(XIII)** (E = Te) was found to reduce (not *via* SIR chemistry) azobenzene (but not phenazine or cyclooctatetraene), Equation 4. The unsolvated complex **(XIV)** (E = Te) reduced phenazine, but not azobenzene or cyclooctatetraene. Reasons for the lack of reactivity with azobenzene were not clear, and represent an interesting reversal of the usual pattern of increased reactivity for unsolvated complexes.

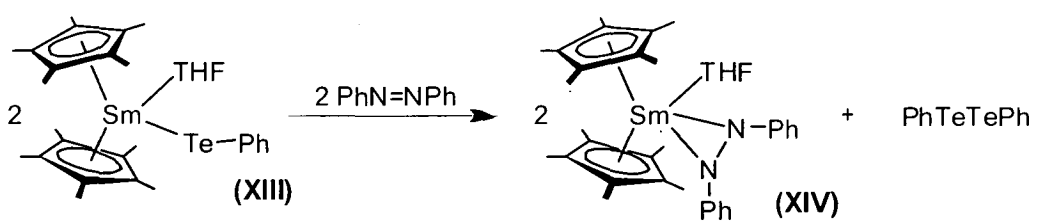

Equation 4

A recent example of ligand based reduction involves the very large $((4\text{-}n\text{-Bu-}C_6H_4)_5C_5)^-$ ($\equiv Cp^{BIG}$) ligand, Equation 5.[19] Reaction of the Sm(III) precursor $[(2\text{-}Me_2N\text{-}C_6H_4\text{-}CH_2)_3Sm]$, **(XV)**, with $Cp^{BIG}H$ resulted in formation of the Sm(II) metallocene $[(Cp^{BIG})_2Sm]$, **(XVI)**, *N,N'*-dimethyl-*o*-toluidine and 1,2-di(2-Me_2N-phenyl)ethane, the latter product formed by the coupling of two $(2\text{-}Me_2N\text{-}C_6H_4\text{-}CH_2)^-$ ligands. Driving forces suggested by the authors for the remarkable spontaneous Sm(III)-Sm(II) transformation included the steric bulk of the Cp^{BIG} ligand, and the stability of the Sm(II) samarocene.

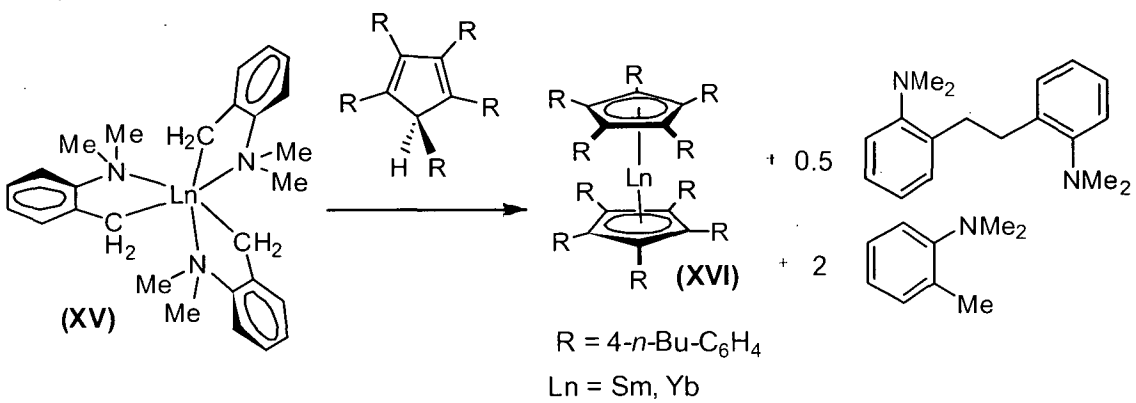

Equation 5

There are examples of porphyrinogen ligands participating in ligand-based reduction chemistry in transition metal complexes.[20,21] Oxidation of Fe(II), Co(II), Ni(II) and Co(II) complexes of the $(Et_4N_4)^{4-}$ porphyrinogen were reported to result in 2 or 4 electron oxidation of the macrocycle, resulting in a porphyrinogen containing 1 or 2 cyclopropane units, respectively.[21,22] The porphyrinogen thereby acts as an electron source, Scheme 4.

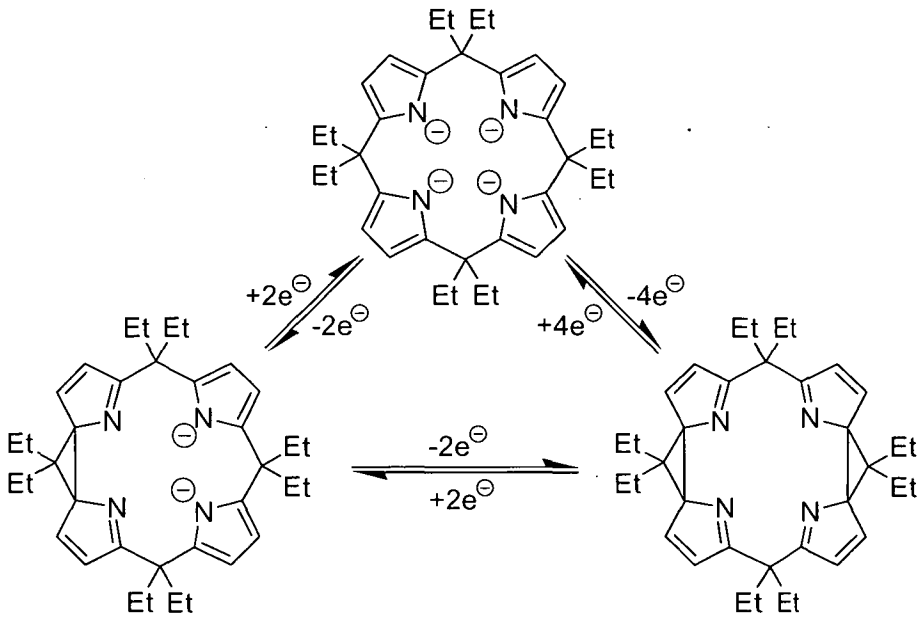

Scheme 4: Intramolecular electron transfer in the $(Et_8N_4)^{4-}$ system.

The transformations of the cobalt(II) complex $[(Et_8N_4)CoLi_2(THF)_4]$, **(XVII)**, are representative of those observed in the analogous Fe(II), Ni(II) and Cu(II) complexes. Complex **(XVII)** was oxidised with 1,4-benzoquinone, molecular O_2 or $CuCl_2$ to give $[(Et_8N_4)(\Delta)Co]$, **(XVIII)**, where $\Delta \equiv$ intramolecular cyclopropyl unit. Further oxidation with $CuCl_2$ led to the formation of $[(Et_8N_4)(\Delta_2)CoCl][Cu_4Cl_5]$, **(XIX)**, Scheme 2. The oxidised porphyrinogens **(XVIII)** and **(XIX)** could be reductively demetallated with H_2S to give the fully reduced porphyringoen $Et_8N_4H_4$, **(XX)**, effectively reversing the redox chemistry.

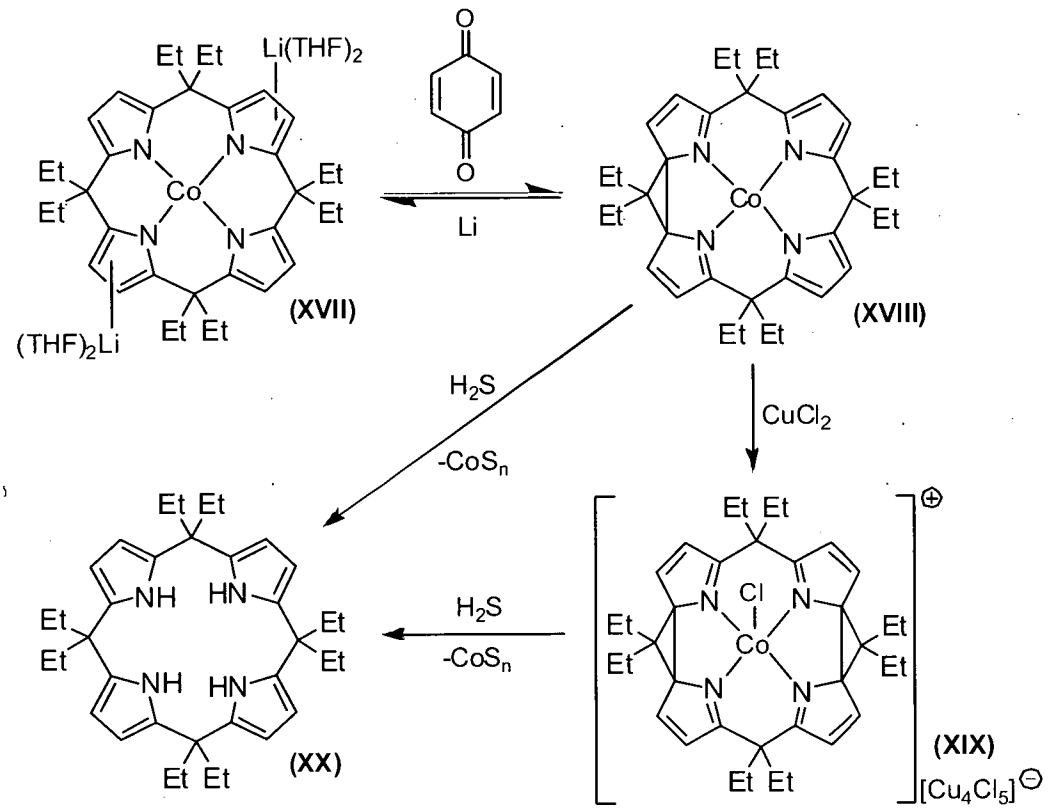

Scheme 2: Reversible electron transfer at a $(porphyrinogen)^{4-}$ ligand

The cobalt complex $[(Et_8N_4)Co]^-[Li(THF)_4]^+$, **(XXI)**, underwent solvent-mediated disproportionation in hydrocarbon solvents to give a mixture of $[(Et_8N_4)CoLi_2(THF)_4]$, **(XVII)**, and $[(Et_8N_4)(\Delta)Co]$, **(XVIII)**, Equation 6. The process reverses upon addition of THF due to formation of the $[Li(THF)_4]^+$ cation, present in **(XXI)**.

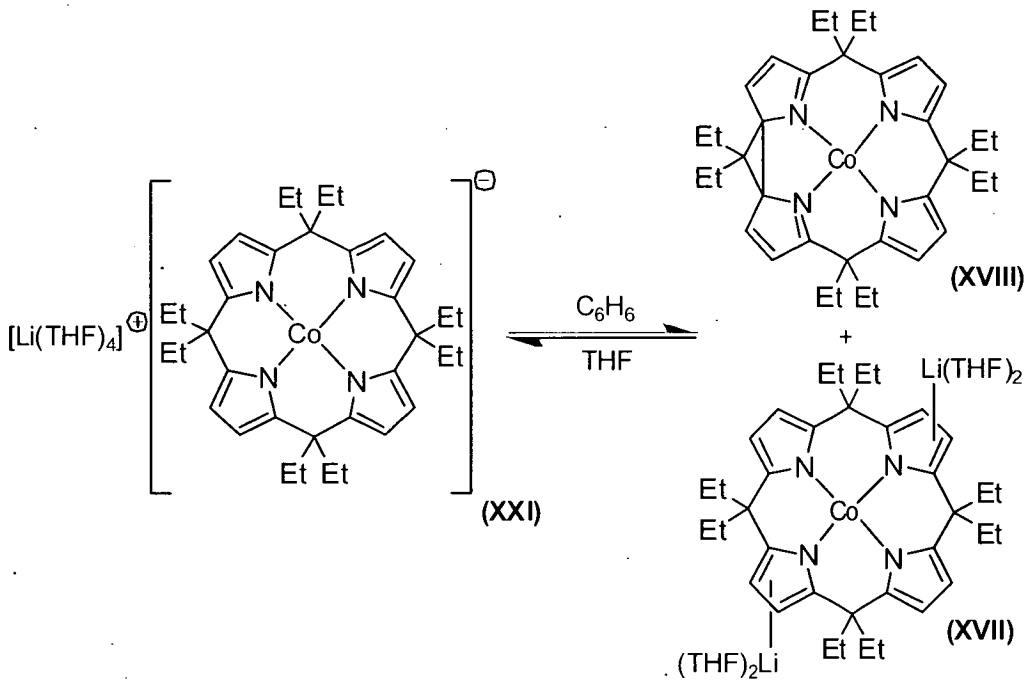

Equation 6

5.2 Research aim

The sterically demanding nature of the $(Et_8N_4Me_2)^{2-}$ macrocycle makes Sm(III) complexes featuring large auxiliary ligands likely to display unusual reactivty. Sm(III) complexes containing *t*-BuDAB, *i*-PrDAB and $(C_5H_5)^-$ auxiliary ligands were to be reacted with one or more reducible substrates (cyclooctatetraene, benzil and benzophenone). Reduction of one of these substrates to form the corresponding Sm(III) complex was expected to be accompanied by formation of neutral *t*-BuDAB, *i*-PrDAB or $(C_5H_5)_2$, thus representing an overall electron transfer between ligands.

5.3 Results and discussion

5.3.1 Complex syntheses

The Sm(III) *t*-BuDAB complex $[\{(Et_8N_4Me_2)Sm\}_2(t\text{-BuDAB})]$, **(18)**, was observed to revert to the Sm(II) complex $[(Et_8N_4Me_2)Sm(THF)_2]$, **(12)**, immediately upon dissolution in THF at room temperature, Equation 7.

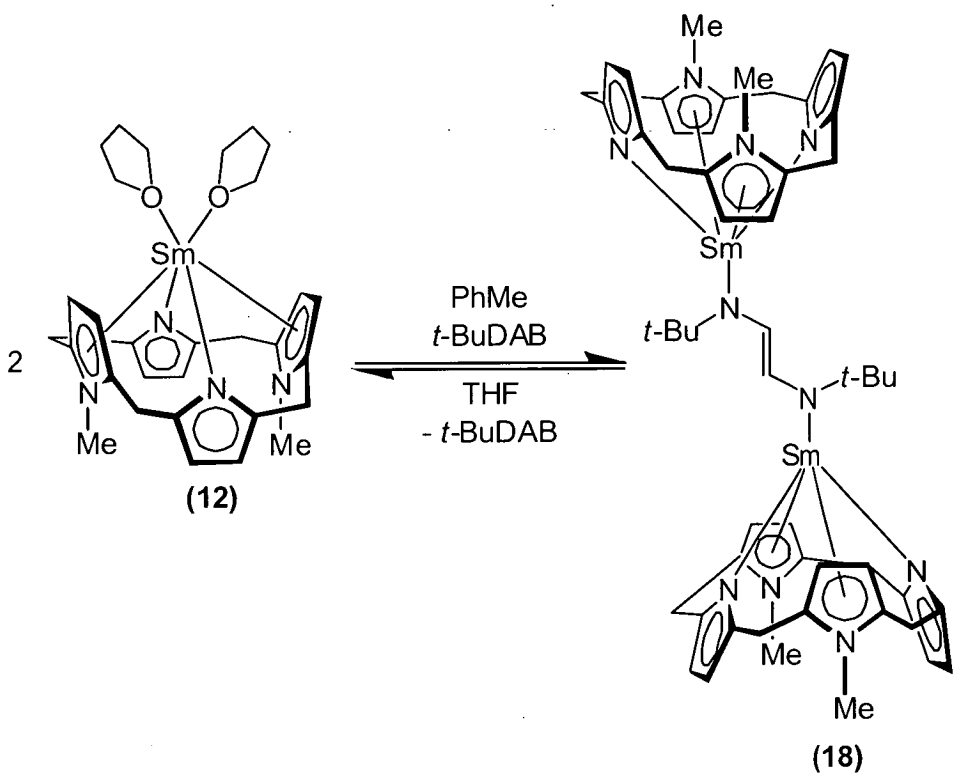

Equation 7

This solvent-mediated reversible redox reactivity suggested the possibility of using **(18)** to conduct reduction chemistry by adding THF to provide an *in situ* source of Sm(II) complex **(12)**. Further to this, it was speculated that **(18)** may be capable of reducing substrates directly in non-polar solvents, without the addition of THF to explicitly create the Sm(II) complex **(12)**. The experiments described in this chapter were all performed on an NMR scale (3×10^{-5} mol).

A solution of **(18)** in benzene-d_6 was added to a solution of benzil in benzene-d_6, Scheme 6. There was a change in colour within a minute from green to the maroon colour of the reduced complex $[\{(Et_8N_4Me_2)Sm\}_2\{OC(Ph)C(Ph)O\}]$, **(29)**. The reaction mixture was heated to effect complete dissolution of **(18)**, which produced a further darkening of colour. Dark maroon crystals formed upon cooling to room temperature, and were separated from the mother liquor. The ^{1}H NMR spectrum of the isolated crystalline product in benzene-d_6 was identical to that of an authentic sample of **(29)**,[23] and free *t*-BuDAB was also observed, indicating that complex **(18)** had acted as a reducing agent. The crystals produced in the reaction were suitable for X-ray structure determination, and the molecular structure agreed with that obtained for the authentic product. The authentic sample of **(29)** was prepared by the addition of a toluene solution

of benzil to a toluene solution of $[(Et_8N_4Me_2)Sm(THF)_2]$, **(12)**, Scheme 6. Crystals suitable for X-ray structure determination were grown by slow cooling of a hot toluene solution to room temperature.

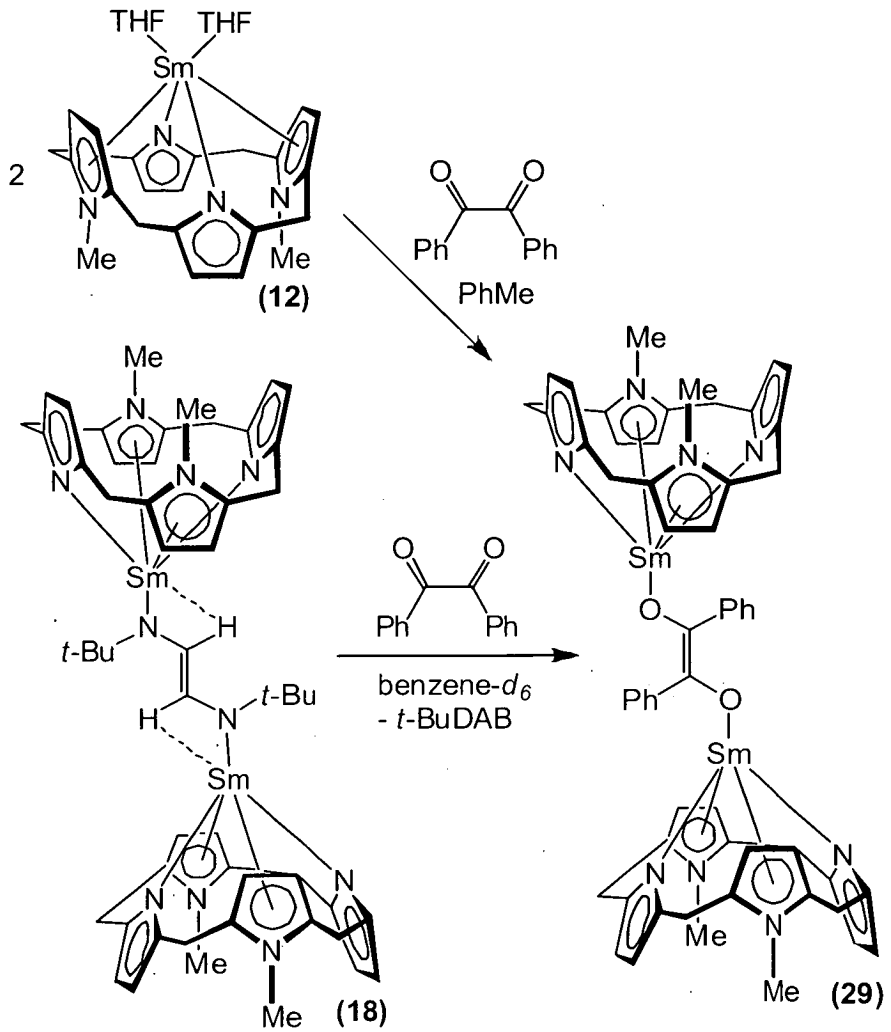

Scheme 6: Syntheses of $[\{(Et_8N_4Me_2)Sm\}_2\{OC(Ph)C(Ph)O\}]$, **(29)**.

The reduction chemistry of the *i*-PrDAB analogue of **(18)**, $[\{(Et_8N_4Me_2)Sm\}_2(i\text{-PrDAB})]$, **(20)**, which features less bulky *i*-Pr groups in place of *t*-butyl substituents on the bridging 1,4-diazabuta-1,3-diene dianion, was also investigated. Unlike **(18)**, the *i*-propyl complex **(20)** does not revert to **(12)** upon dissolution in THF. Trialling **(20)** for Sm(II)-like reactivity was of interest in determining whether a Sm(III) complex which doesn't undergo solvent-mediated reversible redox chemistry would still be able to reduce benzil. A solution of **(20)** in benzene-d_6 was added to a solution of benzil in benzene-d_6, Equation 8. There was a change in colour from green to maroon at room temperature, and upon heating at 80 °C for 30 minutes the colour darkened further. The

presence of **(29)** in the reaction mixture was confirmed by ^{1}H NMR spectroscopy, which also showed the presence of neutral *i*-PrDAB.

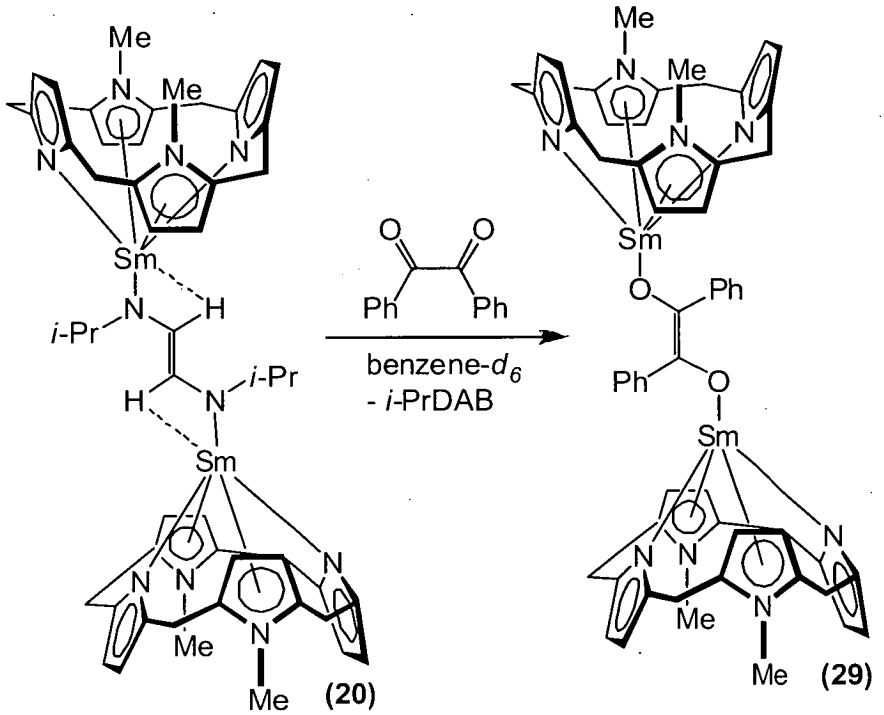

Equation 8

The successful reduction of benzil by the *i*-PrDAB Sm(III) complex **(20)** indicated that the solvent-mediated chemistry observed for **(18)** was not necessary for ligand-based reduction reactivity to occur with reducible substrates. There are direct parallels between this set of results and those obtained with the ytterbium(II) complex [$(C_5H_5)_2$Yb(*t*-BuDAB)], **(XI)**. Like **(20)**, complex **(XI)** does not revert to the Ln(II) precursor upon dissolution in THF. Further, **(XI)** was able to undergo reaction with a reducible substrate (9-fluorenone) to give a reduced product and free DAB, albeit conducted in THF. The ability of **(18)** and **(20)** to undergo ligand redistribution reactions is perhaps more surprising, since the reduction potential for Sm(III)/Sm(II) (-1.55 V) is higher than that for Yb(III)/Yb(II) (-1.15 V).[24] Trials with the even less bulky *n*-BuDAB Sm(III) complex [{$(Et_8N_4Me_2)$Sm}$_2$(*n*-BuDAB)], **(21)**, were not possible due to the difficulties encountered preparing pure samples on a preparative scale (see Chapter 3.3.1.2).

To summarise the [{$(Et_8N_4Me_2)$Sm}$_2$(RDAB)] reductive chemistry, solvent-mediated reversible redox chemistry is specific to the *t*-BuDAB complex [{$(Et_8N_4Me_2)$Sm}$_2$(*t*-BuDAB)], **(18)**, whilst ligand-based reduction chemistry is more

general. The particular ease with which the *t*-BuDAB complex **(18)** undergoes reversible redox chemistry may be due to the electron-donating effect of the *t*-butyl group reducing the stability of the *t*-BuDAB dianion, thereby making the reverse reaction more facile than in the dinuclear *i*-propyl **(20)** or *n*-butyl **(21)** analogues. The more generally observed ligand-based reductive chemistry may be due to the presence of an equilibrium between bridging Sm(III) and chelating Sm(III) complexes resulting in the formation of Sm(II) *in situ*, such as that postulated in the formation of the unsolvated Sm(II) dimer [{($Et_8N_4Me_2$)Sm}$_2$], **(22)**, (Chapter 3.3.1.2, Scheme 8). Although Sm(II) species were not observed in the ^{1}H or ^{13}C NMR spectra of the Sm(III) complexes, the equilibrium concentration of [Sm(II)] required for reduction chemistry may be significantly lower than that observable by NMR spectroscopy.

The Sm(III) cyclopentadienyl complex [($Et_8N_4Me_2$)Sm(C_5H_5)], **(26)**, was trialled for Sm(II)-like reactivity on the basis of the steric strain contained within the macrocyclic skeleton. The η^5-bound cyclopentadienyl ring forces one of the macrocyclic *N*-methylpyrrolyl *N*-methyl groups 27.4(2) ° out of the plane of the heterocycle. The strain of this deformation was calculated to be 11.5 kJ mol^{-1}.[25] For comparison, the strain due to each 0.52 Å methyl displacement in [(C_5Me_5)$_3$Sm] is 9.6 kJ mol^{-1}, although the presence of intramolecular strain does not necessarily indicate a capacity for sterically induced reduction activity (Section 5.1).[5] The energy benefit in releasing this strain, though modest, may potentially result in unusual reactivity. Reaction was attempted with 1,4-benzoquinone, benzil and cyclooctatetraene.

Complex **(26)** was reacted on an NMR scale with 1,4-benzoquinone. A solution of 1,4-benzoquinone in toluene was added to a solution of [($Et_8N_4Me_2$)Sm(C_5H_5)], **(26)**, in toluene and heated in a sealed tube for 5 minutes at 130 °C, giving a tan coloured solution. The temperature of 130 °C was chosen as the highest which the sealed tube containing toluene could safely be operated at. Comparison of the ^{1}H NMR spectrum of the reaction mixture with that of an authentic sample confirmed the presence of [{($Et_8N_4Me_2$)Sm}$_2${O(C_6H_4)O}], **(30)**, indicating that ligand substitution had taken place, Equation 9. The authentic sample of [{($Et_8N_4Me_2$)Sm}$_2${O(C_6H_4)O}], **(30)**, was previously prepared by reduction of 1,4-benzoquinone with [($Et_8N_4Me_2$)Sm(THF)$_2$], **(12)**.[23] The presumed mechanisms involve coupling of two $(C_5H_5)^-$ rings to supply the electrons required to produce the

1,4-benzoquinone dianion, or a Diels-Alder reaction between $(C_5H_5)^-$ and the benzoquinone substrate. However, neither $(C_5H_5)_2$ or other coupled products were identified in the crude reaction mixture by either ^{1}H NMR spectroscopy or GC/MS analysis and thus the proposed mechanisms remain unconfirmed.

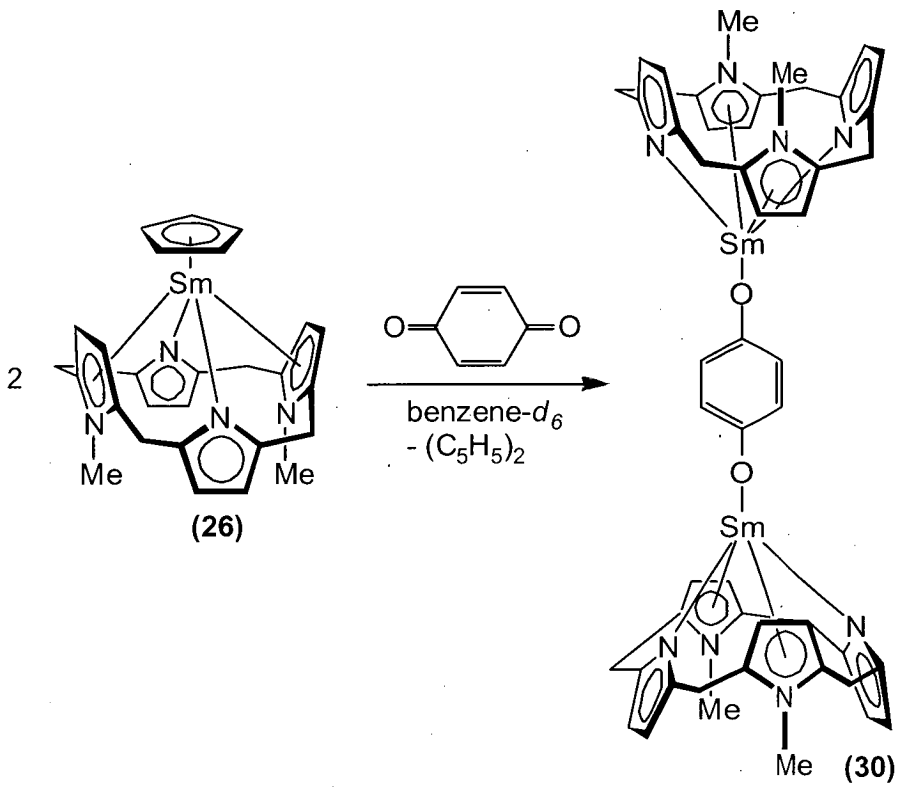

Equation 9

Reaction of complex **(26)** with benzil was attempted on an NMR scale, Equation 10. A solution of **(26)** in benzene-d_6 was added to a solution of benzil in benzene-d_6 and heated overnight at 70 °C in a sealed tube. The reaction had changed colour from orange to purple, however the expected reduction product, $[\{(Et_8N_4Me_2)Sm\}_2\{(OC(Ph)C(Ph)O\}]$, **(29)**, was absent in the reaction mixture (determined by ^{1}H NMR spectroscopy), indicating that ligand redistribution had not taken place. The reaction of complex **(26)** with cyclooctatetraene was attempted on an NMR scale, Equation 11. A solution of **(26)** in toluene was added to a solution of cyclooctatetraene in toluene and heated at 130 °C in a sealed tube for 2 d, with no change in appearance. The expected product of ligand redistribution in this case was $[\{(Et_8N_4Me_2)Sm\}_2(COT)]$, **(28)**, which is bright green and insoluble in toluene. The lack of colour change or precipitation indicated that ligand redistribution had not taken place.

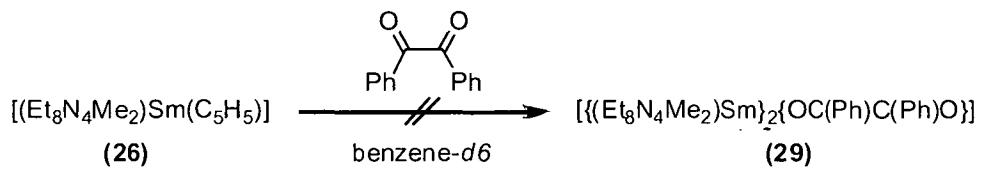

Equation 10

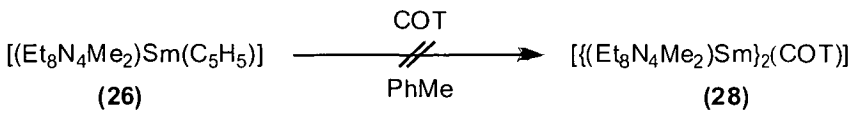

Equation 11

In summary, the Sm(III) cyclopentadienyl complex $[(Et_8N_4Me_2)Sm(C_5H_5)]$, is stable in THF, and does not undergo the solvent-mediated reversible redox chemistry displayed by $[\{(Et_8N_4Me_2)Sm\}_2(t\text{-BuDAB})]$, **(18)**. Complex **(26)** undergoes a ligand redistribution reaction with 1,4-benzoquinone, but analogous chemistry is not observed with either benzil or cyclooctatetraene substrates.

5.3.2 Molecular structure of $[\{(Et_8N_4Me_2)Sm\}_2(OC(Ph)C(Ph)O)]$, (29)

Dark maroon crystals of $[\{(Et_8N_4Me_2)Sm\}_2\{OC(Ph)C(Ph)O\}]$, **(29)**, suitable for X-ray crystal structure determination were grown by either cooling a hot toluene solution of the complex, or cooling the hot benzene-d_6 reaction mixture of benzil and $[\{(Et_8N_4Me_2)Sm\}_2(t\text{-BuDAB})]$, **(18)**. The crystals obtained by the latter method provided a better crystallographic refinement, and they form the basis of the discussion below.

The crystals belong to the monoclinic space group *C*2/*c* (No. 15), a = 16.054(13), b = 20.063(9), c = 30.959(8) Å, β = 102.38(4) °, with 4 molecules in the unit cell, the asymmetric unit consisting of one half of a molecule of $[\{(Et_8N_4Me_2)Sm\}_2\{OC(Ph)C(Ph)O\}]$, **(29)** residing on a crystallographic inversion centre. The molecule has only C_i symmetry, with reduction from C_{2h} being due to the geometry of the bridging benzil dianion. The structure of **(29)** is shown in Figure 1.

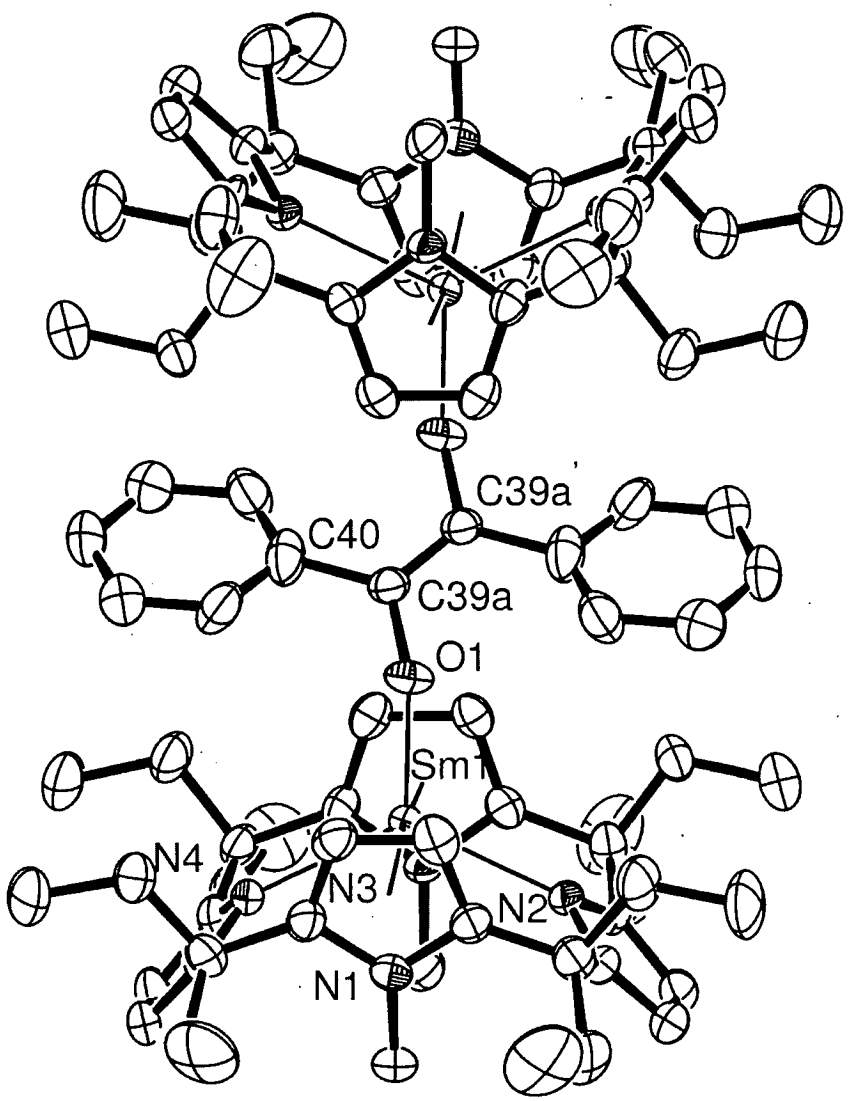

Figure 1: Molecular structure of **(29)**, with thermal ellipsoids drawn at the level of 50% probability (protons removed for clarity).

The molecular structure of **(29)** is dinuclear with each Sm centre bound within its respective macrocyclic cavity in the usual $\eta^1:\eta^5:\eta^1:\eta^5$ fashion. The Sm-N(pyrrolide) distances of 2.470(4), 2.495(4) Å are typical for a Sm(III) centre bound to the $(Et_8N_4Me_2)^{2-}$ macrocycle, as are the Sm-centroid distances of 2.59_5, 2.63_1 Å. The metallocene bend angle is 162.6_2 °, which is similar to the range of values observed in the dinuclear Sm(III) complexes **(18)**, **(19)** and **(21)** featuring bridging RDAB dianions (161.5_3-166.3_6 °). The pyrrolide ring tilt angles of 47.3_9, 49.1_7 ° and *N*-methylpyrrolyl ring tilt angles of 79.5_3, 79.5_8 ° are again within the range of values observed in complexes **(18)**, **(19)** and **(21)** (45.1_0-54.7_1 ° and 77.0_5-79.3_7 °, respectively).

The doubly reduced benzil dianion is bound to each Sm centre *via* the O centres with a bond length of 2.120(4) Å. Disorder in the crystal resulted in a refinement model containing two positions for the alkenyl carbons within the benzil dianion, with disparate bond lengths and angles, Figure 2. The double bond character of the central C=C bond is evident in each of the disordered benzil units, thus implying a doubly reduced dianion: O(1)-C(39A)-C(39A)-O(1) = 1.391(9)-1.323(19)-1.391(9) Å; O(1)-C(39B)-C(39B)-O(1) = 1.41(2)-1.37(5)-1.41.(2) Å. The central benzil atoms O(1), C(39A), C(39B) and C(40) are coplanar, and to which plane the adjoining phenyl groups display a small twist of 27.6_6 °.

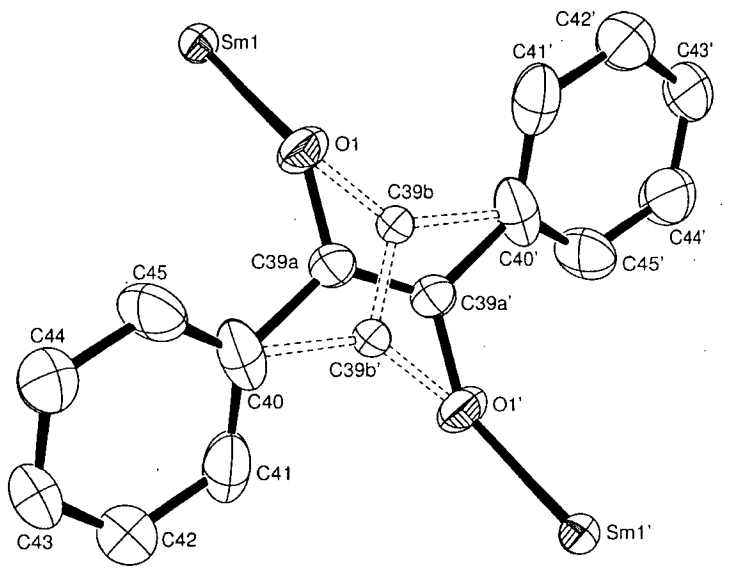

Figure 2: Detail of disordered benzil dianion in the molecular structure of **(29)**.

5.4 Experimental

Synthesis of [{($Et_8N_4Me_2$)Sm}$_2$(OC(Ph)C(Ph)O)], (29)

Dark maroon crystals of [{($Et_8N_4Me_2$)Sm}$_2${OC(Ph)C(Ph)O}], **(29)**, suitable for X-ray crystal structure determination were grown by adding a solution of benzil (1.5×10^{-5} mol) in benzene-d_6 (0.3 mL) and [{($Et_8N_4Me_2$)Sm}$_2$(*t*-BuDAB)], **(18)**, (3×10^{-5} mol) in benzene-d_6 (0.3 mL), briefly heating to reflux in a sealed tube and cooling to room temperature.

^{1}H NMR (300 MHz, C_6D_6, 25 °C): δ = -0.38 (t, 24H, CH_3), 1.16 (m, 8H, CH_2), 1.24 (t, 24H, CH_3), 1.72 (m, 8H, CH_2), 2.57 (m, 8H, CH_2), 3.97 (s, 8H, =CH, pyrMe), 4.22 (s, 12H, CH_3), 6.75 (s, 8H, =CH, pyr), 7.50 (t, 2H, =CH, benz), 7.64 (t, 4H, =CH, benz), 8.86 (d, 4H, =CH, benz).

5.5 References

1. G.A. Molander, C.R. Harris, *Chem. Rev.*, 1996, **96**, 307.

2. W.J. Evans, S.L. Gonzales, J.W. Ziller, *J. Am. Chem. Soc.*, 1991, **113**, 7423.

3. W.J. Evans, B.L. Davis, *Chem. Rev.*, 2002, **102**, 2119.

4. W.J. Evans, T.A. Ulibarri, *J. Am. Chem. Soc.*, 1987, **109**, 4292.

5. W.J. Evans, S.A. Kozimor, J.W. Ziller, *Inorg. Chem.*, 2005, **44**, 7960.

6. W.J. Evans, K.J. Forrestal, J.W. Ziller, *J. Am. Chem. Soc.*, 1998, **120**, 9273.

7. W.J. Evans, *Coord. Chem. Rev.*, 2000, **206**, 263.

8. W.J. Evans, G.W. Nyce, R.D. Clark, R.J. Doedens, J.W. Ziller, *Angew. Chem. Int. Ed.*, 1999, **38**, 1801.

9. W.J. Evans, J.M. Perotti, S.A. Kozimor, T.M. Champagne, B.L. Davis, G.W. Nyce, C.H. Fujimoto, R.D. Clark, M.A. Johnston, J.W. Ziller, *Organometallics*, 2005, **24**, 3916.

10. **a**. W.J. Evans, D.K. Drummond, S.G. Bott, J.L. Atwood, *Organometallics*, 1986, **5**, 2389.
b. W.J. Evans, D.K. Drummond, L.R. Chamberlain, R.J. Doedens, S.G. Bott, H. Zhang, J.L. Atwood, *J. Am. Chem. Soc.*, 1988, **110**, 4983.

11. W.J. Evans, S.L. Gonzales, J.W. Ziller, *J. Am. Chem. Soc.*, 1994, **116**, 2600.

12. K. Vasudevan, A.H. Cowley, *Chem. Commun.*, 2007, 3464.

13. W.J. Evans, T.A. Ulibarri, J.W. Ziller, *J. Am. Chem. Soc.*, 1990, **112**, 219.

14. **a**. A.A. Trifonov, E.A. Fedorova, G.K. Fukin, V.N. Ikorskii, Y.A. Kurskii,

S. Dechert, H. Schumann, M.N. Bochkarev,
Russ. Chem. Bull., Int. Ed., 2004, **53**, 2736.
b. A.A. Trifonov, E.A. Fedorova, V.N. Ikorskii, S. Dechert, H. Schumann, M.N. Bochkarev, *Eu. J. Inorg. Chem.*, 2005, 2812.

15. **a**. A.A. Trifonov, Y.A. Kurskii, M.N. Bochkarev, S. Muehle, S. Dechert, H. Schumann, *Russ. Chem. Bull., Int Ed.*, 2003, **52**, 601.
b. A.A. Trifonov, E.N. Kirillov, M.N. Bochkarev, H. Schumann, S. Muehle, *Russ. Chem. Bull.*, 1999, **48**, 384.

16. J.A. Moore, A.H. Cowley, J.C. Gordon, *Organometallics*, 2006, **25**, 5207.

17. J.H. Melman, T.J. Emge, J.G. Brennan, *Inorg. Chem.*, 1999, **38**, 2117.

18. W.J. Evans, K.A. Miller, D.S. Lee, J.W. Ziller, *Inorg. Chem.*, 2005, **44**, 4326.

19. C. Ruspic, J.R. Moss, M. Schürmann, S. Harder,
Angew. Chem. Int. Ed., 2008, **47**, 2121.

20. **a**. J. Jubb, C. Floriani, A. Chiesi-Villa, C. Rizzoli,
J. Am. Chem. Soc., 1992, **114**, 6571.
b. M. Rosi, A. Sgamellotti, F. Franceschi, C. Floriani,
Chem. Eu. J., 1999, **5**, 2914.
c. C. Floriani, E. Solari, F. Franceschi, R. Scopelliti, P. Belanzoni, M. Rosi,
Chem. Eu. J., 2001, **7**, 3052.

21. S. De Angelis, E. Solari, C. Floriani, A. Chiesi-Villa, C. Rizzoli,
J. Am. Chem. Soc., 1994, **116**, 5702.

22. **a**. S. De Angelis, E. Solari, C. Floriani, A. Chiesi-Villa, C. Rizzoli,
J. Am. Chem. Soc., 1994, **116**, 5691.

23. J. Wang, Unpublished results, University of Tasmania, 2003.

24. L.R. Morss, *Chem. Rev.*, 1976, **76**, 827.

25. B3LYP/6-311+G(2d,p)//B3LYP/6-31G(d): Gaussian 03 (Revision D.01), M.J. Frisch et al.

Chapter 6

Carbon Dioxide and Transmetallation Reduction Chemistry

6.1 Introduction

6.1.1 Lanthanide CO_2 reduction chemistry

Organometallic compounds of carbon dioxide have been prepared with η^1-C and η^2-CO binding, as well as a variety of bridging modes, Figure 1.[1] In addition a number of activation and reduction pathways have been observed in main group and transition metal systems, including various stoichiometric and catalytic insertions, reductive coupling (to oxalate), reductive deoxygenation (to CO and O^{2-}) and reductive disproportionation (to CO and CO_3^{2-}).

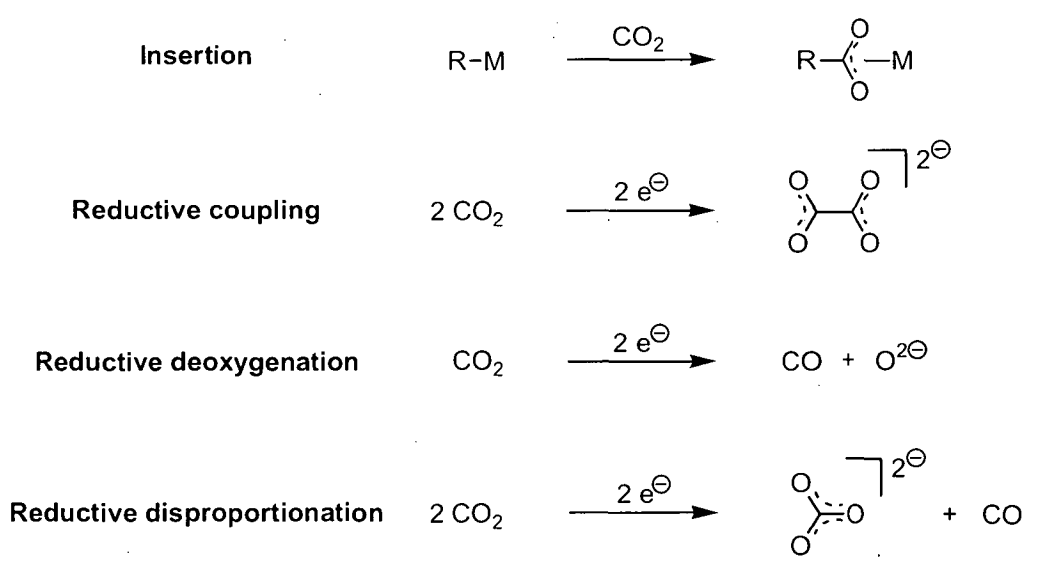

Figure 1: Transition metal mediated activation and reduction of carbon dioxide

A spectroscopically characterised example of carbon dioxide insertion in f-element chemistry is the reaction of CO_2 with the uranium(IV) complex $[(C_5Me_5)_2U(S\text{-}t\text{-}Bu)_2]$, **(I)**, to give $[(C_5Me_2)_2U(O_2CS\text{-}t\text{-}Bu)_2]$, **(II)**, Equation 2.[2] Complex **(II)** represented the first isolated example of CO_2 insertion into a metal-sulfur bond.

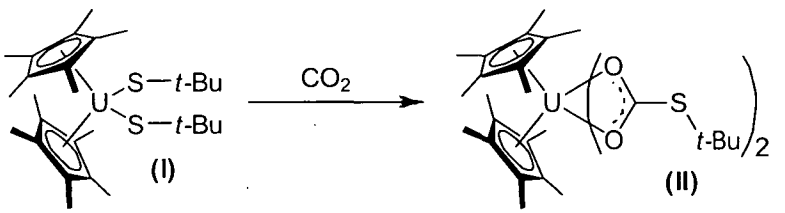

Equation 1

Studies of CO_2 insertion into samarium-chalcogen bonds have also been undertaken with the samarium(III) complexes $[\{(C_5Me_5)_2Sm(\mu\text{-}EPh)\}_2]$ (E = S, Se, Te), Equation 2. The resultant S and Se complexes **(III)** and **(IV)** were structurally authenticated.[3]

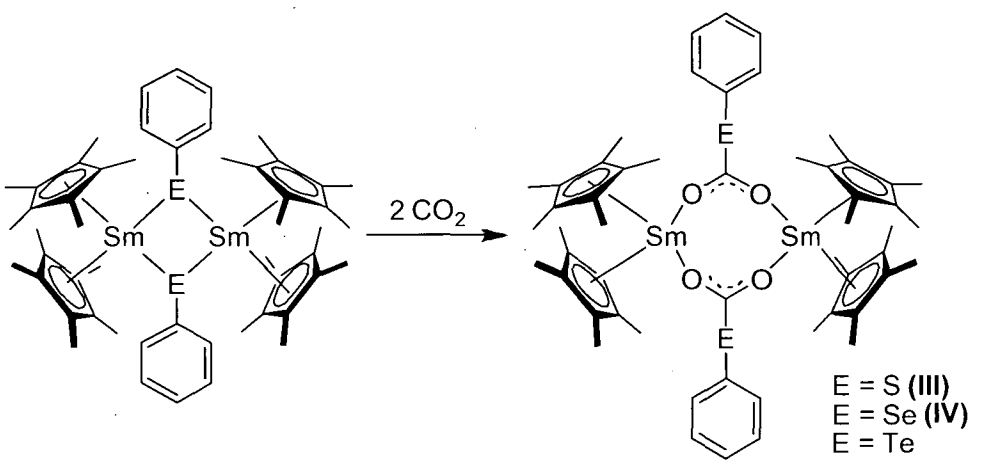

Equation 2

Insertion products were also obtained by reactions of the extremely sterically crowded $(C_5Me_5)_3Ln$ (Ln = Nd, Sm) with CO_2 to give a C_5Me_5-substituted carboxylate **(V)**. Insertion into a Ln-C σ-bond is known for $(C_5Me_5)_3Ln$ reactivity, given the sometimes alkyl-like character of the $(C_5Me_5)^-$ ligands in the crowded complex.[4]

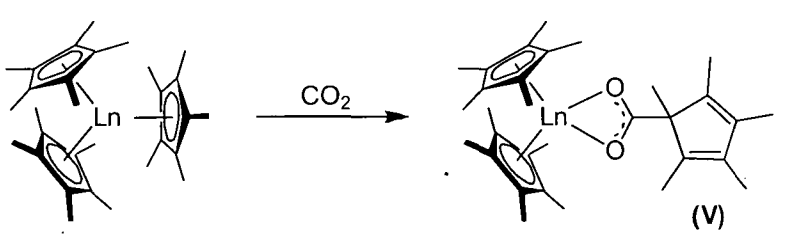

Equation 3

Reductive coupling of two CO_2 molecules has been reported by reaction of carbon dioxide with the samarium(II) complex $[(C_5Me_5)_2Sm(THF)_2]$ to give the dianionic bridging oxalate complex $[\{(C_5Me_5)_2Sm\}_2(\mu\text{-}\eta^2\text{-}\eta^2\text{-}O_2CCO_2)]$, **(VI)**.[5] The derivatised samarium(II) complex $[\{(C_5Me_4SiMe_2(CH_2CH{=}CH_2)\}_2Sm]$ also reacted with carbon dioxide to give the analogous oxalate complex **(VII)**, Equation 4.[6] In complexes **(VI)** and **(VII)** the bridging oxalate dianions bind to the lanthanide centre "side-on", forming a five-membered ring rather than the possible four-membered ring.

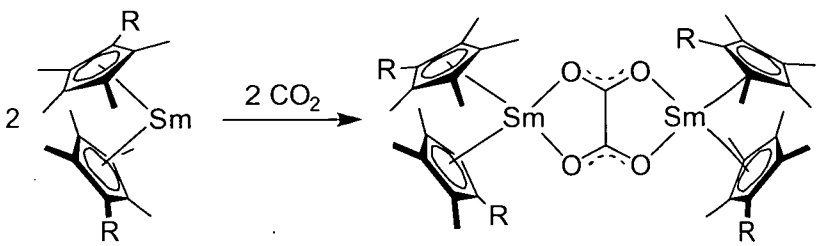

Equation 4

Reductive deoxygenation was observed in the reaction of the functionalised triazacyclononanone uranium(III) complex **(VIII)** with carbon dioxide, Equation 4. The reaction was thought to proceed *via* a putative end-on bridging CO_2 intermediate **(IX)**, before reduction to give the μ-oxo-bridged dinuclear U(IV) complex **(X)**.[7] The mononuclear U(IV) complex **(XI)** featuring end-on bound CO_2 was subsequently isolated and structurally characterised by reaction of the bulkier adamantyl substituted complex **(XII)** with CO_2.

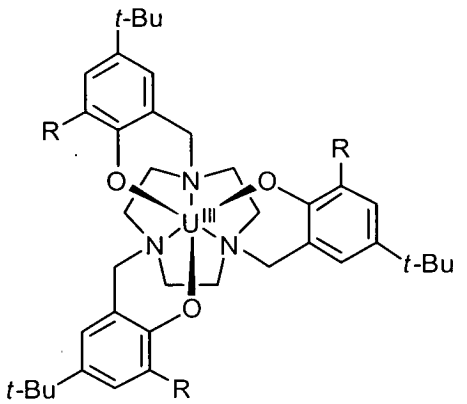

≡ LU(*t*-Bu), R = *t*-Bu, **(VIII)**

≡ LU(Ad), R = adamantyl, **(XII)**

$$\underset{\textbf{(VIII)}}{\text{LU}(t\text{-Bu})} \xrightarrow{CO_2} \underset{\textbf{(IX)}}{\text{L}(t\text{-Bu})\text{U}-\text{O}=\text{C}=\text{O}-\text{UL}(t\text{-Bu})} \longrightarrow \text{CO} + \underset{\textbf{(X)}}{\text{L}(t\text{-Bu})\text{U-O-UL}(t\text{-Bu})}$$

$$\underset{\textbf{(XII)}}{\text{LU(Ad)}} \xrightarrow{CO_2} \underset{\textbf{(XI)}}{\text{L(Ad)U}-\text{O}=\text{C}=\text{O}}$$

Equation 5

Reductive disproportionation of carbon dioxide to give carbon monoxide and a carbonate dianion has been demonstrated in transition metal chemistry, *e.g.*, the reaction of $Li_2[W(CO)_5(CO_2)]$ with an additional equivalent of carbon dioxide to give $[W(CO)_6]$ and lithium carbonate.[8] However, no examples of reductive disproportionation in f-block complexes have appeared in the literature.

6.1.2 Lanthanide redox transmetallation chemistry

Redox transmetallation exploits the ability of lanthanide(II) metal centres to reduce a metal salt, producing a lanthanide(III) complex and, typically, elemental metal, Equation 6. Salts of silver, thallium, lead and mercury are most frequently employed due to the ease with which they are reduced to the element.

$$\text{M}-\text{X} + [\text{Ln}]^{\text{II}} \longrightarrow [\text{Ln}]^{\text{III}}\text{X} + \text{M}\downarrow$$

M = Ag, Hg, Tl, Pb

Equation 6

An example of the synthetic utility of the procedure is an early synthesis of the highly crowded $[(C_5Me_5)_3Sm]$, **(XIII)**. The reduction of $[(C_5Me_5)_2Pb]$ with $[(C_5Me_5)_2Sm(OEt_2)]$ resulted in **(XIII)** as the sole samarium containing product in high

yield, Equation 7.[9] The driving force of the reaction is the precipitation of metallic lead, which is effectively an irreversible process.

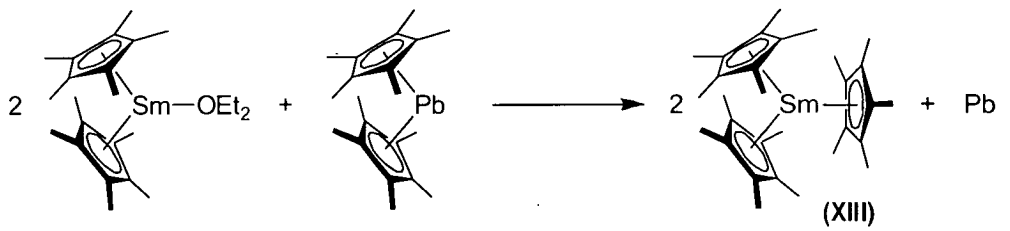

Equation 7

Reduction of the transmetallation reagent can be carried out by metallic Ln in the presence of free ligand, as in the preparation of $[Yb(OAr)_2(THF)_3]$, **(XIV)** (Ar = C_6H_2-2,6-*t*-Bu-4-OMe), Equation 8. The $Yb(C_6F_5)_2$ intermediate deprotonates the phenol, resulting in the coordinated phenoxide product in one step from the free ligand and metallic Yb.[10]

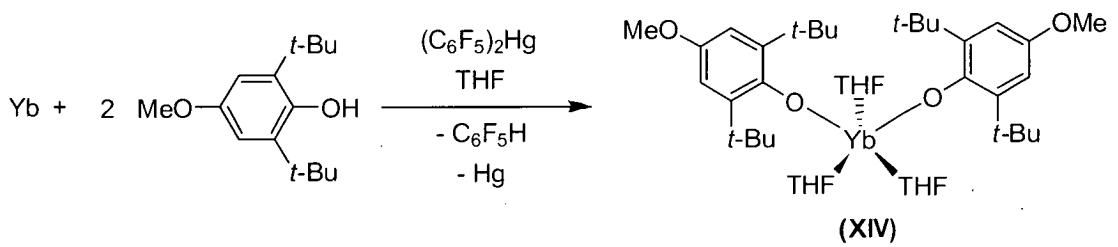

Equation 8

6.2 Research aim

We wished to investigate the reduction of CO_2 by samarium(II) in the context of the sterically demanding $(Et_8N_4Me_2)^{2-}$ ligand set. The bulky nature of the modified porphyrinogen ligand was thought capable of inducing unusual reactivity and/or structural outcomes. Similarly, we wished to exploit the strongly reducing $[(Et_8N_4Me_2)Sm(THF)_2]$, **(12)**, complex in the preparation of samarium(III) tetrafluoroborate and fluoride derivatives by reaction with metal tetrafluoroborate and fluoride salts. Solubility and subsequent salt metathesis reactivity of the tetrafluoroborate salt were also investigated.

6.3 Results and discussion

6.3.1 Carbon dioxide reduction

Reduction of carbon dioxide was investigated by reacting gaseous carbon dioxide with the Sm(II) precursor $[(Et_8N_4Me_2)Sm(THF)_2]$, **(12)**, Equation 7. An evacuated Schlenk flask containing phosphorous pentoxide was filled with carbon dioxide (1 atm) and stood overnight to dry. The Sm(II) precursor **(12)** was dissolved in toluene at room temperature and the flask carefully evacuated until the solvent began to reflux. The dried carbon dioxide was admitted *via* an evacuated line to the solution of **(12)**, and the reaction stirred. After 30 min the dark purple colour of the **(12)** had changed to light orange, and pale yellow solids had formed. The headspace was sampled with an air-tight syringe for GC/MS analysis. The reaction mixture was filtered *via* cannula and the solvent removed *in vacuo* to give a yellow solid. The solid was extracted into hot THF, filtered and concentrated *in vacuo* to give $[\{(Et_8N_4Me_2)Sm\}_2(CO_3)]$, **(31)**, as orange prisms suitable for X-ray structure determination in a yield of 54 %.

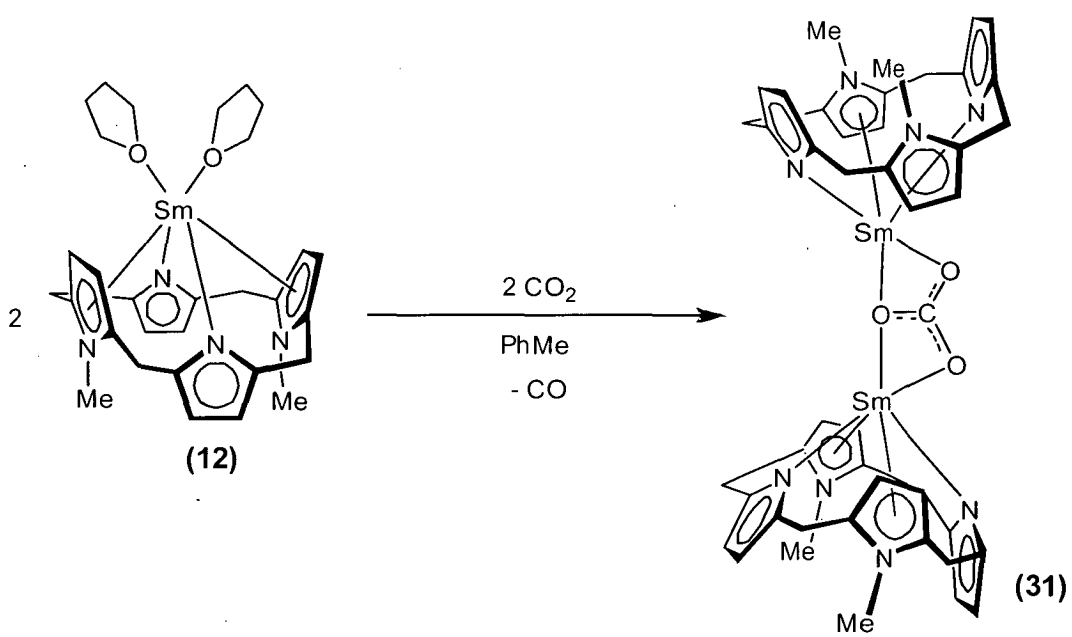

Equation 7

The molecular structure of **(31)** is dinuclear with a bridging CO_3^{2-} moiety. The constitution of **(31)** implied that carbon monoxide was produced *via* reductive disproportionation. GC/MS analysis of the headspace was performed by sampling directly from the reaction vessel with a fixed needle 1 mL hypodermic insulin syringe

(Terumo Medical Corporation, Maryland, USA) and the needle immediately sealed with a silicone rubber GC septum. A 200 μL aliquot of this sample was analysed by combined GC-MS using a HP5890 GC coupled to a Kratos ISQ high resolution magnetic sector mass spectrometer. The mass spectrometer was fitted with an electron ionisation source operating at 70 eV and a full accelerating voltage of 5.3 kV was used. Data was collected using the selected ion monitoring mode with accelerating voltage switching, at a resolution of 8,000 (10 % valley definition), and collecting full ion profiles over a 500 ppm voltage sweep about the monitored m/z values. Ions monitored within a full cycle time of 0.3 s were 28.0061 for N_2, 27.9949 for CO and 31.9898 for O_2, with 28.0061 also being used as a lock mass. A J&W 30 m x 0.53 mm internal diameter PLOT column was used with helium as carrier gas at a head pressure of 7 psi and an oven temperature of 60 °C, and the sample was injected with a 50:1 split ratio. Using standard gases, these conditions easily separated CO_2 from a mixed chromatographic peak containing N_2, O_2 and CO. While there was only a fractional offset observed in the retention times for N_2 and CO under these conditions, these two gases were fully resolved by their mass/charge ratio. An intense chromatographic peak was observed at the correct retention time in the CO channel from the reaction vessel headspace sample, and the centroid of this ion was measured as 27.9948, giving unequivocal confirmation of the presence of CO. A second peak in the CO channel 8 seconds after the retention time of CO and of similar intensity was due to the CO^+ fragment ion derived from CO_2. N_2 and O_2 were also detected in the reaction headspace, with the latter giving a significantly less intense signal than CO and the former giving a stronger signal than CO.

The reductive disproportionation reaction resulting from reduction of CO_2 by $[(Et_8N_4Me_2)Sm(THF)_2]$, **(12)**, contrasts with the reductive coupling observed in the reaction of $[(C_5Me_5)_2Sm(THF)_2]$ with CO_2.[5] The differing reaction outcomes are possibly the result of steric differences between the two ligand systems. In at least some regards the $(Et_8N_4Me_2)^{2-}$ macrocycle can be considered more sterically demanding than the $\{(C_5Me_5)_2\}^{2-}$ ligand set (*viz*, the structural differences recently established for the monomeric and trimeric structures of the $Sm^{III}Me$ derivatives).[11]

Many binding modes for oxalate are known in f-element chemistry. The "side-on" η^2-binding mode forms at least a component of the binding type in all cases, except for $[NH_4]_4[U(C_2O_4)_3(O)_2]$, which features one of the three oxalates bound in an "end-on" η^2-O,O' fashion to form a four-membered chelate ring.[12] The carbonate formation

presented here could be the result of the destabilisation of an initially formed oxalate complex that is prevented from binding with the seemingly preferred "side-on" η^2- binding mode due to the narrow, short binding groove limiting oxalate binding to "end-on", or carboxylate type η^2- binding. However, the observation of a chelating binding mode in the *i*-PrDAB complex [$(Et_8N_4Me_2)$Sm(*i*-PrDAB)], **(19)**, would suggest that a side-on η^2-oxalate binding mode can not be excluded on steric grounds alone, thus leaving the rationale for the observed reductive disproportionation open to speculation.

6.3.1.1 NMR spectroscopic characterisation

The carbonate complex [$\{(Et_8N_4Me_2)Sm\}_2(CO_3)$], **(31)**, was analysed by ^1H, ^{13}C, gHMQC , gHMBC and VT NMR spectroscopy. The resonances in the room temperature ^1H NMR spectrum of **(31)** in benzene-d_6 were observed between 6.79 and -0.51 ppm, a range typical for Sm(III) complexes of the $(Et_8Me_2H_2)^{2-}$ ligand with only minor paramagnetic shifts observed. The ^1H NMR resonances were fully assigned on the basis of signal integration and multiplicity, Table 1. The pyrrolide protons appear as a singlet at 6.79 ppm and the *N*-methylpyrrolyl protons as a singlet at 2.43 ppm. The *N*-methylpyrrolyl *N*-CH_3 groups appear as a single resonance at 1.09 ppm. The two sets of chemically inequivalent *meso*-CH_3 groups appear as triplets at -0.51 and 2.57 ppm, whilst the four *meso*-CH_2 groups appear as multiplets at 1.22, 2.13, 2.26 and 6.14 ppm.

	Pyrrolide CH	***N*-MePyrrolyl CH**	***N*-CH_3**	***meso*-Et CH_2**	***meso*-Et CH_3**
(31)	6.79	2.43	1.09	1.22, 2.13, 2.26, 6.14	-0.51, 3.57

Table 1: ^1H NMR spectroscopic data for [$\{(Et_8N_4Me_2)Sm\}_2(CO_3)$], **(31)** (benzene-$d_6$, 300 MHz, 298 K, ppm).

The ^{13}C NMR spectrum contains 11 resonances, which were completely assigned by gHMQC and gHMBC 2D experiments, Table 2. The macrocyclic quaternary carbon resonances were assigned by long-range through-bond coupling in the gHMBC

spectrum, these are noted beside each assignment. The remaining macrocyclic carbon resonances were assigned on the basis of C-H correlations in the gHMQC spectrum. The ^{13}C resonances at 7.5 and 9.6 ppm are from *meso*-CH_3 carbons and those at 21.0 and 33.9 ppm from *meso*-CH_2 groups. The *N*-CH_3 carbon resonance appears at 31.6 ppm and the *meso*-quaternary carbon at 47.3 ppm ($^2J_{CH}$ correlation to the *meso*-CH_2 protons; $^3J_{CH}$ correlation to the *meso*-CH_3 protons and to the *N*-methylpyrrolyl and pyrrolide CH protons). The aromatic carbons appear at 97.0 (*N*-methylpyrrolyl CH), 101.3 (pyrrolide CH), 133.8 (*N*-methylpyrrolyl quaternary C; $^2J_{CH}$ correlation to the *N*-methylpyrrolyl CH protons, $^3J_{CH}$ correlation to the *N*-CH_3 protons) and 154.6 ppm (pyrrolide quaternary C; $^2J_{CH}$ correlation to the pyrrolide CH protons). The remaining resonance at 190.8 ppm was assigned to the CO_3^{2-} group.

	Pyrrolide =CH	**Pyrrolide quaternary C**	***N*-MePyrrolyl =CH**	***N*-MePyrrolyl quaternary C**	***N*-CH_3**
(31)	101.3	154.6	97.0	133.8	31.6

	***meso*-CH_2**	***meso*-CH_3**	***meso*-CH_3 quaternary C**	**CO_3**
(31)	21.0, 33.9	7.5, 9.6	47.3	190.8

Table 2: ^{13}C NMR spectroscopic data for [{($Et_8N_4Me_2$)Sm}$_2$(CO_3)], **(31)** (toluene-d_8, 75 MHz, 298 K, ppm).

The ^1H NMR spectrum of **(31)** in benzene-d_6 at room temperature indicates a fluxional process giving rise to effective C_{2v} macrocyclic symmetry (overall D_{2h} symmetry for the bimetallic structure). This is suggestive of the frailty of the long Sm-O bonds involving the bridging O-centre of the carbonate. Lability of these interactions (chelate ring opening) would allow rotation of the macrocyclic unit about the remaining Sm-O bond, Figure 2. This is the minimum fluctionality required to explain the symmetry of the room temperature ^1H NMR spectrum of **(31)** (*e.g.* the equivalence of the pyrrolide CH protons). A more extensive fluctional process may also account for the appearance of the room temperature ^1H NMR spectrum of **(31)**, *e.g.* rotation of the

macrocyclic units about intact Sm-O-C-O chelate rings, although this is not likely given the narrow binding groove available for auxiliary ligands that the macrocycle offers.

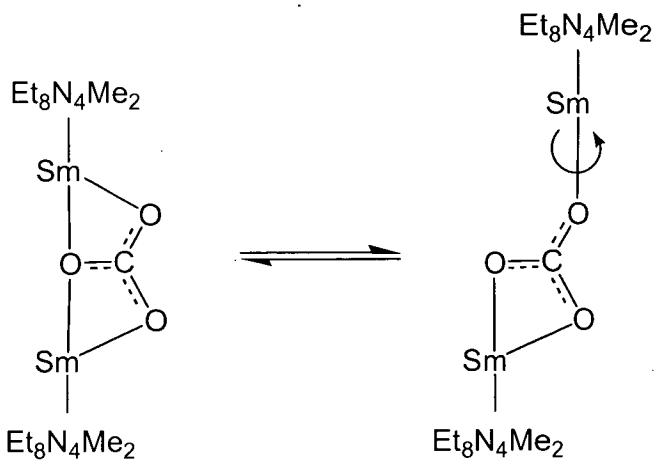

Figure 2: Fluctionality of [{(Et$_8$N$_4$Me$_2$)Sm}$_2$(CO$_3$)], **(31),** in solution.

Low temperature ^{1}H NMR studies were undertaken to investigate the fluctionality further. The ^{1}H NMR spectrum was obtained at 10 degree increments from 20 °C to -60 °C, and the resonances of all protons were observed to vary linearly with 1/T following the Curie-Weiss law. The range of chemical shifts in toluene-d_8 solution was 6.71 to -0.49 ppm at 20 °C and 6.72 to -0.28 ppm at -60 °C. The very small change in chemical shifts between 20 and -60 °C is significantly less than that observed in the Sm(II) complexes [(Et$_8$N$_4$Me$_2$)Sm(THF)$_2$], **(12)**,[13] [(Me$_8$N$_2$Ph$_2$)Sm(THF)$_2$], **(40)**, and [(Me$_8$N$_2$Ph$_2$)Sm(THF)], **(43)** (see Section 7.3.2). The smaller variation of chemical shift with temperature in the Sm(III) complex **(31)** is in keeping with the lower μ_{eff} of Sm(III) compared with Sm(II) (typical μ_{eff} values for Sm(II) = 3.6, Sm(III) = 1.7).[14] The lack of coalescence between any of the resonances indicated no significant change in the average molecular structure, and persistence of fluctionality in solution, over the range of temperatures studied.

6.3.1.2 Molecular structure of [{(Et$_8$N$_4$Me$_2$)Sm}$_2$(CO$_3$)], (31)

Orange crystals of [{(Et$_8$N$_4$Me$_2$)Sm}$_2$(CO$_3$)].3THF suitable for X-ray diffraction were grown overnight by cooling a hot solution of **(31)** in THF. The crystals belong to the monoclinic space group *C2/c* (No. 15), a = 16.838(7), b = 22.858(3), c = 22.177(1) Å, β = 95.27(4) °, with 4 molecules in the unit cell. The asymmetric unit

consists of one dimeric unit residing on a crystallographic C_2 axis. Two THF solvent molecules were located in the refinement. One THF is well defined, whilst the second THF is disordered across a crystallographic twofold symmetry axis, such that two ring atoms lie on the rotation axis (modelled with five anisotropic carbon atoms without hydrogens included). The overall solid state molecular symmetry approximates to C_2, Figure 3.

The molecular structure of **(31)** confirms the dinuclear formulation with a bridging CO_3^{2-} unit. The well-established η^5:η^1:η^5:η^1 macrocyclic binding mode was observed, and Sm-N(pyrrolide) and Sm-(*N*-methylpyrrolyl centroid) distances to the η^1-bound pyrrolide and η^5-bound *N*-methyl pyrrolyl units are in accord with previously reported Sm(III) complexes (see Sections 3.3.3, 4.3.3 and 5.3.2). The Sm centre is bound to the macrocyclic pyrrolide nitrogen centres with Sm-N distances of 2.483(4) and 2.534(4) Å whilst the distances between the Sm centre and the macrocyclic *N*-methylpyrrolyl ring centroids are 2.61_0 and 2.63_6 Å. The metallocene bend angle is 163.5_3 °. The pyrrolide ring tilt angles are 47.8_7 and 50.8_8 °, and the *N*-methylpyrrolyl ring tilt angles are 79.2_5 and 80.1_0 °.

The sterically demanding macrocycle limits the coordination environment of the carbonate fragment, which bridges Sm centres in μ_2:η^2(*O*,*O'*):η^2(*O*,*O''*)- fashion. The Sm-O distances are disparate (2.340(3), 2.5797(13) Å), with those to the bridging *O*-centre being the longer of the two. This binding mode leads to steric interactions between the macrocycles involving *meso*-ethyl groups and 3,4-positions of the *N*-methylpyrrolyl units, which induce a twist in the bimetallic species that reduces the overall symmetry in the solid state to C_2.

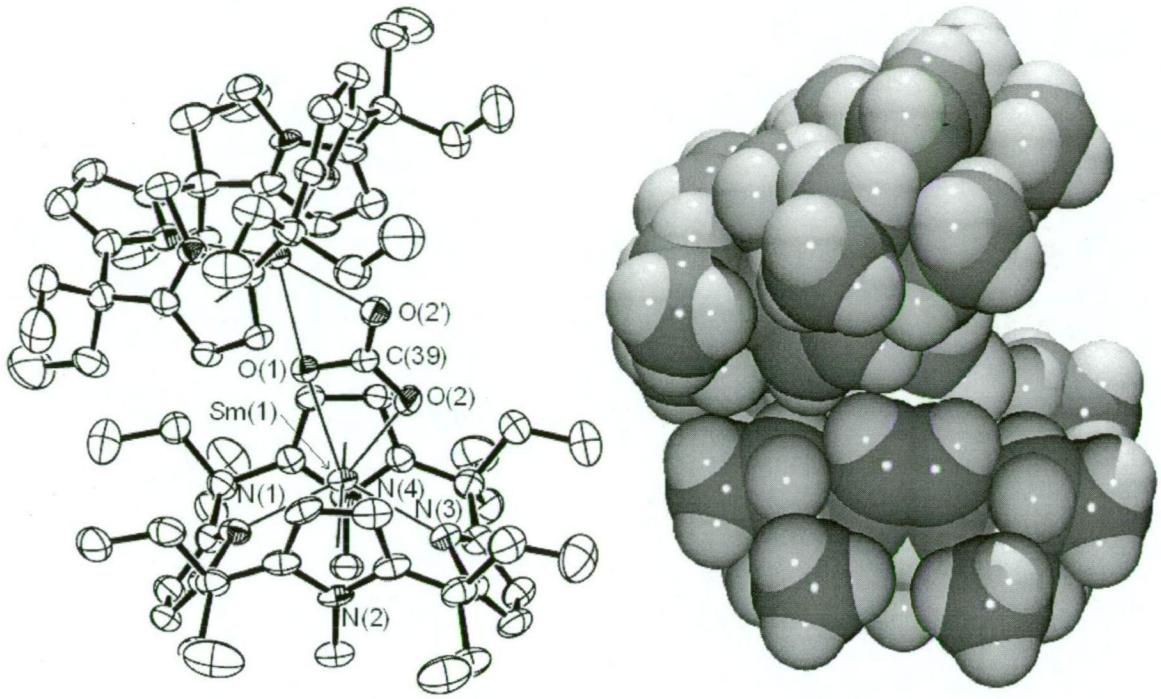

Figure 3: Molecular structure of $[\{(Et_8N_4Me_2)Sm\}_2(CO_3)]$, **(31)**, with thermal ellipsoids drawn at the level of 50% probability (protons removed for clarity) (left), and space filling model (right).

6.3.2 Redox transmetallation chemistry

The Sm(II) precursor $[(Et_8N_4Me_2)Sm(THF)_2]$, **(12)**, was expected to reduce $AgBF_4$ to give the solvated tetrafluoroborate salt $[(Et_8N_4Me_2)Sm(THF)_n][BF_4]$, **(32)**, Equation 8.

$$[(Et_8N_4Me_2)Sm(THF)_2] \xrightarrow[-\ Ag]{AgBF_4} [(Et_8N_4Me_2)Sm(THF)_n][BF_4]$$

(12) **(32)**

Equation 8

The tetrafluoroborate salt was of interest as a potential precursor for subsequent salt metathesis reactions, and as a possible example of a charge-separated solvated Sm(III) complex. A suspension of $AgBF_4$ in THF was added to a solution of one equivalent of $[(Et_8N_4Me_2)Sm(THF)_2]$, **(12)**, in toluene at 75 °C. There was immediate change in colour from dark purple to brown, and stirring at 75 °C was continued for 3 d. The reaction mixture was filtered through Celite to remove the metallic silver byproduct

and reduced *in vacuo* to give the product as a tan coloured powder. Analysis by ^{1}H NMR spectroscopy revealed the presence of *ca.* 25 % protonated porphyrinogen ($Et_8N_4Me_2H_2$).

Complex $(Et_8N_4Me_2)Sm(BF_4)$, **(32)**, was extremely soluble in toluene, benzene, THF and hexanes, giving red-brown solutions, and as a result the $Et_8N_4Me_2H_2$ contaminant could not be removed by rinsing or recrystallisation, and remained present in subsequent reactions. The complex was characterised by ^{1}H NMR spectroscopy alone, and the extreme solubility of **(32)** frustrated efforts to grow crystals suitable for X-ray crystal structure determination. The possibility of **(32)** existing as a charge-separated species with THF-molecules bound to the Sm(III) centre was considered, but the ^{1}H NMR spectrum of **(32)** in benzene-d_6 did not contain any resonances indicating the presence of bound THF. Therefore the THF-free formulation $(Et_8N_4Me_2)Sm(BF_4)$ was used in stoichiometry calculations in subsequent reactions. The yield of $(Et_8N_4Me_2)Sm(BF_4)$, **(32)**, taking into account the presence of *ca.* 25 % $Et_8N_4Me_2H_2$, was calculated to be *ca.* 58 %.

Complex $(Et_8N_4Me_2)Sm(BF_4)$, **(32),** was characterised by ^{1}H NMR spectroscopy alone. The spectrum was assigned on the basis of signal integration and signal multiplicites, although pyrrolide and *N*-methylpyrrolyl aromatic proton resonances could not be distinguished from one another. The ^{1}H NMR spectrum displays resonances over the range 8 to -3 ppm. The *meso*-CH_3 resonances appeared as triplets at 0.41 and 2.95 ppm, whilst the *meso*-CH_2 resonances appeared as multiplets over a wide range: 1.22, 1.92, 3.49 and 7.37 ppm. The *N*-methylpyrrolyl and pyrrolide aromatic protons appeared as singlets at 6.18 and 6.73 ppm. The *N*-methyl protons appeared considerably further upfield than in most $(Et_8N_4Me_2)Sm(III)$ complexes, at -2.24 ppm. The results are summarised in Table 3.

	Pyrrolide and *N*-MePyrrolyl CH	***N*-CH_3**	***meso*-Et CH_2**	***meso*-Et CH_3**
(32)	6.18, 6.73	-2.24	1.22, 1.92, 3.49, 7.37	0.41, 2.95

Table 3: ^{1}H NMR spectroscopic data of $(Et_8N_4Me_2)Sm(BF_4)$, **(32)** (benzene-d_6, 300 MHz, 298 K, ppm).

Synthesis of the tetrafluoroborate salt **(32)** had previously been attempted *via* a salt metathesis reaction between KBF_4 and $[\{(Et_8N_4Me_2)SmCl\}_2]$, **(27)**, which resulted in no reaction, Equation 9. The failure of reaction between a Group 1 tetrafluoroborate and samarium halide complex suggested the reverse reaction may be feasible. Reactions between **(32)** and a number of Group 1 salts were trialled on an NMR scale (0.01 to 0.03 mmol).

$$\underset{\textbf{(27)}}{[\{(Et_8N_4Me_2)SmCl\}_2]} \xrightarrow[\text{- KCl}]{KBF_4,\ THF} \underset{\textbf{(32)}}{(Et_8N_4Me_2)Sm(BF_4)}$$

Equation 9

Synthesis of the samarium(III) iodide $[(Et_8N_4Me_2)SmI]$, **(33)**, was carried out on NMR scale by addition of dried lithium iodide to a solution of $(Et_8N_4Me_2)Sm(BF_4)$, **(32)**, in benzene-d_6 which was heated in a sealed tube at 95 °C for 20 h, Equation 10. The ^1H NMR spectrum of the reaction mixture matched that of an authentic sample of **(33)** prepared by oxidation of $[(Et_8N_4Me_2)Sm(THF)_2]$, **(12)**, with iodine.[15] The *meso*-CH_3 protons appeared as broad triplets at 0.4 and 2.5 ppm, *meso*-ethyl CH_2 protons as multiplets at 1.3, 2.3, 3.1 and 5.9 ppm, pyrrolide/*N*-methylpyrrolyl aromatic protons as broadened resonances at 6.2 and 7.0 ppm and the *N*-metyl protons as a broadened singlet at -1.4 ppm. The driving force for the reaction is the insolubility of the lithium tetrafluoroborate salt.

$$\underset{\textbf{(32)}}{(Et_8N_4Me_2)Sm(BF_4)} \xrightarrow[\text{- LiBF}_4]{LiI} \underset{\textbf{(33)}}{\text{Sm(III) iodide complex}}$$

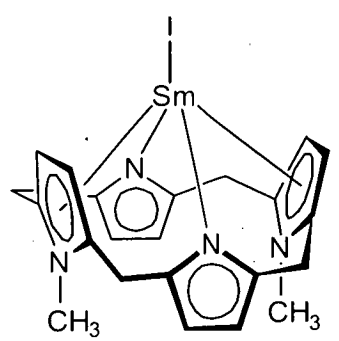

Equation 10

The samarium(III) cyclopentadienyl complex $[(Et_8N_4Me_2)Sm(C_5H_5)]$, **(26)**, was also prepared on an NMR scale, Equation 11. Addition of solid sodium cyclopentadienide to solution of **(32)** in benzene-d_6 resulted in an immediate colour

change from tan to orange, and the formation of pale solids (presumed to be $NaBF_4$). The ^1H NMR spectrum of the reaction mixture matched that of an authentic sample of $[(Et_8N_4Me_2)Sm(C_5H_5)]$, **(26)**, prepared *via* the method outlined in Section 4.3.

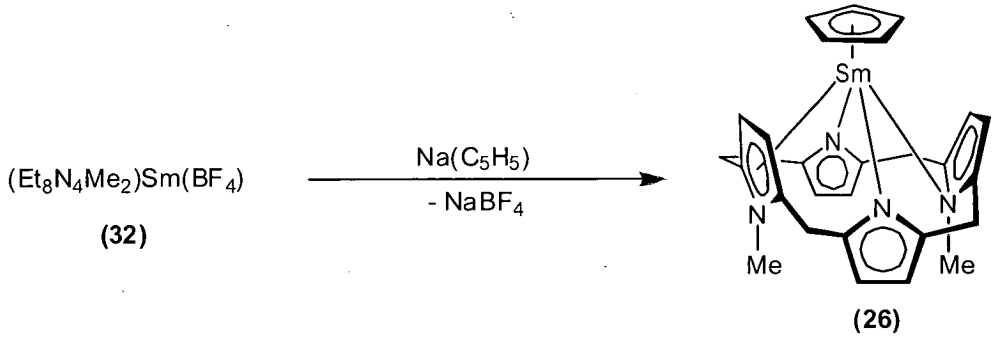

(26)

Equation 11

The reaction of $[(Et_8N_4Me_2)Sm(BF_4)]$, **(32)**, with potassium pentamethylcyclopentadienide was attempted on an NMR scale to investigate the possibility of preparing the extremely crowded $[(Et_8N_4Me_2)Sm(C_5Me_5)]$, **(34)**, Equation 12. Previous attempts to synthesise **(34)** by metathetical exchange between $[\{(Et_8N_4Me_2)SmCl\}_2]$, **(27)**, and $(C_5Me_5)K$ led to reaction mixtures from which no products could be isolated or characterised. A suspension of $(C_5Me_5)K$ in benzene-d_6 was added to a solution of **(32)** in benzene-d_6 and heated in a sealed tube at 90 °C for 5 minutes during which time the colour changed from tan to dark brown. The ^1H NMR spectrum of the reaction mixture showed the presence of more than one product. Repeat reactions using benzene-d_6 and toluene as solvents, longer reaction times and various temperatures failed to produce a product characterisable either by ^1H NMR spectroscopy or X-ray crystal structure determination. The difficulty in isolating the expected complex may be due to extreme steric crowding resulting in a highly reactive species which undergoes further reaction before isolation is possible. Such a highly crowded molecule may indeed to impossible to prepare on steric grounds alone.

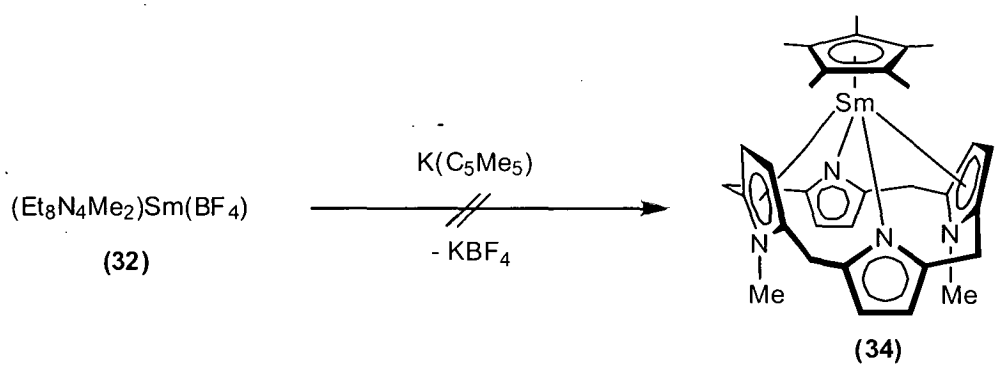

Equation 12

Use of $[(Et_8N_4Me_2)Sm(BF_4)]$, **(32)**, as a metathesis reagent was also investigated in the attempted synthesis of the samarium(III) fluoride derivative. The samarium(III) halide derivatives $[(Et_8N_4Me_2)SmX]$ have been prepared previously for iodide,[16] bromide[15] and chloride,[13] Scheme 1.

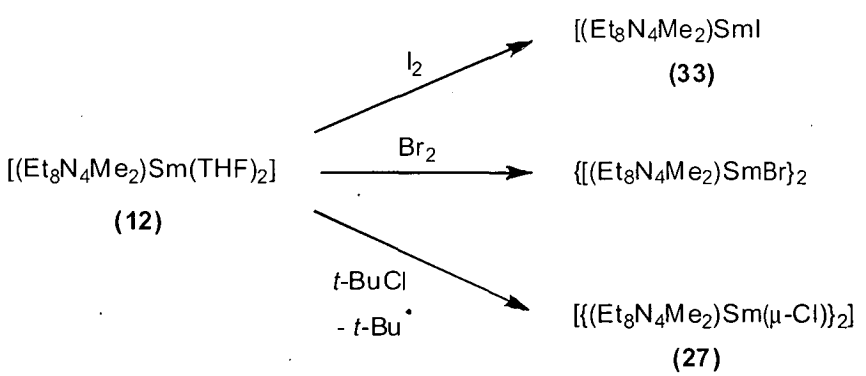

Scheme 1: Established syntheses of samarium(III) halide derivatives of the $(Et_8N_4Me_2)^{2-}$ porphyrinogen

The putative fluoride derivative $(Et_8N_4Me_2)SmF$, **(35)**, is expected to be monomeric, since there is not enough space for a bridging dimeric structure without a reduction in the macrocyclic hapticity such as that observed in the *N*-methylpyrrolyl rings as a result of steric crowding in $[(Et_8N_4Me_2)Sm(C_5H_5)]$, **(26)**, (Chapter 4.3.1). Preparation of the fluoride derivative was attempted *via* salt metathesis reactions with the tetrafluoroborate salt $[(Et_8N_4Me_2)Sm(BF_4)]$, **(32)**, and various redox transmetallation reactions. Solid KF (dried by heating at 250 °C / 5 x 10^{-2} mmHg for 20 h) was added to a solution of **(32)** in THF on an NMR scale and heated in a sealed tube at 100 °C for 2 h, Equation 12. Removal of THF *in vacuo*, addition of benzene-d_6 and analysis by ^{1}H NMR

spectroscopy showed the presence of unreacted **(32)** and no new species had formed. The reaction in benzene-d_6 was heated for a further 14 h at 100 °C without any change to the ^{1}H NMR spectrum. A reaction using solid CsF (dried by heating at 250 °C / 5 x 10^{-2} mmHg for 20 h) in place of KF and benzene-d_6 in place of THF was trialled. After heating at 100 °C for 18 h the ^{1}H NMR spectrum also showed the starting material was unreacted and no new species were present.

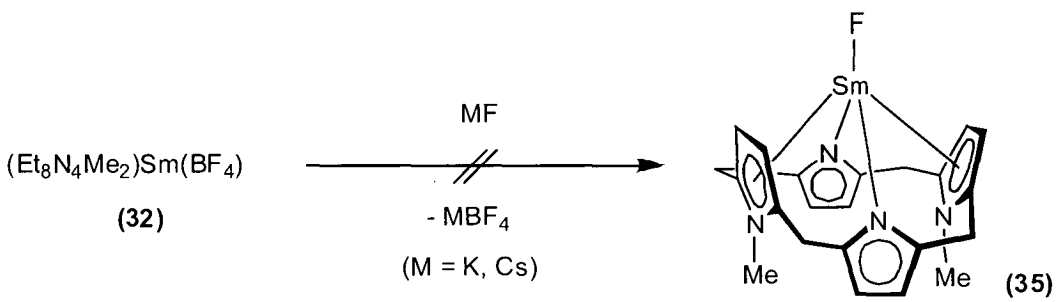

Equation 12

Further attempts to secure the fluoride derivative [$(Et_8N_4Me_2)$SmF], **(35)**, were attempted *via* transmetallation of the samarium(II) precursor [$(Et_8N_4Me_2)Sm(THF)_2$], **(12)**, with various potential fluoride sources, Equations 13,14. The reaction with thallium(I) fluoride was conducted on an NMR scale with benzene-d_6 solvent. A solution of [$(Et_8N_4Me_2)Sm(THF)_2$], **(12)**, in benzene-d_6 was added to a suspension of thallium(I) fluoride in benzene-d_6 and heated overnight at 75 °C in a sealed tube. The ^{1}H spectrum of the resultant reaction mixture contained unreacted **(12)** and no macrocycle-containing samarium(III) species.

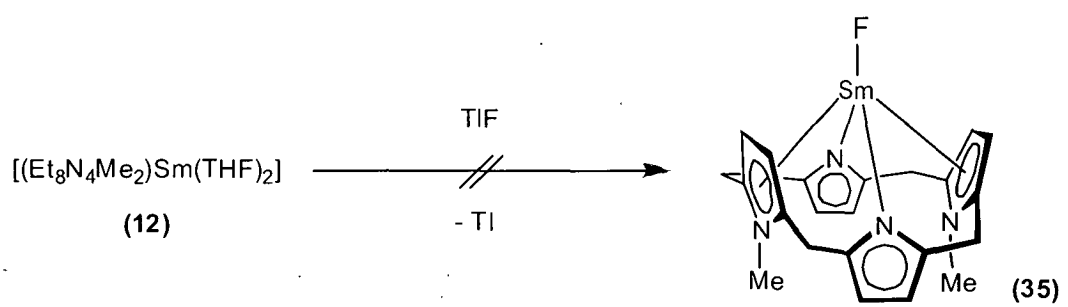

Equation 13

Reaction with silver(I) fluoride was carried out using THF as solvent. A solution of [$(Et_8N_4Me_2)Sm(THF)_2$], **(12)**, in THF was added to a suspension of silver(I) fluoride in THF and heated for 1.5 h at 75 °C in a sealed tube causing a change in colour from the

dark purple of the Sm(II) precursor to red-purple, with a tan precipitate and metallic particles (presumably metallic silver) visible under the microscope. The reaction was heated for a further 2 h, solvent removed *in vacuo* and benzene-d_6 added. The ^{1}H NMR spectrum of the resultant reaction mixture indicated one new macrocycle-containing samarium(III) species as the major product. Resonances in the ^{1}H NMR spectrum were partially assigned on the basis of signal multiplicity and signal integration. Broadened triplets at -0.81 and 2.91 ppm were assigned to the *meso*-ethyl CH_3 groups, and a broad singlet at 3.42 ppm was assigned to the *N*-CH_3 group. The *meso*-ethyl CH_2 groups were tentatively assigned to variously broadened multiplets at 0.80, 1.59, 1.93 and 2.23 ppm whilst the pyrrolide/*N*-methylpyrrolyl aromatic protons were tentatively assigned to resonances at 4.64 and 7.28 ppm. Broad resonances at 1.41 and 3.57 ppm were assigned to free THF in the reaction mixture. Attempts to recrystallise the tan coloured precipitate from THF and benzene-d_6 were unsuccessful, as were attempts to grow crystals by slow diffusion of the starting materials in THF solution. The spectroscopically unique product is presumed to be the flouride [$(Et_8N_4Me_2)$SmF], **(35)**.

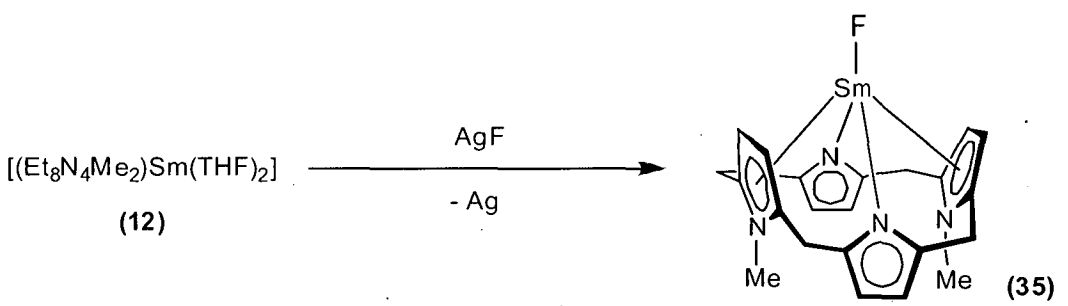

Equation 14

Bis-(pentafluorophenyl)mercury(II) was trialled as a potential fluoride source on an NMR scale, Scheme 2. A solution of [$(Et_8N_4Me_2)$Sm$(THF)_2$], **(12)**, in benzene-d_6 was added to a solution of $(C_6F_5)_2Hg$ in benzene-d_6 in a sealed tube, with no visible sign of immediate reaction. Over the course of 3 d at room temperature the solution changed colour from dark purple to tan with brown solids and metallic mercury visible under the microscope. Analysis by ^{1}H NMR spectroscopy showed the presence of one major product, different to that obtained from the reduction of AgF. Singlets at 4.73 and 6.41 ppm were tentatively assigned to pyrrolide/*N*-methylpyrrolyl aromatic protons, and a singlet at 0.97 ppm assigned to the *N*-CH_3 group. Triplets at -0.10 and 1.81 ppm were assigned to *meso*-ethyl CH_3 protons whilst the *meso*-ethyl CH_2 protons appeared as multiplets at 0.77, 1.33, 2.12 and 2.21 ppm.

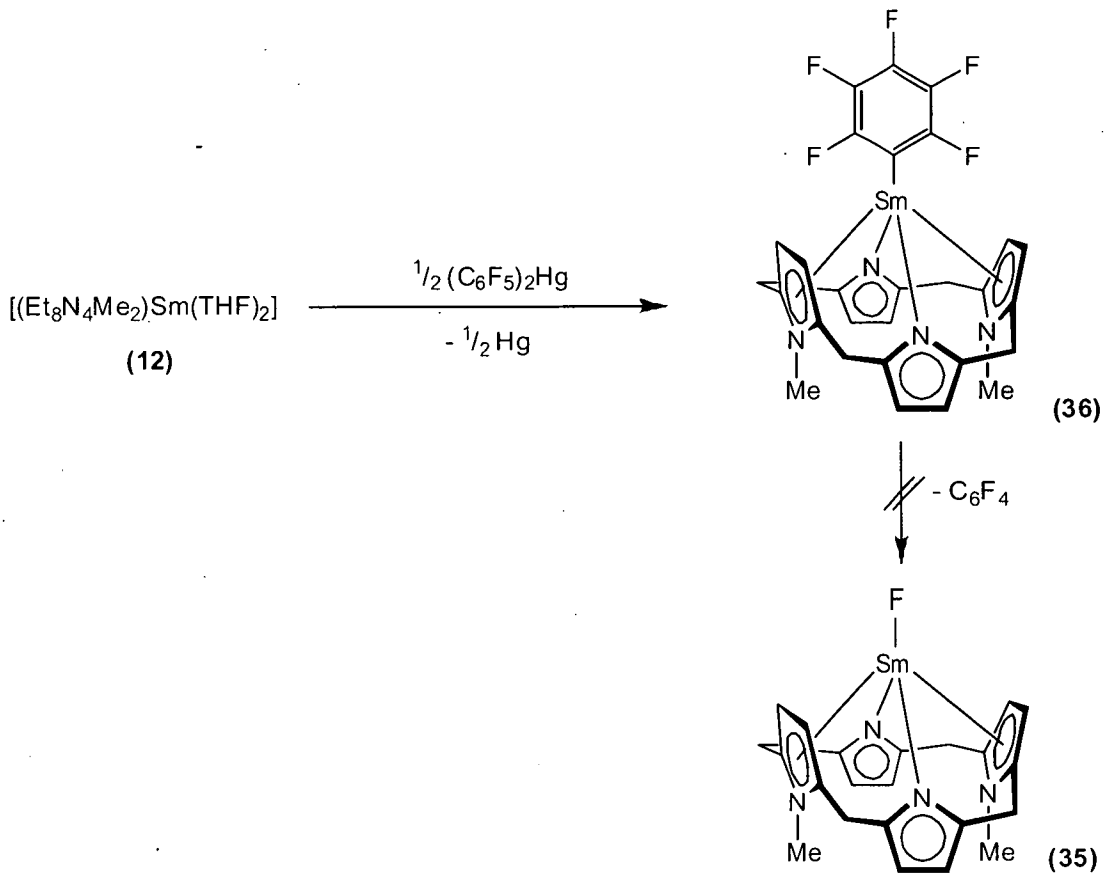

Scheme 2: Reduction of $(C_6F_5)_2Hg$ to give (C_6F_5)-functionalised Sm(III) complex **(35)**.

The reaction was repeated on a preparative scale (0.23 mmol) using THF as solvent. Reaction proceeded as per the NMR scale reaction, and after removal of the solvent, extraction into toluene and filtration an orange solid was obtained. However, ^1H NMR analysis of the orange product showed the presence of protonated $Et_8N_4Me_2H_2$ and no other macrocycle-containing species. The spectroscopically unique compound is presumed to be the Sm(III) pentafluorophenyl complex $[(Et_8N_4Me_2)Sm(C_6F_5)]$, **(36)**. Unfortunately, ^{19}F NMR spectroscopy was not available at the time to confirm this assertion.

6.4 Experimental

Synthesis of $[\{(Et_8N_4Me_2)Sm\}_2(CO_3)]$, (31)

The headspace above a stirred toluene solution (80 mL) of $[(Et_8N_4Me_2)Sm(THF)_2]$, **(12)**, (0.86 g, 1.00 mmol) was carefully evacuated until the solvent started refluxing. An excess of dry carbon dioxide (over P_2O_5) was introduced to the reaction vessel. The colour of the solution changed from purple to light orange and a pale yellow solid formed over 30 mins. The solution was filtered *via* cannula, toluene was removed *in vacuo* and the orange product redissolved in hot THF. Filtration and partial removal of solvent *in vacuo* gave a crystalline orange product on standing overnight (0.40 g, 54 %).

^{1}H NMR (benzene-d_6, 300 MHz, 298 K, ppm): -0.51 (24 H, m, CCH_3), 1.09 (12H, s, NCH_3), 1.22 (8H, m, CH_2), 2.13 (8H, m, CH_2), 2.26 (8H, m, CH_2), 2.43 (8H, s, =CH, pyrMe), 3.57 (24H, m, CH_3), 6.14 (8H, m, CH_2), 6.79 (8H, s, =CH, pyr).

^{13}C NMR (benzene-d_6, 75 MHz, 298 K, ppm): 7.5 (CCH_3), 10.4 (CCH_3), 21.0 (CH_2), 33.9 (CH_2), 31.6 (NCH_3), 47.3 (C), 97.0 (=CH, pyrMe), 101.3 (=CH, pyr), 133.8 (=CR, pyrMe), 154.6 (=CR, pyr), 190.8 (C, CO_3).

Anal. Calcd.: C, 61.88; H, 7.28; N, 7.50 ($C_{77}H_{108}N_8O_3Sm_2$, MW 1782.83)
Found: C, 62.05; H, 7.48; N, 7.70

Synthesis of $Et_8N_4Me_2Sm(BF_4)$, (32)

$AgBF_4$ (0.15 g, 7.7 x 10^{-4} mol) in THF (8 mL) and $Et_8N_4Me_2Sm(THF)_2$, **(12)**, (0.66 g, 7.7 x 10^{-4} mol) in PhMe (25 mL) were each heated in an oil bath at 75 °C. The $AgBF_4$ suspension was added to the solution of **(12)**, producing an immediate colour change from dark purple to brown. Heating was continued for 3 d, and the mixture filtered *via* cannula. The volume of the brown, turbid filtrate was reduced to half *in vacuo*, and filtered through Celite to give a transparent red-brown solution. This solution was reduced to dryness *in vacuo* to give the title compound as a tan coloured powder contaminated with *ca.* 25 % protonated $Et_8N_4Me_2H_2$ (total mass 0.48 g, mass of **(32)** *ca.* 0.36 g, yield *ca.* 58 %).

^{1}H NMR (benzene-d_6, 300 MHz, 298 K, ppm): -2.24 (s, 6H, NCH_3), 0.41 (t, 12H, CH_3), 1.22 (m, 4H, CH_2), 2.57 (m, 4H, CH_2), 2.95 (t, 12H, CH_3), 3.49 (m, 4H, CH_2), 6.18 (s, 4H, =CH, pyr or pyrMe), 6.73 (s, 4H, =CH, pyr or pyrMe), 7.37 (m, 4H, CH_2).

6.5 References

1. For reviews, see:
   a. D. H. Gibson, *Chem. Rev.*, 1996, **96**, 2063.
   b. W. Leitner, *Coord. Chem. Rev.*, 1996, **153**, 257.
   c. X. Ling, J. R. Moss, *Coord. Chem. Rev.*, 1999, **181**, 27.

2. C. Lescop, T. Arliguie, M. Lance, M. Nierlich, M. Ephritikhine, *J. Organomet. Chem.*, 1999, **580**, 137.

3. W. J. Evans, K. A. Miller, J. W. Ziller, *Inorg. Chem.*, 2006, **45**, 424.

4. W. J. Evans, J. M. Perotti, S. A. Kozimor, T. M. Champage, B. L. Davis, G.W. Nyce, C. H. Fujimoto, R. D. Clark, M. A. Johnston, J. W. Ziller, *Organometallics*, 2005, **24**, 3916.

5. W. J. Evans, C. A. Seibel, J. W. Ziller, *Inorg. Chem.*, 1998, **37**, 770.

6. W. J. Evans, J. M. Perotti, J. C. Brady J. W. Ziller, *J. Am. Chem. Soc.*, 2003, **125**, 5204.

7. **a**. I. Castro-Rodríguez, K. Meyer, *Chem. Commun.*, 2006, 1354.
   b. I. Castro-Rodriguez, H. Nakai, L.N. Zakharov, A.L. Rheingold, K. Meyer, *Science*, 2004, **305**, 1757.

8. G.R. Lee, N.J. Cooper, *Organometallics*, 1985, **4**, 1467.

9. W.J. Evans, K.J. Forrestal, J.T. Leman, J.W. Ziller, *Organometallics*, 1996, **15**, 527.

10. G.B Deacon, G.D. Fallon, C.M. Forsyth, S.C. Harris, P.C. Junk, B.W. Skelton, A.H. White, *Dalton Trans.*, 2006, 802.

11. **a**. J. Wang, M. G. Gardiner, B. W. Skelton, A. H. White, *Organometallics*, 2005, **24**, 815.
b. W. J. Evans, J. M. Perotti, J. W. Ziller, *J. Am. Chem. Soc.*, 2005, **127**, 3894.

12. N. W. Alcock, *J. Chem. Soc., Dalton Trans.*, 1973, 1610.

13. J. Wang, A. K. J. Dick, M. G. Gardiner, B. F. Yates, E. J. Peacock, B.W. Skelton and A. H. White, *Eur. J. Inorg. Chem.*, 2004, 1992.

14. W.J. Evans, M.A. Hozbor, *J. Organomet. Chem.*, 1987, **326**, 299.

15. J. Wang, Unpublished results, University of Tasmania, 2003.

16. J. Wang, Ph.D. Thesis, University of Tasmania, 2003.

Chapter 7

trans-Calix[2]benzene[2]pyrrolide Samarium Chemistry

7.1 Introduction

Trans-annular interaction between the *N*-methyl substituents in the $(Et_8N_4Me_2)^{2-}$ ligand, Figure 1(a), restrict the ability of the *N*-methylpyrrolyl rings to splay apart to accommodate very sterically demanding auxiliary ligands. This conformational rigidity leads to a high degree of strain in [$(Et_8N_4Me_2)$SmCp], **(26)**, reduced COT hapticity in [{$(Et_8N_4Me_2)$Sm}$_2$(COT)], **(28)**, and may be implicated in the solvent-mediated reversible redox behaviour of [{$(Et_8N_4Me_2)$Sm}$_2$(*t*-BuDAB)], **(18)**. All complexes of the $(Et_8N_4Me_2)^{2-}$ ligand prepared to date adopt a 1,3-alternate conformation and a predictable η^5:η^1:η^5:η^1 binding environment to the metal centre, with the sole exception of the highly strained **(26)**, in which the hapticity of one of the *N*-methylpyrrolyl groups is reduced to δ-bonding through the nitrogen centre. Similarly, NMR spectroscopic studies have shown no macrocycle-based fluctionality in solutions of Group 1 metal or lanthanide complexes of the $(Et_8N_4Me_2)^{2-}$ ligand.

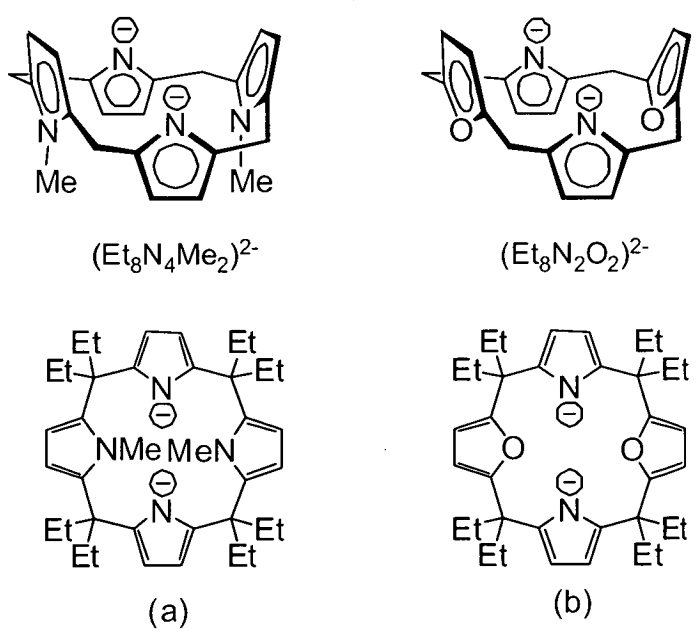

Figure 1: 3D and 2D representations of (a) doubly deprotonated *trans-N,N'*-dimethyl-*meso*-octaethylporphyrinogen $(Et_8N_4Me_2)^{2-}$ and (b) *trans*-dioxa-*meso*-octaethylporphyrinogen, $(Et_8N_2O_2)^{2-}$.

Trans-dioxa-*meso*-octaethylporphyrinogen (≡ $Et_8N_2O_2H_2$), Figure 1(b), contains furanyl rings in place of the *N*-methylpyrrolyl rings in $Et_8N_4Me_2H_2$, consequently the furanyl ligand would be expected to display a greater degree of conformational freedom. The free macrocycle exists in a 1,3-alternate conformation in the solid state,[1] as do all potassium and samarium(II) and samarium(III) complexes structurally authenticated to date.[2] However, flipping of the macrocyclic conformation has been observed in solution by NMR spectroscopy of the free macrocycle and complexes.[3] Chemically equivalent *meso*-ethyl groups are observed in the ^1H and ^{13}C NMR spectra of neutral $Et_8N_2O_2H_2$ and the structurally uncharacterised dilithium salt $[(Et_8N_2O_2)Li_2(TMEDA)_2]$, suggesting a rapid fluctional process involving flipping of the furan or pyrrolide rings in these compounds, resulting in a time-averaged symmetry across the N_2O_2 plane at room temperature, Figure 2. The disodium salt of the related *trans*-dioxa-*meso*-octamethylporphyrinogen $[(Me_8N_2O_2)Na_2(DME)_2]$ also featured chemically equivalent *meso*-methyl groups due to the same effect; its solid state molecular structure displays a partially flattened double cone conformation.[4]

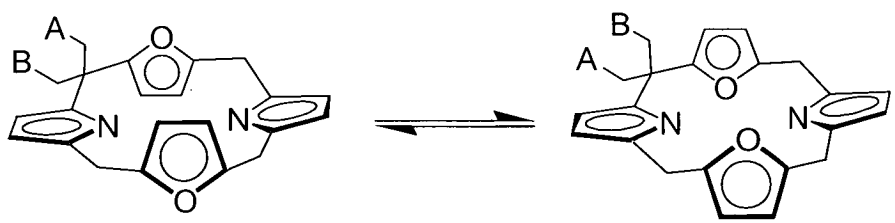

Figure 2: Proposed fluctionality of macrocycle conformations in $(Et_8N_2O_2)^{2-}$

Chemically equivalent *meso*-ethyl groups were not observed in the NMR spectra of samarium(II) complex $[\{(THF)_2K(Et_8N_2O_2)Sm(I)\}_2]$, **(I)**, Figure 3. However this does not imply an absence of fluctionality, since inherent asymmetry between the potassium-bound face and the samarium-bound face of the macrocycle ensures the *meso*-ethyl substituents remain chemically inequivalent even if fluctional flipping of the macrocyclic conformation was taking place between η^5-pyrrolide, η^1-furanyl, and η^1-pyrrolide, η^5-furanyl binding modes.

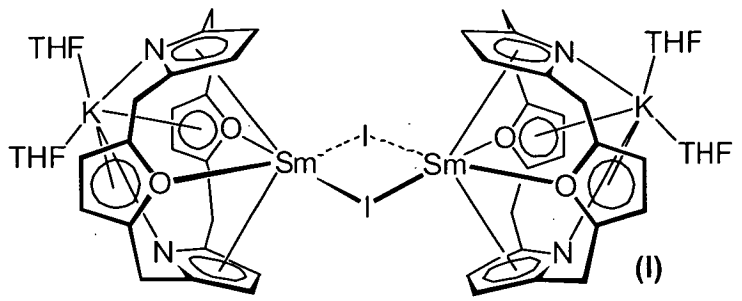

Figure 3: $[\{(THF)_2K(Et_8N_2O_2)Sm(\mu\text{-}I)\}_2]$, **(I)**.

The lanthanide chemistry of the $(Et_8N_2O_2)^{2-}$ system is complicated by the presence of oxygen-containing furanyl rings which can act as Lewis base donors along with the formally anionic pyrrolide nitrogen centres. In the common 1,3-alternate macrocyclic conformation this results in two oxygen atoms on one face of the cavity and two nitrogens at the other. Therefore Sm(II) complexes of $(Et_8N_2O_2)^{2-}$ prepared to date are bimetallic species featuring the samarium centre bound to one face of the macrocycle, and an alkali metal bound to the opposite face (retained from metathesis precursors), see Figure 3 above.[2,3,5]

trans-Calix[2]benzene[2]pyrrole, $Me_8N_2Ph_2H_2$, **(II)**, contains no Lewis basic atoms other than the two pyrrolide nitrogens which can be deprotonated to give the dianionic macrocycle, Figure 4.[6] The absence of extraneous Lewis-basic donor atoms is expected to disfavour the retention of alkali metals in subsequent metathesis reactions, thereby promoting the formation of mononuclear lanthanide complexes. The neutral ligand exists in a 1,3-alternate conformation forming a cavity with two opposite pyrrolide N-H rings and two *m*-phenylene groups extending above the macrocyclic plane. The phenylene groups define two walls of the cavity and, similarly to the *N*-methylpyrrolyl groups in $Et_8N_4Me_2H_2$, they are aromatic and expected to coordinate *via* metal-π interactions. The numbering convention used throughout this section to describe positions on the phenylene rings is shown in Figure 4. The phenylene 1-position C-H groups at the bottom of the macrocyclic cavity are incapable of *trans*-annular interaction with one another, suggesting a wide range of conformational freedom. This is in contrast to the *N*-methylpyrrolyl substituted porphyrinogen $Et_8N_4Me_2H_2$ in which the conformational freedom of the molecule is severely restricted by *trans*-annular interactions between the *N*-methyl groups at the bottom of the cavity. This conformational freedom may result in greater degrees of fluctionality and binding mode

variation in metal complexes of the $(Me_8N_2Ph_2)^{2-}$ macrocycle compared with those of the $(Et_8N_4Me_2)^{2-}$ system.

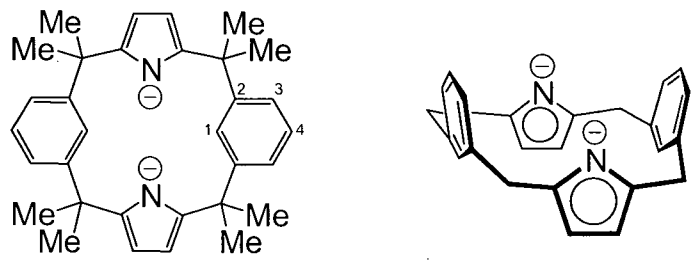

Figure 4: Doubly deprotonated *trans*-calix[2]benzene[2]pyrrole, $(Me_8N_2Ph_2)^{2-}$.

Conformational freedom in the $Me_8N_2Ph_2H_2$ system was demonstrated in neutral molecule and anion binding studies.[6] The molecular structure of the dichloromethane-bound macrocycle $Me_8N_2Ph_2H_2.CH_2Cl_2$, **(III)**, was significantly different to that of the solvent-free starting material, Figure 5. Dichloromethane binds within the macrocyclic cavity defined by the phenylene rings, pulling them inwards and resulting in steeper tilt angles (49.4_7 and 50.3_5 ° in **(II)**; 66.9_2, 67.0_2 ° in **(III)**). The torsion in the macrocyclic skeleton ("twist", resulting in non-planarity of the four *meso*-carbon centres) observed in the molecular structure of **(II)** also changes upon binding to CH_2Cl_2, and instead **(III)** features eclipsed pyrrolide and phenylene rings.

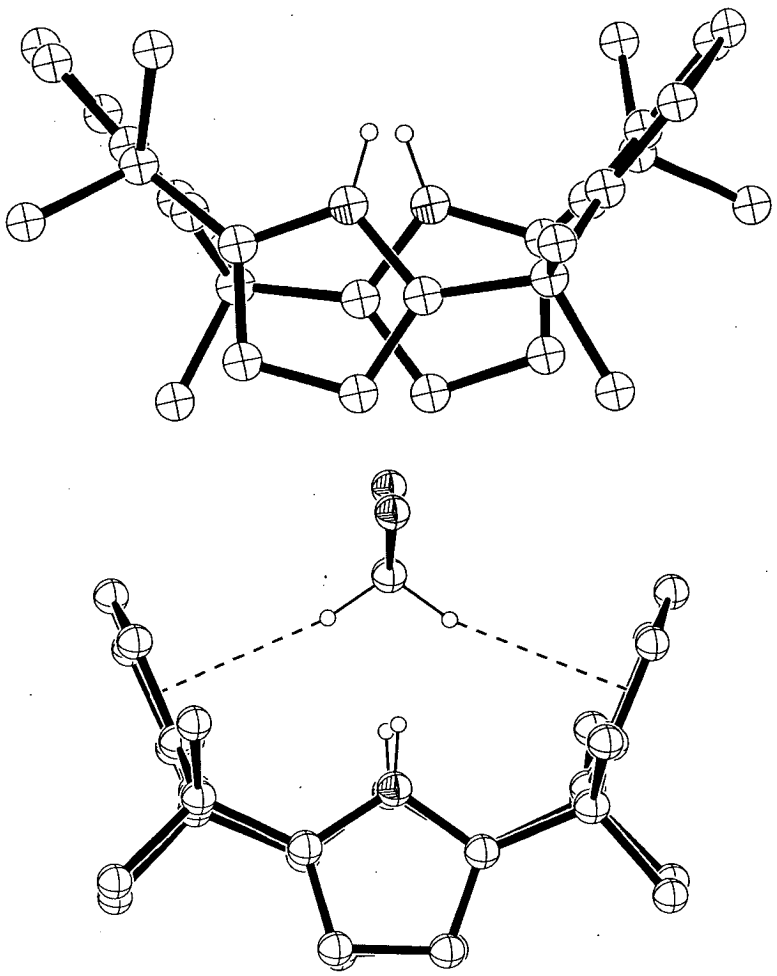

Figure 5: Conformation of $Me_8N_2Ph_2H_2$ (**(II)**, above) and $Me_8N_2Ph_2H_2.CH_2Cl_2$ (**(III)**, below) (all except for N-H protons removed for clarity).

The synthesis of *trans*-calix[2]benzene[2]pyrrole was reported by condensation of equimolar amounts of 1,3-bis(1',1'-dimethylhydroxymethyl)benzene, pyrrole and $BF_3.OEt_2$ in MeCN.[6] Although the yield was low (16 %), the procedure represented a one-step synthesis from inexpensive, commercially available starting materials which would be amenable to large scale preparations.

7.2 Research Aim

The lanthanide coordination chemistry of the *trans*-calix[2]benzene[2]pyrrole ($Me_8N_2Ph_2H_2$) macrocycle was approached by deprotonation of the two pyrrolyl N-H groups in the neutral ligand with potassium metal. The dipotassium salt thus obtained was to be used in a salt metathesis reaction with SmI_2 to produce a complex bearing a

Sm(II) centre coordinated to the two pyrrolide nitrogen donors within the macrocyclic cavity. The lack of Lewis basic functionalities in the $(Me_8N_2Ph_2)^{2-}$ ligand was expected to make retention of alkali metals less likely than in the case of the $(Et_8N_2O_2)^{2-}$ macrocyclic ligand, thus leading to a mononuclear Sm(II) complex. The greater conformational flexibility of the $(Me_8N_2Ph_2)^{2-}$ ligand was expected to result in greater coordination sphere available for further chemistry, and thus provide an interesting counterpoint to the conformationally restricted $(Et_8N_4Me_2)^{2-}$ macrocycle. Investigation of the behaviour of the $(Me_8N_2Ph_2)^{2-}$ ligand in a sterically crowded environment was approached by reaction of the Sm(II) complex with a large, reducible auxiliary ligand such as cyclooctatetraene to provide a Sm(III) complex featuring steric competition between the bulky, oblate auxiliary ligand and the $(Me_8N_2Ph_2)^{2-}$ macrocycle.

7.3 Results and discussion

7.3.1 Macrocycle and complex syntheses

trans-Calix[2]benzene[2]pyrrole, **(II)**, was synthesised by the condensation of equimolar amounts of 1,3-bis(1',1'-dimethylhydroxymethyl)benzene and pyrrole in MeCN. The published procedure[6] used an equimolar amount of $BF_3.OEt_2$ to catalyse reaction over the course of 1 h, followed by quenching with aqueous NaOH, extraction with EtOAc, chromatographic separation and recrystallisation from EtOH to obtain the target macrocycle in 16 % yield. This was modified by the use of 0.5 mol % scandium trifluoromethanesulfonate ($Sc(OTf)_3$) as Lewis acid catalyst in place of $BF_3.OEt_2$, Equation 1.

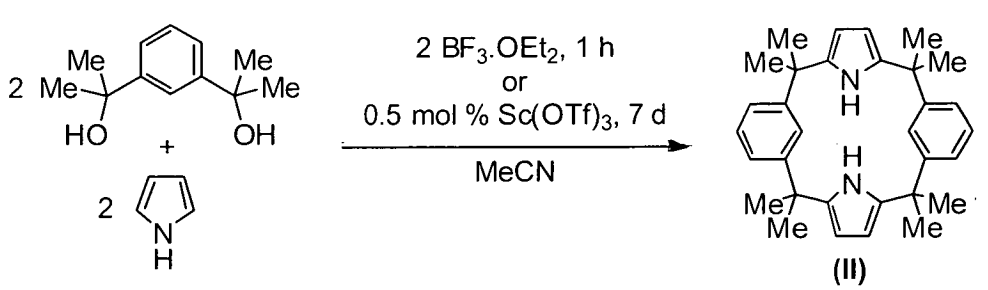

(II)

Equation 1

The use of $Sc(OTf)_3$ followed on from its success in catalysing the "3+1" cyclisation in the synthesis of $Me_8N_4Me_2H_2$ (Chapter 2.3.1). Reaction took place over

7 days at room temperature without stirring, over which time the crude product crystallised from the reaction mixture as colourless rosettes which were filtered off and rinsed with MeCN. The green supernatant was reduced to a small volume *in vacuo*, stood for 2 d at -20 °C, filtered and rinsed with MeCN to yield an additional crop of crude product. The combined solids were dried and sublimed *in vacuo* (250 °C / 1 x 10^{-2} mmHg) to give the target macrocycle as a white crystalline powder in 16 % yield. The mass of discoloured residue remaining after sublimation was less than 10 % of the sublimed mass, indicating that little or no decomposition took place over the course of the sublimation (*ca.* 20 - 30 minutes). The ^{1}H and ^{13}C NMR spectra of the product obtained *via* this alternate procedure were identical to the published NMR spectroscopic data. Despite requiring a longer reaction time, the use of $Sc(OTf)_3$ was found to be convenient, allowing the modified porphyrinogen to be obtained without the need for extraction and chromatographic separation.

Complex $(Me_8N_2Ph_2)K_2(THF)_2$, **(37)**, was prepared by deprotonation of $Me_8N_2Ph_2H_2$. Potassium metal was added to a solution of $Me_8N_2Ph_2H_2$ in THF/PhMe (1:1), yielding the complex as an off-white powder, Equation 2.

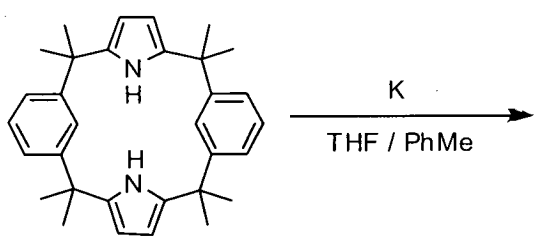

$Me_8N_2Ph_2H_2$ **(II)**

Equation 2

The reaction was carried out under an atmosphere of argon at a temperature just sufficient to melt the potassium metal (*ca.* 70 °C). Hydrogen evolution was observed, and long reaction times (1 - 3 d) employed to ensure complete deprotonation. During reaction the product partially precipitated as an off-white powdery precipitate, and on completion was collected by removal of solvents *in vacuo*. The yield of dipotassium salt was typically 80-95 %. Carrying out the deprotonation in neat THF led to the formation of the product as a gelatinous mass which impeded stirring of the reaction mixture. The product is insoluble in hexanes, toluene and benzene-d_6, and very slightly soluble in THF.

Determination of the number of THF molecules in the structure was attempted by ^{1}H NMR analysis of hydrolysed samples of **(37)** in benzene-d_6, but results varied with different batches over the range ⅔ - 2 THF molecules per macrocycle. The presumed formulation used in subsequent experiments was two THF molecules per macrocycle. The THF-free complex $\{(Me_8N_2Ph_2)K_2\}_n \cdot ⅔(C_6H_5CH_3)$, **(38)**, was prepared by heating a sealed tube containing **(37)** and toluene at 125 °C for 7 d, over which time colourless crystals of **(38)** formed, Equation 3. Both 1,2-alternate and 1,3-alternate macrocyclic conformations are present in the molecular structure of **(38)**, each containing two endo-bound K centres in addition to π-bound K-(pyrrolide) *exo* contacts and weak Me contacts to toluene.

$$\underset{\textbf{(37)}}{(Me_8N_2Ph_2)K_2(THF)_2} \xrightarrow[-\ THF]{PhMe,\ \Delta} \underset{\textbf{(38)}}{\{(Me_8N_2Ph_2)K_2\}_n.{}^2/_3(PhMe)}$$

Equation 3

Whilst suitable crystals of **(37)** could not be obtained by crystallisation from THF in order to determine the molecular structure of **(37)**, the key dipotassiated nature and possible structural features of the THF solvated complex **(37)** can be inferred from the molecular structure of **(38)** (Section 7.3.3.1). Microanalytical data were only obtained for the THF-free complex **(38)**; the carbon content in **(38)** was low (calculated 74.86 %, found 73.76%). The molecular structure of **(38)** contains *endo*- and *exo*- bound potassium centres, creating a linear polymeric structure with resultant low solubility in organic solvents. The low solubility of **(37)** may also imply the presence of a similar polymeric structure, *viz.* $[(Et_8N_4Me_2)K_2(THF)_2]_n$, **(11)**.[3,7] Attempts to obtain NMR spectra of **(37)** and **(38)** in benzene-d_6 and THF-d_8 were not successful due to low solubility.

The preparation of samarium(II) complexes of $(Me_8N_2Ph_2)^{2-}$ were undertaken by salt metathesis reactions of $(Me_8N_2Ph_2)K_2(THF)_2$, **(37)**, with samarium(II) iodide in THF at ambient temperature. A solution of SmI_2 in THF was added to a suspension of $(Me_8N_2Ph_2)K_2(THF)_2$, **(37)**, in THF, resulting in an immediate colour change from beige to deep brown-purple. The mixture was stirred at ambient temperature for 1.5 h and THF removed *in vacuo*. Toluene was added to dissolve the Sm(II) complex and allow separation from potassium iodide formed in the metathesis reaction. The resulting dark green-black mixture was filtered *via* cannula and the toluene subsequently removed *in*

vacuo to give black, non-crystalline solids. The solids were dissolved by the addition of THF, which gave a dark violet-black solution. THF was then carefully removed *in vacuo* until solids just began to form at room temperature. The flask was stood at -20 °C for 4 d, forming a crop of solids. The supernatant was decanted away and the solids dried *in vacuo* to give a crude product, **(39)**, as a purple powder.

^{1}H NMR spectroscopy of crude **(39)** in benzene-d_6 was consistent with the presence of one new species bearing an effective C_{2v} symmetry of the macrocycle, but no further structural information could be inferred. Heating **(39)** in THF lead to the formation of dark red-brown crystals, **(40)**. ^{1}H NMR spectroscopy of **(40)** indicated a single major product with C_{2v} symmetry of the macrocycle, with a different ^{1}H NMR spectrum to **(39)**. The differing NMR data suggested that the process of heating **(39)** in THF caused a change in composition. The molecular structure of **(40)** was determined by X-ray crystal structure determination to be $[(Me_8N_2Ph_2)Sm(THF)_2]$, Scheme 1.

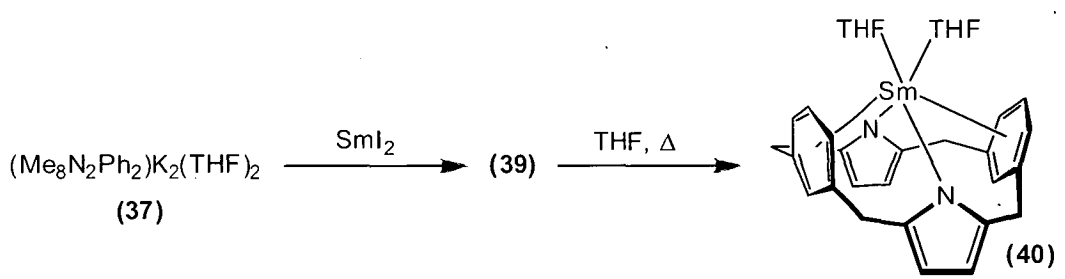

Scheme 1: Synthesis of $[(Me_8N_2Ph_2)Sm(THF)_2]$, **(40)**, *via* uncharacterised intermediate **(39)**.

The molecular structure of **(40)** features a Sm(II) metal centre bound η^1 to each pyrrolide unit and η^6 to each phenylene unit. Two THF molecules bind to the metal at the top of the macrocyclic cavity, whilst the bottom of the cavity is defined by two downwards-pointing phenylene 1-H groups and two downwards-pointing *meso*-methyl groups. These presence of these groups restricts access to the bottom of the Sm centre, although not as completely as the *N*-methylpyrrolyl methyl groups in the $(Et_8N_4Me_2)^{2-}$ macrocyclic system; the positions of the *meso*-methyl groups in **(40)** are dependant upon the twisted conformation adopted by the macrocycle skeleton in this particular complex, though the phenylene 1-H groups would be expected to remain downwards facing in any 1,3-alternate conformation. This in contrast to the *N*-methylpyrrolide macrocycle

$(Et_8N_4Me_2)^{2-}$, which posseses two *N*-CH_3 groups in direct steric contact at the bottom of the macrocycle cavity in all observed conformations, preventing binding to the metal centre or pyrrolide rings from that face of the cavity.

Crystallisation of the Sm(II) intermediate **(39)** from THF at low temperature was attempted to avoid conversion to **(40)**, but crystals suitable for X-ray structural analysis could not be produced. Microanalysis of the crude **(39)** were variable, showing significantly lower amounts of C and N than the bis-(THF) adduct **(40)** which is consistent with KI incorporation, although this may also be due to impurities present in the crude sample. The composition of the crude reaction product **(39)** was investigated *via* preparation of a reduced cyclooctatetraenediyl derivative.

Complex **(39)** was expected to reduce cyclooctatetraene, with the subsequent production of a binuclear Sm(III) species. The structure of this Sm(III) species might allow the composition/structure of the intermediate **(39)** to be inferred. Reaction of crude **(39)** with cyclooctatetraene in benzene-d_6 resulted in the separation of a violet solid, **(41)**, from a green supernatant. Crystals of complex **(41)** were obtained from THF/toluene and charcterised by X-ray crystal structure determination.

The molecular structure of **(41)** was found to be $[(Me_8N_2Ph_2)Sm(COT)K(THF)]_n$. The structure contains a samarium centre bound η^1 to each pyrrolide nitrogen and η^1 to the phenylene rings, which are splayed back allow the planar, aromatic COT dianion to bind η^8 to the metal centre. On the underside of the macrocycle a potassium centre is η^2-bound to each C(pyrrolide-3,4 positions), η^3-bound to COT and one THF molecule.

The phenylene rings of the macrocyclic ligand in **(41)** are splayed back towards the macrocyclic plane, allowing the cyclooctatetraenediyl access to the Sm centre in its preferred η^8 binding mode. This behaviour is in marked contrast to $[\{(Et_8N_4Me_2)Sm\}_2(COT)]$, **(28)**, in which the COT ligand was forced to adopt η^2 binding due to the conformational rigidity of the *trans-N,N'*-dimethyl substituted $(Et_8N_4Me_2)^{2-}$ macrocycle.

The presence of potassium in the molecular structure implies that **(39)**, which appeared as a single compound in both ^1H and ^{13}C NMR spectroscopy, is a

heterometallic complex incorporating both samarium(II) and potassium centres. A possible formulation would be $K(Me_8N_2Ph_2)Sm(THF)_nI$, in which a potassium centre binds to the back of the macrocycle pyrrolide rings in a similar fashion to that observed in **(41)**. Alternately, **(41)** may be the result of potassium iodide contamination present in the crude **(39)** sample. A possible set of reactions which would lead to **(41)** via the proposed formulation of **(39)** is shown in Scheme 2.

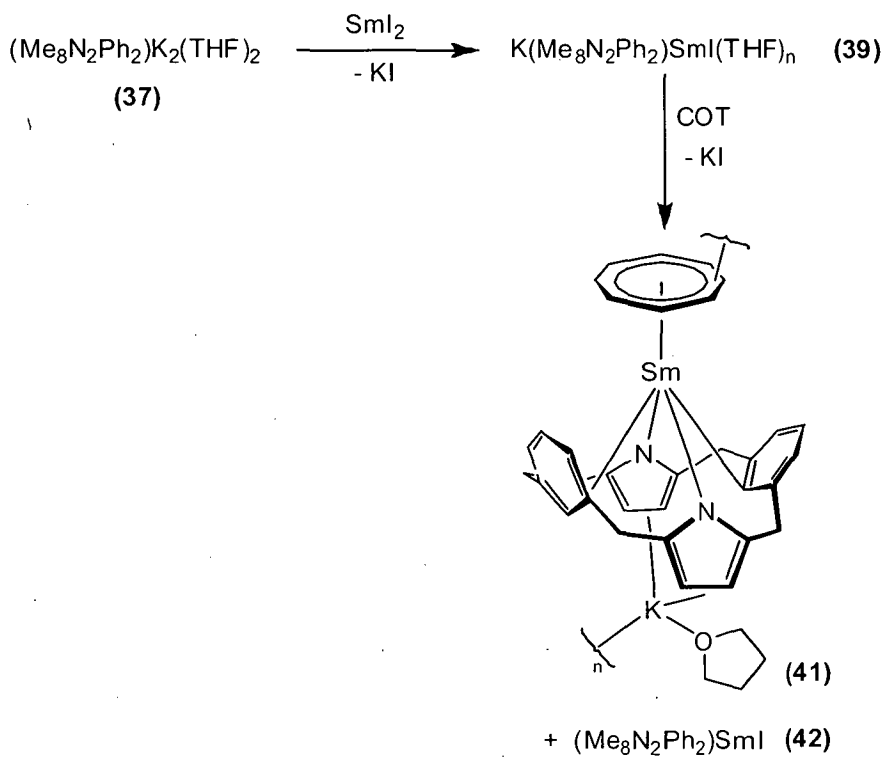

Scheme 2: Synthesis of $[(Me_8N_2Ph_2)Sm(COT)K(THF)]_n$, **(41)**, *via* uncharacterised complex **(39)**.

Complex $(Me_8N_2Ph_2)SmI$, **(42)**, is implied as the byprodut of the reaction. Attempts to crystallise the tentative Sm(III) byproduct, $(Me_8N_2Ph_2)SmI$, **(42)**, were unsuccessful, and the ^1H NMR spectrum of the reaction supernatant was not informative due to the presence of multiple species. Likewise, attempts to isolate, identify or independently synthesise **(42)** were not successful. Although structural charcterisation of the crude metathesis product **(39)** was not possible, the well characterised homometallic bis-(THF) adduct, $[(Me_8N_2Ph_2)Sm(THF)_2]$, **(40)**, was subsequently synthesised on a preparative scale by heating the crude metathesis product **(39)** in THF, see below. This provided a Sm(II) precursor free of metathesis by-products for subsequent Sm(II) and (III) chemistry.

The divalent samarium complex $[(Me_8N_2Ph_2)Sm(THF)_2]$, **(40)**, was obtained directly from the metathesis reaction of $(Me_8N_2Ph_2)K_2(THF)_2$, **(37)**, with SmI_2 in THF, Equation 4. Conditions were similar to those used in the synthesis of **(39)**, except the reaction was run at elevated temperature (70 °C), and the crude product hence obtained was heated overnight in THF to ensure formation of the desired potassium-free complex.

$$\underset{\textbf{(37)}}{(Me_8N_2Ph_2)K_2(THF)_2} \xrightarrow[THF,\ \Delta]{SmI_2} \underset{\textbf{(40)}}{[(Me_8N_2Ph_2)Sm(THF)_2]}$$

Equation 4

After reaction at 70 °C for 3 d, pale solids were visible under a dark purple supernatant, consistent with the expected production of potassium iodide. THF was removed *in vacuo* and the solids extracted twice with toluene and filtered. Solvent was removed from the combined extracts, THF added and the flask heated to 70 °C overnight before being cooled to -20 °C to give the product as a dark purple powder. Yields were low, typically 16 - 25 % based on the dipotassium starting material.

Complex **(40)** is insoluble in hexanes and slightly soluble in toluene, benzene and THF at room temperature. Recrystallisation of complex **(40)** from refluxing benzene-d_6 or toluene gives the mono-(THF) adduct, $[(Me_8N_2Ph_2)Sm(THF)]$, **(43)**, as dark indigo crystals, Equation 5. The structural features of **(40)** and **(43)** are exapanded on in Section 7.3.3.3.

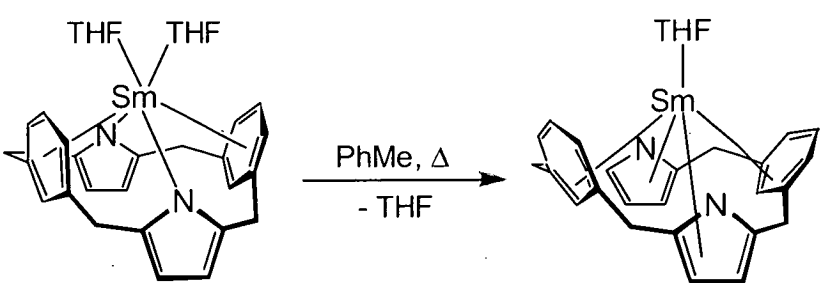

(40) **(43)**

Equation 5

Complexes **(40)** and **(43)** gave satisfactory microanalyses and their structures have been confirmed by X-ray crystal structure determinations. Complexes **(40)** and **(43)**

were characterised by VT ^{1}H NMR spectroscopy, but low solubility in deuterated solvents prevented the acquisition of useful ^{13}C or 2D NMR spectra.

In addition to $[(Me_8N_2Ph_2)Sm(THF)_2]$, **(40)**, and $[(Me_8N_2Ph_2)Sm(THF)]$, **(43)**, a dimeric Sm(II) *N*-confused complex was also isolated from the reaction of $(Me_8N_2Ph_2)K_2(THF)_2$, **(37)**, with SmI_2 in THF at room temperature. Filtration of the reaction mixture *via* cannula and removal of solvent *in vacuo* was followed by the addition of toluene and heating at 90 °C for 3 h. The supernatant was decanted from the solids, which were dried *in vacuo* to give $[\{(Me_8NN'Ph_2)Sm\}_2]$, **(44)**, as a grey-green powder in 49 % yield, Equation 6. The main difference between this procedure and that employed in the synthesis of **(40)** is heating in PhMe at 90 °C for 3 h rather than THF at 70 °C for 3 d. Complex **(44)** was only slightly soluble in THF, toluene and benzene-d_6, and the dilute solutions thus obtained were pale green in colour. Microanalytical data were obtained; the percentages of carbon and hydrogen were low (calculated 66.81 and 7.08 %, found 65.27 and 6.06 % respectively).

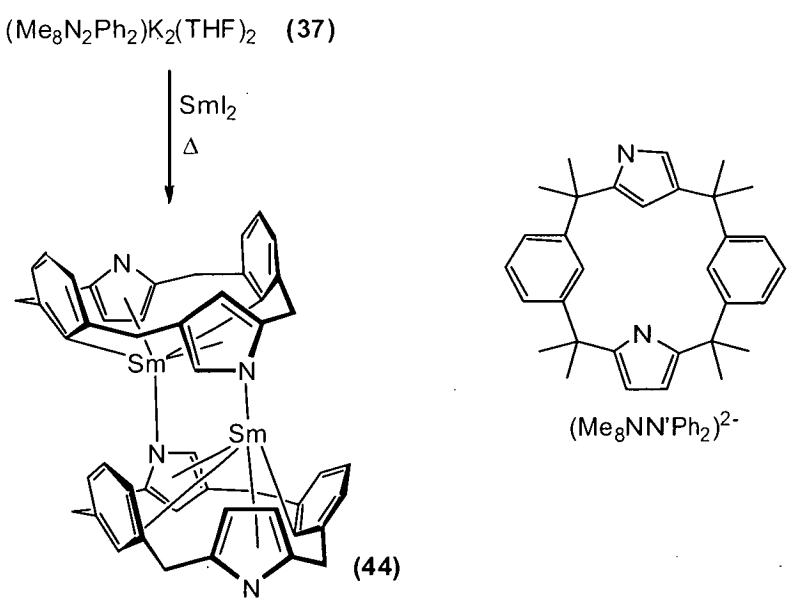

Equation 6

The structure of the usual bis(phenylene) macrocycle $((Me_8N_2Ph_2)^{2-})$ contains two pyrrolide units joined to *meso*-carbons at the 2 and 5 positions. The *N*-confused macrocycle $((Me_8NN'Ph_2)^{2-})$ in **(44)** differs in that one of the pyrrolide rings is bound to the adjacent *meso*-carbons at the 2 and 4 positions. The macrocycles are in full cone conformations, and each pyrrolide unit binds to a samarium centre within the macrocycle

via η^5 interactions. In addition, the *N*-confusion results in one of the pyrrolide nitrogens being present at the open face of each macrocycle, allowing σ-bonding to the opposite samarium centre in preference to binding THF. The result is a binuclear, solvent-free complex of C_i symmetry.

An alternate interpretation of the molecular structure of **(44)** is a Sm(III) complex containing unconfused $(Me_8N_2Ph_2)^{2-}$ macrocyclic units in which the coordinating pyrrolide 3-postion is metallated by the opposite Sm centre. Hydrolysis of such a complex would reprotonate the pyrrolide 3-position and regenerate $Me_8N_2Ph_2H_2$. However, ^{1}H NMR analysis of a hydrolysed sample of $[\{(Me_8NN'Ph_2)Sm\}_2]$, **(44)**, in benzene-d_6 showed the presence of the protonated *N*-confused macrocycle $Me_8NN'Ph_2H_2$. The spectrum displayed eight *meso*-methyl resonances, congruent with the loss of symmetry due to *N*-confusion of one pyrrolide unit in each macrocycle, thus ruling out 3-pyrrolide metallation of an unconfused macrocycle in **(44)**.

Analysis of the starting materials ruled out the presence of *N*-confused macrocycle in either the starting $Me_8N_2Ph_2H_2$ or intermediate $(Me_8N_2Ph_2)K_2$, hence confirming its formation during the above reaction. The low solubility of **(44)** may drive its formation as a result of precipitation. There is a literature report of an *N*-confused samarium(III) complex forming as a minor product (7 % yield) from the reaction of $[Li_2(Et_8N_4)SmH]$ with acetylene, although no mechanistic details were offered.[8]

Reaction between $[(Me_8N_2Ph_2)Sm(THF)_2]$, **(40)**, and cyclooctatetraene was undertaken on NMR scale to isolate a homometallic Sm(III) COT complex, Equation 7. Cyclooctatetraene was added to a solution of two equivalents of $[(Me_8N_2Ph_2)Sm(THF)_2]$, **(40)**, in benzene-d_6 producing a violet precipitate under an almost colourless supernatant. The violet solids were insoluble in deuterated solvents, thus precluding NMR spectroscopy, and microanalysis was not undertaken due to the small scale of reactions and time constraints.

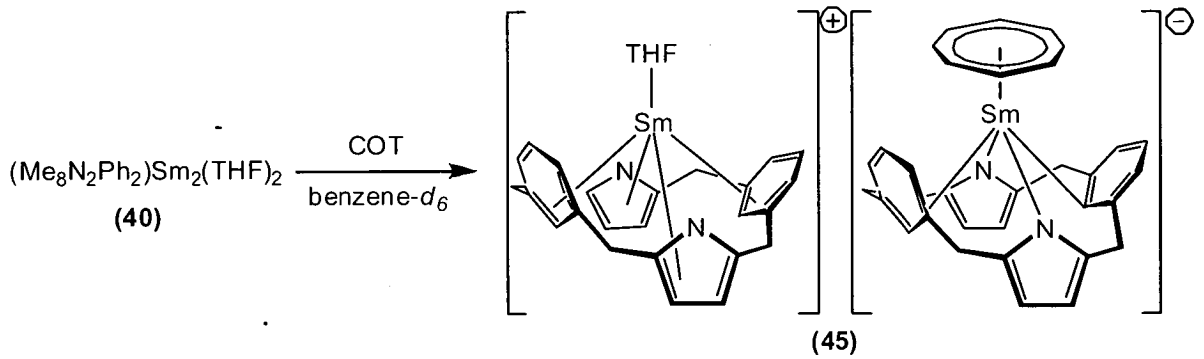

Equation 7

In a separate reaction diffusion of cyclooctatetraene vapour into a toluene solution of **(40)** over a period of 2 weeks produced $[(Me_8N_2Ph_2)Sm(COT)][(Me_8N_2Ph_2)Sm(THF)]$, **(45)**, as a violet precipitate of sufficient crystallinity for crystal structure determination to be undertaken using a synchrotron X-ray source. The molecular structure is a binuclear Sm(III) ion pair displaying two different macrocyclic environments. The anionic unit contains a Sm(III) centre η^1-bound to the two pyrrolide nitrogens, η^1-bound to each phenylene C-1, and η^8-bound to the COT dianion, while the cationic unit displays a Sm(III) centre bound η^5- to the face of each pyrrolide ring, η^1-binding to the phenylene C-1 and a single THF molecule completing the coordination sphere. The result is an ion pair instead of the μ-COT complex, which had been the anticipated product of the reaction.

The formation of the ion pair may be due to the energy penalty associated with splaying back of the macrocyclic phenylene rings to accomodate the large oblate COT ligand. Formation of the μ-COT complex would require two macrocycle units to splay back towards the macrocyclic plane to accommodate the bridging COT. In the ion pair **(45)**, the THF-bearing macrocycle phenylene ring tilt angles are 71.4_4, 73.2_2 ° whilst those of the COT-bearing macrocycle are 31.0_1, 34.2_3 °. For comparison, the phenylene ring tilt angles in the neutral ligand $Me_8N_2Ph_2H_2$ are intermediate, at 49.4_7°, 50.3_5°. Performing an analogous reaction with THF-free starting material (*i.e.* $[(Me_8N_2Ph_2)Sm]$, presently unsynthesised) would be of interest, perhaps resulting in the μ-COT complex. The presence of two distorted macrocycle units in such a complex might result in unusual reactivity as the macrocycle(s) attempt to reduce steric strain through subsequent reaction.

A reaction between $[(Me_8N_2Ph_2)Sm(THF)_2]$, **(40)**, cyclooctatetraene and KI was undertaken on NMR scale in an attempt to synthesise $[(Me_8N_2Ph_2)Sm(COT)K(THF)]_n$, **(41)**. A mixture of KI and one equivalent of $[(Me_8N_2Ph_2)Sm(THF)_2]$, **(40)**, was heated at 85 °C in benzene-d_6 for 18 h, then evacuated to remove solvent, and heated for a further 24 h in THF. One-half equivalent of cyclooctatetraene was added and the mixture heated to give a violet precipitate under a pale yellow supernatant. There was residual, unreacted KI and the violet colour of the precipitate was identical to that of **(45)**, which was thus presumed to be the product.

In summary, both Sm(II) and Sm(III) complexes of the $(Me_8N_2Ph_2)^{2-}$ ligand system were accessed. The conformationally flexible macrocycle allowed greater access to the metal coordination sphere than the rigid $(Et_8N_4Me_2)^{2-}$ system, resulting in a variety of binding modes. This loss of control over the macrocyclic coordination environment may result in uncharacterised by-products in addition to those isolated and characterised. This may be responsible for the low yields of the metathesis reactions used to access the Sm(II) chemistry.

7.3.2 NMR spectroscopic characterisation

Complexes $[(Me_8N_2Ph_2)Sm(THF)_2]$, **(40)**, and $[(Me_8N_2Ph_2)Sm(THF)]$, **(43)** were characterised by ^1H NMR spectroscopy. The ^1H NMR spectrum of $[(Me_8N_2Ph_2)Sm(THF)_2]$, **(40)**, in benzene-d_6 showed a series of variously broadened and shifted resonances over a chemical shift range of approximately 11 to -4 ppm owing to the influence of the paramagnetic Sm(II) centre. Singlet resonances at 10.44 and -3.54 ppm were assigned to the *meso*-methyl groups, the disparate chemical shifts being possibly due to the conformation adopted by **(40)** which places the downwards facing *meso*-methyl groups in closer proximity to the Sm centre. The THF resonances appeared at -1.40 and -4.52 ppm. Singlet resonances at 6.43 and 5.91 ppm were due to 3-H phenylene protons and pyrrolide protons. Only one of the two remaining phenylene resonances was visible as a singlet at 7.20 ppm, and was assigned to the 4-H phenylene protons. The 1-H phenylene protons were not observed, presumably due to the extreme line broadening effect of the paramagnetic samarium(II) centre which binds very close in the conformations displayed by **(40)** and **(43)**.

The ^{1}H NMR spectrum of **(43)** in benzene-d_6 is similar to that of **(40)**. The greatest difference in chemical shift is displayed by the THF protons which appear at -4.10 and -12.33 ppm whilst all other resonances appear within 0.3 ppm of the respsective resonances in **(40)**, Figure 6.

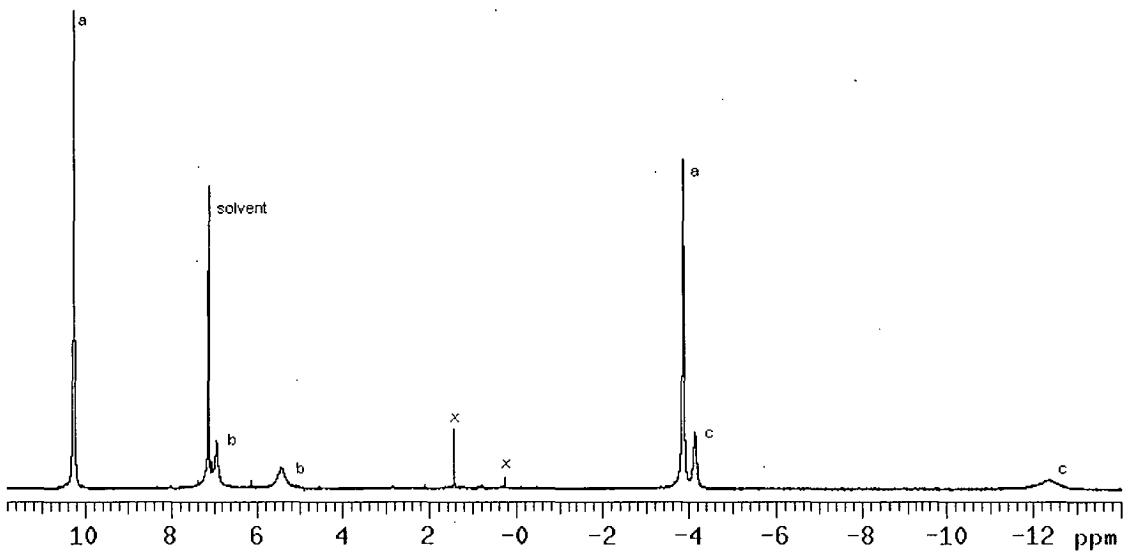

Figure 6: ^{1}H NMR spectrum of complex $[(Me_8N_2Ph_2)Sm(THF)]$, **(43)** (benzene-d_6, 300 MHz, 298 K, ppm) (a. *meso*-CH_3 protons, b. aromatic protons, c. THF protons; x = impurity).

Variable temperature ^{1}H NMR spectroscopic studies of $[(Me_8N_2Ph_2)Sm(THF)_2]$, **(40)**, and $[(Me_8N_2Ph_2)Sm(THF)]$, **(43)**, in the temperature range -80 to 20 °C were investigated using toluene-d_8 as solvent, Figure 7. The chemical shifts observed for **(40)** and **(43)** varied approximately linearly with 1/T according to the Curie-Weiss law, Figure 7. The THF proton resonances in **(40)** could not be located below 0 and -20 °C due to line broadening. The chemical shifts observed in the ^{1}H spectra of **(40)** and **(43)** converge at temperatures below *ca.* -40 °C, suggesting a common species is present in solution at low temperature. This common species is presumed to be a mono(THF) adduct which exists at low temperature even in the presence of the extra equivalent of THF.

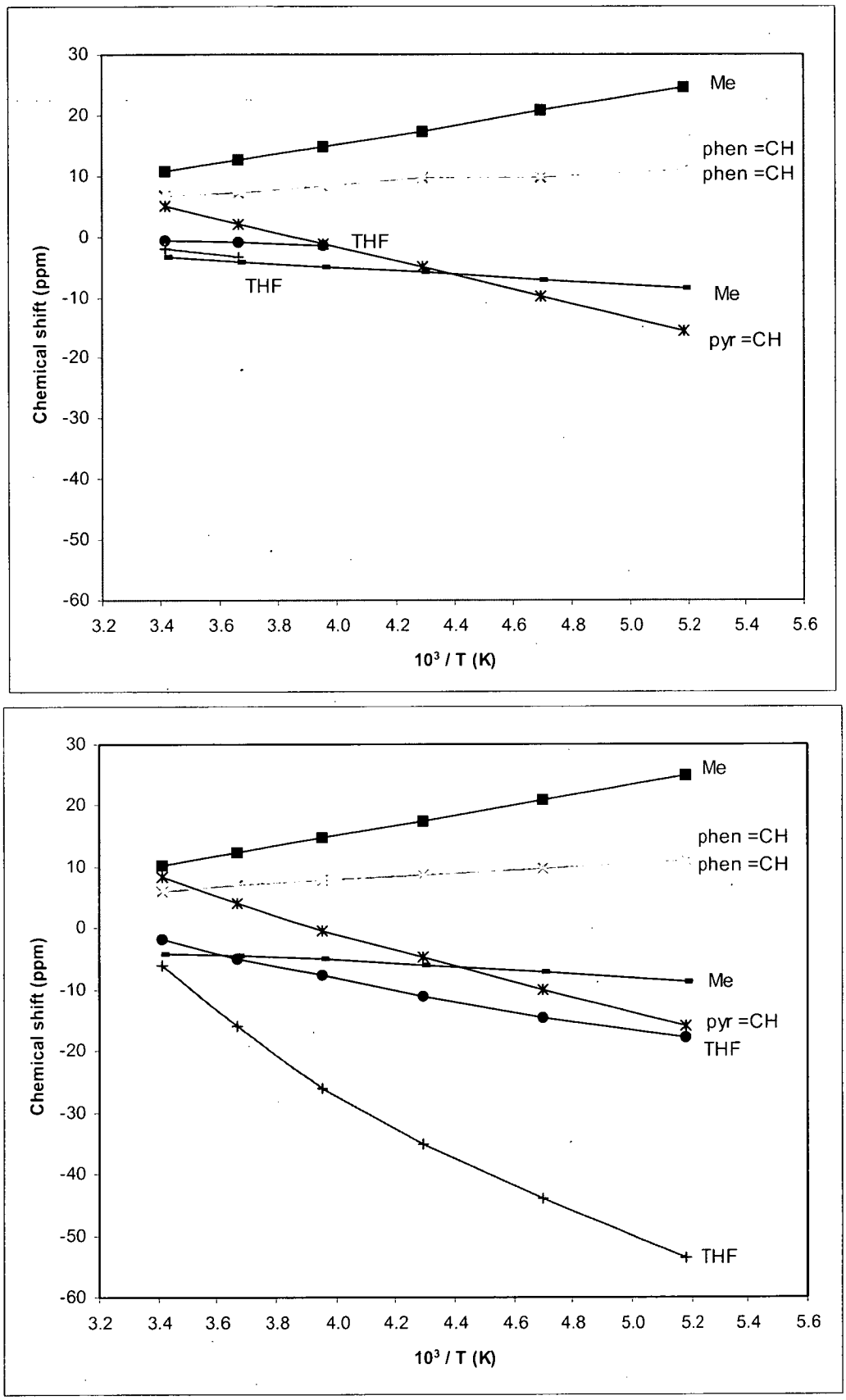

Figure 7: Variable temperature ^{1}H NMR spectra of [$(Me_8N_2Ph_2)Sm(THF)_2$], **(40)** (above), and [$(Me_8N_2Ph_2)Sm(THF)$], **(43)** (below) (toluene-d_8, 300 MHz, ppm).

The *N*-confused Sm(II) complex [{($Me_8NN'Ph_2$)Sm}$_2$] **(44)** was analysed by ^{1}H NMR spectroscopy, but low solubility in benzene-d_6 and THF-d_8 prevented ^{13}C or 2D NMR spectroscopy to be undertaken. The *N*-confusion present in the macrocyclic skeletons of **(44)** results in a loss of symmetry and a corresponding increase in the number of chemically unique protons compared with $(Me_8N_2Ph_2)^{2-}$. The ^{1}H NMR spectrum of **(44)** in benzene-d_6 contains a series of singlet resonances over the approximate range 41 to -20 ppm, presumably due to line broadening caused by the paramagnetic samarium(II) centres. Due to the wide range of chemical shifts, line broadening (loss of multiplicity information) and the inability to perform 2D NMR experiments, the ^{1}H NMR spectrum could only be partially assigned according to resonance integrals. Resonances were assigned to each of the 8 chemically independent *meso*-methyl groups at -4.78, -2.58, -2.25, -0.93, 1.55, 1.98, 8.04 and 26.63 ppm. Referring to the solid state molecular structure of **(44)**, one of the eight *meso*-methyl groups is significantly closer to a Sm(II) centre (C-Sm distance 3.91_6 Å) than the other seven (C-Sm distances > 4.50_0 Å); the proximity of this methyl group may be responsible for the single low field resonance at 26.63 ppm.

7.3.3 Molecular structures

7.3.3.1 Molecular structure of $\{(Me_8N_2Ph_2)K_2\}_n \cdot \frac{2}{3}(C_6H_5CH_3)$, (38)

Colourless crystals of $\{(Me_8N_2Ph_2)K_2\}_n \cdot \frac{2}{3}(C_6H_5CH_3)$ suitable for X-ray crystal structure determination were grown by heating $(Me_8N_2Ph_2)K_2(THF)_2$, **(37)**, in toluene at 125 °C for 7 days in a sealed tube. The crystals belong to the triclinic space group *P*1 (No. 2), a = 10.4318(12), b = 12.953(2), c = 16.853(3) Å, α = 92.730(9), β = 101.825(7), γ = 93.985(7) °, with 3 macrocyclic units in the unit cell. The asymmetric unit consists of 1.5 macrocyclic units (one full unit and one on an inversion centre) as well as half of a disordered toluene molecule lying on an inversion centre, Figure 8.

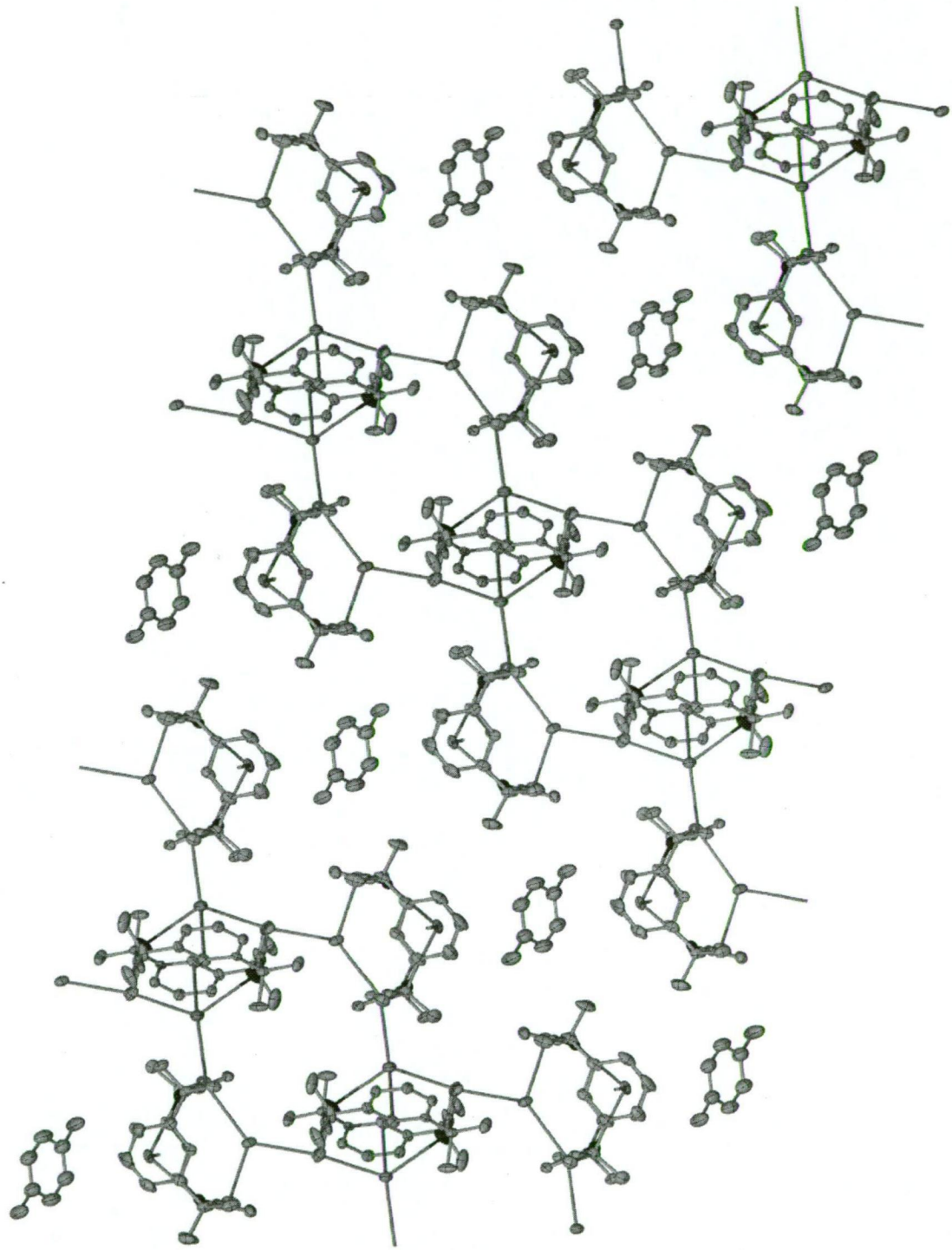

Figure 8: Solid state packing in $\{(Me_8N_2Ph_2)K_2\}_n \cdot \frac{2}{3}(C_6H_5CH_3)$, **(38)**, with thermal ellipsoids drawn at the level of 50% probability (protons removed for clarity).

The molecular structure of **(38)** features the $(Me_8N_2Ph_2)^{2-}$ macrocycle in two conformations. The first macrocyclic unit is in the 1,3-alternate conformation, with both pyrrolide units facing one side of the macrocyclic cavity, and the phenylene rings facing

the other, Figure 9. One potassium cation is η^5-bound to each pyrrolide unit and has a close contact (2.87$_9$ Å) to the phenylene 1-H proton and is *exo*-η^2-bound to the 1,2-alternate macrocycle *via* 3,4-positions of a pyrrolide unit. The second potassium cation is η^1-bound to the pyrrolide nitrogen, η^6-bound to the two phenylene rings and has a K···Me contact to a toluene molecule. There is a long K···K contact between the two potassium centres (4.17$_8$ Å).

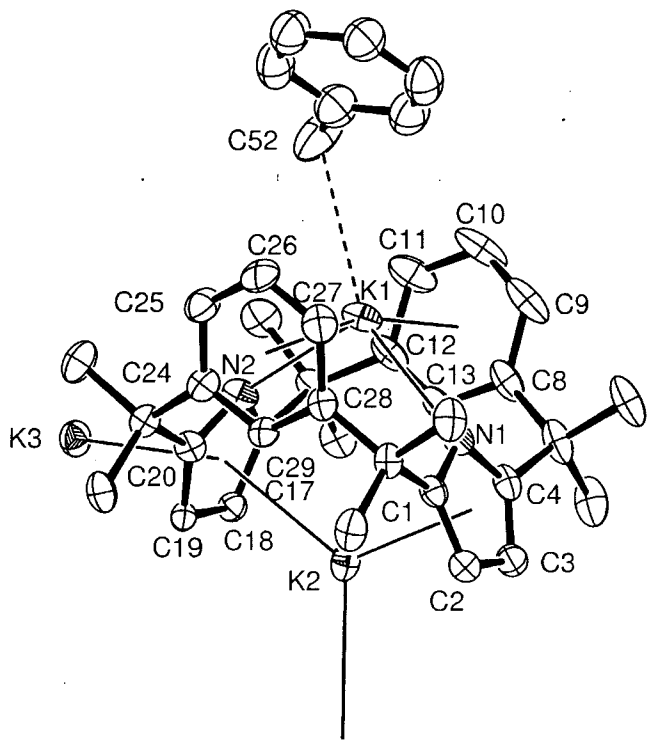

Figure 9: Detail of 1,3-alternate macrocyclic unit in $\{(Me_8N_2Ph_2)K_2\}_n \cdot \frac{2}{3}(C_6H_5CH_3)$, **(38)**, with thermal ellipsoids drawn at the level of 50% probability (protons removed for clarity).

The second macrocyclic unit exhibits a shallow 1,2-alternate conformation, *i.e.*, phenylene rings splayed back towards a partially flattened double cone conformation, with adjacent pyrrolide and phenylene units oriented towards each cavity, Figure 10. Each of the crystallographically identical *endo*-bound potassium cations features η^1 binding to the anionic pyrrolide nitrogen, contacts with the other pyrrolide ring (2.943(4) - 3.367(4) Å) and η^1 binding to a phenylene ring. The coordination sphere of these potassium centres is completed by *exo*-η^5-binding to a pyrrolide unit of an adjacent 1,3-alternate macrocycle. The overall structure is two dimensional polymeric due to the abovementioned *exo*-binding interactions in this Lewis basic solvent free complex.

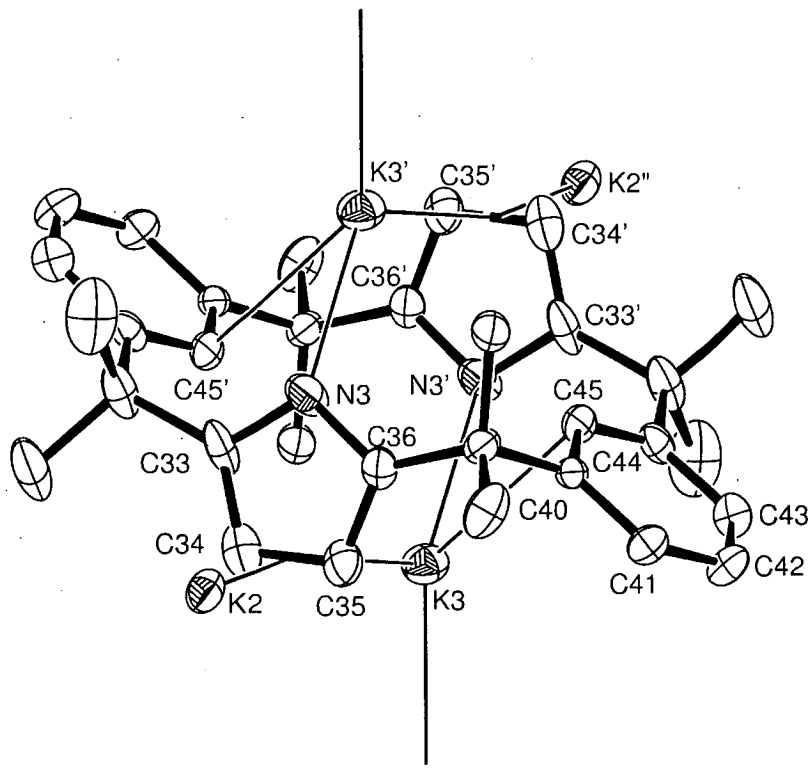

Figure 10: Detail of 1,2-alternate macrocyclic unit in $\{(Me_8N_2Ph_2)K_2\}_n \cdot \frac{2}{3}(C_6H_5CH_3)$, **(38)**, with thermal ellipsoids drawn at the level of 50% probability (protons removed for clarity).

The presence of the 1,2-alternate conformation in complex **(38)** clearly demonstrates the greater conformational freedom of $(Me_8N_2Ph_2)^{2-}$ relative to the $(Et_8N_4Me_2)^{2-}$ modified porphyrinogen derived ligand. This is possible due to lack of *trans*-annular interactions between the phenylene rings. The presence of such interaction makes the analogous 1,2-alternate conformation impossible in the $(Et_8N_4Me_2)^{2-}$ macrocycle. Two *endo*-bound potassium centres are present in the structure despite the lack of Lewis basic donor atoms in the phenylene rings.

The potassium centre K(1) is η^6-bound to both phenylene rings of the 1,3-alternate macrocycle with K-centroid distances of 2.83_8 Å and 2.91_7 Å, whilst the K-C distances vary between 3.071(4) - 3.381(4) Å. K(1) also coordinates to the pyrrolide nitrogens with K-N distances of 2.793(3) and 2.875(3) Å. Present on the other side of the 1,3-alternate macrocycle is K(2), which is bound through η^5 interactions to the pyrrolide rings with K-centroid distances of 2.86_8 and 3.01_8 Å. The metallocene bite angles for K(1) and K(2) are 163.7_2 and 126.3_7 ° respectively. K(1) engages in a short contact with the toluene methyl group, K(1)-C(52) = 3.45_2 Å, K(1)-H(52C) = 2.61_8 Å.

The 1,3-alternate macrocycle contains pyrrolide rings tilted at 66.9_3 ° and 77.1_1 ° to the macrocyclic plane, whilst the phenylene ring tilt angles are 74.2_5 ° and 81.8_8 °. Although of nominally similar conformation, these tilt angles differ considerably from those observed in the uncoordinated free ligand, (pyrrolide tilt angles 86.1_4, 87.5_7 °, phenylene tilt angles 49.4_7, 50.5_3 °).

The remaining potassium centre in the asymmetric unit is K(3), which is *endo*-bound to the 1,2-alternate macrocycle and bridges to the 1,3-alternate macrocycle through an *exo*-interaction with the pyrrolide ring (K-C(pyrrolide) distances of 2.983(3) - 3.362(3) Å). The bond lengths of K(3) to the 1,2-alternate macrocycle are 2.895(3) Å (η^1 to pyrrolide nitrogen), 2.943(4) - 3.367(4) Å (to rear of pyrrolide ring) and 3.117(4) Å (η^1 to phenylene ring). The tilt angles of the pyrrolide rings are 85.2_4 ° and those of the phenylene rings are 33.5_8 °. The low phenylene angle reflects the flattened morphology of the 1,2-alternate macrocycle, with the phenylene rings lying at relatively shallow angle to the macrocyclic plane compared with those in the 1,3-alternate conformation (74.2_5 ° and 81.8_8 °).

7.3.3.2 Molecular structure of $[(Me_8N_2Ph_2)Sm(COT)K(THF)]_n$, (41)

Violet crystals of **(41)** suitable for X-ray structure determination were grown by cooling a hot solution in THF/toluene to ambient temperature. The crystals belong to the orthorhombic space group *Pnma* (No. 62), a = 17.9849(3), b = 15.0322(3), c = 15.8123(3) Å, with 4 macrocyclic units in the unit cell. The asymmetric unit consists of one half of the macrocyclic unit, and one half of an unbound THF molecule disordered across a mirror plane. The K-bound THF molecule has a two-site occupancy disorder in both β-methylene units. The overall crystallographic molecular symmetry is C_s, Figure 11.

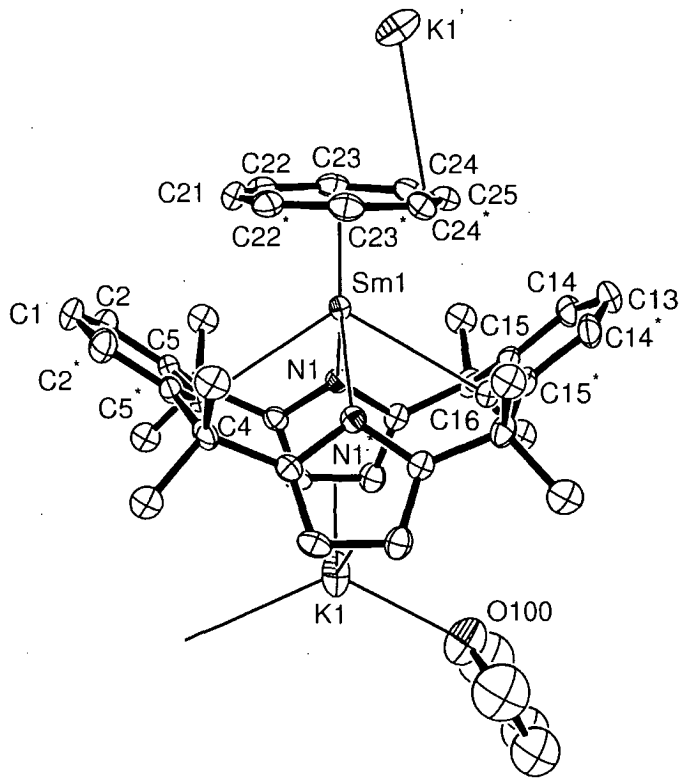

Figure 11: Molecular structure of $[(Me_8N_2Ph_2)Sm(COT)K(THF)]_n$, **(41)**, with thermal ellipsoids drawn at the level of 50% probability (protons removed for clarity).

Complex **(41)** contains a samarium(III) centre σ-bound to two pyrrolide nitrogens with Sm-N distances of 2.60_0 Å. There is also an η^1 interaction between the samarium centre and a phenylene carbon (Sm-C distance 2.94_9 Å). The COT is η^8-bound to the samarium centre with a Sm-centroid bond length of 1.94_7 Å, and Sm-C bond lengths of 2.65_1 - 2.70_2 Å. Present on the other face of the macrocycle is a potassium cation η^2-bound to the 3,4-positions of the pyrrolide units (K-C distances 3.13_8, 3.18_9 Å). The potassium is also η^3-bound to the COT ligand of the adjacent molecule, forming a linear polymeric structure. The coordination sphere of the potassium centre is completed by a single THF molecule.

The macrocycle in complex **(41)** displays a 1,3-alternate conformation. The phenylene rings are splayed back towards the macrocyclic plane to accommodate the COT dianion resulting in a low η^1 hapticity to the samarium cente, and shallow phenylene ring tilt angles of 34.6_7, 38.8_8 ° which are similar to those observed in the COT-containing macrocycle in the potassium-free complex $[(Me_8N_2Ph_2)Sm(COT)][(Me_8N_2Ph_2)Sm(THF)]$, **(45)**, ($31.0_1$, 34.2_3 °, *vide infra*). The pyrrolide ring tilt angle of 67.9_1 ° is also similar to those observed in complex **(45)**,

(60.8_5, 64.0_9 °, *vide infra*). The pyrrolide and phenylene rings are eclipsed as there is no twist in the macrocyclic skeleton (absolute deviation of *meso*-carbons from the least squares macrocyclic plane 0.00_0 Å).

7.3.3.3 Molecular structures of $[(Me_8N_2Ph_2)Sm(THF)_2]$, (40), and $[(Me_8N_2Ph_2)Sm(THF)]$, (43)

Dark red-brown crystals of **(40)** suitable for X-ray crystal structure determination were grown by heating the complex with THF in a sealed tube at 50 °C overnight, then 90 °C for 7 h followed by slow cooling to ambient temperature and standing for 24 h. The crystals belong to the orthorhombic space group $P2_12_12$ (No. 15), a = 13.2103(1), b = 13.3956(2), c = 9.3869(1) Å, with 2 molecules in the unit cell. The asymmetric unit consists of half a molecule lying on a C_2 axis. The overall molecular symmetry is C_2, reduced from C_{2v} by a large "twist" of the macrocycle and THF molecule orientations, see Figure 12.

Complex **(40)** is mononuclear, with a single samarium centre σ-bound to the pyrrolide nitrogen centres with a distance of 2.614(3) Å. Two THF molecules bind to the samarium centre at the top of the macrocyclic cavity with Sm-O bond lengths of 2.638(3) Å. The samarium centre is η^6-bound to the phenylene rings with a Sm-centroid distance of 2.77_1 Å and Sm-C distances in the range 2.938(4) - 3.258(4) Å. The metallocene bend angle is 167.5_5 ° and the tilt angles of the phenylene rings are 76.2_0 °. The pyrrolide ring tilt angles are 26.4_3 °.

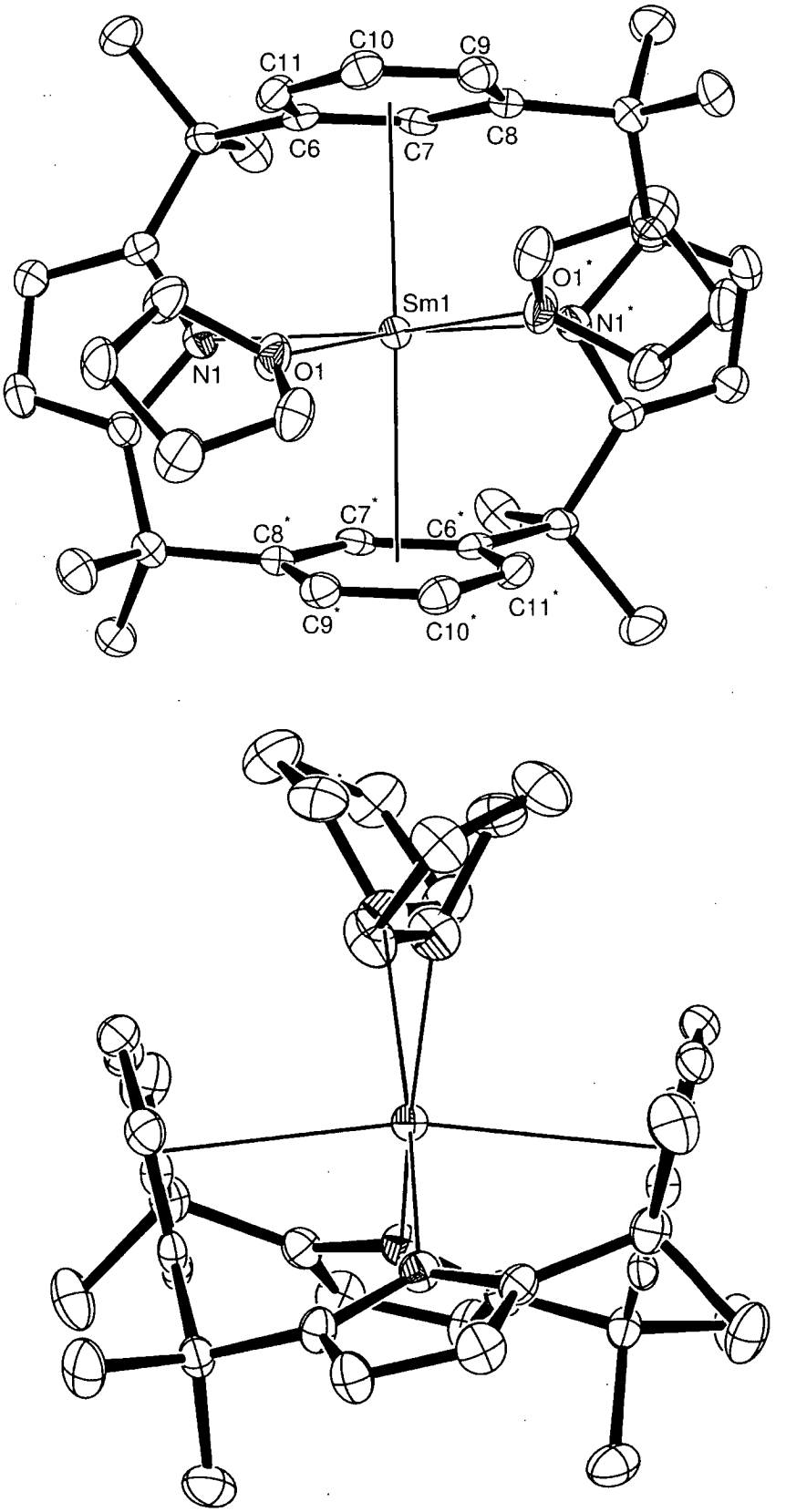

Figure 12: Molecular structure of $[(Me_8N_2Ph_2)Sm(THF)_2]$, **(40)**, with thermal ellipsoids drawn at the level of 50% probability (protons removed for clarity).

The 1,3-alternate macrocycle skeleton of **(40)** displays a large degree of twist, unobserved in other structurally characterised K and Sm complexes of the $(Me_8N_2Ph_2)^{2-}$ ligand. This is reflected in the large absolute deviation of the *meso*-carbons from the least-squares macrocyclic plane (0.67_7 Å). Similar twisting is observed in the neutral $Me_8N_2Ph_2H_2$ ligand, in which the absolute deviation of *meso*-carbons from the least-squares macrocyclic plane of the neutral ligand is 0.71_2 - 0.71_7 Å. Conversely, the 1,3-alternate macrocyclic unit in the dipotassium salt $\{(Me_8N_2Ph_2)K_2\}_n \cdot \frac{2}{3}(C_6H_5CH_3)$, **(38)**, displays only a very minor degree of twist (absolute deviation of *meso*-carbons from the least squares macrocyclic plane 0.06_8 - 0.06_9 Å), similar to that observed in $Me_8N_2Ph_2H_2.CH_2Cl_2$ (absolute deviation of *meso*-carbons from the least squares macrocyclic plane 0.06_3 Å). The twist in **(40)** and $Me_8N_2Ph_2H_2$ results in the phenylene rings adopting a staggered conformation, Figure 13.

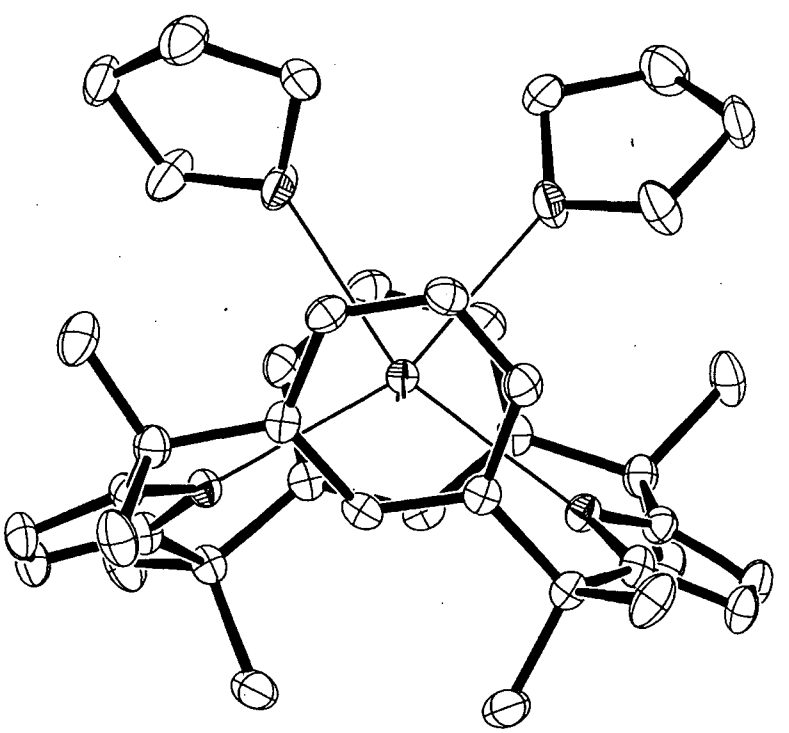

Figure 13: Molecular structure of $[(Me_8N_2Ph_2)Sm(THF)_2]$, **(40)**, showing staggered phenylene ring conformation, with thermal ellipsoids drawn at the level of 50% probability (protons removed for clarity).

Dark indigo crystals of **(43)** suitable for X-ray crystal structure determination were grown by heating $[(Me_8N_2Ph_2)Sm(THF)_2]$, **(40)**, in toluene at 130 °C for 24 h followed by slow cooling to room temperature. The crystals belong to the orthorhombic

space group $P2_12_12$ (No. 19), a = 10.495(2), b = 15.478(3), c = 18.759(4) Å, with 4 molecules in the unit cell. The asymmetric unit consists of 1 molecule. The overall molecular symmetry approximates to C_s (including THF molecule orientation) whilst the symmetry of the macrocycle is C_{2v}, Figure 14.

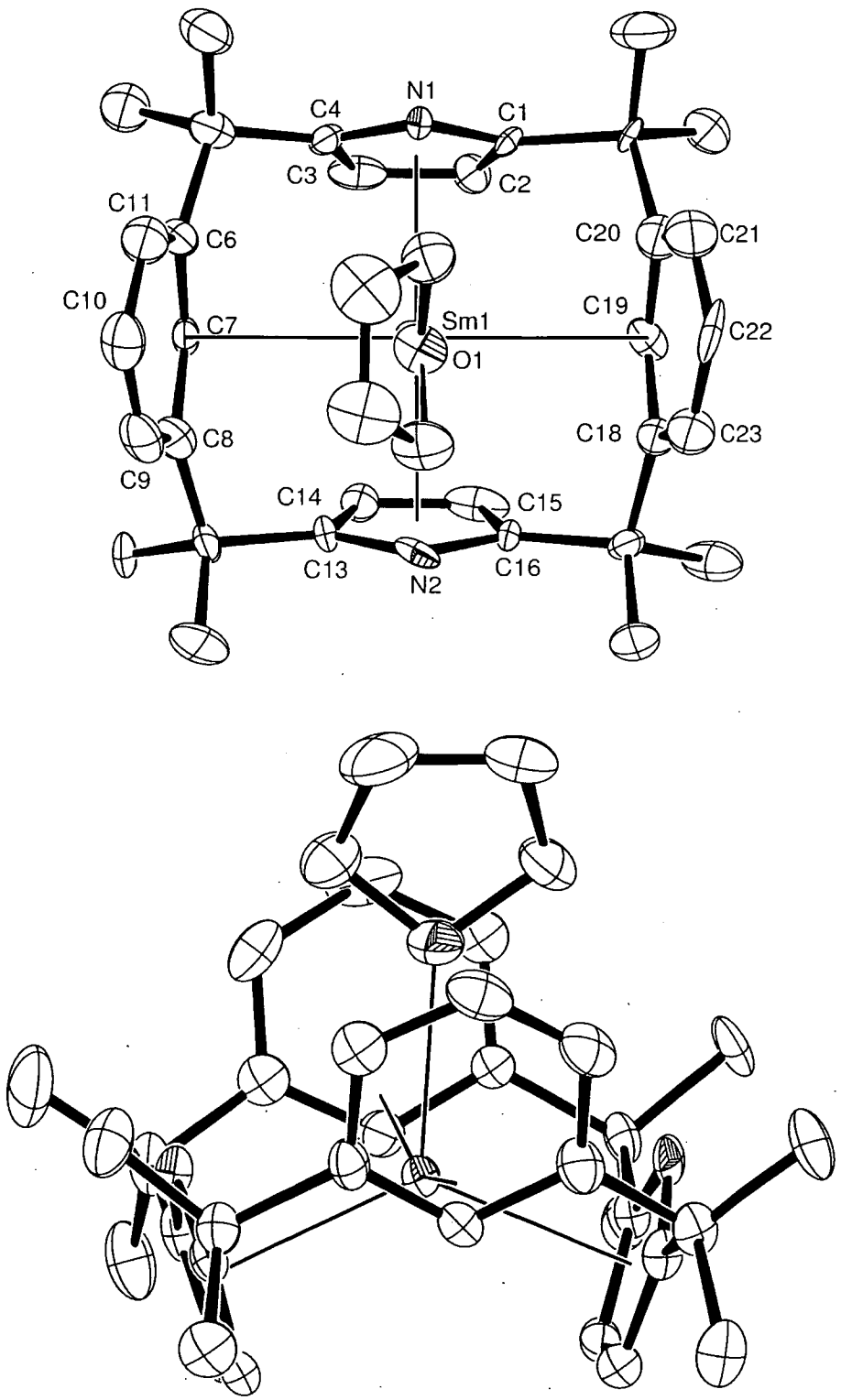

Figure 14: Molecular structure of [($Me_8N_2Ph_2$)Sm(THF)], **(43)**, with thermal ellipsoids drawn at the level of 50% probability (protons removed for clarity).

The macrocyclic binding modes in **(43)** are different to those observed in **(40)**. The macrocycle skeleton in **(40)** is 1,3-alternate, with η^1-Sm-N binding, and η^6-bound phenylene rings. In contrast, the macrocyclic unit in the mono-THF adduct **(43)** displays η^5-bound pyrrolide rings and η^3-bound to the phenylene rings in a non-conventional full-cone conformation, *c.f.*, conformation of $[\{(Me_8NN'Ph_2)Sm\}_2]$, **(44)**, Section 7.3.3.4. The disposition of the nitrogen centres with respect to the phenylene rings in **(43)** is typical of a 1,3-alternate conformation, however there is also a full-cone aspect in that all four arene rings present to the same face of the macrocyclic cavity for π-interactions to an *endo*-bound samarium centre. The overall hapticity of the macrocycle in the mono(THF) complex thus increases to compensate for the presence of only one THF molecule.

The reduction in coordination number and/or electronic saturation also results in a shorter Sm-O distance in **(43)** (2.523(4) Å) than in the bis-(THF) adduct (2.6552(14) Å). The three shortest Sm-C(phenylene) distances are 2.797(9) - 3.22_9 and 2.809(9) - 3.24_7 Å; the remaining Sm-C distances are 4.02_9 - 4.39_9 and 4.04_3 - 4.41_6 Å, thus indicating an η^3-Sm-phenylene interaction to each ring. The Sm-phenylene centroid distances are 2.52_9 and 2.53_5 Å, defining a metallocene bend angle of 131.5_5°. The Sm-pyrrolide nitrogen bond lengths are 2.639(5) and 2.651(5) Å whilst the Sm-pyrrolide carbon bond lengths are 2.745(6) - 2.907(6) and 2.751(7) - 2.92_5 Å, congruent with an η^5-pyrrolide interaction.

The phenylene ring tilt angles are 72.6_5 and 73.8_7 ° and the pyrrolide ring tilt angles are 106.3_0 and 107.0_8 °. The obtuse values for the pyrrolide ring tilt angles are representative of the degree of rotation required to produce the conformation observed in **(16)** from a theoretical, planar macrocycle in which the pyrrolide rings are coplanar to the macrocyclic plane, and the pyrrolide nitrogens and phenylene 1-carbon centres point towards the centre of the cavity. The macrocyclic skeleton of **(43)** displays only a very slight degree of twist, in contrast to the bis(THF) adduct. The absolute deviation of each *meso*-carbon from the least squares macrocyclic plane is 0.07_1 Å.

7.3.3.4 Molecular structure of [{($Me_8NN'Ph_2$)Sm}$_2$].4C_6D_6, (44)

Grey-green crystals of **(44)** suitable for X-ray diffraction determination were grown by allowing a suspension of **(18)** to stand in benzene-d_6 at room temperature for 2 weeks. The crystals belong to the triclinic space group $P\bar{1}$ (No. 2), a = 12.655(3), b = 13.010(3), c = 13.201(3) Å, α = 70.64(3), β = 62.47(3), γ = 77.28(3) °, with 1 molecule in the unit cell. The asymmetric unit consists of one half of a centrosymmetric dimer and two benzene-d_6 molecules, Figure 15.

The molecular structure is binuclear, with each samarium centre *endo*-bound within an *N*-confused macrocyclic cavity, and *exo*-bound to a pyrrolide nitrogen of the other macrocycle, resulting in a centrosymmetric structure. Within the cavity the samarium centres are η^5-bound to each pyrrolide ring (Sm-centroid distances = 2.58_3, 2.66_0 Å) and η^1-bound to the phenylene rings (the shortest Sm-C distances to each ring are 3.011(7) and 3.02_2 Å, the next closest are 3.56_0, 3.56_7 and 3.58_1, 3.65_3 Å). The bond length between each samarium centre and the *exo*-bound pyrrolide nitrogen is 2.519(9) Å.

The macrocycle units adopt a full cone-type conformation in which both the pyrrolide and phenylene rings present to the same face of the macrocyclic cavity. In addition, the pyrrolide and phenylene carbons are all present on the same side of the macrocyclic plane. This differs from the full cone-type conformation displayed in [($Me_8N_2Ph_2$)Sm(THF)], **(43)**, in which the phenylene carbons are present on the same side as the bound THF molecule, with the pyrrolide carbons on the opposite side of the macrocyclic plane. The tilt angles of the phenylene rings in **(44)** are 30.9_8 and 37.3_5 °, whilst those of the pyrrolide rings are 78.7_0 and 79.9_2 Å. There is a small amount of twist in each macrocycle resulting in the absolute deviation of each *meso*-carbon from the least squares macrocyclic plane being 0.25_5 - 0.26_4 Å.

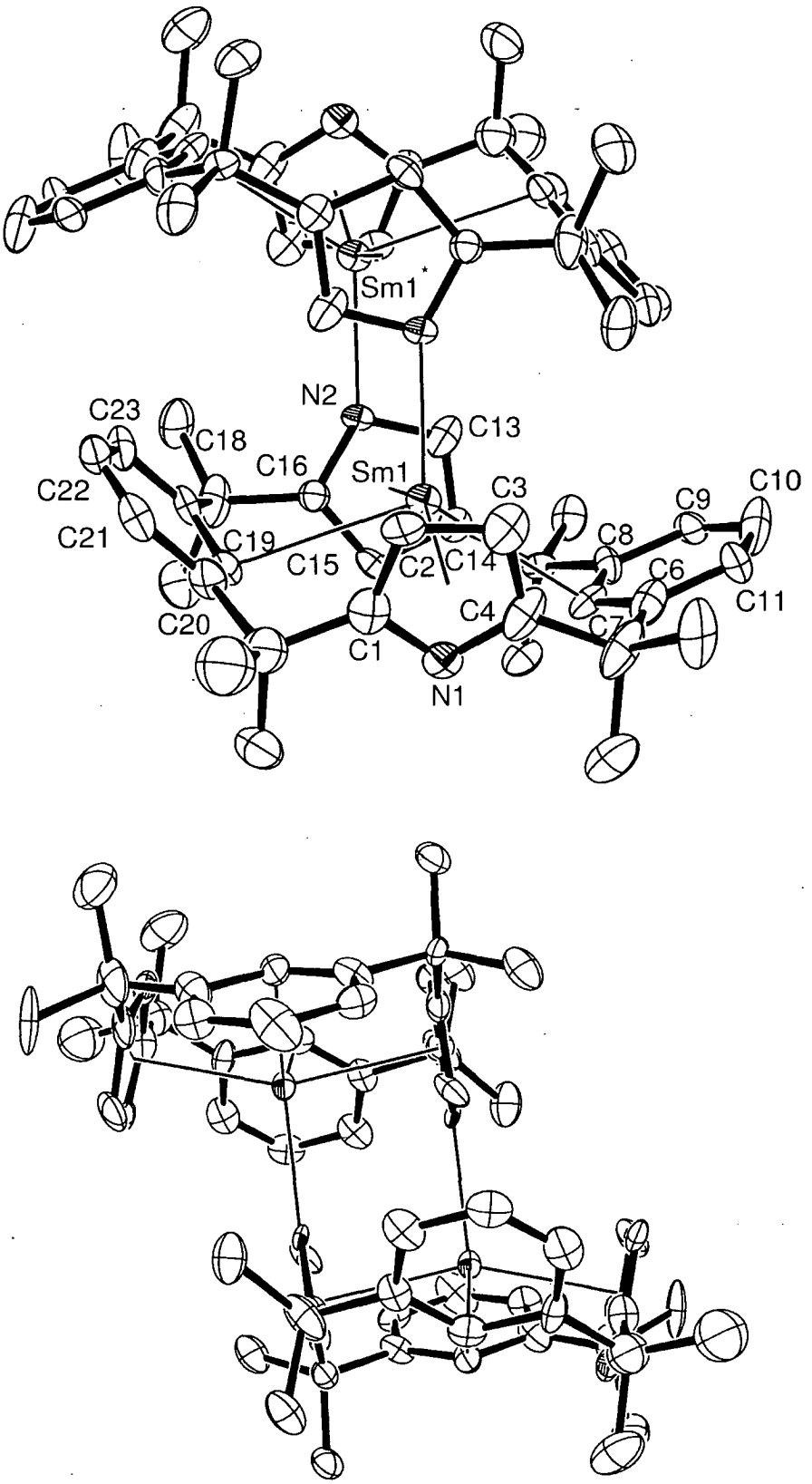

Figure 15: Molecular structure of [{($Me_8NN'Ph_2$)Sm}$_2$], **(44)**, with thermal ellipsoids drawn at the level of 50% probability (protons removed for clarity).

7.3.3.5 Molecular structure of $[(Me_8N_2Ph_2)Sm(THF)][(Me_8N_2Ph_2)Sm(COT)]$, (45)

Complex **(45)** was obtained as a violet crystalline precipitate by diffusion of cyclooctatetraene vapour into a solution of $[(Me_8N_2Ph_2)Sm(THF)_2]$, **(40)**, over the course of 2 weeks. A single crystal was isolated from the precipitate and analysed using a synchrotron X-ray source. The crystal belongs to the monoclinic space group $P2_1/n$ (No. 14), a = 10.341(5), b = 32.455(5), c = 18.467(5) Å, β = 93.688(5) °, with 4 cation/anion pairs in the unit cell. The asymmetric unit consists of two macrocyclic units, one cationic with a Sm(III) centre bound to a molecule of THF, the other anionic with a Sm(III) centre bound to a COT dianion, Figure 16.

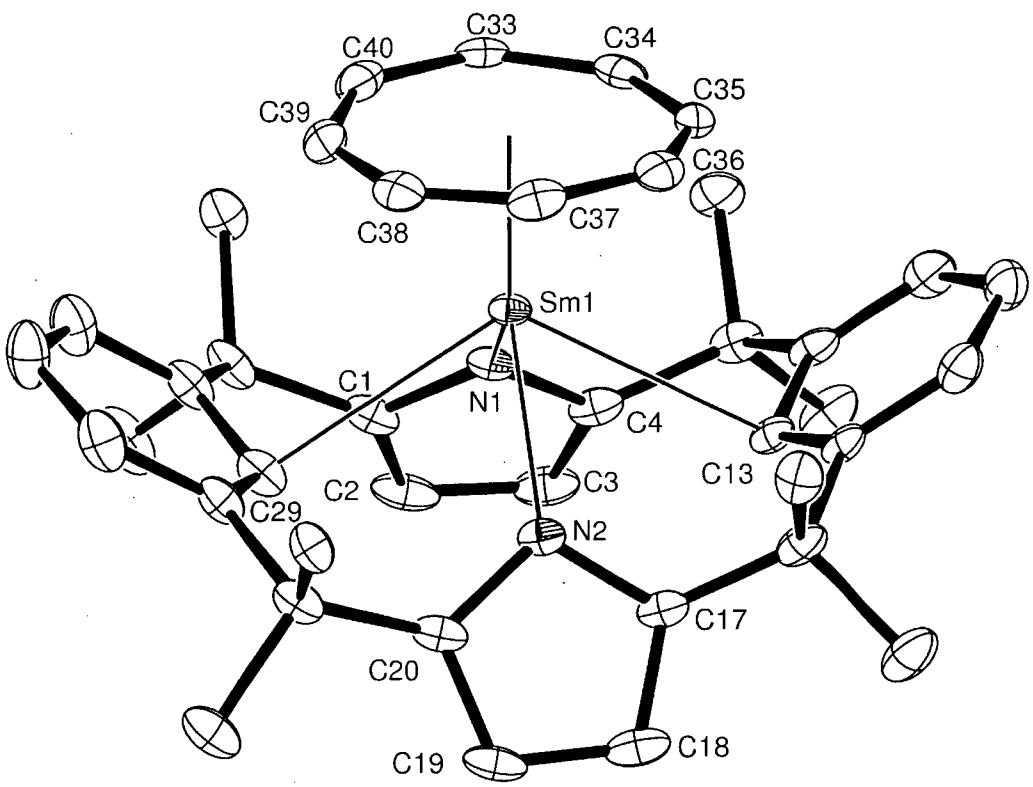

Figure 16: Molecular structure of the anionic COT-bound macrocycle in complex **(45)**, with ellipses shown at the level of 50% probability (protons removed for clarity).

The COT-bound macrocycle consists of a Sm(III) centre η^8-bound to a COT dianion with a Sm-centroid distance of 1.97$_4$ Å, and Sm-C distances of 2.658(4)-2.732(4) Å. These values can be compared with those in $[\{(Et_8N_4Me_2)Sm\}_2(COT)]$, **(28)**, which displays a Sm-centroid distance of 3.61$_3$ Å and shortest Sm-C distances of 2.704(1) and 2.751(1) Å. The more flexible $(Me_8N_2Ph_2)^{2-}$ macrocycle accomodates the

COT ligand in it's preferred η^8-binding mode, and allows closer contact between the Sm centre and COT carbons.

The Sm-N(pyrrolide) bond lengths are 2.562(3), 2.552(3) Å, and binding to the phenylene rings is η^1-, with Sm-C1 distances of 2.966(4), 3.008(4) Å. The large oblate COT dianion has a profound effect on the macrocyclic conformation as the phenylene rings splay back towards the macrocyclic plane, which is reflected in the phenylene ring tilt angles (31.0_1, 34.2_3 °). The pyrrolide ring tilt angles are 60.8_5 and 64.0_9 °.

The macrocyclic conformation in the COT-bound macrocyclic unit is qualitatively similar to $[(Me_8N_2Ph_2)Sm(COT)K(THF)]_n$, **(41)**, which also features a Sm(III) centre η^8-bound to a COT dianion, with η^1-binding to the pyrrolide nitrogens and phenylene C1 carbons. The main difference in quantitative data between the two molecular structures is due to the THF-solvated K centre which bridges the COT dianion and pyrrolide 3,4-carbons in **(41)**. Selected bond lengths and angles are shown in Table 1.

	(45), COT-bound macrocycle	**(41)**
Sm-N(pyrrolide)	2.552(3), 2.562(3)	2.60_0
Sm-C1	2.966(4), 3.008(4)	2.94_9
Sm-COT centroid	1.97_4	1.94_7
Sm-C(COT)	2.658(4) - 2.732(4)	2.65_1 - 2.70_2
Pyrrolide ring tilt	60.8_5, 64.0_9	67.9_1
Phenylene ring tilt	31.0_1, 34.2_3	34.6_7, 38.8_8

Table 1: Selected bond lengths (Å) and angles (°) for the COT-bound macrocycle in complex **(45)**, and $[(Me_8N_2Ph_2)Sm(COT)K(THF)]_n$, **(41)**.

The cationic THF-bound macrocyclic unit consists of a Sm(III) centre η^5-bound to the macrocyclic pyrrolide rings with Sm-centroid distances of 2.39_3, 2.39_4 Å, and a resultant metallocene bend angle of 131.4_1 °. The Sm-phenylene interaction is best described as η^1, with a Sm-C1 distance of 2.729(4) Å and Sm-C2 distances of 3.20_0 - 3.24_0 Å. A single THF molecule binds to the Sm(III) centre with a Sm-O(THF) bond distance of 2.411(3) Å, Figure 1.7.

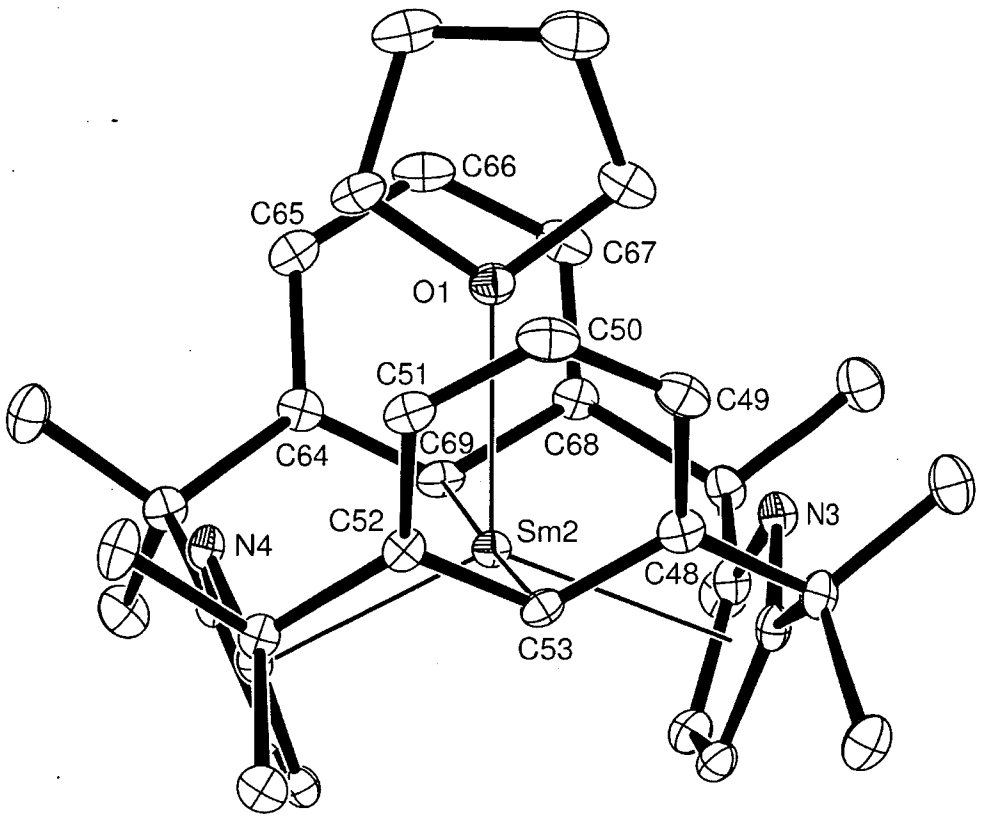

Figure 17: Molecular structure of the cationic COT-bound macrocycle in complex **(45)**, with ellipses shown at the level of 50% probability (protons removed for clarity).

The pyrrolide ring tilt angles are 108.4_7, $109.3_4°$, whilst the phenylene ring tilt angles are 71.4_4, $73.2_2°$. The Sm(III) centre is bound in an identical conformation to the Sm(II) centre in $[(Me_8N_2Ph_2)Sm(THF)]$, **(43)**, allowing an interesting comparison between the two molecules which differ in the oxidation state of the Sm centre, Table 2. The Sm-O, C1 and pyrrolide centroid distances are all shorter in complex **(45)**, as expected from the higher effective nuclear charge of the Sm(III) centre. Minor differences in ring tilt angles are also noted between the two complexes, reflecting the changes required to maintain optimal binding to the different size Sm centres.

	(45), THF-bound macrocycle	**(43)**
Sm-pyrrolide centroid	2.39_3, 2.39_4	2.52_9, 2.53_5
Sm-Cl	2.729(4)	2.797(9), 2.809(9)
Sm-O(THF)	2.411(3)	2.523(4)
Metallocene bend angle	131.4_1	131.5_5
Pyrrolide ring tilt	108.4_7, 109.3_4	106.3_0, 107.0_8
Phenylene ring tilt	71.4_4, 73.2_2	72.6_5, 73.8_7

Table 2: Selected bond lengths (Å) and angles (°) for the THF-bound macrocycle in complex **(45)**, and [($Me_8N_2Ph_2$)Sm(THF)], **(43)**.

7.4 Experimental

Synthesis of $Me_8N_2Ph_2H_2$, (II)

1,3-bis(1',1'-dimethylhydroxymethyl)benzene (6.8×10^{-2} mol, 13.2 g) and pyrrole (6.8×10^{-2} mol, 4.56 g) were added to MeCN (1 L) with stirring to effect dissolution. $Sc(OTf)_3$ (3.4×10^{-4} mol, 167 mg) in MeCN (3 mL) was added and the solution left without stirring for 8 d, during which time the crude product formed as colourless rosettes. The deep green supernatant was decanted away and the white crystals rinsed with MeCN. The supernatant was reduced to 200 mL and kept at -20 °C for 2 d to give a second crop of product which was collected and rinsed with MeCN. The combined solids were dried *in vacuo* and purified by sublimation at 250 °C / 1×10^{-2} mmHg to give $Me_8N_2Ph_2H_2$ as a white crystalline powder (2.42 g, 16 %).

^{1}H NMR (300 MHz, $CDCl_3$, 25 °C): δ = 1.51 (s, 24H, *meso*-CH_3), 5.94 (d, 4H, β-pyrrole CH), 6.59 (s, br, 2H, NH), 6.74 (s, 2H, phenylene C(1)H), 7.19 (m, 6H, phenylene C(3)H and C(4)H)

Synthesis of $(Me_8N_2Ph_2)K_2(THF)_2$, (37)

$Me_8N_2Ph_2H_2$ (3.2×10^{-3} mol, 1.45 g) was added to THF (30 mL) and PhMe (30 mL) with stirring. K metal (0.64 g, 1.6×10^{-2} mol) was added and the mixture heated with gentle stirring in an oil bath at 75 °C for 2 d. The suspension of $Me_8N_2Ph_2H_2$ was filtered from excess K metal and the solvent removed *in vacuo*, affording the product as an off-white powder (1.75 g, 94 %).

Synthesis of $[(Me_8N_2Ph_2)K_2(C_6H_5CH_3)_{2/3}]_n$, (38)

$(Me_8N_2Ph_2)K_2(THF)_2$, **(37)**, (2.6×10^{-5} mol, 15 mg) was suspended in toluene (1 mL) and heated at 125 °C for 7 d in a sealed tube to form the product as colourless crystals. The turbid supernatant was decanted, and the crystals rinsed with toluene and dried *in vacuo* (mass and yield not recorded).

Anal. Calcd.: C, 74.86; H, 7.08; N, 4.76 ($C_{36.67}H_{41.33}N_2K_2$, MW = 588.29)
Found: C, 73.76; H, 6.80; N, 5.05.

Synthesis of Sm(II) intermediate (39) (postulated formula [K($Me_8N_2Ph_2$)SmI])

$(Me_8N_2Ph_2)K_2(THF)_2$, **(37)**, (1.18×10^{-3} mol, 0.68 g) was suspended in THF (20 mL). Dropwise addition of samarium(II) iodide (1.00×10^{-3} mol, 10.0 mL of 0.1 M solution in THF) to the stirred, off-white suspension resulted in a colour change to dark brown and the formation of a white precipitate (presumably KI). Stirring was continued for 1.5 h, then solvent was removed *in vacuo* and toluene (30 mL) added to the dark purple solids. The mixture was stirred for 0.5 h, filtered *via* cannula and the toluene removed *in vacuo* to give black solids. THF (20 mL) was added with stirring to effect complete dissolution, then partially removed *in vacuo* until solids began to form. The mixture was stood at -20 °C for 3 d forming dark purple crystalline solid. The supernatant was removed *via* cannula and the crude product dried *in vacuo* (95 mg, yield not calculated).

Synthesis of [($Me_8N_2Ph_2$)Sm(THF)$_2$], (40)

Samarium(II) iodide (7.5×10^{-4} mol, 7.5 mL of 0.1M solution in THF) was added dropwise to a suspension of $(Me_8N_2Ph_2)K_2(THF)_2$, **(37)**, (8.8×10^{-3} mol, 0.50 g) in THF (10 mL). The mixture was heated at 70 °C for 3 d and solvent removed *in vacuo*. The grey solids were extracted with toluene (30 mL and 15 mL) *via* filter cannula and the solvent removed from the combined filtrates *in vacuo*. THF (15 mL) was added and the suspension heated at 75 °C overnight before being stood at -20 °C overnight to complete the precipitation. Supernatant was removed *via* cannula and the solids dried *in vacuo* to give the product as a purple powder (0.14 g, 25 % based on Sm).

^{1}H NMR (300 MHz, C_6D_6, 25 °C; partially assigned): δ = -4.52 (br, 8H, THF), -3.54 (s, 12H, CH_3), -1.40 (br, 8H, THF), 5.91 (br, 4H, =CH), 6.43 (br, 4H, =CH), 7.20 (s, 2H, =CH), 10.44 (s, 12H, CH_3).

Anal. Calcd.: C, 64.64; H, 7.05; N, 3.77 ($C_{40}H_{52}N_2O_2Sm$, MW = 743.23)
Found: C, 64.19; H, 6.90; N, 3.72.

Synthesis of $[(Me_8N_2Ph_2)Sm(COT)K(THF)]_n$, (41)

Cyclooctatetraene (9.6×10^{-6} mol, 25 μL of 0.384 M solution in benzene-d_6) was added to a solution of complex **(39)** (14 mg) in toluene (1 mL) in a sealed tube. The mixture was briefly heated to reflux and left at room temperature overnight to give violet solids under a yellow-green supernatant. The supernatant was decanted and the solids rinsed with benzene-d_6. The solids were recrystallised from a hot THF/toluene solution to give violet crystals suitable for X-ray structure analysis. The mass and yield of product were not recorded.

Synthesis of $[(Me_8N_2Ph_2)Sm(THF)]$, (43)

$[(Me_8N_2Ph_2)Sm(THF)_2]$ **(40)** (50 mg, 6.73×10^{-5} mol) and toluene (0.5 mL) were heated for 24 h at 130 °C. Slow cooling to room temperature and removal of the supernatant afforded the product as dark indigo crystals suitable for X-ray diffraction analysis (28 mg, 62 %).

^{1}H NMR (300 MHz, C_6D_6, 25 °C; partially assigned): δ = -12.33 (br, 4H, THF), 4.10 (s, 4H, THF), -3.83 (s, 12H, CH_3), 5.47 (br, 4H, =CH, pyrrolide), 6.97 (s, 4H, =CH, phenylene), *ca.* 7.16 ppm (s, 2H, =CH, phenylene), 10.29 (s, 12H, CH_3).

Anal. Calcd.: C, 64.43; H, 6.61; N, 4.17 ($C_{36}H_{44}N_2OSm$, MW = 671.13)
Found: C, 64.69; H, 6.33; N, 3.97.

Synthesis of $[\{(Me_8NN'Ph_2)Sm\}_2]$, (44)

Samarium iodide (8.9×10^{-4} mol, 8.9 mL of 0.1 M solution in THF) was added dropwise to a stirred suspension of $(Me_8N_2Ph_2)K_2(THF)_2$, **(37)**, (1.0×10^{-3} mol, 0.60 g), in THF (20 mL). Stirring was continued overnight and the mixture filtered *via* cannula. Solvent was removed *in vacuo*, toluene (20 mL) added and the olive green mixture stirred at room temperature overnight then heated to 90 °C for 3 h. The colourless supernatant was decanted away and the solids dried *in vacuo* to give the product as a pale grey-green powder (0.26 g, 49 %).

^{1}H NMR (300 MHz, C_6D_6, 25 °C; partially assigned): δ = -4.78 (s, 6H, CH_3), -2.58 (s, 6H, CH_3), -2.25 (s, 6H, CH_3), -0.93 (s, 6H, CH_3), 1.55 (s, 6H, CH_3), 1.98 (s, 6H, CH_3), 8.04 (s, 6H, CH_3), 26.63 (s, 6H, CH_3).

Anal. ($C_{64}H_{72}N_4Sm_2.2(C_6D_6)$, MW = 1366.32)

Calcd.: C, 66.81; H+D, 7.08; N, 4.10

Found: C, 65.27; H+D, 6.06; N, 3.70.

7.5 References

1. Y.-S. Jang, H.-J. Kim, P.-H. Lee and C.-H. Lee, *Tetrahedron Lett.*, 2000, **41**, 2919.

2. J. Wang, M.G. Gardiner, *Chem. Commun.*, 2005, 1589.

3. J. Wang, Ph.D. Thesis, University of Tasmania, 2003.

4. R. Crescenzi, E. Solari, C. Floriani, A. Chiesi-Villa, C. Rizzoli, *Inorg. Chem.*, 1996, **35**, 2413.

5. D.N. Stringer, Ph.D. Thesis, University of Tasmania, 2008.

6. J.L. Sessler, W.-S. Cho, V. Lynch, V. Král, *Chem. Eur. J.*, 2002, **8**, 1134.

7. J. Wang, M.G. Gardiner, E.J. Peacock, B.W. Skelton, A.H. White, *Dalton Trans.*, 2003, 161.

8. T. Dubé, J. Guan, S. Gambarotta, G.P.A. Yap, *Chem. Eu. J.*, 2001, **7**, 374.

Chapter 8
Conclusion

8.1 Concluding remarks

This thesis describes studies into the synthesis, characterisation and reactivity of samarium(II) and (III), europium(II) and ytterbium(II) complexes derived from the modified porphyrinogens *trans-N,N'*-dimethyl-*meso*-octaethylporphyrinogen, $Et_8N_4Me_2H_2$, and *trans*-calix[2]benzene[2]pyrrole, $Me_8N_2Ph_2H_2$.

Chapter 2 details the synthesis of the new modified porphyrinogen $Me_8N_4Me_2H_2$, which was prepared in a "3+1" condensation reaction between 1-methyl-2,5-bis(1,1'-dimethylhydroxymethyl)pyrrole with 1-methyl-2,5-bis{(2'-pyrrolyl)dimethylmethyl}pyrrole in acetonitrile in the presence of scandium trifluoromethanesulfonate. The target macrocycle and the intermediate compounds were characterised by NMR spectroscopy and/or X-ray crystal structure determination. Future work may exploit the stepwise nature of the synthesis to functionalise various parts of the molecule, *e.g.*, adding an alkyl pendant to the 3,4-positions of the *N*-methylpyrrolyl units of the macrocycle to examine agostic interactions at the samarium centre.

Chapter 3 deals with the preparation of lanthanide(II) precursors and their subsequent reactivity with 1,4-diazabuta-1,3-dienes of various steric bulk. The europium(II) complex $[(Et_8N_4Me_2)Eu(THF)_2]$, **(15)**, was synthesised from $Et_8N_4Me_2H_2$ using a modification of the procedure already established for the samarium(II) and ytterbium(II) complexes. The neutral ligand $Et_8N_4Me_2H_2$ was deprotonated with potassium metal and the dipotassium salt was reacted with europium(II) iodide in a salt metathesis reaction. The europium(II) bis(THF) adduct hence obtained was found to lose a molecule of THF upon crystallisation from toluene, giving $[(Et_8N_4Me_2)Eu(THF)]$ **(16)**. Both europium complexes were isostructural and isomorphous with the analogous Sm(II) complexes previously prepared. Reduction of *t*-BuDAB, *i*-PrDAB, and *n*-BuDAB by $[(Et_8N_4Me_2)Sm(THF)_2]$, **(12)**, gave the samarium(III) complexes $[\{(Et_8N_4Me_2)Sm\}_2$(*t*-BuDAB)], **(18)**, $[(Et_8N_4Me_2)Sm$(*i*-PrDAB)], **(19)**, and $[\{(Et_8N_4Me_2)Sm\}_2$(*n*-BuDAB)], **(21)**, respectively. Complex **(19)** was found to react with another equivalent of **(12)** to give $[\{(Et_8N_4Me_2)Sm\}_2$(*i*-PrDAB)], **(20)**. Crystals of an unsolvated samarium(II) dimer

[{($Et_8N_4Me_2$)Sm}$_2$], **(22)**, were recovered from a reaction between *n*-BuDAB and **(12)**; a mechanism for the formation of **(22)** *via* disproportionation of the bridging samarium(III) complex **(21)** was postulated. Analogous reactions between the ytterbium(II) precursor [($Et_8N_4Me_2$)Yb(THF)], **(13)**, and the same 1,4-diazabuta-1,3-dienes led to ytterbium(II) RDAB Lewis base adducts in the case of *i*-PrDAB ([($Et_8N_4Me_2$)Yb(*i*-PrDAB)], **(24)**) and *n*-BuDAB ([{($Et_8N_4Me_2$)Yb}$_2$(*n*-BuDAB)], **(25)**). However, *t*-BuDAB failed to react with **(13)**. The formation of Yb(II) Lewis base adducts rather than Yb(III) complexes was attributed to steric factors preventing sufficient access for the 1,4-diazabuta-1,3-dienes to engage in redox chemistry with the ytterbium centre and/or the lower reduction potential of ytterbium(II) compared with samarium(II). Attempted reactions between the europium(II) precursor [($Et_8N_4Me_2$)Eu(THF)$_2$], **(15)**, and *t*-BuDAB, *i*-PrDAB and *n*-BuDAB were unsuccessful. All the above complexes were characterised by X-ray crystallography. In adddition, **(18)** and **(19)** were characterised by ^{1}H, ^{13}C and 2D NMR spectroscopy.

Chapter 4 details the reduction of cyclooctatetraene by [($Et_8N_4Me_2$)Sm(THF)$_2$] **(12)**, leading to the binuclear bridging COT complex [{($Et_8N_4Me_2$)Sm}$_2$(μ:η^2:η^2-COT)], **(28)**. The molecular structure of **(28)** showed a reduction in hapticity of the cyclooctatetraenediyl moeity from its preferred η^8- to η^2- binding mode. This result highlights the degree of structural control attainable *via* use of the $(Et_8N_4Me_2)^{2-}$ modified porphyrinogen ligand. The mononuclear cyclopentadienyl samarium(III) complex [($Et_8N_4Me_2$)Sm(C_5H_5)], **(26)**, was prepared by salt metathesis between the samarium(III) chloride [{($Et_8N_4Me_2$)SmCl}$_2$], **(27)**, and sodium cyclopentadienide. Complex **(26)** was characterised by ^{1}H, ^{13}C, 2D and VT NMR spectroscopy and X-ray crystallography which showed the cyclopentadienyl ring bound η^5 to the samarium metal, with a concomitant reduction in hapticity of one of the *N*-methylpyrrolide rings from η^5- to η^1-binding. The complex represents the only structurally characterised example of steric competition between an auxiliary ligand and the $(Et_8N_4Me_2)^{2-}$ macrocycle leading to a reduction of hapticity in the latter.

Chapter 5 describes ligand based reduction reactions in which Sm(III) complexes of 1,4-diazabuta-1,3-dienes and $(C_5H_5)^-$ were reacted with reducible substrates. Samarium(III) complexes of *t*-BuDAB and *i*-PrDAB were found to reduce benzil to give the binuclear complex [{($Et_8N_4Me_2$)Sm}$_2${OC(Ph)C(Ph)O}], **(29)**, with the concomitant

formation of free 1,4-diazabuta-1,3-diene. The strained [($Et_8N_4Me_2$)Sm(C_5H_5)] was found to undergo a ligand replacement reaction with 1,4-benzoquinonone to give the binuclear [{($Et_8N_4Me_2$)Sm}$_2${O(C_6H_4)O}], **(30)**, whilst benzil and cyclooctatetraene produced no reaction.

Chapter 6 describes further examples of the reductive chemistry of [($Et_8N_4Me_2$)Sm($THF)_2$], **(12)**. The Sm(II) complex was found to reduce CO_2 in a disproportionation reaction to give carbon monoxide and a bridging CO_3^{2-} moiety. The resulting binuclear samarium(III) complex [{($Et_8N_4Me_2$)Sm}$_2$(CO_3)], **(31)**, was characterised by X-ray crystal structure determination and NMR spectroscopy. The presence of the carbon monoxide disproportionation byproduct was confirmed by GC/MS analysis of the reaction headspace. The samarium(II) complex was also used in redox transmetallation reactions with mercury, thallium and silver salts. The reaction with silver tetrafluoroborate gave a samarium(III) tetrafluoroborate intermediate which underwent subsequent salt metathesis reactions with sodium cyclopentadienide and lithium iodide to give the respective samarium(III) derivatives. Redox transmetallation reactions were underaken on an NMR scale between [($Et_8N_4Me_2$)Sm($THF)_2$], **(12)**, and AgF and Hg(C_6F_5)$_2$ to give solutions containing spectroscopically unique species postulated to be the flouride and pentamethylphenyl complexes [($Et_8N_4Me_2$)SmF], **(35)**, and [($Et_8N_4Me_2$)Sm(C_6F_5)], **(36)**, respectively.

Chapter 7 details the synthesis of *trans*-calix[2]benzene[2]pyrrole by condensation of pyrrole with 1,3-bis(1',1'-dimethylhydroxymethyl)benzene in acetonitrile. The literature procedure was improved by the use of a catalytic amount of scandium trifluoromethanesulfonate, thus allowing lengthy extraction and column chromatography steps to be omitted. As a counterpoint to the conformationally restricted *N,N'*-dimethyl-*meso*-octaethylporphyrinogen, the less rigid doubly deprotonated *trans*-calix[2]benzene[2]pyrrole was investigated as a ligand for lanthanide metals. The dipotassium salt was sythesised by deprotonation of the neutral macrocycle with potassium metal. The Sm(II) and Sm(III) chemistry was investigated by reaction of the dipotassium salt with SmI_2. The reaction was sensitive to conditions and resulted in mixtures from which a number of Sm(II) complexes featuring varying degrees of solvation, residual potassium iodide retention and an unsolvated *N*-confused dimer were isolated. Molecular structures of the dipotassium salt, mono- and bis-(THF) Sm(II) adducts, Sm(II) *N*-confused dimer, a heterometallic Sm(III) cyclooctatetraenediyl

complex and a homometallic, binuclear ion pair Sm(III) cyclooctatetraenediyl complex were obtained by X-ray crystal structure determinations. Macrocyclic binding modes observed fell between the extremes of the samarium(II) mono-(THF) adduct (featuring a bis(η^3-arene) structural motif with only a slight metallocene bend angle) and cyclooctatetraenediyl samarium(III) complexes in which the macrocycle splays back to allow the large, planar COT full access to the Sm coordination sphere, resulting in an η^8 Sm-COT interaction and concomitant reduction in the arene interaction to a slipped η^1-arrangement. The samarium(II) complexes were also characterised by ^{1}H NMR and/or variable temperature ^{1}H NMR spectroscopy.

APPENDIX I

General experimental procedures

Unless otherwise stated all manipulations of complexes were carried out under an argon atmosphere (high purity) by using standard Schlenk techniques. Solvents for the preparation of complexes were dried over Na metal or Na/K alloy. Storage of complexes and preparation of samples for various analyses required the use of a dry, nitrogen atmosphere glove box. For the preparation of organic intermediates or ligands, solvents including methanol, ethanol, dichloromethane, toluene, hexanes and diethyl ether were used as received or after degassing in some cases. All chemicals were obtained from Aldrich and used as received, except pyrrole which was used in reactions after being freshly redistilled. 18-crown-6 was prepared according to the literature procedure.[1]

NMR spectra were recorded in chloroform-*d*, acetone-d_6 or appropriately dried benzene-d_6, THF-d_8, toluene-d_8 and 1,4-dioxane-d_8 using a Varian Mercury Plus 300 operating at 299.91 MHz (^{1}H) and 75.42 MHz (^{13}C) or Bruker AMX 400 spectrometer operating at 400.13 MHz (^{1}H) and 100.61 MHz (^{13}C). The ^{1}H NMR spectra were referenced to the residual ^{1}H resonances of acetone-d_6 (2.05), chloroform-*d* (7.26), benzene-d_6 (7.15), toluene-d_8 (2.09), THF-d_8 (1.73 or 3.75) and 1,4-dioxane-d_8 (3.53), and ^{13}C NMR were referenced to the ^{13}C resonances of $CDCl_3$ (77.2), C_6D_6 (128.4), THF-d^8 (67.6 or 25.4) and toluene-d_8 (20.4). GC/MS spectra were performed using a HP5890 gas chromatograph equipped with an HP5790 Mass Selective Detector and a 25 m x 0.32 mm HPI column. Elemental analyses were performed by the Central Science Laboratory at the University of Tasmania. (Carlo Erba EA1108 Elemental Analyser) or the Chemical and Analytical Services Pty. Ltd., Melbourne. X-ray crystal structure determinations were carried out by Prof. Allan H. White and Dr. Brian W. Skelton of the University of Western Australia or Dr. Michael G. Gardiner and Dr. Gary D. Fallon at Monash University, or Dr. Peter Turner at the University of Sydney.

[1] G.W. Gokel, D.J. Cram, *J. Org. Chem.*, 1974, **39**, 2445.